

University of Bath



PHD

Asymptotic analysis of mathematical models for elastic composite media

Serkov, S. K.

Award date:
1998

Awarding institution:
University of Bath

[Link to publication](#)

General rights

Copyright and moral rights for the publications made accessible in the public portal are retained by the authors and/or other copyright owners and it is a condition of accessing publications that users recognise and abide by the legal requirements associated with these rights.

- Users may download and print one copy of any publication from the public portal for the purpose of private study or research.
- You may not further distribute the material or use it for any profit-making activity or commercial gain
- You may freely distribute the URL identifying the publication in the public portal ?

Take down policy

If you believe that this document breaches copyright please contact us providing details, and we will remove access to the work immediately and investigate your claim.

Download date: 23. May. 2019

Asymptotic Analysis of Mathematical Models for Elastic Composite Media

submitted by

S. K. Serkov

for the degree of Ph.D

of the

University of Bath

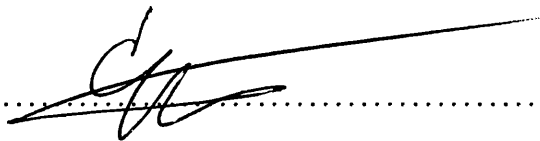
1998

COPYRIGHT

Attention is drawn to the fact that copyright of this thesis rests with its author. This copy of the thesis has been supplied on the condition that anyone who consults it is understood to recognise that its copyright rests with its author and that no quotation from the thesis and no information derived from it may be published without the prior written consent of the author.

This thesis may be made available for consultation within the University Library and may be photocopied or lent to other libraries for the purposes of consultation.

Signature of Author



S. K. Serkov

UMI Number: U601510

All rights reserved

INFORMATION TO ALL USERS

The quality of this reproduction is dependent upon the quality of the copy submitted.

In the unlikely event that the author did not send a complete manuscript and there are missing pages, these will be noted. Also, if material had to be removed, a note will indicate the deletion.



UMI U601510

Published by ProQuest LLC 2013. Copyright in the Dissertation held by the Author.
Microform Edition © ProQuest LLC.

All rights reserved. This work is protected against
unauthorized copying under Title 17, United States Code.



ProQuest LLC
789 East Eisenhower Parkway
P.O. Box 1346
Ann Arbor, MI 48106-1346

UNIVERSITY OF BATH LIBRARY	
22	29 APR 1998
Ph.D	

5121473

Summary

The main subject of the thesis is the asymptotic analysis of models in mechanics of composite materials. It is based on the extension of the theory of the Pólya-Szegő tensors to the problems of homogenization and fracture. Such a technique allows one to obtain an asymptotic solution to a problem where most of numerical algorithms fail due to the presence of a singular perturbation. As a result of this work, a number of interesting effects have been found in optimization of composites and inverse problems of crack-inclusion interaction.

Chapter 1 is an introductory chapter that contains the main definitions and bibliographical remarks.

In Chapter 2 the Pólya-Szegő dipole tensors are employed for analysis of plane elasticity problems in non-homogeneous media. Classes of equivalence for defects (cavities and rigid inclusions) are specified for the Laplace and Navier operators: composite materials with defects of the same class have the same effective elastic moduli. Explicit asymptotic formulae for the effective compliance matrices of dilute composites are obtained.

The problem of the optimal cavity shape is analyzed in Chapter 3. The analysis uses the Pólya-Szegő tensors calculated in Chapter 2. A new type of structure which is optimal for shear loading has been found. Properties of the optimal cavity are described.

The crack-inclusion interaction problem considered in Chapter 4 has been solved by the asymptotic methods. An analysis of crack trajectories is performed in Chapter 5 for different types of defects and interface conditions. The algorithm employs the Pólya-Szegő tensors as integral characteristics describing the defect. Comparison with experimental data (Ceramic Centre, Bologna) is presented.

In Chapter 6 we use the method of compound asymptotic expansions to treat the homogenization problem for thin-walled composites. The technique of boundary layer fields is employed to derive the junction condition in the region connecting thin walls. The asymptotic formulae are derived for the effective elastic, thermal conductive and thermal expansion moduli of thin-walled periodic structures.

Acknowledgments

I would like to thank the Department of Mathematical Sciences at the University of Bath, where this thesis has been written. I am grateful for the financial support of the University Scholarship and ORS student research award.

I would very much like to thank Dr. Alexander Movchan, my supervisor, for his encouragement, fruitful and helpful discussions and support. Also, I wish to thank Prof. Graeme Milton, Prof. Andrej Cherkaev and Dr. Yury Grabovsky of the Department of Mathematics, University of Utah, for interesting discussions during my visit to the Department. I would also like to thank Dr. Davide Bigoni of the University of Bologna for his hospitality and Ms Monica Valentini of the Ceramic Centre (Bologna) for the experimental data. I am grateful to Dr. Natasha Movchan, Dr. Valery Smyshlyaev and Prof. Yury Antipov for their useful comments.

Finally, my thanks go to Mr and Mrs Pakeman, in whose house I lived during the last year.

Contents

1	Introduction	6
1.1	Background, motivation and structure of the thesis	6
1.2	Definitions	13
1.2.1	The dipole form matrices	13
1.2.2	The Pólya-Szegő matrices	15
	The case of the Laplace operator	15
	Pólya-Szegő and energy matrices	16
2	The Pólya - Szegő matrices in elasticity	19
2.1	Definition of Pólya-Szegő matrix for the Navier equations	19
2.2	Explicit formulae for Pólya-Szegő matrices	21
2.2.1	Plane strain: cavities	21
2.2.2	Plane strain: rigid inclusions	27
2.2.3	Anti-plane shear: cavities and rigid inclusions	31
2.2.4	Circular elastic inclusions	33
2.3	Effective moduli of dilute composites	34
2.3.1	Anti-plane shear	34
	Asymptotic formulae	34
	Comparison with previous results	36
2.3.2	Plane strain	37
	Classes of equivalent domains	37
	The compliance matrix	38
	Examples of effective moduli	41
2.4	Mapping to a composite material with elliptical voids	42
2.5	Conclusions	46

3	Pólya-Szegő matrices in optimization problem	47
3.1	Recent results	47
3.2	Formulation of the problem	48
3.3	Minimization technique	53
3.4	Optimal shape of the cavity	53
3.4.1	Optimization of the shape by the direct method	54
3.4.2	Properties of the optimal hole	56
3.5	Solution of the inverse problem	61
3.6	Asymptotic expansion of the optimal solution near the corners	64
3.7	Numerical procedure and existence of the solution	68
3.8	Conclusions	70
4	Crack-inclusion interaction problem	71
4.1	Background and motivation	71
4.2	Crack geometry and field equations	72
4.3	Asymptotic expansion for a solution of a thermo-elasticity problem	75
4.4	Unperturbed crack	79
4.5	Perturbation of the crack	80
4.5.1	Asymptotic analysis	80
4.5.2	Crack trajectory	84
4.5.3	Effect of thermal stresses	85
4.6	Conclusions	86
5	Fracture propagation due to different inhomogeneities	88
5.1	Some examples of the crack path	89
5.1.1	Interaction between a semi-infinite crack and a cavity	89
5.1.2	Interaction between a crack and a circular elastic inclusion	93
5.2	The influence of an elliptic elastic inclusion on the crack trajectory	96
5.2.1	Model problem	96
5.2.2	Conformal mapping	98
5.2.3	Series representation for potentials	99
5.2.4	Pólya-Szegő matrix	104
5.2.5	Trajectory of a perturbed crack	106
5.3	Fracture in thermo-elastic media	109

5.3.1	Interaction of a crack with a circular thermoelastic inclusion . . .	109
5.3.2	Interaction of a crack with an elliptical thermoelastic inclusion .	111
5.3.3	Numerical experiments	114
5.4	Mathematical model of a debonding-type interface	119
5.4.1	Asymptotic derivation of linear interface conditions	120
5.4.2	Circular inclusion with imperfect bonding	123
5.5	Crack trajectory in a dilute composite	129
5.5.1	Pólya-Szegő matrix	129
5.5.2	Crack trajectory	130
5.6	Conclusions	133
6	Asymptotic analysis of thin-walled composites	134
6.1	Honeycomb structure under remote loading: formal asymptotic approach	134
6.1.1	First-order boundary layer	138
6.1.2	Second-order boundary layer	140
6.2	Asymptotic expansion of the solution in thin bridges	143
6.2.1	Thin bridge of a constant thickness	143
6.2.2	Thin bridge of an orthotropic material	145
6.2.3	Thin bridge of a varying thickness	146
6.3	The leading order approximation for the effective moduli	149
6.3.1	Effective elastic moduli for square honeycombs	151
6.3.2	Effective elastic moduli for triangular honeycombs	153
6.3.3	Effective elastic moduli for hexagonal honeycombs	156
6.3.4	Second term in effective moduli expansion	160
6.4	3D effective elastic moduli	162
6.5	Application of the homogenization procedure	165
6.5.1	Closely-located rigid inclusions: elasticity problem	165
6.5.2	Thin-walled composites: conductive media	167
6.5.3	Closely-located rigid inclusions: conductive media	168
6.5.4	Thin-walled composites: thermo-elastic media	169
6.6	Comparison with numerical experiments	170
6.7	Conclusions	172
A	Homogenisation of the linear elasticity equations	173

Chapter 1

Introduction

1.1 Background, motivation and structure of the thesis

The main objective of the thesis is to apply asymptotic methods to the problems of homogenization and fracture in composite materials. In particular, the problem of evaluating the effective moduli of dilute media filled with cavities or rigid inclusions of arbitrary shape and crack propagation in such a medium are of main interest. An asymptotic approach to homogenization of thin-walled composites with periodic structure is considered in the last chapter. Both these topics - composite materials and asymptotics - have been studied by many authors in recent years. They often have been treated as two separate topics with no common links. However, if a composite medium can be characterized by a small parameter, the asymptotics allow one to obtain some closed-form solutions. In fact, any dilute suspension or cellular solid is an example of such a structure.

Due to a wide application of the computer technology, problems of solid mechanics are often treated numerically. Advanced finite element packages have been designed for elasticity, conductivity, fluid dynamics (e.g. COSMOS/M package [120] developed by Structural Research and Construction Corporation). Usually this technique enables one to obtain good results applicable to the industrial problems. At the same time there is a number of singularly perturbed problems where, due to the presence of a small parameter associated with a non-regularity of the problem or small coefficients multiplying the high derivatives, the application of the finite element or finite difference methods requires a very fine mesh or in many cases fail. Examples include elasticity or conductivity problems in dilute media (perturbation of the boundary due to additional

interface of inclusion) or cellular solids with perturbed boundary of walls or rods. The convergence of such schemes is often unsatisfactory for the problems with small parameters. Asymptotic methods are free of these disadvantages. Conversely they allow one to construct the leading terms (or all terms in some cases) of the expansion explicitly and, as a result, to analyse qualitatively the solutions of either direct or inverse problems. Asymptotic methods for singularly perturbed problems have been extensively studied during the last ten years. Various topics of the asymptotic theory of partial differential equations and calculus of approximation have been considered. The theory is based on the results of Kondrat'ev [54], who analysed the behaviour of the solution of elliptic boundary value problems near the conical and angular points. Speaking about asymptotic methods it is important to refer to the works by Maz'ya (for example, Maz'ya, Nazarov and Plamenevsky [65]). They used the method of compound asymptotic expansions in singularly perturbed boundary value problems. Elliptic boundary value problems have been considered by Nazarov and Plamenevsky [84] in domains with edges of different geometries (polygons, cones, cusps). Monograph by Movchan and Movchan [75] deals with some particular areas of fracture mechanics, such as modelling of cracks, thin inclusions and domains with conical points and sharp edges. Asymptotic expansions of the solutions of linear elasticity boundary value problems have been analysed.

It is important to mention that the main subject of the investigation is composite and inhomogeneous media, a widely presented subject in mathematical and engineering literature. It is appropriate to refer to some monographs where composite materials are described (Sendekyj [99], Christensen [18], Jones [49]). Overall elastic moduli have been studied by Willis in [122] where the well-known bounds obtained by Hill [43] have been compared with Hashin-Shtrikman bounds and with bounds of a higher order. In [123] three principal methods for studying randomly inhomogeneous media (perturbation theory, variational principles and self-consistent methods) have been considered. Self-consistent analysis has been applied to wave propagation problems in composites with spherical inclusions or small cracks by Sabina, Smyshlyaev and Willis [96]. Properties of different types of composite materials have been studied by Nemat-Nasser and Hori [85]. Properties of laminates, as the optimal structures, have been considered by Milton [68]. Specific types of heterogeneous structures - cellular solids - have been described by Gibson and Ashby [30] and Kalamkarov and Kolpakov [50]. They analysed thin-walled

two- and three-dimensional composite media using engineering hypotheses. Hashin [40], [37] considered thermo-elastic properties of composites. Budiansky [12] analysed the overall moduli of a multiphase material using approximate methods.

An important application of the method of asymptotic expansions is in homogenization of composite materials where the asymptotic technique allows one to derive the homogenized operator by considering multiple scale asymptotic expansions. We can refer to monographs by Bensoussan, Lions and Papanicolaou [8], Bakhvalov and Panasenko [4] and Jikov, Koslov and Oleinik [47]. They discuss a technique based on two different scales. The first one is the macro-scale which characterizes the size of the domain, the second one corresponds to the micro-scale which describes the size of an elementary periodic cell. In the monograph by Bensoussan, Lions and Papanicolaou [8] the multiple scale method is used to treat boundary value problems with rapidly oscillating coefficients. Rigorous theory of homogenization is presented in the monograph by Jikov, Koslov and Oleinik [47], where the method of asymptotic expansion has been used to justify homogenization for second order elliptic operators with periodic coefficients. Jikov, Koslov and Oleinik [47] also considered homogenization of parabolic operators, homogenization in linear elasticity and nonlinear variational problems. “Averaging technique” of defining the effective constants for layered and multi-rod structures has been considered by Bakhvalov and Panasenko [4].

The optimal design of composite materials is one of the areas in mechanics widely studied at the present time. A number of monographs have been written on this subject, for example, Haug, Choi and Komkov [41] on application of numerical methods in optimization, Pironneau [89] and Sokolowski and Zolesio [104] on variational techniques. It is important to mention the work by Rozvany, Bendsoe and Kirsch [94] that includes mathematical and numerical analyses of shape sensitivity associated with elliptic boundary value problems, and “First World Congress of Structural and Multidisciplinary Optimization” [87] where the new problems in structural optimization have been discussed. Structural optimization using FEM is considered by Schnack [98]. The existence of solutions of optimal control problems for the Laplace operator is analyzed by Chenais [15].

Since one part of this work deals with fracture in inhomogeneous media filled with defects of different type, it is appropriate here to refer on papers on fracture mechanics. Fracture propagation is an area of mechanics where asymptotic methods have wide applications.

Stress intensity factors at the tip of a slightly curved or kinked 2D crack have been found by Cotterell and Rice [20]. Initial development of a crack path has been analysed. Later Sumi, Nemat-Nasser and Keer [107] analysed quasi-static growth of slightly non-collinear crack in a finite brittle solid using Muskhelishvili complex potentials. They supposed the crack extension to be of special polynomial form. Crack path caused by a residual stress field has been simulated numerically by Sumi [106]. Rubinstein [95] analysed an interaction of a macrocrack with microdefects in an elastic body. He derived the increment in stress intensity factors due to microdefects by solving the integral equation for the potentials. Movchan, Nazarov and Polyakova [77] have obtained a similar expression by asymptotic methods using the weight functions. These functions have been introduced by Bueckner [13] and have many applications. For 3D dynamical crack they have been derived by Willis and Movchan [124], Movchan and Willis [82]. Another application is in a wavy crack problem analysed by Willis and Movchan [125], Gao [25] and Xu, Bower and Ortiz [126] where 3D perturbation of a crack front has been analysed. In-plane perturbation of a flat crack in 3D space has been analysed by Martin [61] using integral equations technique. Perturbed conformal mapping on the penny-shaped crack has been introduced and hypersingular equation for the crack opening has been solved. Similar technique was applied to nearly circular tensile cracks by Martin [62].

The asymptotic technique has been employed for the solution of elliptic boundary value problems in regions with a non-smooth boundary. One can mention the following works: investigation of cracks with smoothly closed edges carried out by Movchan, Morozov and Nazarov [74]; defects with sharp edges studied by Movchan and Nazarov [76]; cusps and conical points on the boundary treated by Maz'ya and Nazarov [64]; asymptotic expansions of solutions in the vicinity of conical and angular points found by Kondrat'ev [54] and Kondrat'ev and Oleinik [55]. Crack in the form of a rectangular hole has been considered by Movchan [71] and Movchan and Serkov [78]. The effects which occur under the longitudinal loading of a thin rectangular hole have been analysed and the mechanism which causes crack branching has been explained.

The technique based on the analysis of the Pólya-Szegő tensors is closely connected to the method of asymptotic expansions. This is an alternative way of describing an inclusion in terms of the energy of perturbation field associated with a finite defect in an infinite plane. This tensor was introduced in 1951 by Pólya and Szegő [90] and Taylor

[110] for electrostatic problems. They considered the Dirichlet and Neumann boundary value problems for the Laplace operator. It has been proved that in this case the Pólya-Szegő matrices represent second rank tensors and are independent of the right-hand sides in equations and boundary conditions.

Later this technique has been applied to elasticity problems by Babich, Zorin, Ivanov, Movchan and Nazarov [3], Movchan [72], Movchan and Serkov [79], [81], [80] and Zorin, Movchan and Nazarov [127]. It is important that a lot of characteristics in linear elasticity, such as energy increment and effective moduli of composite, can be expressed in terms of the Pólya-Szegő tensor. Asymptotic behaviour of the solution of boundary value problems in an infinite plane with an inclusion is specified in terms of this tensor also. Using the Pólya-Szegő tensors, the elasticity problems in an infinite plane with defects can be treated without any restriction on the geometry of inclusion provided the inclusion is finite. The knowledge of the tensors gives sufficient information about energy characteristics of defects and allows one to solve a number of new problems of homogenization, fracture mechanics and optimal control.

The Pólya-Szegő tensor can be considered as an alternative characteristic of an inclusion and can be compared with the Eshelby tensor [24]. The first one describes the field far away from the inclusion, the second one within the inclusion. On the other hand, the Pólya-Szegő tensor characterises an inclusion of an arbitrary shape. The Eshelby tensor is usually used for an elliptical inclusion (Eshelby [24]).

An extension of the method of compound asymptotic expansions (technique of the Pólya-Szegő tensors) to the problem of homogenization, fracture mechanics and optimal design is the main subject of this thesis. The key-point is the investigation of the properties of the Pólya-Szegő tensor naturally occurring in the problems listed above. The major advantage of this technique is in the analysis of the boundary value problems in domains with defects of an arbitrary shape (provided the perturbed inclusion or cavity is finite).

In Chapter 2 the main properties of the Pólya-Szegő tensors are discussed. The elements of the tensor are defined as the coefficients in the asymptotic expansion at infinity for the solution of a model boundary value problem imposed in an infinite region with a defect. Calculations of these tensors for cavities, rigid inclusions in conductive and elastic media are carried out. The boundary integral equations of the Kolosov-Muskhelishvili type are employed for this purpose. Correspondence between the energy increment due to

an inclusion and the Pólya-Szegő tensor is given. Homogenization procedure for dilute composites with defects of arbitrary shape is carried out. An analytical representation for the leading terms of the effective moduli is given in terms of components of the Pólya-Szegő tensor.

The analysis of the effective moduli results in a number of interesting effects: equivalence between domains possessing the same effective moduli, equivalence between elliptical and non-elliptical defects (for conductivity problem and elasticity after certain affine transform of the coordinates). In particular, for the case of the Laplace operator (anti-plane shear) it is shown that the displacement field for an arbitrary inclusion or cavity occupying a bounded simply connected region is equivalent (in the energy norm) to the field associated with an elliptical inclusion. Dilute composite medium is also considered where an elementary cell contains a small inclusion or cavity. Following Olver [88] (also, see Milton and Movchan [70]) one can choose an affine transformation which yields a new system of equations represented in the canonical form corresponding to an orthotropic material. The matrix of elastic moduli has a block-diagonal structure. It is shown that under some conditions imposed on the Pólya-Szegő matrix there exists a transformation which relates a homogenization problem for a medium with small holes (of arbitrary shape) to a medium with elliptical cavities. It has been shown that the correction term of the compliance matrix for composites with voids is independent of the Poisson ratio. Chapter 3 deals with the extension of Pólya-Szegő technique to the optimal design problem. Here we follow the idea of Milton [69], Grabovsky and Kohn [34], [35], and Vigdergauz [118], who analysed the optimality of composites. Different types of optimal structures, such as laminates and confocal ellipses, have been found. Here different technique has been applied and some special type of loading conditions (i.e. shear loading) has been analysed. Application of the Pólya-Szegő technique to these problems has led to a new type of optimal microstructures subjected to shear. A cavity of fixed area is said to be optimal if it provides a minimal energy change associated with introducing the cavity in an infinite plane. One shows that for shear loading the contour of the optimal cavity is not smooth and shaped as a curved quadrilateral. The shape is specified in terms of conformal mapping coefficients and the proof of optimal behaviour of this structure is presented.

In Chapters 4 and 5 the asymptotic technique is applied to problems of fracture mechanics. The method of compound asymptotic expansions is employed to treat the problem

of interaction between a crack and an elastic inclusion (so called crack-inclusion interaction problem). This method allows one to derive an asymptotic formula for the crack trajectory in terms of the Pólya-Szegő tensor and, hence, to analyse the trajectory without laborious finite-element calculations (Sumi and Wang [108]).

In Chapter 4 two-dimensional asymptotic solution for description of the trajectory of a quasi-static crack in thermo-elastic isotropic medium containing small defects is presented. First, the asymptotic procedure is applied to uncoupled thermo-elasticity problems imposed in an infinite plane with a crack and an inclusion. Asymptotic formulae for crack trajectories are derived. The defects are described by the Pólya-Szegő matrices, and examples of the crack trajectories for different types of defects (elliptical cavities, circular and elliptical elastic inclusions) are given in Chapter 5. The results of the asymptotic analysis agree with existing numerical solutions and give a qualitative description of crack trajectories observed in brittle materials, such as porous ceramics. Finally, comparison with the experimental data provided by the Ceramic Centre (Bologna) is presented. The second part of the Chapter 5 deals with the effect of temperature on the crack trajectory. It also describes non-perfect interface conditions and how they affect the crack trajectory. The situation when debonding causes the shield effect is analysed.

Chapter 6 does not employ the technique of the Pólya-Szegő matrices. It is based on the compound asymptotic expansions constructed for thin regions. This Chapter has a logical link with Chapter 2, where homogenization of dilute composites is studied. The Pólya-Szegő technique works well in these problems. In Chapter 6 the homogenization of thin-walled composites is studied. Full asymptotic expansions are constructed and the boundary layer solutions are analysed. Junction conditions are deduced from the analysis of junction boundary layer solutions. Thus, they are obtained without any simplifying hypothesis widely used in engineering approaches. Using the homogenization procedure, we analyse the honeycomb, square and triangular thin-walled composites. Both thermal and elastic effects are taken into account. The effective moduli are evaluated for different types of structures consisting of conductive, elastic or thermo-elastic constituents.

1.2 Definitions

1.2.1 The dipole form matrices

Consider a two-dimensional irrotational flow of incompressible inviscid fluid with the velocity $\mathbf{v}^{(i)} = \mathbf{e}^{(i)}$, $i = 1, 2$. Introduce a finite body G . The flow of fluid will be perturbed and the perturbation field decays at infinity. One is looking for solutions of the Neumann boundary value problems

$$\Delta \Phi^{(i)}(\mathbf{x}) = 0, \quad \mathbf{x} \in \mathbb{R}^2 \setminus \overline{G}, \quad (1.2.1)$$

$$\frac{\partial \Phi^{(i)}}{\partial n} = 0, \quad \mathbf{x} \in \partial G, \quad (1.2.2)$$

which satisfy the following condition at infinity

$$\Phi^{(i)} \sim x_i \quad \text{as} \quad \|\mathbf{x}\| \rightarrow \infty. \quad (1.2.3)$$

In (1.2.2) \mathbf{n} is the unit outward normal vector with respect to $\mathbb{R}^2 \setminus \overline{G}$. The idea of Pólya and Szegő [90] was to compensate the discrepancy in the boundary condition (1.2.2) produced by the originally homogeneous field by taking the functions $\Phi^{(i)}$ in the form

$$\Phi^{(i)} = x_i + \varphi^{(i)}, \quad (1.2.4)$$

where $\varphi^{(i)}$ are harmonic in $\mathbb{R}^2 \setminus \overline{G}$ and satisfy the Neumann boundary conditions

$$\frac{\partial \varphi^{(i)}}{\partial n} = -n_i \quad \text{on} \quad \partial G, \quad (1.2.5)$$

and the conditions of decay at infinity (in 2D case)

$$\varphi^{(i)}(\mathbf{x}) \sim \sum_{k=1}^2 \mathcal{D}_{ik}(G) \frac{x_k}{\|\mathbf{x}\|^2}, \quad \text{as} \quad \|\mathbf{x}\| \rightarrow \infty. \quad (1.2.6)$$

The matrix $\mathcal{D} = \{\mathcal{D}_{ik}\}_{i,k=1}^2$ in the above expression is said to be *the matrix of the dipole form*

$$\sum_{i,k=1,2} \mathcal{D}_{ik} \varepsilon_i \varepsilon_k.$$

Let

$$\mathcal{W}_{ik} = (\varphi^{(i)}, \varphi^{(k)}) = \int_{R^2 \setminus \bar{G}} \nabla \varphi^{(i)} \nabla \varphi^{(k)} dx. \quad (1.2.7)$$

Then, the following relation between the energy matrix \mathcal{W} and the matrix \mathcal{D} holds (see Taylor [110])

$$\boxed{\mathcal{W}(G) = 2\pi\mathcal{D}(G) - mes_2(G)\mathbf{I}}, \quad (1.2.8)$$

where \mathbf{I} is the identity matrix. It follows from (1.2.7) that the matrix \mathcal{D} is positive definite.

Now, recall the definition of the dipole matrix for the Dirichlet problem. Consider a homogeneous electrostatic field of the constant intensity $\mathbf{E} = e^{(i)}$, $i = 1, 2$, in an infinite plane. Introduce a finite conductor G , and assume that its total charge is equal to zero. The two-dimensional defect G yields a perturbation of the electrostatic field which decays like $O(\|\mathbf{x}\|^{-1})$ at infinity. For the corresponding Dirichlet problem with the condition (1.2.3) at infinity the electrostatic potential $\Phi^{(i)}$ admits the representation

$$\Phi^{(i)} = x_i + \psi^{(i)}. \quad (1.2.9)$$

Here, the function $\psi^{(i)}$ compensates the discrepancy, produced by the first term on the right-hand side of (1.2.9) in the Dirichlet boundary condition, and it is characterized by the following asymptotic formula at infinity

$$\psi^{(i)}(x) \sim \sum_{k=1}^2 \mathcal{H}_{ik}(G) \frac{x_k}{\|\mathbf{x}\|^2}, \quad \text{as } \|\mathbf{x}\| \rightarrow \infty. \quad (1.2.10)$$

The matrix $\|\mathcal{H}_{ik}\|$ is called *the dipole form matrix* or the matrix of dipole coefficients.

The energy matrix

$$\mathcal{P}_{ik} = (\psi^{(i)}, \psi^{(k)}) = \int_{R^2 \setminus \bar{G}} \nabla \psi^{(i)} \nabla \psi^{(k)} dx. \quad (1.2.11)$$

and the matrix \mathcal{H} of the dipole coefficients are related by

$$\boxed{\mathcal{P}(G) = -2\pi\mathcal{H}(G) - mes_2(G)\mathbf{I}}. \quad (1.2.12)$$

This formula has been proved by Taylor [110], and it also can be found in Pólya and Szegő [90]. As follows from (1.2.11) and (1.2.12), the matrix \mathcal{H} is negative definite.

Analysis of elasticity problems which generalises the results of Pólya and Szegő is pre-

sented in Movchan [72], Movchan and Serkov [79], Movchan and Movchan [75] and Zorin, Movchan and Nazarov [127]. In the next section we shall consider the problem for an inclusion with the interface boundary conditions posed on ∂G .

1.2.2 The Pólya-Szegő matrices

The case of the Laplace operator

Consider an anti-plane shear of an infinite plane containing a finite inclusion G . The third (transversal to the plane) component $u(\mathbf{x})$ of the displacement satisfies the boundary value problem

$$-\mu\Delta u(\mathbf{x}) = 0, \quad \mathbf{x} \in \mathbb{R}^2 \setminus \overline{G}, \quad (1.2.13)$$

$$-\mu_0\Delta u^{(0)}(\mathbf{x}) = 0, \quad \mathbf{x} \in G, \quad (1.2.14)$$

$$\mu \frac{\partial u}{\partial n} = \mu_0 \frac{\partial u^{(0)}}{\partial n}, \quad u = u^{(0)}, \quad \mathbf{x} \in \partial G, \quad (1.2.15)$$

with the following condition at infinity

$$u(\mathbf{x}) \sim \sum_{i=1}^2 C_i x_i \quad \text{as } \|\mathbf{x}\| \rightarrow \infty. \quad (1.2.16)$$

In (1.2.16) C_i are constants. The solution of (1.2.13)-(1.2.15) with the conditions at infinity (1.2.16) can be found in the form

$$u(\mathbf{x}) = \sum_{i=1}^2 C_i \left\{ x_i + w^{(i)}(\mathbf{x}) \right\}. \quad (1.2.17)$$

The harmonic functions $w^{(i)}$, $i = 1, 2$, decay at infinity and can be specified by the asymptotic formula

$$w^{(i)} = -\frac{1}{2\pi\mu} \sum_{j=1}^2 M_{ij} \frac{x_j}{\|\mathbf{x}\|^2} + O\left(\frac{1}{\|\mathbf{x}\|^2}\right), \quad \|\mathbf{x}\| \rightarrow \infty. \quad (1.2.18)$$

Note that the matrix $\|M_{ij}\|$ differs from the matrix $\|D_{ij}\|$ introduced in Section 1.2.1 by a constant coefficient. The equivalent form of (1.2.18) is

$$w^{(i)} = \sum_{j=1}^2 M_{ij} \frac{\partial}{\partial x_j} T(\mathbf{x}) + O\left(\frac{1}{\|\mathbf{x}\|^2}\right), \quad \|\mathbf{x}\| \rightarrow \infty, \quad (1.2.19)$$

where $T(\mathbf{x}) = -(2\pi\mu)^{-1} \ln \|\mathbf{x}\|$ is the fundamental solution of the Laplace equation in a plane. Further in the text the matrix $\{M_{ij}\}$ will be called the *Pólya-Szegő matrix*.

It should be mentioned that for the case of a cavity G with the contour ∂G (Neumann boundary condition), the displacement $u(\mathbf{x})$ satisfies (1.2.13) and the boundary conditions (1.2.15) should be replaced by

$$\frac{\partial u}{\partial n} = 0, \quad \mathbf{x} \in \partial G. \quad (1.2.20)$$

If G is a rigid inclusion (Dirichlet boundary conditions), the displacement vector $u(\mathbf{x})$ satisfies (1.2.13) and the condition

$$u(\mathbf{x}) = a, \quad \mathbf{x} \in \partial G, \quad (1.2.21)$$

where the constant a is chosen in such a way that the field $u(\mathbf{x})$ admits the representation (1.2.17) with the functions $w^{(i)}$ characterized by the asymptotic formula (1.2.19) at infinity (the term corresponding to a point force is absent).

Pólya-Szegő and energy matrices

Here we consider the boundary value problem (1.2.13)-(1.2.15) and seek its solution in the form

$$u(\mathbf{x}) = \sum_{i=1}^2 C_i \{x_i + w^{(i)}(\mathbf{x})\}, \quad \mathbf{x} \in \mathbb{R}^2 \setminus \overline{G},$$

$$u^{(0)}(\mathbf{x}) = \sum_{i=1}^2 C_i \{x_i + w^{(0,i)}(\mathbf{x})\}, \quad \mathbf{x} \in G,$$

where the functions $w^{(i)}(\mathbf{x})$ and $w^{(0,i)}(\mathbf{x})$ are harmonic in $\mathbb{R}^2 \setminus \overline{G}$ and G , respectively, and satisfy the following interface conditions on ∂G

$$\mu \frac{\partial w^{(i)}}{\partial n} - \mu_0 \frac{\partial w^{(0,i)}}{\partial n} = (\mu_0 - \mu)n_i, \quad w(\mathbf{x}) = w^{(0,i)}(\mathbf{x}), \quad \mathbf{x} \in \partial G. \quad (1.2.22)$$

Then one can see that the harmonic fields $w^{(i)} + x_i$, $w^{(0,i)} + x_i$ satisfy the interface boundary conditions (1.2.15). Using the Green's formula one verifies (see also Movchan [72]) that

$$\boxed{\mathcal{M}(G) = -M(G) + (\mu_0 - \mu)mes_2GI,} \quad (1.2.23)$$

where

$$\mathcal{M}_{ij} = \mu \int_{R^2 \setminus \bar{G}} \nabla w^{(i)} \cdot \nabla w^{(j)} d\mathbf{x} + \mu_0 \int_G \nabla w^{(0,i)} \cdot \nabla w^{(0,j)} d\mathbf{x}. \quad (1.2.24)$$

Taking the limit when $\mu_0 \rightarrow 0$ we arrive at the problem for a cavity with the Neumann boundary conditions. In this case the Pólya-Szegő matrix \mathbf{M} is related to the dipole form matrix \mathcal{D} introduced in Section 1.2.1 by

$$\mathbf{M} = -2\pi\mu\mathcal{D}.$$

Consider a different way of extension of the polynomial fields x_i , $i = 1, 2$, into the inclusion G . Namely, introduce a harmonic function $w^{*(0,i)}$ such that

$$\mu \frac{\partial w^{(i)}}{\partial n} - \mu_0 \frac{\partial w^{*(0,i)}}{\partial n} = 0, \quad w(\mathbf{x}) - w^{*(0,i)}(\mathbf{x}) = \left(\frac{\mu}{\mu_0} - 1\right)x_i, \quad \mathbf{x} \in \partial G. \quad (1.2.25)$$

Then the fields $w^{(i)} + x_i$, $w^{*(0,i)} + \mu x_i / \mu_0$ satisfy the interface boundary conditions (1.2.15). In other words, we have extended the field $w^{(i)}$ into the inclusion in such a way that the shear tractions are continuous on the interface. Application of the Green's formula shows that

$$\boxed{\mathcal{N}(G) = \mathbf{M}(G) - \mu \left[1 - \frac{\mu}{\mu_0}\right] mes_2 G \mathbf{I}}, \quad (1.2.26)$$

where

$$\mathcal{N}_{ij} = \mu \int_{R^2 \setminus \bar{G}} \nabla w^{(i)} \cdot \nabla w^{(j)} d\mathbf{x} + \mu_0 \int_G \nabla w^{*(0,i)} \cdot \nabla w^{*(0,j)} d\mathbf{x}. \quad (1.2.27)$$

Taking the limit when $\mu_0 \rightarrow \infty$, we obtain the equality

$$\mathbf{M} = -2\pi\mu\mathcal{H},$$

where \mathcal{H} is the dipole form matrix for the "rigid inclusion" introduced in Section 1.2.1. Note that the Pólya-Szegő matrix \mathbf{M} is positive definite for a cavity (the boundary conditions of the Neumann type), and it is negative definite for a rigid inclusion (the Dirichlet boundary conditions).

In conclusion to Chapter 1 it should be mentioned that Pólya-Szegő tensors introduced here in the simplest case of the Laplace operator have interesting applications in elasticity. In Chapter 2 the Pólya-Szegő tensors will be constructed for different types of inhomogeneities and then applied to the problems of composite media and fracture propagation.

Chapter 2

The Pólya - Szegő matrices in elasticity

2.1 Definition of Pólya-Szegő matrix for the Navier equations

Consider the same region $\mathbb{R}^2 \setminus \overline{G}$ as in Section 1.2.2, and assume that the displacement field $\mathbf{u}(\mathbf{x})$ satisfies the system of Navier equations and the interface boundary conditions on ∂G

$$\mu \nabla^2 \mathbf{u} + (\lambda + \mu) \nabla \nabla \cdot \mathbf{u} = 0, \quad \mathbf{x} \in \mathbb{R}^2 \setminus \overline{G}, \quad (2.1.1)$$

$$\mu_0 \nabla^2 \mathbf{u}^{(0)} + (\lambda_0 + \mu_0) \nabla \nabla \cdot \mathbf{u}^{(0)} = 0, \quad \mathbf{x} \in G, \quad (2.1.2)$$

$$\sigma^{(n)}(\mathbf{u}; \mathbf{x}) = \sigma^{(n,0)}(\mathbf{u}^{(0)}; \mathbf{x}), \quad \mathbf{u} = \mathbf{u}^{(0)}, \quad \mathbf{x} \in \partial G, \quad (2.1.3)$$

$$\sigma^{(n)}(\mathbf{u}; \mathbf{x}) = \begin{pmatrix} (2\mu + \lambda) \frac{\partial u_1}{\partial x_1} + \lambda \frac{\partial u_2}{\partial x_2} & \mu \left[\frac{\partial u_2}{\partial x_1} + \frac{\partial u_1}{\partial x_2} \right] \\ \mu \left[\frac{\partial u_2}{\partial x_1} + \frac{\partial u_1}{\partial x_2} \right] & (2\mu + \lambda) \frac{\partial u_1}{\partial x_1} + \lambda \frac{\partial u_2}{\partial x_2} \end{pmatrix} \begin{pmatrix} n_1 \\ n_2 \end{pmatrix}. \quad (2.1.4)$$

At infinity the vector function $\mathbf{u}(\mathbf{x})$ is characterised by

$$\mathbf{u} \sim \sum_{i=1}^3 C_i \mathbf{V}^{(i)}(\mathbf{x}), \quad (2.1.5)$$

where C_i , $i = 1, 2, 3$ are constants, and

$$\mathbf{V}^{(1)} = \begin{pmatrix} x_1 \\ 0 \end{pmatrix}, \mathbf{V}^{(2)} = \begin{pmatrix} 0 \\ x_2 \end{pmatrix}, \mathbf{V}^{(3)} = \frac{1}{\sqrt{2}} \begin{pmatrix} x_2 \\ x_1 \end{pmatrix}. \quad (2.1.6)$$

2.1. DEFINITION OF PÓLYA-SZEGÖ MATRIX FOR THE NAVIER EQUATIONS

As in (1.2.17) the field $\mathbf{u}(\mathbf{x})$ is taken in the form

$$\mathbf{u}(\mathbf{x}) = \sum_{i=1}^3 C_i (\mathbf{V}^{(i)}(\mathbf{x}) + \mathbf{W}^{(i)}(\mathbf{x})), \quad (2.1.7)$$

where the vector functions $\mathbf{W}^{(i)}$, $i = 1, 2, 3$, compensate a discrepancy left by $\mathbf{V}^{(i)}$, $i = 1, 2, 3$, in the first interface boundary condition (2.1.3); and they also satisfy the homogeneous Navier equations and the second interface condition (2.1.3). At infinity the vector fields $\mathbf{W}^{(i)}$ are characterised by the asymptotic formulae

$$\mathbf{W}^{(i)} = \sum_{k=1}^3 \mathcal{P}_{ik} \mathbf{V}^{(k)} \left(\frac{\partial}{\partial \mathbf{x}} \right) \cdot \mathbf{T}(\mathbf{x}) + O(\|\mathbf{x}\|^{-2}), \quad i = 1, 2, 3, \quad (2.1.8)$$

where $\mathbf{T}(\mathbf{x})$ represents the Green's tensor for the 2D Navier system

$$\mathbf{T}(\mathbf{x}) = q \begin{pmatrix} -2\kappa \ln R + \frac{2x_1^2}{R^2} & \frac{2x_1 x_2}{R^2} \\ \frac{2x_1 x_2}{R^2} & -2\kappa \ln R + \frac{2x_2^2}{R^2} \end{pmatrix},$$

$$q = \frac{\lambda + \mu}{8\pi\mu(\lambda + 2\mu)}, \quad R = \sqrt{x_1^2 + x_2^2}$$

The matrix $\{\mathcal{P}_{ij}\}_{i,j=1}^3$ is called *the Pólya-Szegö matrix in elasticity*. It is important to mention that the components of this matrix specify 4th rank Pólya-Szegö (“polarisation”) tensor $\{\mathcal{P}_{klmn}\}_{k,l,m,n=1}^2$. Further in the text one will use the Pólya-Szegö matrices in order to evaluate the effective moduli of periodic composites.

Note that if G is a cavity with a contour ∂G , the displacement \mathbf{u} satisfies (2.1.1) and ∂G is free of tractions

$$\sigma^{(n)}(\mathbf{u}; \mathbf{x}) = 0, \quad \mathbf{x} \in \partial G. \quad (2.1.9)$$

If G is a rigid inclusion, which does not resist translations and rotations, the displacement vector \mathbf{u} satisfies (2.1.1), and instead of (2.1.3) one has

$$\mathbf{u}(\mathbf{x}) = \mathbf{a} + \mathbf{b} \times \mathbf{x}, \quad \mathbf{x} \in \partial G, \quad (2.1.10)$$

where the constant vectors \mathbf{a} and \mathbf{b} are such that the field \mathbf{u} admits the representation (2.1.7), where the vector function $\mathbf{W}^{(i)}$ are characterised by the asymptotic formula (2.1.8) at infinity (the terms corresponding to point forces and moments are absent).

2.2 Explicit formulae for Pólya-Szegö matrices

Here we evaluate the Pólya-Szegö matrices for arbitrary simply connected 2D regions occupied by rigid inclusions or cavities. The Kolosov-Muskhelishvili representations for displacements and stresses in terms of complex potentials are employed.

2.2.1 Plane strain: cavities

Consider an infinite elastic plane containing a finite cavity G . The displacement field $\mathbf{u}(\mathbf{x})$ satisfies the homogeneous Navier system (2.1.1) and the traction boundary condition (2.1.9). The field $\mathbf{u}(\mathbf{x})$ admits the representation (2.1.7) which takes into account the conditions at infinity (2.1.5). We introduce the Kolosov-Muskhelishvili complex potentials φ , ψ such that

$$u_1 + iu_2 = (2\mu)^{-1} \{ \kappa\varphi(z) - z\bar{\varphi}'(z) - \bar{\psi}(z) \},$$

where $z = x_1 + ix_2$, μ is the shear modulus and $\kappa = 3 - 4\nu$ with ν being the Poisson ratio.

Introduce the conformal mapping function

$$z = \omega(\xi), \quad z = x_1 + ix_2,$$

which relates the exterior of the unit circle $|\xi| = 1$ and $\mathbb{R}^2 \setminus \bar{G}$. It admits the series representation

$$\omega(\xi) = c_1\xi + \sum_{n=1}^N \frac{c_{-n}}{\xi^n}, \quad (2.2.1)$$

with c_1, c_{-n} being constants.

Then the boundary condition (2.1.9) can be written in the form

$$\varphi(\xi) + \frac{\omega(\xi)}{\omega'(\xi)} \overline{\varphi'(\xi)} + \overline{\psi(\xi)} = 0, \quad |\xi| = 1, \quad (2.2.2)$$

The complex potentials φ and ψ are assumed to satisfy the following conditions

$$\varphi(\xi) \sim \alpha\xi, \quad \psi(\xi) \sim \gamma\xi \quad \text{as } |\xi| \rightarrow \infty, \quad (2.2.3)$$

with given complex coefficients α, γ .

We seek two functions φ and ψ , which are analytic in the exterior of the unit circle and satisfy the equation (2.2.2) and the conditions (2.2.3) at infinity. Using the Kolosov-Muskhelishvili method (see, for example, [83]) one can reduce the problem to a system of integral equations

$$\begin{aligned} \oint_L \frac{\varphi(\sigma)}{\sigma - \xi} d\sigma + \oint_L \frac{\omega(\sigma)\overline{\varphi'(\sigma)}}{\omega'(\sigma)(\sigma - \xi)} d\sigma + \oint_L \frac{\overline{\psi(\sigma)}}{\sigma - \xi} d\sigma &= 0, \\ \oint_L \frac{\overline{\varphi(\sigma)}}{\sigma - \xi} d\sigma + \oint_L \frac{\overline{\omega(\sigma)\varphi'(\sigma)}}{\omega'(\sigma)(\sigma - \xi)} d\sigma + \oint_L \frac{\psi(\sigma)}{\sigma - \xi} d\sigma &= 0, \end{aligned} \quad (2.2.4)$$

where $L = \{\xi \in \mathbb{C} : |\xi| = 1\}$. The complex potentials are sought in the form

$$\begin{aligned} \varphi(\xi) &= \alpha\xi + \frac{\beta}{\xi} + \sum_{k=2}^{\infty} \frac{\beta^{(k)}}{\xi^k}, \\ \psi(\xi) &= \gamma\xi + \frac{\delta}{\xi} + \sum_{k=2}^{\infty} \frac{\delta^{(k)}}{\xi^k}. \end{aligned} \quad (2.2.5)$$

Let S^+ and S^- be the interior and exterior of the unit circle L . Using the Cauchy theorem, one can evaluate the integrals in (2.2.4). Since $\varphi(\xi)$ is holomorphic in S^- except infinity where it has the first order pole with the principal part $\alpha\xi$, the following relation holds

$$\frac{1}{2\pi i} \oint_L \frac{\varphi(\sigma)}{\sigma - \xi} d\sigma = -\varphi(\xi) + \alpha\xi, \quad \xi \in S^-.$$

The function $\overline{\varphi}(1/\xi)$ is holomorphic in S^+ except the origin. It has a pole at $\xi = 0$ with the principal part $\overline{\alpha}/\xi$. Thus,

$$\frac{1}{2\pi i} \oint_L \frac{\overline{\varphi(\sigma)}}{\sigma - \xi} d\sigma = \frac{1}{2\pi i} \oint_L \frac{\overline{\varphi}(1/\sigma)}{\sigma - \xi} d\sigma = -\frac{\overline{\alpha}}{\xi}, \quad \xi \in S^-.$$

Similarly, one can write

$$\frac{1}{2\pi i} \oint_L \frac{\psi(\sigma)}{\sigma - \xi} d\sigma = -\psi(\xi) + \gamma\xi, \quad \xi \in S^-,$$

$$\frac{1}{2\pi i} \oint_L \frac{\overline{\psi(\sigma)}}{\sigma - \xi} d\sigma = \frac{1}{2\pi i} \oint_L \frac{\overline{\psi}(1/\sigma)}{\sigma - \xi} d\sigma = -\frac{\overline{\gamma}}{\xi}, \quad \xi \in S^-.$$

The function $\omega(\xi)\overline{\varphi}'(1/\xi)(\overline{\omega}'(1/\xi))^{-1}$ has a multiple pole of order N at the origin and,

therefore, the Cauchy integral can be evaluated as follows

$$\frac{1}{2\pi i} \oint_L \frac{\omega(\sigma)\overline{\varphi'(\sigma)}}{\omega'(\sigma)(\sigma - \xi)} d\sigma = - \sum_{m=1}^N \frac{a_m}{\xi^m}, \quad \xi \in S^-,$$

where

$$a_m = \bar{\alpha}\rho_{N-m} - \rho_{N-m-2}\bar{\beta} - \sum_{n=2}^{N-m-1} \rho_{N-m-n-1}n\bar{\beta}^{(n)},$$

$$\rho_k = \frac{1}{k!} \frac{d^k}{d\xi^k} \left[\frac{c_1\xi^{N+1} + \sum_{n=1}^N c_{-n}\xi^{N-n}}{\bar{c}_1 - \sum_{n=1}^N n\bar{c}_{-n}\xi^{n+1}} \right] \Big|_{\xi=0}, \quad k \geq 0. \quad (2.2.6)$$

In (2.2.6) the coefficients ρ_k with negative indices are equal to zero.

$$\frac{1}{2\pi i} \oint_L \frac{\overline{\omega(\sigma)}\varphi'(\sigma)}{\omega'(\sigma)(\sigma - \xi)} d\sigma = -\frac{\bar{\omega}(1/\xi)\varphi'(\xi)}{\omega'(\xi)} + \sum_{m=0}^N \bar{a}_m\xi^m, \quad \xi \in S^-.$$

The Cauchy theorem enables one to obtain a system of linear algebraic equations with respect to the coefficients in (2.2.5). In particular, the quantities β and δ can be represented as functions of α , γ and the coefficients in the expansion (2.2.6) of the mapping function. One considers three sets of complex potentials which correspond to the following choice of α and γ

$$\begin{aligned} \gamma_1 &= -\mu c_1, & \gamma_2 &= \mu c_1, & \gamma_3 &= \sqrt{2}\mu c_1 i, \\ \alpha_1 &= \frac{\mu c_1}{\varkappa - 1}, & \alpha_2 &= \frac{\mu c_1}{\varkappa - 1}, & \alpha_3 &= 0. \end{aligned} \quad (2.2.7)$$

The potentials have the following expansion at infinity

$$\begin{aligned} \varphi_j(z) &= \frac{\alpha_j z}{c_1} + \frac{B_j}{z} + O\left(\frac{1}{|z|^2}\right), \quad |z| \rightarrow \infty, \\ \psi_j(z) &= \frac{\gamma_j z}{c_1} + \frac{D_j}{z} + O\left(\frac{1}{|z|^2}\right), \quad |z| \rightarrow \infty, \end{aligned} \quad (2.2.8)$$

where

$$\begin{aligned} B_j &= \beta_j c_1 - \alpha_j c_{-1} = -\bar{\gamma}_j c_1 - b_j c_1 - \alpha_j c_{-1}, \\ D_j &= \delta_j c_1 - \gamma_j c_{-1} = -\bar{\alpha}_j c_1 - \bar{d}_j c_1 - \gamma_j c_{-1}, \end{aligned}$$

Here j is the index associated with the model problem, whose solution approaches to $\mathbf{V}^{(j)}$ at infinity. In other words, φ and ψ are the potentials associated with the field $\mathbf{V}^{(j)} + \mathbf{W}^{(j)}$ (see (2.1.8)). Substitution of the expressions (2.2.7) in formulae for B_j and

D_j leads to the following identities

$$\begin{aligned} B_1 &= \mu|c_1|^2 - \frac{\mu c_1 c_{-1}}{\varkappa - 1} - b_1 c_1, & D_1 &= \mu c_1 c_{-1} - \frac{\mu|c_1|^2}{\varkappa - 1} - \bar{d}_1 c_1, \\ B_2 &= -\mu|c_1|^2 - \frac{\mu c_1 c_{-1}}{\varkappa - 1} - b_2 c_1, & D_2 &= -\mu c_1 c_{-1} - \frac{\mu|c_1|^2}{\varkappa - 1} - \bar{d}_2 c_1, \\ B_3 &= \sqrt{2}\mu|c_1|^2 i - b_3 c_1, & D_3 &= -\sqrt{2}\mu c_1 c_{-1} i - \bar{d}_3 c_1. \end{aligned}$$

Coefficients b_j and d_j are given by

$$\begin{aligned} b_j &= \bar{\alpha}_j \rho_{N-1} + \rho_{N-3}(\bar{a}_{1,j} + \gamma_j) + \sum_{k=2}^{N-2} k \rho_{N-k-2} \bar{a}_{k,j}, & j &= 1, 2, 3, \\ d_j &= \bar{\alpha}_j \rho_{N+1} + \rho_{N-1}(\bar{a}_{1,j} + \gamma_j) + \sum_{k=2}^N k \rho_{N-k} \bar{a}_{k,j}, & j &= 1, 2, 3, \end{aligned} \quad (2.2.9)$$

where coefficients $a_{k,j}$, $j = 1, 2, 3$, $k = 1, 2, \dots, N$, solve the algebraic system

$$a_{m,j} - \rho_{N-m-2}(\bar{a}_{1,j} + \gamma_j) - \sum_{k=2}^{N-m-1} k \rho_{N-k-m-1} \bar{a}_{k,j} = \bar{\alpha}_j \rho_{N-m},$$

with ρ_k being the same as in (2.2.6). We note that coefficients b_j and d_j are related to $a_{m,j}$, by the identities $b_j = a_{1,j}$ and $d_j = a_{-1,j}$.

In terms of complex potentials the displacement field $\mathbf{W}^{(i)}$ is given in the form

$$\begin{aligned} \mathbf{W}^{(i)}(z) &= \frac{1}{2\mu} [\varkappa \varphi(z) - z \overline{\varphi'(z)} - \overline{\psi(z)}] \\ &= \frac{1}{2\mu} [\varkappa B_i \frac{1}{z} + \bar{B}_i \frac{z}{z^2} - \bar{D}_i \frac{1}{z}] + O\left(\frac{1}{|z|^2}\right), \quad |z| \rightarrow \infty. \end{aligned} \quad (2.2.10)$$

The asymptotic formula (2.1.8) can be rewritten as follows

$$\begin{aligned} \mathbf{W}^{(i)}(z) &= \mathcal{P}_{i1} \left(\frac{\partial}{\partial z} [T_{11} + iT_{12}] + \frac{\partial}{\partial \bar{z}} [T_{11} + iT_{12}] \right) \\ &\quad + \mathcal{P}_{i2} \left(\frac{\partial}{\partial z} [-T_{22} + iT_{12}] + \frac{\partial}{\partial \bar{z}} [T_{22} - iT_{12}] \right) \\ &\quad + \frac{1}{\sqrt{2}} \mathcal{P}_{i3} \left(i \frac{\partial}{\partial z} [T_{11} + T_{22}] + \frac{\partial}{\partial \bar{z}} [2T_{12} + i(T_{22} - T_{11})] \right) + O\left(\frac{1}{|z|^2}\right). \end{aligned} \quad (2.2.11)$$

Here

$$\mathbf{T} = q \begin{pmatrix} -2\varkappa \ln |z| + \frac{z^2 + \bar{z}^2 + 2z\bar{z}}{2z\bar{z}} & \frac{z^2 - \bar{z}^2}{2iz\bar{z}} \\ \frac{z^2 - \bar{z}^2}{2iz\bar{z}} & -2\varkappa \ln |z| - \frac{z^2 + \bar{z}^2 - 2z\bar{z}}{2z\bar{z}} \end{pmatrix} \quad (2.2.12)$$

is the 2D Green's tensor, and q is given by (2.1.8).

Then it follows from the definition of the Pólya-Szegö matrix (see (2.1.8)) that

$$\mathcal{P} = \frac{1}{4\mu q} \begin{pmatrix} -\operatorname{Re}B_1 + \frac{1}{\varkappa-1}\operatorname{Re}D_1 & \operatorname{Re}B_1 + \frac{1}{\varkappa-1}\operatorname{Re}D_1 & -\sqrt{2}\operatorname{Im}B_1 \\ \operatorname{Re}B_1 + \frac{1}{\varkappa-1}\operatorname{Re}D_1 & \operatorname{Re}B_2 + \frac{1}{\varkappa-1}\operatorname{Re}D_2 & -\sqrt{2}\operatorname{Im}B_2 \\ -\sqrt{2}\operatorname{Im}B_1 & -\sqrt{2}\operatorname{Im}B_2 & -\sqrt{2}\operatorname{Im}B_3 \end{pmatrix}, \quad (2.2.13)$$

or, equivalently,

$$\mathcal{P} = \frac{1}{4q} \begin{pmatrix} -\Omega + \frac{\Sigma}{\varkappa-1} - \frac{\Xi}{(\varkappa-1)^2} & \Omega - \frac{\Xi}{(\varkappa-1)^2} & -\Theta + \frac{\Lambda}{\varkappa-1} \\ \Omega - \frac{\Xi}{(\varkappa-1)^2} & -\Omega - \frac{\Sigma}{\varkappa-1} - \frac{\Xi}{(\varkappa-1)^2} & \Theta + \frac{\Lambda}{\varkappa-1} \\ -\Theta + \frac{\Lambda}{\varkappa-1} & \Theta + \frac{\Lambda}{\varkappa-1} & \Upsilon \end{pmatrix}, \quad (2.2.14)$$

where

$$\begin{aligned} \Omega &= |c_1|^2 + \operatorname{Re}(a_1^\gamma c_1), & \Sigma &= 2\operatorname{Re}(c_1 c_{-1}) + \operatorname{Re}(a_1^\alpha c_1) + \operatorname{Re}(\bar{a}_{-1}^\gamma c_1), \\ \Xi &= |c_1|^2 + \operatorname{Re}(\bar{a}_{-1}^\alpha c_1), & \Upsilon &= -2|c_1|^2 + 2\operatorname{Im}(a_1^\tau c_1), \\ \Theta &= \sqrt{2}\operatorname{Im}(a_1^\gamma c_1), & \Lambda &= \sqrt{2}\operatorname{Im}(c_1 c_{-1}) + \sqrt{2}\operatorname{Im}(a_1^\alpha c_1), \end{aligned} \quad (2.2.15)$$

and a^γ , a^α and a^τ are the solutions of the following system of linear algebraic equations:

$$\begin{aligned} a_m^\alpha - \rho_{N-m-2}\bar{a}_1^\alpha - \sum_{k=2}^{N-m-1} \rho_{N-m-k-1}k\bar{a}_k^\alpha &= \rho_{N-m}\bar{c}_1, \\ a_m^\gamma - \rho_{N-m-2}\bar{a}_1^\gamma - \sum_{k=2}^{N-m-1} \rho_{N-m-k-1}k\bar{a}_k^\gamma &= \rho_{N-m-2}c_1, \\ a_m^\tau - \rho_{N-m-2}\bar{a}_1^\tau - \sum_{k=2}^{N-m-1} \rho_{N-m-k-1}k\bar{a}_k^\tau &= \rho_{N-m-2}ic_1, \end{aligned} \quad (2.2.16)$$

where $m = -1, 1, \dots, N$.

The last result can be formulated as a theorem:

Theorem 2.1 *The Pólya-Szegö matrix characterising a finite size cavity admits the representation (2.2.14), where the coefficients $\Omega, \Sigma, \Theta, \Xi, \Upsilon, \Lambda$ depend on the conformal mapping coefficients $c_n, n = 1, -1, -2, \dots$ only and are given by (2.2.15).*

Note that the coefficients a_1^α and a_{-1}^γ possess the property $\operatorname{Re}(a_1^\alpha c_1) = \operatorname{Re}(\bar{a}_{-1}^\gamma c_1)$ which follows from the symmetry of the Pólya-Szegö matrix and leads to further simplification of formulae (2.2.15).

The quantities b_1, b_2, b_3, d_1, d_2 and d_3 in (2.2.9) and a_m^α, a_m^γ and a_m^τ in (2.2.16) are related by

$$\begin{aligned} b_1 &= \frac{\mu a_1^\alpha}{\varkappa - 1} - \mu a_1^\gamma, & b_2 &= \frac{\mu a_1^\alpha}{\varkappa - 1} + \mu a_1^\gamma, & b_3 &= \sqrt{2} \mu a_1^\tau, \\ d_1 &= \frac{\mu a_{-1}^\alpha}{\varkappa - 1} - \mu a_{-1}^\gamma, & d_2 &= \frac{\mu a_{-1}^\alpha}{\varkappa - 1} + \mu a_{-1}^\gamma, & d_3 &= \sqrt{2} \mu a_{-1}^\tau. \end{aligned}$$

Examples:

The following formulae represent the Pólya-Szegö matrices for regions which are close to polygons.

1. If the conformal mapping $\omega(\xi)$ has only three non-zero coefficients c_1, c_{-1}, c_{-2} , then

$$\begin{aligned} \rho_0 &= \frac{c_{-2}}{\bar{c}_1}, & \rho_1 &= \frac{c_{-1}}{\bar{c}_1}, & \rho_2 &= \frac{c_{-2}\bar{c}_{-1}}{\bar{c}_1^2}, & \rho_3 &= \frac{|c_1|^2 + |c_{-1}|^2 + 2|c_{-2}|^2}{\bar{c}_1^2}, \\ a_1^\alpha &= c_{-1}, & a_1^\gamma &= 0, & a_1^\tau &= 0, \\ a_{-1}^\alpha &= \frac{|c_1|^2 + 2|c_{-1}|^2 + 4|c_{-2}|^2}{\bar{c}_1}, & a_{-1}^\gamma &= \frac{c_{-1}c_1}{\bar{c}_1}, & a_{-1}^\tau &= \frac{c_{-1}c_1}{\bar{c}_1}i. \end{aligned}$$

Substituting the expressions above into (2.2.15) we obtain

$$\mathcal{P} = \frac{1}{4q} \begin{pmatrix} \frac{\Sigma}{\varkappa-1} - |c_1|^2 - \frac{\Xi}{(\varkappa-1)^2} & |c_1|^2 - \frac{\Xi}{(\varkappa-1)^2} & \frac{\Lambda}{\varkappa-1} \\ |c_1|^2 - \frac{\Xi}{(\varkappa-1)^2} & -\frac{\Sigma}{\varkappa-1} - |c_1|^2 - \frac{\Xi}{(\varkappa-1)^2} & \frac{\Lambda}{\varkappa-1} \\ \frac{\Lambda}{\varkappa-1} & \frac{\Lambda}{\varkappa-1} & -2|c_1|^2 \end{pmatrix}, \quad (2.2.17)$$

$$\Xi = 2(|c_1|^2 + |c_{-1}|^2 + 2|c_{-2}|^2), \quad \Sigma = 4\operatorname{Re}(c_{-1}c_1), \quad \Lambda = 2\sqrt{2}\operatorname{Im}(c_1c_{-1}).$$

2. For the case of the conformal mapping with non-zero coefficients $c_1, c_{-1}, c_{-2}, c_{-3}$ we have the following representations for the quantities $\rho_k, a_m^\alpha, a_m^\gamma, a_m^\tau$

$$\begin{aligned} \rho_0 &= \frac{c_{-3}}{\bar{c}_1}, & \rho_1 &= \frac{c_{-2}}{\bar{c}_1}, & \rho_2 &= \frac{c_{-1}}{\bar{c}_1} + \frac{c_{-3}\bar{c}_{-1}}{\bar{c}_1^2}, \\ \rho_3 &= \frac{c_{-2}\bar{c}_{-1}}{\bar{c}_1^2} + 2\frac{c_{-3}\bar{c}_{-2}}{\bar{c}_1^2}, & \rho_4 &= \frac{|c_1|^2 + |c_{-1}|^2 + 2|c_{-2}|^2 + 3|c_{-3}|^2}{\bar{c}_1^2} + \frac{c_{-3}\bar{c}_{-1}^2}{\bar{c}_1^3}, \\ a_1^\alpha &= \frac{c_{-1}(|c_1|^2 + |c_{-3}|^2) + 2c_1c_{-3}\bar{c}_{-1}}{|c_1|^2 - |c_{-3}|^2}, & a_1^\gamma &= \frac{c_{-3}c_1^2 + \bar{c}_1|c_{-3}|^2}{|c_1|^2 - |c_{-3}|^2}, & a_1^\tau &= \frac{c_{-3}c_1^2 - \bar{c}_1|c_{-3}|^2}{|c_1|^2 - |c_{-3}|^2}i, \\ a_{-1}^\alpha &= \frac{|c_1|^2 + 4|c_{-2}|^2 + 6|c_{-3}|^2}{\bar{c}_1} + \frac{2|c_{-1}|^2(|c_1|^2 + |c_{-3}|^2) + 4\operatorname{Re}(c_1c_{-3}\bar{c}_{-1}^2)}{\bar{c}_1(|c_1|^2 - |c_{-3}|^2)}, \end{aligned}$$

$$a_{-1}^{\gamma} = \frac{c_1 c_{-1} |c_1|^2 + \overline{c_1 c_{-1}} |c_{-3}|^2 + 2\operatorname{Re}(c_1^2 c_{-3} \overline{c_{-1}})}{\overline{c_1} (|c_1|^2 - |c_{-3}|^2)},$$

$$a_{-1}^{\theta} = \frac{c_1 c_{-1} |c_1|^2 - \overline{c_1 c_{-1}} |c_{-3}|^2 + 2i\operatorname{Im}(c_1^2 c_{-3} \overline{c_{-1}})}{\overline{c_1} (|c_1|^2 - |c_{-3}|^2)} i.$$

The matrix \mathcal{P} is given by (2.2.14), where the coefficients $\Omega, \Xi, \Theta, \Sigma, \Lambda, \Upsilon$ are of the form

$$\Omega = \frac{\operatorname{Re}(c_{-3} c_1^3) + |c_1|^4}{|c_1|^2 - |c_{-3}|^2}, \quad \Sigma = 4 \left[\frac{\operatorname{Re}(c_1 c_{-1})}{|c_1|^2 - |c_{-3}|^2} |c_1|^2 + \frac{\operatorname{Re}(c_1^2 c_{-3} \overline{c_{-1}})}{|c_1|^2 - |c_{-3}|^2} \right],$$

$$\Xi = 2|c_1|^2 + 4|c_{-2}|^2 + 6|c_{-3}|^2 + 2|c_{-1}|^2 \frac{|c_1|^2 + |c_{-3}|^2}{|c_1|^2 - |c_{-3}|^2} + \frac{4\operatorname{Re}(\overline{c_1} c_{-1}^2 \overline{c_{-3}})}{|c_1|^2 - |c_{-3}|^2},$$

$$\Theta = \sqrt{2} \frac{\operatorname{Im}(c_1^3 c_{-3})}{|c_1|^2 - |c_{-3}|^2}, \quad \Lambda = 2\sqrt{2} \left[\frac{\operatorname{Im}(c_1 c_{-1})}{|c_1|^2 - |c_{-3}|^2} |c_1|^2 + \frac{\operatorname{Im}(c_1^2 c_{-3} \overline{c_{-1}})}{|c_1|^2 - |c_{-3}|^2} \right],$$

$$\Upsilon = 2 \frac{\operatorname{Re}(c_{-3} c_1^3) - |c_1|^4}{|c_1|^2 - |c_{-3}|^2}. \quad (2.2.18)$$

The formulae (2.2.17) and (2.2.18) will be used further in Section 2.3.

2.2.2 Plane strain: rigid inclusions

Consider a finite rigid inclusion which is not fixed in the matrix. If the matrix is under external loading the translation or rotation of such an inclusion occur. The inclusion can be considered as absolutely rigid kernel: there is no any deformation for internal points. The displacement field \mathbf{u} in the matrix satisfies the system (2.1.1), the boundary condition (2.1.10) and admits the representation (2.1.7) at infinity. In terms of complex potentials the boundary condition (2.1.10) can be written as

$$\varkappa \varphi(\xi) - \frac{\omega(\xi)}{\omega'(\xi)} \overline{\varphi'(\xi)} - \overline{\psi(\xi)} = 2\mu\theta i \omega(\xi), \quad |\xi| = 1, \quad (2.2.19)$$

where $\omega(\xi)$ is the same mapping function as in (2.2.1), θ is the angle of rigid rotation.

In general, the complex potentials have the form (see [83])

$$\varphi_j(z) = \frac{\alpha_j z}{c_1} - \frac{X + iY}{2\pi(\varkappa + 1)} \ln z + \frac{B_j}{z} + O\left(\frac{1}{|z|^2}\right), \quad |z| \rightarrow \infty,$$

$$\psi_j(z) = \frac{\gamma_j z}{c_1} + \frac{\varkappa(X - iY)}{2\pi(\varkappa + 1)} \ln z + \frac{D_j}{z} + O\left(\frac{1}{|z|^2}\right), \quad |z| \rightarrow \infty, \quad (2.2.20)$$

where $\alpha_j, \gamma_j, B_j, D_j, X$ and Y are constants.

One follows the Muskhelishvili method and derives the following system of integral

equations

$$\varkappa \oint_L \frac{\varphi(\sigma)}{\sigma - \xi} d\sigma - \oint_L \frac{\omega(\sigma) \overline{\varphi'(\sigma)}}{\omega'(\sigma)(\sigma - \xi)} d\sigma - \oint_L \frac{\overline{\psi(\sigma)}}{\sigma - \xi} d\sigma = 2\mu\theta i \oint_L \frac{\omega(\sigma)}{\sigma - \xi} d\sigma,$$

$$\varkappa \oint_L \frac{\overline{\varphi(\sigma)}}{\sigma - \xi} d\sigma - \oint_L \frac{\overline{\omega(\sigma)} \varphi'(\sigma)}{\omega'(\sigma)(\sigma - \xi)} d\sigma - \oint_L \frac{\psi(\sigma)}{\sigma - \xi} d\sigma = -2\mu\theta i \oint_L \frac{\overline{\omega(\sigma)}}{\sigma - \xi} d\sigma.$$

Since the load is self-balanced the logarithmic terms in (2.2.20) are absent, and therefore the solution has the form:

$$\varphi_j(z) = \frac{\alpha_j z}{c_1} + \frac{B_j}{z} + \sum_{k=2}^{\infty} \frac{B_j^{(k)}}{z^k}, \quad (2.2.21)$$

$$\psi_j(z) = \frac{\gamma_j z}{c_1} + \frac{D_j}{z} + \sum_{k=2}^{\infty} \frac{D_j^{(k)}}{z^k}. \quad (2.2.22)$$

Here φ_j and ψ_j are the potentials associated with the function $\mathbf{V}^{(j)} + \mathbf{W}^{(j)}$ of (2.1.6) and (2.1.8). As before, the integrals are evaluated using the Cauchy theorem. As a result, we have

$$\begin{aligned} B_j &= \beta c_1 - \alpha_j c_{-1} = \frac{1}{\varkappa} \left(\overline{\gamma}_j c_1 + b_j c_1 + 2\mu\theta_j c_1 c_{-1} i \right) - \alpha_j c_{-1}, \\ D_j &= \delta c_1 - \gamma_j c_{-1} = \varkappa \overline{\alpha}_j c_1 - \overline{d}_j c_1 + 2\mu\theta_j |c_1|^2 i - \gamma_j c_{-1}. \end{aligned} \quad (2.2.23)$$

Introduce the quantities a_m^α , a_m^γ , a_m^τ , a_m^θ such that

$$\begin{aligned} b_1 &= \frac{\mu a_1^\alpha}{k-1} - \mu a_1^\gamma + 2\mu\theta_1 a_1^\theta, & d_1 &= \frac{\mu a_{-1}^\alpha}{k-1} - \mu a_{-1}^\gamma + 2\mu\theta_1 a_{-1}^\theta, \\ b_2 &= \frac{\mu a_1^\alpha}{k-1} + \mu a_1^\gamma + 2\mu\theta_2 a_1^\theta, & d_2 &= \frac{\mu a_{-1}^\alpha}{k-1} + \mu a_{-1}^\gamma + 2\mu\theta_2 a_{-1}^\theta, \\ b_3 &= \sqrt{2}\mu a_1^\tau + 2\mu\theta_3 a_1^\theta, & d_3 &= \sqrt{2}\mu a_{-1}^\tau + 2\mu\theta_3 a_{-1}^\theta. \end{aligned} \quad (2.2.24)$$

Then one can rewrite formulae (2.2.23) as

$$\begin{aligned} B_1 &= \frac{1}{\varkappa} \left(-\mu |c_1|^2 - \mu a_1^\gamma c_1 + 2\mu\theta_1 a_1^\theta c_1 + 2\mu\theta_1 c_1 c_{-1} i \right) - \frac{\mu c_1 c_{-1}}{\varkappa - 1} + \frac{\mu a_1^\alpha c_1}{\varkappa(\varkappa - 1)}, \\ D_1 &= \frac{\varkappa \mu |c_1|^2}{\varkappa - 1} - \frac{\mu \overline{a}_{-1}^\alpha c_1}{\varkappa - 1} + \mu \overline{a}_{-1}^\gamma c_1 - 2\mu\theta_1 \overline{a}_{-1}^\theta c_1 + 2\mu\theta_1 |c_1|^2 i + \mu c_1 c_{-1}, \\ B_2 &= \frac{1}{\varkappa} \left(\mu |c_1|^2 + \mu a_1^\gamma c_1 + 2\mu\theta_2 a_1^\theta c_1 + 2\mu\theta_2 c_1 c_{-1} i \right) - \frac{\mu c_1 c_{-1}}{\varkappa - 1} + \frac{\mu a_1^\alpha c_1}{\varkappa(\varkappa - 1)}, \end{aligned}$$

$$\begin{aligned}
 D_2 &= \frac{\varkappa\mu|c_1|^2}{\varkappa-1} - \frac{\mu\bar{a}_{-1}^\alpha c_1}{\varkappa-1} - \mu\bar{a}_{-1}^\gamma c_1 - 2\mu\theta_2\bar{a}_{-1}^\theta c_1 + 2\mu\theta_2|c_1|^2 i - \mu c_1 c_{-1}, \\
 B_3 &= \frac{1}{\varkappa} \left(-\sqrt{2}\mu|c_1|^2 i + \sqrt{2}\mu a_1^\tau c_1 + 2\mu\theta_3 a_1^\theta c_1 + 2\mu\theta_3 c_1 c_{-1} i \right), \\
 D_3 &= -\sqrt{2}\mu\bar{a}_{-1}^\tau c_1 - 2\mu\theta_3\bar{a}_{-1}^\theta c_1 + 2\mu\theta_3|c_1|^2 i - \sqrt{2}\mu c_1 c_{-1} i.
 \end{aligned}$$

The coefficients a_m^α , a_m^γ , a_m^τ and a_m^θ are the solution of the linear system of algebraic equations:

$$\begin{aligned}
 a_m^\alpha + \frac{1}{\varkappa}\rho_{N-m-2}\bar{a}_1^\alpha + \frac{1}{\varkappa}\sum_{k=2}^{N-m-1}\rho_{N-m-k-1}k\bar{a}_k^\alpha &= \rho_{N-m}\bar{c}_1, \\
 a_m^\gamma + \frac{1}{\varkappa}\rho_{N-m-2}\bar{a}_1^\gamma + \frac{1}{\varkappa}\sum_{k=2}^{N-m-1}\rho_{N-m-k-1}k\bar{a}_k^\gamma &= -\frac{1}{\varkappa}\rho_{N-m-2}c_1, \\
 a_m^\tau + \frac{1}{\varkappa}\rho_{N-m-2}\bar{a}_1^\tau + \frac{1}{\varkappa}\sum_{k=2}^{N-m-1}\rho_{N-m-k-1}k\bar{a}_k^\tau &= -\frac{1}{\varkappa}\rho_{N-m-2}i c_1, \\
 a_m^\theta + \frac{1}{\varkappa}\rho_{N-m-2}\bar{a}_1^\theta + \frac{1}{\varkappa}\sum_{k=2}^{N-m-1}\rho_{N-m-k-1}k\bar{a}_k^\theta &= \frac{i}{\varkappa}\sum_{k=1}^{N-m-1}k\bar{c}_{-k}\rho_{N-m-k-1},
 \end{aligned}$$

and, therefore, depend on the coefficients in the expansion of the conformal mapping function.

Using the definition of the principal moment (see Muskhelishvili [83], p.356)

$$M = \operatorname{Re}\left[\int_L \psi(z)dz\right] = \operatorname{Re}\left[\int_L \psi(\xi)\omega'(\xi)d\xi\right]$$

one can represent the balance condition for M in the form

$$\operatorname{Im}(D_j)\operatorname{arg}z = 0. \quad (2.2.25)$$

The condition (2.2.25) gives the value θ of the angle of the rigid rotation (see the right-hand side (2.2.19)). Thus,

$$\begin{aligned}
 \theta_1 &= \frac{(\varkappa-1)^{-1}\operatorname{Im}(\bar{a}_{-1}^\alpha c_1) - \operatorname{Im}(c_1 c_{-1}) - \operatorname{Im}(\bar{a}_{-1}^\gamma c_1)}{2(|c_1|^2 - \operatorname{Im}(\bar{a}_{-1}^\theta c_1))}, \\
 \theta_2 &= \frac{(\varkappa-1)^{-1}\operatorname{Im}(\bar{a}_{-1}^\alpha c_1) + \operatorname{Im}(c_1 c_{-1}) + \operatorname{Im}(\bar{a}_{-1}^\gamma c_1)}{2(|c_1|^2 - \operatorname{Im}(\bar{a}_{-1}^\theta c_1))}, \\
 \theta_3 &= \sqrt{2}\frac{\operatorname{Re}(c_1 c_{-1}) + \operatorname{Im}(\bar{a}_{-1}^\tau c_1)}{2(|c_1|^2 - \operatorname{Im}(\bar{a}_{-1}^\theta c_1))},
 \end{aligned}$$

where θ_j corresponds to the pair of complex potentials φ_j, ψ_j . Note that due to symmetry of the matrix \mathcal{P}

$$\operatorname{Im}(\bar{a}_{-1}^\alpha c_1) = 0 \quad \text{and} \quad \theta_1 = -\theta_2.$$

Therefore the Pólya-Szegő matrix can be represented in the form (2.2.14) where

$$\begin{aligned} \Omega &= -\frac{1}{\varkappa} \left(|c_1|^2 + \operatorname{Re}(a_1^\gamma c_1) + 2\theta_1 \left[\operatorname{Im}(c_{-1}c_1) - \operatorname{Re}(a_1^\theta c_1) \right] \right), \\ \Sigma &= 2\operatorname{Re}(c_1c_{-1}) + \operatorname{Re}(\bar{a}_{-1}^\gamma c_1) - 2\theta_1 \operatorname{Re}(\bar{a}_{-1}^\theta c_1) - \frac{1}{\varkappa} \operatorname{Re}(a_1^\alpha c_1), \\ \Xi &= -\varkappa |c_1|^2 + \operatorname{Re}(\bar{a}_{-1}^\alpha c_1), \\ \Upsilon &= \frac{2}{\varkappa} \left(|c_1|^2 - \operatorname{Im}(a_1^\tau c_1) - \sqrt{2}\theta_3 \left[\operatorname{Im}(a_1^\theta c_1) + \operatorname{Re}(c_1c_{-1}) \right] \right), \\ \Theta &= -\frac{\sqrt{2}}{\varkappa} \left(\operatorname{Im}(a_1^\gamma c_1) - 2\theta_1 \left[\operatorname{Im}(a_1^\theta c_1) + \operatorname{Re}(c_1c_{-1}) \right] \right), \\ \Lambda &= \sqrt{2} \left(\operatorname{Im}(c_1c_{-1}) - \frac{1}{\varkappa} \operatorname{Im}(a_1^\alpha c_1) \right). \end{aligned} \quad (2.2.26)$$

Examples.

1. In particular, when the mapping function has only three non-zero coefficients c_1, c_{-1}, c_{-2} we have

$$\begin{aligned} \rho_0 &= \frac{c_{-2}}{\bar{c}_1}, \quad \rho_1 = \frac{c_{-1}}{\bar{c}_1}, \quad \rho_2 = \frac{c_{-2}\bar{c}_{-1}}{\bar{c}_1^2}, \quad \rho_3 = \frac{|c_1|^2 + |c_{-1}|^2 + 2|c_{-2}|^2}{\bar{c}_1^2}, \\ a_1^\alpha &= c_{-1}, \quad a_1^\gamma = 0, \quad a_1^\tau = 0, \quad a_1^\theta = 0, \\ a_{-1}^\alpha &= \frac{|c_1|^2 + |c_{-1}|^2 + 2|c_{-2}|^2}{\bar{c}_1} - \frac{|c_{-1}|^2 + 2|c_{-2}|^2}{\varkappa \bar{c}_1}, \quad a_{-1}^\gamma = -\frac{c_{-1}c_1}{\varkappa \bar{c}_1}, \\ a_{-1}^\tau &= -\frac{c_{-1}c_1}{\varkappa \bar{c}_1} i, \quad a_{-1}^\theta = \frac{|c_{-1}|^2 + 2|c_{-2}|^2}{\varkappa \bar{c}_1} i. \end{aligned}$$

The formulae (2.2.26) are reduced to

$$\begin{aligned} \Omega &= -\frac{1}{\varkappa} \left(|c_1|^2 + 2\theta_1 \operatorname{Im}(c_{-1}c_1) \right), \quad \Sigma = \frac{2(\varkappa - 1)}{\varkappa} \operatorname{Re}(c_1c_{-1}), \\ \Xi &= |c_1|^2(1 - \varkappa) + (|c_{-1}|^2 + 2|c_{-2}|^2) \frac{\varkappa - 1}{\varkappa}, \quad \Theta = \frac{2\sqrt{2}}{\varkappa} \theta_3 \operatorname{Re}(c_1c_{-1}), \end{aligned}$$

$$\Upsilon = \frac{2}{\varkappa} \left(|c_1|^2 - \sqrt{2}\theta_3 \operatorname{Re}(c_{-1}c_1) \right), \quad \Lambda = \frac{\sqrt{2}(\varkappa - 1)}{\varkappa} \operatorname{Im}(c_1c_{-1}), \quad (2.2.27)$$

where the rotation angles are given by

$$\begin{aligned} \theta_1 &= -\frac{\varkappa + 1}{2\varkappa} \frac{\operatorname{Im}(c_1c_{-1})}{|c_1|^2 + \frac{1}{\varkappa}(|c_{-1}|^2 + 2|c_{-2}|^2)} = -\theta_2, \\ \theta_3 &= \frac{\varkappa + 1}{\sqrt{2}\varkappa} \frac{\operatorname{Re}(c_1c_{-1})}{|c_1|^2 + \frac{1}{\varkappa}(|c_{-1}|^2 + 2|c_{-2}|^2)}. \end{aligned} \quad (2.2.28)$$

2. For n -sided regular polygons the quantities θ_i are zero and the coefficients of the Pólya-Szegö matrix (2.2.14) are

$$\begin{aligned} \Omega &= -\frac{1}{\varkappa} (\operatorname{Re}(a_1^\gamma c_1) + |c_1|^2), \quad \Sigma = 2\operatorname{Re}(c_1c_{-1}) + \operatorname{Re}(\bar{a}_{-1}^\gamma c_1) - \frac{1}{\varkappa} \operatorname{Re}(a_1^\alpha c_1), \\ \Xi &= -\varkappa |c_1|^2 + \operatorname{Re}(\bar{a}_{-1}^\alpha c_1), \quad \Upsilon = \frac{2}{\varkappa} (|c_1|^2 - \operatorname{Im}(a_1^\gamma c_1)), \\ \Theta &= -\frac{\sqrt{2}}{\varkappa} \operatorname{Im}(a_1^\gamma c_1), \quad \Lambda = \sqrt{2} (\operatorname{Im}(c_1c_{-1}) - \frac{1}{\varkappa} \operatorname{Im}(a_1^\alpha c_1)). \end{aligned} \quad (2.2.29)$$

2.2.3 Anti-plane shear: cavities and rigid inclusions

In order to evaluate the matrix M (see (1.2.18)) we analyse the model problems (1.2.13),(1.2.20),(1.2.21) and introduce the complex valued function $\vartheta_j(z)$, $j = 1, 2$, $z = x_1 + ix_2$, such that

$$\operatorname{Re}\vartheta_j(z) = x_j + w^{(j)}.$$

Then, for a rigid inclusion the Dirichlet boundary condition (1.2.21) can be written in the form

$$\vartheta(\sigma) + \overline{\vartheta(\sigma)} = \text{const}, \quad |\sigma| = 1, \quad (2.2.30)$$

and for an arbitrary cavity the condition (1.2.20) is equivalent to (see, for example, Muskhelishvili [83], Barenblatt and Cherepanov [6])

$$\vartheta(\sigma) - \overline{\vartheta(\sigma)} = 0, \quad |\sigma| = 1, \quad (2.2.31)$$

where the conformal mapping function $z = \omega(\xi)$ is given by (2.2.1).

One follows the standard technique (see, for example, Milne-Thompson [67]) and derives

the following integral equation

$$\oint_L \frac{\vartheta(\sigma)}{\sigma - \xi} d\sigma - \oint_L \frac{\overline{\vartheta(\sigma)}}{\sigma - \xi} d\sigma = 0 \quad (2.2.32)$$

for the Neumann problem (1.2.13),(1.2.20), and the equation

$$\oint_L \frac{\vartheta(\sigma)}{\sigma - \xi} d\sigma + \oint_L \frac{\overline{\vartheta(\sigma)}}{\sigma - \xi} d\sigma = 0 \quad (2.2.33)$$

for the Dirichlet boundary value problem (1.2.13),(1.2.21).

The functions $\vartheta_j(z)$ are given by the following expansions

$$\vartheta_j(z) = A_j z + \frac{B_j}{z} + \sum_{k=2}^{\infty} \frac{B_j^{(k)}}{z^k}. \quad (2.2.34)$$

In the ξ coordinates corresponding to the exterior of the unit disk ϑ_1 and ϑ_2 admit the asymptotic expansion of the form

$$\vartheta_j(\xi) = A_j c_1 \xi + \left(A_j c_{-1} + \frac{B_j}{c_1} \right) \frac{1}{\xi} + O\left(\frac{1}{|\xi|^2} \right), \quad |\xi| \rightarrow \infty.$$

Then, using the Cauchy theorem for evaluation of the integrals in (2.2.32), (2.2.33) and the conditions (1.2.18) at infinity, we obtain

$$A_1 = 1, \quad B_1 = \pm |c_1|^2 - c_1 c_{-1},$$

$$A_2 = -i, \quad B_2 = (\pm |c_1|^2 + c_1 c_{-1})i.$$

where signs "+" and "-" correspond to the cavity or rigid inclusion, respectively.

The asymptotic formula (1.2.18) can be rewritten in the form

$$w^{(j)}(z) = -\frac{1}{4\pi\mu} \left\{ M_{j1} \left[\frac{1}{z} + \frac{1}{\bar{z}} \right] + M_{j2} \left[\frac{1}{z} - \frac{1}{\bar{z}} \right] i \right\} + O\left(\frac{1}{|z|^2} \right), \quad |z| \rightarrow \infty, \quad (2.2.35)$$

and the Pólya-Szegö matrix \mathbf{M} is given by

$$\mathbf{M} = 2\pi\mu \begin{pmatrix} \mp |c_1|^2 + \operatorname{Re}(c_1 c_{-1}) & \operatorname{Im}(c_1 c_{-1}) \\ \operatorname{Im}(c_1 c_{-1}) & \mp |c_1|^2 - \operatorname{Re}(c_1 c_{-1}) \end{pmatrix}. \quad (2.2.36)$$

The sign "+" is chosen for a rigid inclusion (the matrix \mathbf{M} is positive definite, $|c_1| > |c_{-1}|$)

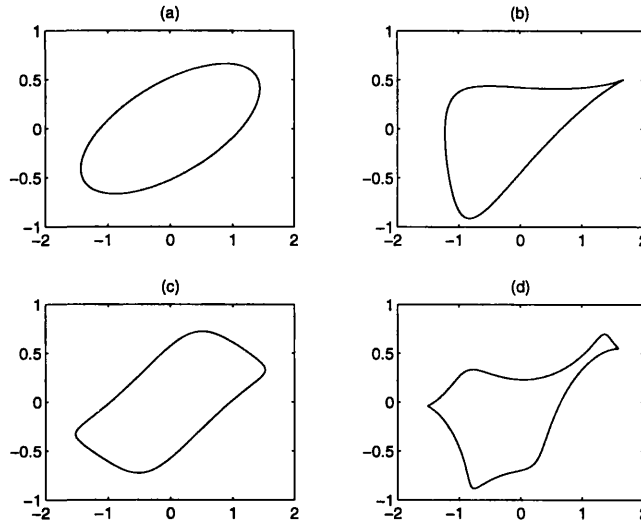


Figure 2-1: The equivalent regions for Laplace operator:

$$(a) \quad \omega(\xi) = \xi + \frac{1}{2} \exp \frac{\pi i}{5} \xi^{-1}; \quad (b) \quad \omega(\xi) = \xi + \frac{1}{2} \exp \frac{\pi i}{5} \xi^{-1} + \frac{1}{4} \exp \frac{\pi i}{4} \xi^{-2};$$

$$(c) \quad \omega(\xi) = \xi + \frac{1}{2} \exp \frac{\pi i}{5} \xi^{-1} + \frac{1}{10} \xi^{-3};$$

$$(d) \quad \omega(\xi) = \xi + \frac{1}{2} \exp \frac{\pi i}{5} \xi^{-1} + \frac{1}{4} \exp \frac{\pi i}{2} \xi^{-2} + \frac{1}{10} \xi^{-5}.$$

for all finite volume inclusions) and the sign "–" for a cavity (the Pólya-Szegő matrix is negative definite). It should be noted that in (2.2.36) only two coefficients c_1 and c_{-1} of the conformal mapping (2.2.1) are involved.

Lemma 2.1 *In the state of anti-plane shear, for any finite cavity (or rigid inclusion) there exists a cavity (or rigid inclusion) of an elliptical shape with the same Pólya-Szegő matrix.*

In Figure 2-1 the examples of equivalent domains are presented.

2.2.4 Circular elastic inclusions

Below a simple example is considered - Pólya-Szegő matrices for an elastic disk of radius R in an infinite elastic isotropic plane. Material of the circular inclusion is specified by the Lamé constants μ_0 and λ_0 , whereas μ and λ are the Lamé constants of the matrix. $\mathbf{1}^0$. For the Laplace operator (anti-plane shear) the coefficients α_j, β_j in (2.2.34) are given by

$$A_1 = 1, \quad B_1 = \frac{\mu - \mu_0}{\mu + \mu_0} R^2,$$

$$A_2 = -i, \quad B_2 = \frac{\mu - \mu_0}{\mu + \mu_0} R^2 i.$$

Then the Pólya-Szegő matrix can be represented in a simple form

$$\mathbf{M} = 2\pi\mu \frac{\mu_0 - \mu}{\mu_0 + \mu} R^2 \mathbf{I},$$

where \mathbf{I} is the identity matrix.

The matrix \mathbf{M} is positive definite for $\mu_0 > \mu$ and negative definite for $\mu_0 < \mu$.

2^0 . For the case of the Navier system given the linear displacement field at infinity, the Kolosov-Muskhelishvili complex potentials are represented by

$$\varphi(z) = \frac{\alpha z}{R} + \frac{\bar{\gamma} R}{z} \frac{\mu_0 - \mu}{\varkappa \mu_0 + \mu}, \quad (2.2.37)$$

$$\psi(z) = \frac{\gamma z}{R} + \frac{2\operatorname{Re}(\alpha)R}{z} \frac{\mu_0(\varkappa - 1) - \mu(\varkappa_0 - 1)}{\mu(\varkappa_0 - 1) + 2\mu_0} + O\left(\frac{1}{|z|^2}\right), \quad (2.2.38)$$

where the constants α and γ are chosen in accordance with (2.2.7).

Thus, the Pólya-Szegő matrix has the form

$$\mathcal{P} = \frac{R^2}{4q} \begin{pmatrix} \Xi + \Theta & \Xi - \Theta & 0 \\ \Xi - \Theta & \Xi + \Theta & 0 \\ 0 & 0 & 2\Theta \end{pmatrix}, \quad (2.2.39)$$

where

$$\Theta = \frac{\mu_0 - \mu}{\varkappa \mu_0 + \mu}, \quad \Xi = \frac{2}{(\varkappa - 1)^2} \frac{\mu_0(\varkappa - 1) - \mu(\varkappa_0 - 1)}{\mu(\varkappa_0 - 1) + 2\mu_0}.$$

The matrix \mathcal{P} is positive definite provided $\mu_0 > \mu$ and $\mu_0(\varkappa - 1) > \mu(\varkappa_0 - 1)$, and it is negative definite when $\mu_0 < \mu$ and $\mu_0(\varkappa - 1) < \mu(\varkappa_0 - 1)$.

2.3 Effective moduli of dilute composites

2.3.1 Anti-plane shear

Asymptotic formulae

The solution of the system (1.2.13)-(1.2.15) in a finite region Ω (e.g. $[-1/2, 1/2] \times [-1/2, 1/2]$) with a small inclusion ω_ε can be represented in the form

$$u(\mathbf{x}) = v(\mathbf{x}) + \varepsilon w(\varepsilon^{-1} \mathbf{x}) + \varepsilon^2 \mathcal{V}(\mathbf{x}) + O(\varepsilon^3), \quad (2.3.1)$$

where

$$w(\varepsilon^{-1}\mathbf{x}) = \sum_{i=1}^2 w^{(i)}(\varepsilon^{-1}\mathbf{x}) \frac{\partial v}{\partial x_i}(0)$$

and $w^{(i)}$ are defined in Section 1.2.2. Region Ω can be regarded as an elementary cell of dilute composite filled with small inclusions ω_ε .

The third term of the asymptotic expansion satisfies the boundary value problem

$$\Delta \mathcal{V} = 0, \quad \mathbf{x} \in \Omega, \quad (2.3.2)$$

$$\mu \frac{\partial \mathcal{V}}{\partial n}(\mathbf{x}) = \frac{1}{2\pi} \frac{\partial}{\partial n} \sum_{j,k=1}^2 M_{jk} \frac{x_k}{\|\mathbf{x}\|^2} \frac{\partial v}{\partial x_j}(0), \quad \mathbf{x} \in \partial\Omega,$$

and admits the representation

$$\mathcal{V}(\mathbf{x}) = \sum_{j,k=1}^2 M_{jk} [T^{(k)}(\mathbf{x}) + \frac{1}{2\pi\mu} \frac{x_k}{\|\mathbf{x}\|^2}] \frac{\partial v}{\partial x_j}(0), \quad (2.3.3)$$

where $T^{(k)}$, $k = 1, 2$, are the dipole fields specified by

$$-\mu \Delta T^{(k)} + \frac{\partial \delta}{\partial x_k}(\mathbf{x}) = 0, \quad \mathbf{x} \in \Omega, \quad (2.3.4)$$

$$\frac{\partial T^{(k)}}{\partial n}(\mathbf{x}) = 0, \quad \mathbf{x} \in \partial\Omega.$$

As follows from Oleinik, Panasenko and Yosifian [86], the effective moduli for a composite with the elementary cell Ω can be calculated as

$$\hat{H}_{nk} = \mu \int_{\Omega \setminus \overline{\omega_\varepsilon}} \nabla u^{(n)} \cdot \nabla u^{(k)} d\mathbf{x} + \mu_0 \int_{\omega_\varepsilon} \nabla u^{(n,0)} \cdot \nabla u^{(k,0)} d\mathbf{x}, \quad (2.3.5)$$

where $u^{(n)}$ satisfies the equations (1.2.13)-(1.2.15) in Ω , the periodic boundary conditions and admits the representation

$$u^{(n)}(\mathbf{x}) = x_n + \varepsilon w^{(n)}(\varepsilon^{-1}\mathbf{x}) + \varepsilon^2 \mathcal{V}^{(n)}(\mathbf{x}) + O(\varepsilon^3). \quad (2.3.6)$$

Using the Green's formula one can rewrite the "energy integral" (2.3.5) in the form

$$\hat{H}_{nk} = \sum_i \mu \left\{ \int_{\Gamma} n_i u^{(n)} \frac{\partial u^{(k)}}{\partial x_i} ds + \int_{\partial\omega_\varepsilon} n_i u^{(n)} \frac{\partial u^{(k)}}{\partial x_i} ds \right\} - \mu_0 \int_{\partial\omega_\varepsilon} n_i u^{(n,0)} \frac{\partial u^{(k,0)}}{\partial x_i} ds,$$

where Γ is the outer boundary of Ω .

Due to (1.2.15), the two last integrals are cancelled down. Then replacing $u^{(n)}$ by (2.3.6) with $v^{(n)} = x_n$ we obtain

$$\begin{aligned}\widehat{H}_{nk} &= \mu\delta_{nk} + \mu\varepsilon^2 \sum_i \int_{\Gamma} n_i \sum_{j,m=1}^2 M_{jm} T^{(m)}(\mathbf{x}) \frac{\partial v^{(k)}}{\partial x_i}(0) \frac{\partial v^{(n)}}{\partial x_j}(0) ds \\ &= \mu\delta_{nk} - \mu\varepsilon^2 \int_{\Omega} \sum_{m=1}^2 M_{nm} x_k \Delta T^{(k)} d\mathbf{x},\end{aligned}$$

and due to (2.3.4),

$$\boxed{\widehat{H}_{nk} = \mu\delta_{nk} + \varepsilon^2 M_{nk} + O(\varepsilon^3)}. \quad (2.3.7)$$

Comparison with previous results

As proved by Hetherington and Thorpe [42], the effective shear modulus $\widehat{\mu}$ for a periodic dilute composite containing cavities or rigid inclusions of a regular polygonal shape is specified by the formula

$$\frac{\widehat{\mu}}{\mu_0} = 1 \pm G(n)f + O(f^2), \quad (2.3.8)$$

where f is the area fraction of inclusions, and for n -sided regular polygons the function G has the form

$$G(n) = \frac{\tan(\pi/n) \Gamma^4(1/n)}{2\pi n \Gamma^2(2/n)}.$$

The conformal mapping of n -sided regular polygon is defined by

$$\omega(\xi) = R \left(\xi + \frac{2}{n(n-1)\xi^{n-1}} + \frac{n-1}{n^2(2n-1)\xi^{2n-1}} + \frac{(n-2)(2n-2)}{3n^3(3n-1)\xi^{3n-1}} + \dots \right). \quad (2.3.9)$$

Jasiuk [44] derived that in terms of coefficients of the expansion (2.2.1) or (2.3.9) the quantity f from (2.3.8) admits the representation

$$f = \pi\varepsilon^2 \left(|c_1|^2 - \sum_{m=1}^{\infty} m |c_{-m}|^2 \right).$$

Here ε is a small non-dimensional positive parameter characterising the size of the defect in comparison with the size of an elementary cell. It was also proved by Jasiuk, Chen

and Thorpe [45] that

$$\pi \left(1 - \sum_{m=1}^{\infty} m |c_{-m}|^2 \right) = \frac{4\pi^2 n}{\tan(\pi/n)} \frac{\Gamma^2(2/n)}{\Gamma^4(1/n)},$$

and therefore, the asymptotic formula (2.3.8) can be written as

$$\frac{\hat{\mu}}{\mu_0} = 1 \pm 2\pi |c_1|^2 \varepsilon^2. \quad (2.3.10)$$

On the other hand, it has been shown that for a dilute periodic composite material the matrix $\hat{\mathbf{H}}$ of effective moduli is specified by (2.3.7). In particular, when the defects are cavities or rigid inclusions of a regular polygonal shape we obtain the result (2.3.8) of Hetherington and Thorpe [42]. Moreover, asymptotic formula (2.3.7) yields the following

Lemma 2.2 *In the state of anti-plane shear for any dilute periodic composite containing small cavities (or rigid inclusions) there exists an equivalent periodic composite medium containing elliptical cavities (or rigid inclusions) with the same (in the asymptotic sense of (2.3.7)) matrix of effective elastic moduli.*

2.3.2 Plane strain

Classes of equivalent domains

Consider the effective moduli of the Navier system. First, we write equation (2.1.1) in the matrix form

$$\mathcal{D}(\partial/\partial x) \mathcal{H} \mathcal{D}^T (\partial/\partial x) \mathbf{u} = 0, \quad (2.3.11)$$

where

$$\mathcal{D} = \begin{pmatrix} x_1 & 0 & \frac{1}{\sqrt{2}}x_2 \\ 0 & x_2 & \frac{1}{\sqrt{2}}x_1 \end{pmatrix}, \quad \mathcal{H} = \begin{pmatrix} 2\mu + \lambda & \lambda & 0 \\ \lambda & 2\mu + \lambda & 0 \\ 0 & 0 & 2\mu \end{pmatrix}. \quad (2.3.12)$$

The matrix of effective elastic moduli of a periodic composite material with an elementary cell containing an arbitrary small inclusion is approximated by (see Babich, Zorin, Ivanov, Movchan and Nazarov [3])

$$\boxed{\hat{\mathcal{H}} = \mathcal{H} + \varepsilon^2 \mathcal{P} + O(\varepsilon^3)}. \quad (2.3.13)$$

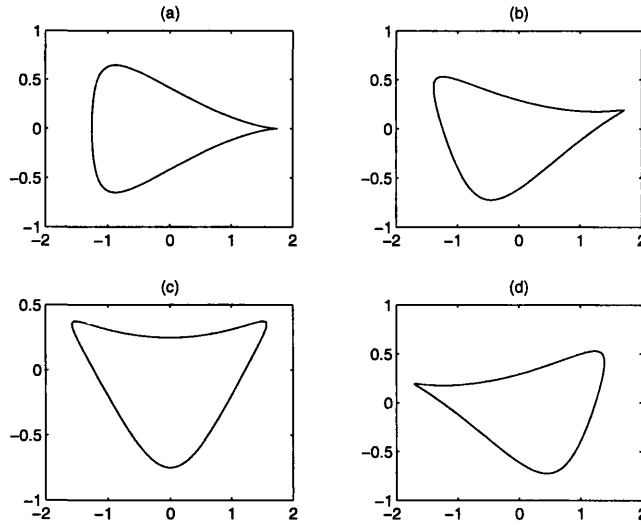


Figure 2-2: Equivalent cavities for the case of plane strain:

$$\begin{aligned}
 \text{(a)} \quad \omega(\xi) &= \xi + \frac{1}{2}\xi^{-1} + \frac{1}{4}\xi^{-2}; & \text{(b)} \quad \omega(\xi) &= \xi + \frac{1}{2}\xi^{-1} + \frac{1}{4}\exp\frac{\pi i}{4}\xi^{-2}; \\
 \text{(c)} \quad \omega(\xi) &= \xi + \frac{1}{2}\xi^{-1} + \frac{1}{4}\exp\frac{\pi i}{2}\xi^{-2}; & \text{(d)} \quad \omega(\xi) &= \xi + \frac{1}{2}\xi^{-1} + \frac{1}{4}\exp\frac{3\pi i}{4}\xi^{-2}.
 \end{aligned}$$

The structure of the matrix of effective moduli can be analysed, and the analysis shows that the same set of effective elastic moduli may characterise composite structures containing different types of small defects. Moreover, one can derive relations between the conformal mapping coefficients which provide equivalence in the above sense. Namely, if the following quantities Ω , Σ , Ξ , Θ , Λ , Υ from (2.2.15) are the same for two different conformal mappings, then the effective moduli matrices also coincide (to first order accuracy).

In particular, equation (2.2.17) implies that if $|c_{-2}| = \text{const}$ and c_1 and c_{-1} are fixed, then the first order approximation for the effective moduli does not depend on $\arg c_{-2}$. Figure 2-2 shows the examples of such cavities.

The compliance matrix

Using the technique mentioned above one calculates the compliance matrix. For a periodic composite material with small inclusions it has the form

$$\boxed{\widehat{\mathbf{c}} = \mathbf{c} - \varepsilon^2 \mathbf{c} \mathcal{P} \mathbf{c} + O(\varepsilon^3) = \mathbf{c} - \varepsilon^2 \mathbf{e} + O(\varepsilon^3)}, \quad (2.3.14)$$

where the compliance matrix of isotropic material

$$\mathbf{C} = \mathcal{H}^{-1} = \begin{pmatrix} \frac{1}{E} & \frac{\nu}{E(\nu-1)} & 0 \\ \frac{\nu}{E(\nu-1)} & \frac{1}{E} & 0 \\ 0 & 0 & \frac{1}{E(1-\nu)} \end{pmatrix},$$

with E is the Young's modulus, ν is the Poisson ratio.

For the case of cavities \mathcal{E} is given by

$$\mathcal{E} = \frac{\pi}{E} \begin{pmatrix} -2\Omega + \Sigma - \frac{1}{2}\Xi & 2\Omega - \frac{1}{2}\Xi & \Lambda - 2\Theta \\ 2\Omega - \frac{1}{2}\Xi & -2\Omega - \Sigma - \frac{1}{2}\Xi & \Lambda + 2\Theta \\ \Lambda - 2\Theta & \Lambda + 2\Theta & 2\Upsilon \end{pmatrix}, \quad (2.3.15)$$

where constants $\Omega, \Sigma, \Xi, \Theta, \Lambda, \Upsilon$ are presented by (2.2.15), and they are independent of the Lamé moduli μ and λ of the elastic material. It follows from (2.3.15) that the correction term \mathcal{E} for the compliance matrix of the homogenised medium is independent of the Poisson ratio of the elastic matrix. Thus, we have proved the following

Theorem 2.2 *The correction term \mathcal{E} in the representation (2.3.14) of the compliance matrix for a periodic composite containing small cavities is independent of the Poisson ratio and depends on the cavity morphology and Young's modulus only.*

Examples:

1. For the case of a crack characterised by the conformal mapping $\omega(\xi) = R(\xi + \frac{1}{\xi})$ the correction term for the effective compliance matrix of the periodic material is given by

$$\mathcal{E} = \frac{\pi}{E} R^2 \varepsilon^2 \begin{pmatrix} 0 & 0 & 0 \\ 0 & -8 & 0 \\ 0 & 0 & -4 \end{pmatrix}.$$

One can see that for a composite material with small cracks aligned along the x_1 -axis the homogenised anisotropic material has the same Young's modulus in x_1 -direction as the unperturbed isotropic material.

2. For the case of a circular cavity characterised by the conformal mapping $\omega(\xi) = R\xi$, the correction term \mathcal{E} is

$$\boldsymbol{\mathcal{E}} = \frac{\pi}{E} \varepsilon^2 R^2 \begin{pmatrix} -3 & 1 & 0 \\ 1 & -3 & 0 \\ 0 & 0 & -4 \end{pmatrix}.$$

3. For an equilateral triangle, one has $\omega(\xi) = R(\xi + \frac{1}{3\xi^2})$ and

$$\boldsymbol{\mathcal{E}} = \frac{\pi}{E} \varepsilon^2 R^2 \begin{pmatrix} -3\frac{2}{9} & \frac{7}{9} & 0 \\ \frac{7}{9} & -3\frac{2}{9} & 0 \\ 0 & 0 & -4 \end{pmatrix}.$$

4. For square cavities characterised by the conformal mapping $\omega(\xi) = R(\xi - \frac{1}{6\xi^3})$, the correction term for the effective compliance matrix is

$$\boldsymbol{\mathcal{E}} = \frac{\pi}{E} \varepsilon^2 R^2 \begin{pmatrix} -2\frac{67}{84} & \frac{53}{84} & 0 \\ \frac{53}{84} & -2\frac{67}{84} & 0 \\ 0 & 0 & -\frac{12}{5} \end{pmatrix}.$$

5. For a square cavity rotated through the angle $\pi/4$, one has $\omega(\xi) = R(\xi + \frac{1}{6\xi^3})$ and

$$\boldsymbol{\mathcal{E}} = \frac{\pi}{E} \varepsilon^2 R^2 \begin{pmatrix} -3\frac{29}{60} & \frac{79}{60} & 0 \\ \frac{79}{60} & -3\frac{29}{60} & 0 \\ 0 & 0 & -\frac{12}{7} \end{pmatrix}.$$

One could mention that the diagonal entries for the compliance matrices in examples 2-5 were evaluated by Jasiuk [44], and our results are consistent with those published in [44].

6. In the case of an ellipse with the conformal mapping function $\omega(\xi) = R(\xi + \frac{m}{\xi})$, the correction term for the effective compliance matrix is given by

$$\boldsymbol{\mathcal{E}} = \frac{\pi}{E} \varepsilon^2 R^2 \begin{pmatrix} -3 - m^2 + 4m & 1 - m^2 & 0 \\ 1 - m^2 & -3 - m^2 - 4m & 0 \\ 0 & 0 & -4 \end{pmatrix}.$$

7. For an elliptical cavity of an arbitrary orientation the mapping is $\omega(\xi) = c_1\xi + \frac{c_{-1}}{\xi}$, where c_1 and c_{-1} are complex coefficients. The matrix $\boldsymbol{\mathcal{E}}$ takes the form

$$\boldsymbol{\mathcal{E}} = \frac{\pi}{E} \varepsilon^2 |c_1|^2 \begin{pmatrix} -3 - \frac{|c_{-1}|^2 - 4\text{Re}(c_1 c_{-1})}{|c_1|^2} & 1 - \frac{|c_{-1}|^2}{|c_1|^2} & 2\sqrt{2} \frac{\text{Im}(c_1 c_{-1})}{|c_1|^2} \\ 1 - \frac{|c_{-1}|^2}{|c_1|^2} & -3 - \frac{|c_{-1}|^2 + 4\text{Re}(c_1 c_{-1})}{|c_1|^2} & 2\sqrt{2} \frac{\text{Im}(c_1 c_{-1})}{|c_1|^2} \\ 2\sqrt{2} \frac{\text{Im}(c_1 c_{-1})}{|c_1|^2} & 2\sqrt{2} \frac{\text{Im}(c_1 c_{-1})}{|c_1|^2} & -4 \end{pmatrix}.$$

Examples of effective moduli

In order to compare this method with results of Jasiuk [44], Jasiuk, Chen and Thorpe [45] and Thorpe and Jasiuk [111], the examples are presented where the effective elastic moduli of periodic composites with small cavities (or rigid inclusions) are evaluated for defects of different shapes.

When only non-zero coefficients of the conformal mapping function are c_1 , c_{-1} , c_{-2} (other coefficients are zero), the explicit formulae for the Pólya-Szegő matrices are given by (2.2.17), and the effective elastic moduli can be evaluated from (2.2.17). In particular, when $Im(c_1 c_{-1}) = 0$ the effective material is orthotropic. For an elliptical cavity $c_{-2} = 0$, the condition $Im(c_1 c_{-1}) = 0$ corresponds to the case when the axes of the ellipse are parallel to the coordinate axes. Periodic composites with small circular cavities (or rigid inclusions) and equilateral triangular cavities (or rigid inclusions) always correspond to effective orthotropic media.

Following Jasiuk [44], one introduces the directional Young's moduli E_1 , E_2 , E_3 such that

$$\frac{1}{E_1} = C_{11}, \quad \frac{1}{E_2} = C_{22}, \quad \frac{1}{E_3} = C_{12} + \frac{1}{2}C_{33},$$

and also the average Young's modulus E is given by

$$\frac{1}{E} = \frac{1}{2} \left\{ \frac{1}{E_1} + \frac{1}{E_2} \right\}.$$

It can be observed that for equilateral polygons the average Young's modulus and the directional Young's moduli are equal. In terms of components of the Pólya-Szegő matrix the average effective Young's modulus \widehat{E} is given by

$$\frac{1}{\widehat{E}} = \frac{1}{E} + \frac{\alpha}{E} \varepsilon^2 + O(\varepsilon^3), \quad (2.3.16)$$

with

$$\alpha = \frac{(\mathcal{P}_{11} + \mathcal{P}_{22})(\lambda^2 + 2\lambda\mu + 2\mu^2) - \mathcal{P}_{12}(\lambda + 2\mu)2\lambda}{4\mu(\lambda + \mu)(2\mu + \lambda)}.$$

Here ε is a small positive parameter which is equal to a normalised diameter of a small defect in an elementary cell.

The table below includes the values of the coefficient α from the expansion (2.3.16) obtained for dilute periodic composites containing cavities or rigid inclusions.

Shape	Conformal mapping	α_0 (cavity) and α_∞ (rigid inclusion)
circle	$\omega(\xi) = R\xi$	$\alpha_0 = 3\pi R^2$ $\alpha_\infty = -\frac{\kappa^2 - \kappa + 4}{2\kappa} \pi R^2$
ellipse	$\omega(\xi) = R(\xi + \frac{m}{\xi})$ $R, m \in \mathbb{R}$	$\alpha_0 = \pi R^2(3 + m^2)$ $\alpha_\infty = [-\frac{\kappa^2 - \kappa + 4}{2\kappa} + m^2 \frac{\kappa - 1}{2\kappa}] \pi R^2$
ellipse	$\omega(\xi) = c_1 \xi + \frac{c_{-1}}{\xi}$ $c_1, c_{-1} \in \mathbb{C}$	$\alpha_0 = \pi[3 c_1 ^2 + c_{-1} ^2]$ $\alpha_\infty = [-\frac{\kappa^2 - \kappa + 4}{2\kappa} c_1 ^2 + \frac{\kappa - 1}{2\kappa} c_{-1} ^2 + \frac{2(\kappa + 1) \operatorname{Im}^2(c_1 c_{-1})}{(\kappa c_1 ^2 + c_{-1} ^2) \kappa} \pi]$
triangle	$\omega(\xi) = R(\xi + \frac{1}{3\xi^2})$	$\alpha_0 = 3\frac{2}{9} \pi R^2$ $\alpha_\infty = -\frac{9\kappa^2 - 11\kappa + 38}{18\kappa} \pi R^2$
square	$\omega(\xi) = R(\xi - \frac{1}{6\xi^3})$	$\alpha_0 = 2\frac{67}{84} \pi R^2$
square (rotated through $\pi/4$)	$\omega(\xi) = R(\xi + \frac{1}{6\xi^3})$	$\alpha_0 = 3\frac{29}{60} \pi R^2$

2.4 Mapping to a composite material with elliptical voids

As proved by Olver [88] (also see Milton and Movchan [70]), for any two-dimensional anisotropic medium there exists an affine transformation which maps the given boundary value problem to a boundary value problem for an orthotropic material. In other words, one can establish a correspondence between a generally anisotropic medium and a medium with an orthotropic symmetry.

Consider a dilute two-dimensional periodic composite containing small cavities, and assume that the matrix of effective elastic moduli is specified by (2.3.13). In this section we show that in certain cases one can find an affine transformation which establishes a correspondence between the given dilute composite and another periodic composite containing small elliptical cavities. We seek the required mapping matrix in the form

$$\mathbf{T} = \mathbf{I} + \varepsilon^2 \begin{pmatrix} t_{11} & t_{12} \\ t_{21} & t_{22} \end{pmatrix}, \quad \det \mathbf{T} = 1. \quad (2.4.1)$$

Then it follows from the results of Milton and Movchan [70] that the modified matrix of elastic moduli is given by

$$\begin{aligned} \tilde{\mathcal{H}} &= (\mathbf{I} + \varepsilon^2 \mathbf{Q})(\mathcal{H} + \varepsilon^2 \mathcal{P})(\mathbf{I} + \varepsilon^2 \mathbf{Q})^T \\ &= \mathcal{H} + \varepsilon^2 \tilde{\mathcal{P}} + O(\varepsilon^4), \end{aligned} \quad (2.4.2)$$

where

$$\mathbf{Q} = \begin{pmatrix} 2t_{11} & 0 & \sqrt{2}t_{12} \\ 0 & 2t_{22} & \sqrt{2}t_{21} \\ \sqrt{2}t_{21} & \sqrt{2}t_{12} & 0 \end{pmatrix},$$

and

$$\tilde{\mathcal{P}} = \mathbf{Q}\mathcal{H} + \mathcal{H}\mathbf{Q}^T + \mathcal{P} \quad (2.4.3)$$

is the transformed Pólya-Szegö matrix. The objective is to choose the mapping matrix (2.4.1) in such a way that the matrix (2.4.3) corresponds to an elliptical cavity, and therefore, (2.4.2) can be interpreted as a matrix of effective elastic moduli for a periodic composite containing small elliptical cavities.

The second condition (2.4.1) implies

$$t_{22} = -t_{11}, \quad t_{21} = -t_{11}^2 t_{12}^{-1}. \quad (2.4.4)$$

First, the matrix $\tilde{\mathcal{H}}$ should be block-diagonal, i.e.

$$\begin{aligned} \tilde{\mathcal{H}}_{13} &= \varepsilon^2 \left\{ \sqrt{2}(\lambda + 2\mu)(t_{12} + t_{21}) + \mathcal{P}_{13} \right\} = 0, \\ \tilde{\mathcal{H}}_{23} &= \varepsilon^2 \left\{ \sqrt{2}(\lambda + 2\mu)(t_{12} + t_{21}) + \mathcal{P}_{23} \right\} = 0. \end{aligned} \quad (2.4.5)$$

One can see that the above system is solvable with respect to t_{12} , t_{21} if and only if

$$\mathcal{P}_{13} = \mathcal{P}_{23}. \quad (2.4.6)$$

Suppose that the original Pólya-Szegö matrix \mathcal{P} satisfies (2.4.6). Then one can choose the transformation matrix (2.4.1) with real components such that relations (2.4.4),

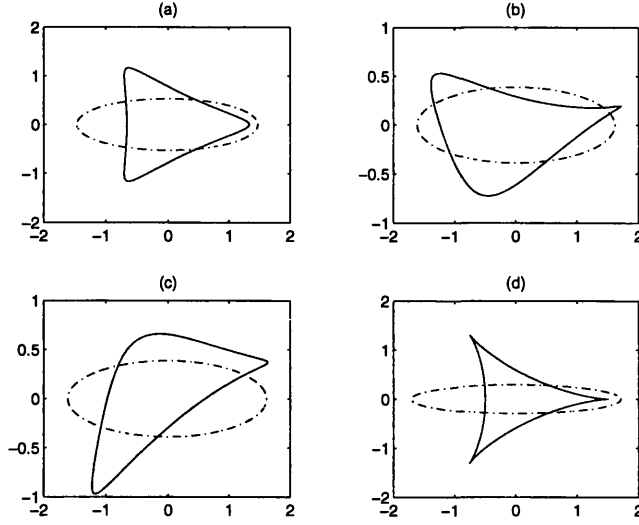


Figure 2-3: The equivalent elliptical and nonelliptical cavities:

$$\begin{aligned}
 \text{(a)} \quad \omega(\xi) &= \xi + \frac{1}{3}\xi^{-2}; & \text{(b)} \quad \omega(\xi) &= \xi + \frac{1}{2}\xi^{-1} + \frac{1}{4}\exp\frac{\pi i}{4}\xi^{-2}; \\
 \text{(c)} \quad \omega(\xi) &= \xi + \frac{1}{2}\exp\frac{\pi i}{4}\xi^{-1} + \frac{1}{4}\xi^{-2}; & \text{(d)} \quad \omega(\xi) &= \xi + \frac{1}{2}\xi^{-2}.
 \end{aligned}$$

(2.4.5) hold. Then, the matrix $\tilde{\mathcal{P}}$ has the form

$$\tilde{\mathcal{P}} = \begin{pmatrix} \mathcal{P}_{11} + 4(2\mu + \lambda)t_{11} & \mathcal{P}_{12} & 0 \\ \mathcal{P}_{12} & \mathcal{P}_{22} - 4(2\mu + \lambda)t_{11} & 0 \\ 0 & 0 & \mathcal{P}_{33} \end{pmatrix}.$$

If

$$\mathcal{P}_{11} + \mathcal{P}_{22} = 2(\mathcal{P}_{12} + \mathcal{P}_{33}), \quad (2.4.7)$$

and

$$2\mathcal{P}_{33} - (\varkappa - 1)^2(2\mathcal{P}_{12} + \mathcal{P}_{33}) > 0, \quad (2.4.8)$$

then by appropriate choice of t_{11} it follows from (2.2.17) (with $c_{-2} = 0$) that $\tilde{\mathcal{P}}$ is the Pólya-Szegő matrix corresponding to an elliptical cavity which can be mapped to the unit disk by

$$\omega(\xi) = \tilde{c}_1\xi + \frac{\tilde{c}_{-1}}{\xi}, \quad (2.4.9)$$

where $\tilde{c}_1, \tilde{c}_{-1}$ are constant coefficients ($\text{Im}(\tilde{c}_1\tilde{c}_{-1}) = 0$) whose moduli are specified by

$$|\tilde{c}_1|^2 = -2q\mathcal{P}_{33},$$

$$|\tilde{c}_{-1}|^2 = q[2\mathcal{P}_{33} - (\mathcal{P}_{33} + 2\mathcal{P}_{12})(\varkappa - 1)^2]. \quad (2.4.10)$$

Note that the choice of \tilde{c}_1 , \tilde{c}_{-1} is not unique.

Thus, one has proved the following

Theorem 2.3 *Let a homogenised composite medium have the effective elastic matrix (2.3.13), where \mathcal{P} is the Pólya-Szegő matrix corresponding to a finite cavity. Also, assume that components \mathcal{P}_{kl} satisfy the conditions (2.4.6)-(2.4.8). Then there exists an affine transformation (2.4.1) which maps (in the sense of Olver [88]) the original boundary value problem to a new boundary value problem associated with the medium perforated by cavities of elliptical shape.*

Example:

Now consider a simple situation where a finite domain is mapped to the unit disk by the conformal mapping with only three non-zero coefficients (see (2.2.17)). In this case after the affine transformation (2.4.1)

$$\mathbf{T} = \mathbf{I} + \varepsilon^2 \begin{pmatrix} t_{11} & t_{12} \\ -\frac{t_{11}^2}{t_{12}} & -t_{11} \end{pmatrix},$$

with

$$t_{11} = \pi|c_1|\sqrt{|c_{-1}|^2 + 2|c_{-2}|^2} - \pi \operatorname{Re}(c_1 c_{-1}),$$

$$t_{12} = \pm \pi \left\{ 2|c_1|^2(|c_{-1}|^2 + |c_{-2}|^2) - 2|c_1| \operatorname{Re}(c_1 c_{-1}) \sqrt{|c_{-1}|^2 + 2|c_{-2}|^2} \right\}^{1/2} - \pi \operatorname{Im}(c_1 c_{-1}),$$

one has the modified equations which are related to the homogenisation problem associated with the medium perforated by small elliptical cavities, and the corresponding coefficients of the conformal mapping are given by

$$\tilde{c}_1 = c_1, \quad |\tilde{c}_{-1}|^2 = |c_{-1}|^2 + 2|c_{-2}|^2.$$

Figure 2-3 shows the geometry of equivalent (in the sense of the Olver transformation) cavities.

2.5 Conclusions

Starting with the definition of the Pólya-Szegő matrix in elasticity we described the algorithm for calculation its coefficients. This algorithm employs the Kolosov-Muskhelishvili potentials and the conformal mapping technique. As a result, the Pólya-Szegő matrices have been obtained for a wide range of defects. That includes cavities and rigid inclusions of arbitrary shapes, some examples for elastic inclusions. The case of anti-plane shear has been considered for different types of defect.

In the second part of the chapter we considered the dilute composite media. The Pólya-Szegő matrix has a simple meaning for such kind of media. It describes the correction term for effective (homogenised) moduli. This result is derived on the basis of the asymptotic procedure. Then we also analysed the properties of the composite media. Two following topics have been considered:

First, the correspondence between different types of cavities in the sense of effective elastic properties of dilute media shows links between cavities of different shapes. In conductivity any cavity has an equivalent elliptical one, in elasticity it is true under certain conditions only.

Second, the perforated materials with the cavities of arbitrary shapes are considered. One shows that the correction term of the compliance matrix for homogenised media is independent of the Poisson ratio. This result has been proved for dilute composite materials analytically.

Chapter 3

Pólya-Szegő matrices in optimization problem

3.1 Recent results

The problem of shape optimization. We will consider the problem of maximization of the stiffness of an elastic plane weakened by a cavity of a fixed area and loaded by a uniform stress field σ at infinity. This problem is equivalent to minimizing the energy decrease stored in the medium under some loading. The total elastic energy stored in the plane is infinite, nevertheless, the energy decrease is finite. One assumes that the cavity occupies a simply-connected domain in \mathbb{R}^2 .

The shape of optimal cavities and the optimal properties of composites have been studied for a uniform hydrostatic loading and a biaxial loading with the principal stresses of the same sign (see Cherepanov [16], Vigdergauz [115], [117]). Several optimal cavities in a body have been described by Vigdergauz [116]. Vigdergauz and Cherkaev [119] studied numerically the optimal cavities under by-axial tension-compression.

In this chapter the case of pure shear loading is considered. One will show that the optimal cavity is a curved quadrilateral, and the angle near the corners is equal to the critical Carothers [14] value $\sim 102.6^\circ$ (see Figure 3-1).

The formulation of the optimization problem and discussion of the necessary conditions of optimality and their applications to dilute composites is considered at the beginning. Next, one presents a minimization algorithm based on the concept of the dipole matrix corresponding to remote field associated with finite cavities in an elastic plane. It enables one to produce explicit representation of the energy increment in terms of the

dipole coefficients. The exterior of a cavity is presented as a conformal image of the interior of the unit disc. The elements of the dipole matrix are evaluated in terms of the coefficients of the truncated series expansion of the conformal map. Finally, the energy increment (given by the dipole tensor) is minimized over all possible values of the coefficients in the expansion. The resulting sequence of cavities approaches to a limiting shape of a quadrilateral.

Afterwards, the complex variable technique which is similar to the method of Cherepanov [16] is used. One uses optimality conditions and Kolosov-Muskhelishvili potentials in conjunction with conformal mapping representation of the unknown domain in order to set up the integral equation for the unknown conformal mapping. The integral equation is reduced to a finite dimensional system of linear equations by expanding all the quantities into truncated power series. Solving the linear system, one finds the same conformal map obtained by the direct minimization procedure described above. Finally, the local behaviour of elastic fields near the corners of the cavity contour is studied using the asymptotic expansion of the solution near the corner and the optimality conditions; in this way the exact value of the angle at the corner is determined.

Correspondence with composite materials. If one removes any restriction on the topology of the structure (number of holes) then one has to consider composites – materials with infinite number of infinitely small holes. The optimization problem for composites has been solved analytically (see, for example, the papers by Kohn and Strang [53], Gibiansky and Cherkaev [28], [29], Milton [68], Bendsoe [7], Grabovsky and Kohn [35]). These analytical solutions have showed that the elliptical hole minimizes the energy increment if the principal stresses have the same sign, even when the topology is unrestricted. However, if the principal stresses have opposite sign then a second rank laminate structure minimizes energy. Shape found in this chapter is the best if one restricts the number of holes to 1. It is important to refer to Cherkaev, Grabovsky, Movchan and Serkov [17], [100], where this idea has been suggested.

3.2 Formulation of the problem

In this section the boundary value problem and the appropriate variational formulation are given and the optimality criteria is discussed.

Elasticity problem. First, one considers the boundary value problem in an elastic domain with a single finite cavity G . The elastic material is characterised by the Lamé constants μ and λ . On ∂G the free-traction boundary conditions are specified, and at infinity the uniform shear stress field is given. The displacement field \mathbf{u} satisfies the following boundary value problem in $\mathcal{B}_\rho = \{(x, y) : x^2 + y^2 < \rho^2\}$ where ρ is sufficiently large and n_j are components of the unit outward normal vector

$$\begin{aligned} \mu \nabla^2 \mathbf{u} + (\lambda + \mu) \nabla \nabla \cdot \mathbf{u} &= 0, & \mathbf{x} \in \mathcal{B}_\rho \setminus \overline{G}, \\ \sigma^{(n)}(\mathbf{u}; \mathbf{x}) &= 0, & \mathbf{x} \in \partial G, \\ \sigma^{(n)}(\mathbf{u}; \mathbf{x}) &= \sigma_{ij}^\infty n_j, & \mathbf{x} \in \partial \mathcal{B}_\rho. \end{aligned} \quad (3.2.1)$$

Following variational technique (see Sokolowski and Zolesio[104]) one defines the energy space $W(\mathcal{B}_\rho \setminus \overline{G})$ for the boundary value problem (3.2.1) and introduces the norm

$$\|\mathbf{u}\|_{\mathcal{B}_\rho \setminus \overline{G}}^2 = \frac{1}{2} \int_{\mathcal{B}_\rho \setminus \overline{G}} \sigma_{ij} \varepsilon_{ij} dx, \quad (3.2.2)$$

The elastic potential energy of the region which is bounded by $\partial \mathcal{B}_\rho$ can be evaluated as a difference between the total strain energy (3.2.2) and the work of external forces (see Sokolnikoff [103], p.384)

$$\mathcal{E}(\mathbf{u}; \mathcal{B}_\rho \setminus \overline{G}) = \|\mathbf{u}\|_{\mathcal{B}_\rho \setminus \overline{G}}^2 - \int_{\partial \mathcal{B}_\rho} \sigma_{ij}^\infty n_j u_i ds, \quad (3.2.3)$$

One remarks that the work of external forces on the boundary ∂G and external body forces is zero due to (3.2.1). The solution of the boundary value problem (3.2.1) minimises the potential energy (3.2.3)

$$\mathcal{E}(\mathbf{u}; \mathcal{B}_\rho \setminus G) = \min_U \mathcal{E}(U; \mathcal{B}_\rho \setminus G), \quad (3.2.4)$$

where U are all possible vector valued fields which provide a finite energy (3.2.3). In a similar way, the potential energy of the homogeneous disk with the radius ρ can be written as

$$\mathcal{E}(\mathbf{u}; \mathcal{B}_\rho) = \|\mathbf{u}\|_{\mathcal{B}_\rho}^2 - \int_{\partial \mathcal{B}_\rho} \sigma_{ij}^\infty n_j u_i ds, \quad (3.2.5)$$

The increment of energy is defined as a difference between two functionals associated with full energy in the homogeneous disk $\mathcal{B}_\rho = \{\mathbf{x} \in \mathbb{R}^2 : \|\mathbf{x}\| < \rho\}$ and in the disk \mathcal{B}_ρ weakened by the cavity G

$$\begin{aligned} \delta W_{G; \sigma_{ij}^\infty} &= \lim_{\rho \rightarrow \infty} \{\mathcal{E}(\mathbf{u}; \mathcal{B}_\rho \setminus \overline{G}) - \mathcal{E}(\mathbf{u}; \mathcal{B}_\rho)\} \\ &= \lim_{\rho \rightarrow \infty} \left(-\frac{1}{2} \int_{\mathcal{B}_\rho \setminus \overline{G}} \sigma_{ij} \varepsilon_{ij} dx + \frac{1}{2} \int_{\mathcal{B}_\rho} \sigma_{ij}^\infty \varepsilon_{ij}^\infty dx \right), \end{aligned} \quad (3.2.6)$$

where $\sigma_{ij}^\infty, \varepsilon_{ij}^\infty$ are components of the stresses and the strains tensors in the homogeneous disk, and $\sigma_{ij}, \varepsilon_{ij}$ are the stresses and strains in the disk \mathcal{B}_ρ with the cavity G .

Optimization problem. The main objective is to find the shape of the cavity which provides the minimal absolute value of the energy increment. Note that the energy increment is negative for the disk with a cavity. The constraints of the fixed area and boundness of the domain are imposed. The optimization problem can be formulated in the following form: find a bounded domain G^* of a fixed area such that

$$\boxed{\delta W_{G^*; \sigma_{ij}^\infty} = \max_G \delta W = \max_G \lim_{\rho \rightarrow \infty} \left\{ \min_U \mathcal{E}(U; \mathcal{B}_\rho \setminus G) - \min_U \mathcal{E}(U; \mathcal{B}_\rho) \right\}}, \quad (3.2.7)$$

where the maximum for G is taken over all simply connected bounded domains of a given area. Let one now discuss the set of admissible minimisers. An infinite plane with an arbitrary single cavity can be mapped to the exterior of the unit disk by the conformal mapping of the form

$$\omega(\xi) = R \left[\frac{1}{\xi} + \sum_{n=1}^{\infty} c_n \xi^n \right], \quad (3.2.8)$$

where R and c_n are constants. The constraint of the fixed area can be written in terms of the conformal mapping coefficients

$$S(G) = \pi R^2 \left(1 - \sum_{n=1}^{\infty} n |c_n|^2 \right) = \text{const.} \quad (3.2.9)$$

One determines the set of admissible cavities by their coefficients R and c_n of conformal mapping to the unit disc. The optimization problem becomes:

Find the set of coefficients R and c_n from (3.2.8) restricted by (3.2.9) such

Applying this condition to our formulation with a pure shear prescribed at infinity, one can observe that it is impossible to have $\sigma_{tt} = \text{const}$ on all parts of boundary. To resolve this contradiction it has to be assumed that σ_{tt} is piece-wise constant function taking values c and $-c$. The points of discontinuity of σ_{tt} must correspond to irregularities of the boundary. Thus one must conclude that the optimal cavity is necessarily bounded by a non-smooth curve. In section 3.6 one will compute the angle at the corners using asymptotic analysis of a stress field near the corner.

Related optimal composites. The possible approach to calculation of the optimal energy of a body with cavities is the following. Consider a periodic structure with cavities, which is characterized by the volume fraction f and by the shape of cavities. The effective compliance tensor $\mathbf{S}^*(f)$ of such a structure can be evaluated and one can find the bounds for the effective shear and bulk moduli which are independent of the cavities shape. The bounds (obtained by Gibiansky and Cherkaev [28], Milton [69]) are proved to be exact, and they correspond to the “second rank” matrix laminates.

Suppose that the optimal composite with a small volume fraction $f \ll 1$ of cavities occupies the volume A and subject to a uniform average stress field $\boldsymbol{\sigma}$ due to an external loading. The total volume of the cavities is equal to fA . The energy change associated with the cavity can be obtained as

$$\delta W = \left(\boldsymbol{\sigma} : \frac{\partial}{\partial f} \mathbf{S}^*(f) \Big|_{f=0} : \boldsymbol{\sigma} \right) fA. \quad (3.2.13)$$

Using the explicit formula for the energy of the optimal composite derived by Gibiansky and Cherkaev [28] one can evaluate the increment

$$\delta W = \begin{cases} \Upsilon c(\sigma_1 + \sigma_2)^2, & \sigma_1 \sigma_2 \geq 0, \\ \Upsilon c(\sigma_1 - \sigma_2)^2, & \sigma_1 \sigma_2 \leq 0, \end{cases} \quad (3.2.14)$$

where $\Upsilon = -(2\mu + \lambda)/(4\mu(\lambda + \mu))$, λ and μ are the Lamé elastic moduli, and σ_1, σ_2 are the principal stresses.

It should be noted that this approach does not pose any restrictions to the connectness of the elastic domain. Therefore, one could expect that the cost of the optimal problem will be greater when an additional restriction – single-connectness of cavities is imposed.

3.3 Minimization technique

This optimization problem can be reduced to minimisation of a function of several variables. The unknown variables are the coefficients of the conformal mapping subject to the restriction $|c_n| < 1/\sqrt{n}$ according to (3.2.9). Our purpose is to find the set of conformal mapping coefficients $\{c_n\}$ minimising the absolute value of the energy increment (3.2.10). In other words, the problem reduces to multi-dimensional minimisation of a function f of $2N$ variables (the conformal mapping coefficients are complex). To do this, one uses the downhill simplex method (see Press et al [91] and section 3.7 for more details).

The calculation confirms that the optimal construction for a uniform loading ($\sigma_{11} = \sigma_{22}$) is a circular cavity and the optimal construction for a uniaxial loading is a crack oriented along the loading line. For the case of composition of two uniaxial loadings of the same sign the optimal shape will be the ellipse oriented along the direction corresponding to the maximal principal stress and specified by the following conformal map (Vigdergauz [116])

$$\omega(\xi) = R \left[\xi + \left(\frac{a-b}{a+b} \right) \frac{1}{\xi} \right], \quad \frac{a}{b} = \frac{\sigma_{11}}{\sigma_{22}}, \quad (3.3.15)$$

where a and b are semi-axes of the ellipse, and σ_{11}, σ_{22} are principal stresses of the same sign.

The energy increment associated with the optimal elliptical cavity of the unit area can be estimated as in Gibiansky and Cherkaev [28]

$$\delta W^{opt} = -\frac{\lambda + 2\mu}{4\mu(\lambda + \mu)}(\sigma_1 + \sigma_2)^2. \quad (3.3.16)$$

The properties of the optimal field for ($\sigma_1\sigma_2 \geq 0$) reduce to the constant dilatation (or constant first invariant of the stress tensor) in the exterior domain and the constant tangential stress on the cavity boundary. In the next section we describe our results for the remaining case when $\sigma_1\sigma_2 < 0$.

3.4 Optimal shape of the cavity

In this section the complex variable technique is used to compute the shape of the optimal cavity that gives minimum for the absolute value of the energy increment in

the state of a shear loading applied at infinity. First, one applies the minimization procedure of Section 3.3 and evaluates numerically the values of the coefficients of the conformal mapping function. Then, this mapping function is used to solve the direct elasticity problem for an optimal domain.

3.4.1 Optimization of the shape by the direct method

Now consider the cavity under a shear loading. The optimal bound for the energy increment is well known (see, for example, Gibiansky and Cherkhev [28]). It corresponds to the multiply connected laminated composites

$$\delta W^{opt} = -\frac{\lambda + 2\mu}{4\mu(\lambda + \mu)} [(\sigma_{11} - \sigma_{22})^2 + 4\sigma_{12}^2]. \quad (3.4.1)$$

The calculations show that the absolute value of the energy increment for a circular cavity is two times greater than the optimal one (3.4.1). Our aim is to find the geometry of the region, which is specified by a smaller energy change than the circular cavity and which is the best among simply-connected domains.

Using the exact representation for the energy increment (3.2.10) together with the minimisation procedure, we find, for $N = 3$,

$$\omega(\xi) = R \left(\frac{1}{\xi} + \frac{\sqrt{2} - 1}{3} \xi^3 \right). \quad (3.4.2)$$

Here the constant R is chosen in such a way that the cavity has a unit area.

Increasing the number of terms in (3.2.8) and taking into account 7th, 11th, 15th and 19th terms we calculate the non-zero conformal mapping coefficients c_n for the optimal domain (see Figure 3-1). The approximate values of c_n are given in Table 1.

Coefficients	$N = 19$	$N = 15$	$N = 11$	$N = 7$	$N = 3$
c_3	0.14445	0.14420	0.14372	0.14251	0.13814
c_7	0.01699	0.01683	0.01652	0.01575	
c_{11}	0.00552	0.00539	0.00513		
c_{15}	0.00250	0.00239			
c_{19}	0.00133				

Table 1. Coefficients of the conformal mapping obtained by the optimization procedure.

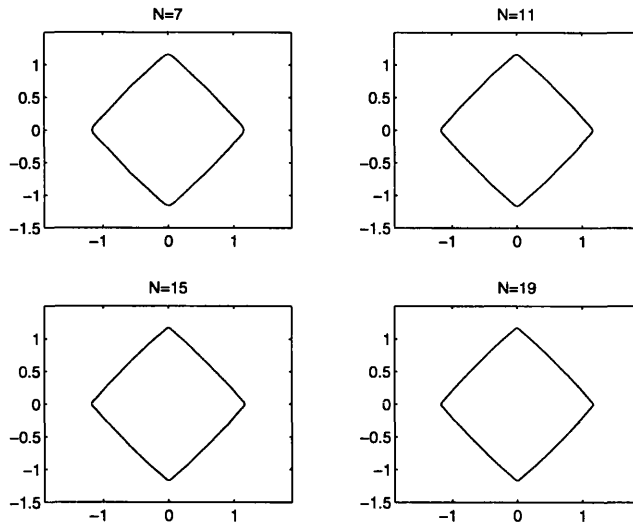


Figure 3-1: The shape of the optimal cavity.

The energy increment for such a domain can be specified as

$$\Delta\mathcal{E} = -\mathcal{K} \frac{\sigma_{12}^2(\lambda + 2\mu)}{2\mu(\lambda + \mu)}, \quad (3.4.3)$$

where the coefficient \mathcal{K} is given in Table 2 as a function of the number N of conformal mapping coefficients.

The number N of coefficients	Coefficient \mathcal{K}
3	3.72792
7	3.71725
11	3.71532
15	3.71473
19	3.71449

Table 2. The dependence of \mathcal{K} on the number of coefficients in the conformal mapping series.

For a circular cavity under pure shear the coefficient \mathcal{K} in the formula (3.4.3) is equal to 4, while the absolute minimum value is 2, as follows from (3.4.1). One can see (Figure 3-1) that the number of coefficients is increased then the optimal domain approaches what looks like a square.

Note that an interesting case arises for non-pure shear. It has been found that the optimal cavity is close to a rectangular one with the sides ratio given in Figure 3-2. The

that the cavity defined by (3.2.8) minimizes (3.2.7).

In other words the goal is to find an optimal single-connected cavity rather than an array of smaller cavities of the same area.

Representation of the energy increment. It is convenient to represent the energy increment in terms of "polarization" tensor (see Babich et al [3], Zorin, Movchan and Nazarov [127]) for precise proof of this representation)

$$\delta W = \frac{1}{2} \boldsymbol{\varepsilon} : \boldsymbol{\mathcal{P}} : \boldsymbol{\varepsilon}, \quad (3.2.10)$$

where \mathcal{P}_{ijkl} , $i, j, k, l = 1, 2$, is the 4-th order "polarization" tensor (also called Pólya-Szegö tensor [90]). It has the same symmetry properties as the Hooke's tensor C_{ijkl} . Namely,

$$\mathcal{P}_{ijkl} = \mathcal{P}_{jikl} = \mathcal{P}_{ijlk} = \mathcal{P}_{klij},$$

and the number of independent elements is six for 2D geometry. The "polarisation" tensor characterizes the remote displacement field associated with the presence of the cavity G . It also characterises the morphology of the cavity and elastic constants of the material. The explicit formulae for the tensor $\boldsymbol{\mathcal{P}}$ corresponding to a single cavity are presented in section 2.2.1 in terms of the coefficients of the conformal mapping (3.2.8). Thus, the mathematical formulation of the optimality problem reduces to the maximization problem for the function of N variables

$$\begin{aligned} \max \quad & (\boldsymbol{\varepsilon} : \boldsymbol{\mathcal{P}} : \boldsymbol{\varepsilon}). \\ c_n, n = 1..N & \\ \text{area}(G) \text{ is fixed} & \end{aligned} \quad (3.2.11)$$

Necessary conditions of optimality. The stationarity conditions for the optimal boundary ∂G are derived using the variational scheme (see Courant and Hilbert [21]). This condition states that an energy density must be constant along the boundary ∂G . For the case of a cavity with zero tractions specified on the boundary, this implies that the only non-zero component of stress $\sigma_{tt} = \boldsymbol{\sigma} : \mathbf{t} \otimes \mathbf{t}$ must be of a constant absolute value on the cavity contour, where \mathbf{t} denotes the unit tangent to the contour:

$$|\sigma_{tt}| = c = \text{const} \quad \text{on an optimal boundary.} \quad (3.2.12)$$

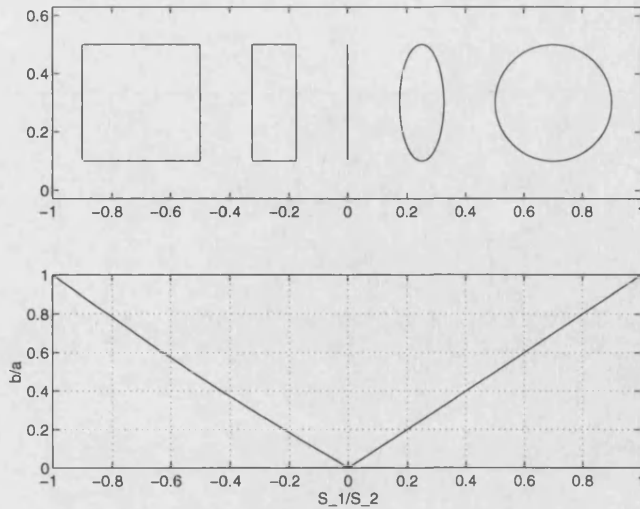


Figure 3-2: Geometry of the optimal cavity as the function of applied stresses.

ratio of the energy increment and the optimal energy (3.4.1) is presented in Figure 3-3. One can see that simply connected inclusions (holes) are not optimal (in sense of lower bound on energy (3.2.14)) when $\sigma_1\sigma_2 < 0$.

The result discussed in this section can be briefly summarised in the following lemma:

Lemma 3.1 *In the state of plane strain in an infinite plane there exists a finite size optimal cavity. It has the following main properties:*

- *Elastic energy in such a plane is maximal among all other planes with different cavities of the same area.*
- *On the boundary of the optimal cavity the condition of the piece-wise tensile stresses hold $|\sigma_{tt}| = \text{const}$.*
- *This cavity is specified in terms of conformal mapping (3.2.8) with the coefficients given in Table 1.*

3.4.2 Properties of the optimal hole

In this section the Kolosov-Muskhelishvili potentials ϕ and ψ are used to represent elastic fields in the exterior of the hole (Muskhelishvili [83]). The components of the displacement vector $(u_1, u_2)^t$ are given by

$$u_1 + iu_2 = \left(\frac{1}{k} + \frac{1}{2\mu}\right)\varphi(z) - \frac{1}{2\mu}(\bar{\psi}(z) + z\bar{\Phi}(z)), \quad k = \lambda + \mu, \quad (3.4.4)$$

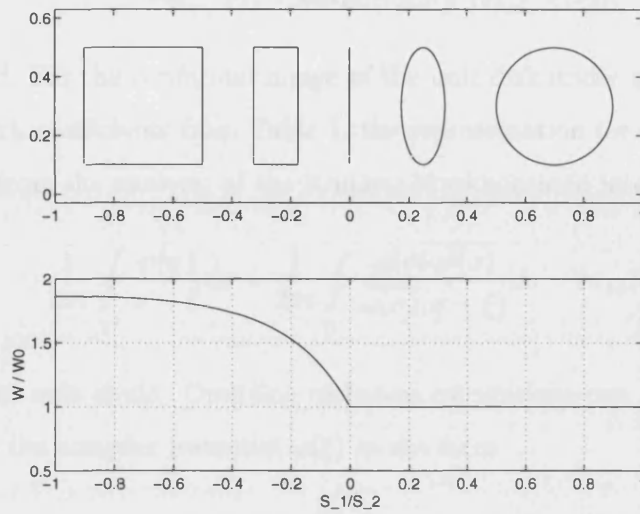


Figure 3-3: The normalized energy change versus applied stress.

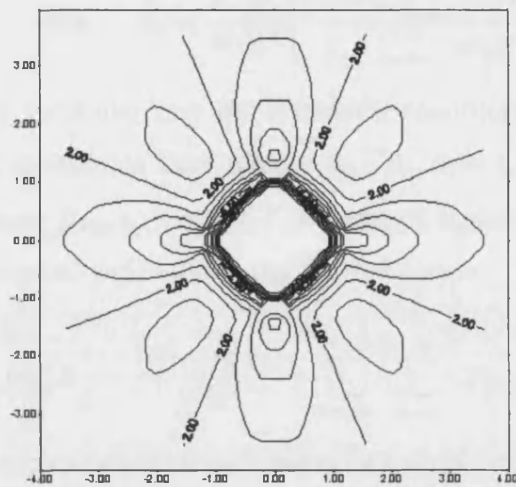


Figure 3-4: The distribution of the energy density for the optimal domain.

where $\Phi = \varphi'$. The elements of the associated stress σ are given by

$$\begin{aligned}\sigma_{11} + \sigma_{22} &= 4\operatorname{Re}\Phi(z), \\ \sigma_{22} - \sigma_{11} + 2i\sigma_{12} &= 2(\bar{z}\Phi'(z) + \Psi(z)),\end{aligned}\tag{3.4.5}$$

where $\Psi = \psi'$. For the conformal image of the unit disk under the mapping $\omega(\xi)$ given by (3.2.8) with coefficients from Table 1, the representation for complex potentials can be obtained from the analysis of the Kolosov-Muskhelishvili integral equation

$$\frac{1}{2\pi i} \oint_{\gamma} \frac{\varphi(\sigma)}{\sigma - \xi} d\sigma + \frac{1}{2\pi i} \oint_{\gamma} \frac{\omega(\sigma)\overline{\varphi'(\sigma)}}{\omega(\sigma)(\sigma - \xi)} d\sigma - i\sigma_{12}R\xi = 0,\tag{3.4.6}$$

where γ is the unit circle. Omitting technical calculations one writes the series representation for the complex potential $\varphi(\xi)$ in the form

$$\varphi(\xi) = \sum_{m=1}^N \beta_m \xi^m, \quad |\xi| \leq 1,\tag{3.4.7}$$

where the coefficients β_m solve the linear system:

$$\beta_m - \sum_{n=1}^{N-m-1} \rho_{N-m-n-1} n \bar{\beta}_n - i\sigma_{12}^{\infty} R \delta_{m1} = 0, \quad m = \overline{1, N},$$

$$\text{with } \rho_k = \frac{1}{k!} \frac{d^k}{d\xi^k} \left[\frac{\xi^{N+1} + \sum_{n=1}^N c_n \xi^{N-n}}{1 - \sum_{n=1}^N n \bar{c}_n \xi^{n+1}} \right] \Big|_{\xi=0}.$$

Note that in our particular case the symmetry conditions yield that all non-zero conformal mapping coefficients have indices $4n - 1$, $n = 1, 2, 3, \dots$. They correspond to non-zero coefficients β_{4n-3} , $n = 1, 2, 3, \dots$, and all remaining coefficients vanish.

The complex potential $\psi(\xi)$ admits the representation

$$\psi(\xi) = i\sigma_{12}^{\infty} R \frac{1}{\xi} - \frac{\bar{\omega}(1/\xi)\varphi'(\xi)}{\omega'(\xi)} - \sum_{m=0}^{N-2} \sum_{n=1}^{N-m-1} \bar{\rho}_{N-m-n-1} n \beta_n \frac{1}{\xi^m}.\tag{3.4.8}$$

Note that the complex potential $\psi(\xi)$ has only a simple pole at the origin (the first term in representation (3.4.8)). At the same time the third term in (3.4.8) compensates the singular part from the second term, resulting in ψ to have the pole of order one only.

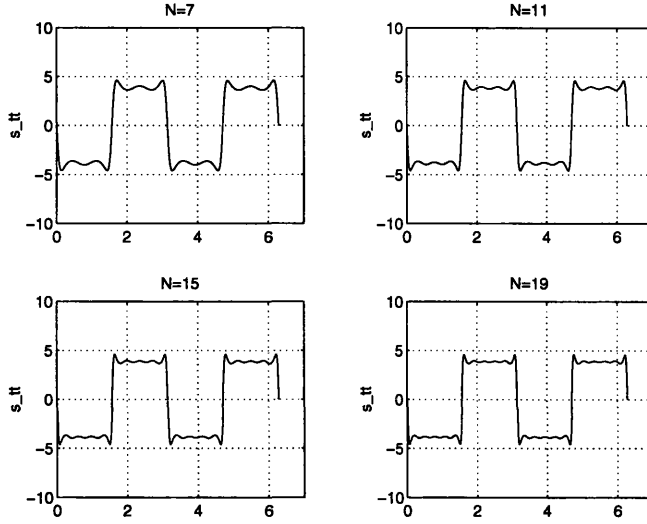


Figure 3-5: The tangential stress on the boundary.

For example, for $N = 3$ we obtain

$$\varphi(\xi) = \frac{3}{2 + \sqrt{2}} i \sigma_{12}^{\infty} R \xi, \quad |\xi| \leq 1,$$

$$\psi(\xi) = i R \sigma_{12}^{\infty} \left(\frac{1}{\xi} + \frac{\xi^3 (6 - 2\sqrt{2})}{(2 + \sqrt{2})(\xi^4 (1 - \sqrt{2}) + 1)} \right). \quad (3.4.9)$$

Taking into account the representation for stress components in terms of the complex potentials

$$\sigma_{11} + \sigma_{22} = 2 \left(\frac{\varphi'(\xi)}{\omega'(\xi)} + \overline{\frac{\varphi'(\xi)}{\omega'(\xi)}} \right),$$

$$\sigma_{22} - \sigma_{11} + 2i\sigma_{12} = 2 \left(\overline{\omega(\xi)} \frac{\varphi''(\xi)\omega'(\xi) - \varphi'(\xi)\omega''(\xi)}{\omega'(\xi)^3} + \frac{\psi'(\xi)}{\omega'(\xi)} \right), \quad (3.4.10)$$

one calculates the hydrostatic $\sigma_{11} + \sigma_{22}$ and deviatoric $\sigma_{22} - \sigma_{11} + 2i\sigma_{12}$ parts of the stress tensor. In Figure 3-4 the energy density of the elastic field is presented for the domain described by (3.4.2). Using (3.4.7) and (3.4.8), one calculates the tangential stress σ_{tt} on the boundary for different number of terms in the conformal mapping function (Table 1). The results are presented in Figure 3-5 for $N = 7, 11, 15, 19$. It is possible to see that the modulus of the tangential stress is constant along the contour except in a small neighbourhood of corners where it vanishes. The diameter of this neighbourhood vanishes as we increase N . *This observation confirms that the necessary condition of optimality (3.2.12) is satisfied for our domain under pure shear.*

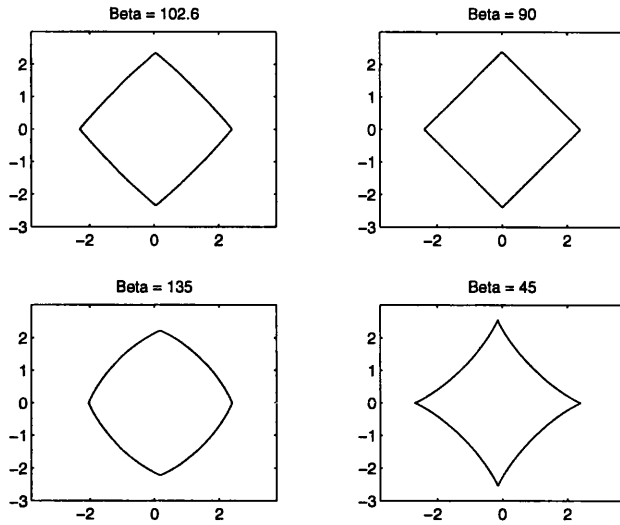


Figure 3-6: The regions obtained by the "modified" conformal mapping

Now one can consider the corners of the optimal hole. The Christoffel-Schwartz integral (Savin [97])

$$\begin{aligned} \omega(\xi) &= R \int_1^\xi \frac{\sqrt{t^4 - 1}}{t^2} dt = R \left(\frac{1}{\xi} + \frac{\xi^3}{6} + \frac{\xi^7}{56} + \frac{\xi^{11}}{176} + \frac{\xi^{15}}{384} + \frac{7\xi^{19}}{4864} + \dots \right) \\ &= R \left(\frac{1}{\xi} + 0.16667\xi^3 + 0.01786\xi^7 + 0.00568\xi^{11} + 0.00260\xi^{15} + \dots \right) \end{aligned}$$

specifies the mapping of the unit disk to the exterior of a square.

The slightly modified conformal mapping

$$\omega(\xi) = R \int_1^\xi \frac{(t^4 - 1)^\alpha}{t^2} dt, \quad \alpha = 1 - \beta\pi^{-1}, \quad (3.4.11)$$

where β is different from $\pi/2$, corresponds to a transformation of the unit disk to a symmetric domain with the angle β near the corners (see Figure 3-6). The opening angle near the vertex of the point $\xi = 1$ can be calculated as

$$\begin{aligned} \beta &= \pi - \left[\arg \omega'(\xi) \Big|_{\xi \rightarrow 1-0i} - \arg \omega'(\xi) \Big|_{\xi \rightarrow 1+0i} \right] \\ &= \pi - \left(\lim_{\xi \rightarrow 1-0i} \frac{(t^4 - 1)^\alpha}{t^2} - \lim_{\xi \rightarrow 1+0i} \frac{(t^4 - 1)^\alpha}{t^2} \right) = \pi - \left(\frac{3\pi\alpha}{2} - \frac{\pi\alpha}{2} \right). \end{aligned}$$

The remaining three angles (near the points $\xi = i, -1, -i$) have the same values. Chang-

ing β one can find the conformal mapping function which is in good agreement with the results of the optimization procedure. If we choose $\beta_* = 102.6^\circ$ then (3.4.11) can be rewritten in the form

$$\omega(\xi) = R \left(\frac{1}{\xi} + 0.14343\xi^3 + 0.01751\xi^7 + 0.00585\xi^{11} + 0.00275\xi^{15} + \dots \right),$$

which agrees with Table 1. This suggests that the quantity β_* is the critical angle in the Carothers problem [105] (more detailed discussion is presented in Section 3.6, where one shows that this is not an accidental agreement).

3.5 Solution of the inverse problem

The objective of this section is to solve the inverse problem: to find the shape of the quadrilateral G from the condition $\sigma_{tt} = c$ or $-c$ on the boundary. One does not refer to the energy evaluation. However, it is shown that the results of the two approaches coincide.

The Kolosov-Muskhelishvili representation of the boundary condition

$$\sigma^{(n)}(\mathbf{u}; \mathbf{x}) = 0, \quad \mathbf{x} \in \partial G,$$

in terms of complex potentials φ and ψ can be written in the form

$$\varphi(z) + z\overline{\varphi'(z)} + \overline{\psi(z)} = 0, \quad z \in \partial G. \tag{3.5.1}$$

Under a pure shear loading the potentials tend to infinity as the following functions

$$\varphi(z) \rightarrow 0, \quad |z| \rightarrow \infty,$$

$$\psi(z) \rightarrow i\sigma_{12}z, \quad |z| \rightarrow \infty.$$

After mapping the exterior of G onto the interior of the unit disc by the conformal mapping $z = \omega(\xi)$, one can rewrite the integral equation (3.4.6) for the potential φ

$$\varphi(\xi) + \frac{1}{2\pi i} \oint_{\gamma} \frac{\omega(\sigma)\overline{\Phi(\sigma)}}{\sigma - \xi} d\sigma - i\sigma_{12}R\xi = 0, \tag{3.5.2}$$

where $\Phi(\sigma) = \frac{\varphi'(\sigma)}{\omega'(\sigma)}$, and $\omega(\sigma)$ is the conformal mapping function. The boundary of the

unit disk is denoted by γ . The condition of the piece-wise constant tangential stresses on the boundary is applied and the conditions (3.2.12) is rewritten as

$$\sigma_{tt} = 4Re \varphi'(z) = 4Re \Phi(\xi) = \pm 4A, \quad z \in \partial G, \quad (3.5.3)$$

where $c = 4A$ is an unknown constant. The unit circle $|\xi| = 1$ is the image of the boundary. The points $1, i, -1, -i$ in the ξ -plane map to the corners of the domain G in z -plane. Therefore

$$Re \Phi(e^{i\alpha}) = \begin{cases} A, & \alpha \in (0, \frac{\pi}{2}) \cup (\pi, \frac{3\pi}{2}), \\ -A, & \alpha \in (\frac{\pi}{2}, \pi) \cup (\frac{3\pi}{2}, 2\pi). \end{cases} \quad (3.5.4)$$

Using the Schwartz formula that recovers the holomorphic function in the unit disk by the values of its real part on the boundary, we obtain

$$\Phi(\xi) = \frac{2}{\pi} Ai \ln \frac{1 - \xi^2}{1 + \xi^2}, \quad |\xi| \leq 1. \quad (3.5.5)$$

Expression (3.5.5) is the explicit representation for the complex potential $\Phi(\xi)$ satisfying the condition (3.2.12).

Taking the derivative of (3.5.2) and using the identity $\overline{\Phi(\sigma)} = 2Re \Phi(\sigma) - \Phi(\sigma)$ and the expression for the derivative of the Cauchy integral, the integral equation (3.5.2) reduces to

$$\Phi(\xi)\omega'(\xi) + \frac{1}{\pi i} \oint_{\gamma} \frac{\omega(\sigma)Re \Phi(\sigma)}{(\sigma - \xi)^2} d\sigma - \frac{1}{2\pi i} \oint_{\gamma} \frac{\omega(\sigma)\Phi(\sigma)}{(\sigma - \xi)^2} d\sigma = \frac{1}{2} R \operatorname{dev} \sigma^{\infty}, \quad (3.5.6)$$

where $\operatorname{dev} \sigma = \sigma_{22} - \sigma_{11} + 2i\sigma_{12}$.

Using the expression (3.5.4) for the real part of the potential $\Phi(\xi)$ and formulae for the derivatives of the Cauchy integral, one represents the integrals on the left hand side of (3.5.6) in the form

$$\frac{1}{2\pi i} \oint_{\gamma} \frac{\omega(\sigma)\Phi(\sigma)}{(\sigma - \xi)^2} d\sigma = \frac{d}{d\xi} \{\omega(\xi)\Phi(\xi)\}$$

and

$$\frac{1}{2\pi i} \oint_{\gamma} \frac{\omega(\sigma)Re \Phi(\sigma)}{(\sigma - \xi)^2} d\sigma = \frac{A}{2\pi i} \left(\int_{\gamma_1} \frac{\omega(\sigma)}{(\sigma - \xi)^2} d\sigma - \int_{\gamma_2} \frac{\omega(\sigma)}{(\sigma - \xi)^2} d\sigma \right)$$

$$\begin{aligned}
 & + \int_{\gamma_3} \frac{\omega(\sigma)}{(\sigma - \xi)^2} d\sigma - \int_{\gamma_4} \frac{\omega(\sigma)}{(\sigma - \xi)^2} d\sigma = \frac{4i A \omega(1)}{\pi(\xi^4 - 1)} \\
 & + \frac{A}{2\pi i} \left(\int_{\gamma_1} \frac{\omega'(\sigma)}{\sigma - \xi} d\sigma - \int_{\gamma_2} \frac{\omega'(\sigma)}{\sigma - \xi} d\sigma + \int_{\gamma_3} \frac{\omega'(\sigma)}{\sigma - \xi} d\sigma - \int_{\gamma_4} \frac{\omega'(\sigma)}{\sigma - \xi} d\sigma \right),
 \end{aligned}$$

where $\gamma_1, \gamma_2, \gamma_3$ and γ_4 are the arcs of the unit disk between points 1 and i , i and -1 , -1 and $-i$, $-i$ and 1, respectively. After some laborious but simple calculations using the symmetry of the conformal map

$$\omega(i) = -i\omega(1), \quad \omega(-1) = -\omega(1), \quad \omega(-i) = i\omega(1),$$

and the Cauchy formula for the holomorphic function in the unit disk, one obtains the integral equation for the unknown function $\omega(\xi)$, $|\xi| \leq 1$, $\xi \neq 1, i, -1, -i$,

$$\begin{aligned}
 & \frac{8i}{\pi(1 - \xi^4)} \left(\xi\omega(\xi) - \omega(1) \right) - 2 \left(\omega'(\xi) + \frac{R}{\xi^2} \right) \\
 & + \frac{2}{\pi i} \int_1^i \frac{\omega'(\sigma)}{\sigma - \xi} d\sigma + \frac{2}{\pi i} \int_{-1}^{-i} \frac{\omega'(\sigma)}{\sigma - \xi} d\sigma = \frac{R}{2A} \operatorname{dev} \sigma^\infty, \quad (3.5.7)
 \end{aligned}$$

where the integrals are taken over the quarter arcs of the unit circle located in the first and third quadrants respectively. Now one represents the conformal mapping function ω by the Laurent expansion about the origin

$$\omega(\xi) = R \left(\frac{1}{\xi} + \sum_{m=1}^{\infty} c_m \xi^m \right) = R \left(\frac{1}{\xi} + c_3 \xi^3 + c_7 \xi^7 + c_{11} \xi^{11} + \dots \right). \quad (3.5.8)$$

The function $\frac{\xi\omega(\xi)}{1 - \xi^4}$ can be represented as the Taylor series

$$\begin{aligned}
 & \frac{1}{1 - \xi^4} = \sum_{k=0}^{\infty} \xi^{4k}, \\
 & \frac{\xi\omega(\xi)}{1 - \xi^4} = R \sum_{k=0}^{\infty} \xi^{4k} + R \sum_{k=0}^{\infty} \left(\sum_{m=1}^k c_{4m-1} \right) \xi^{4k},
 \end{aligned}$$

Integrands in (3.5.7) admit the series expansion in different powers of ξ

$$\frac{\omega'(\sigma)}{\sigma - \xi} = \omega'(\sigma) \sum_{k=0}^{\infty} \frac{1}{\sigma^{k+1}} \xi^k.$$

3.6. ASYMPTOTIC EXPANSION OF THE OPTIMAL SOLUTION NEAR THE
CORNERS

After term by term integration of the series and collecting the coefficients near the same powers of ξ , we obtain

$$\int_1^i \frac{\omega'(\sigma)}{\sigma - \xi} d\sigma + \int_{-1}^{-i} \frac{\omega'(\sigma)}{\sigma - \xi} d\sigma = -R \sum_{k=0}^{\infty} \frac{2\xi^{4k}}{2k+1} - R \sum_{k=0}^{\infty} \left(\sum_{m=1}^{\infty} c_{4m-1} \frac{2(4m-1)}{2m-2k-1} \right) \xi^{4k}.$$

Finally, after truncation of the expansion (3.5.8) by the highest power $4N-1$, the linear system of equations for the coefficients $c_{4m-1}, m = 1..N$ is obtained

$$\sum_{m=1}^N \frac{2(4m-1)}{2(m-n)-1} c_{4m-1} - 4 \sum_{m=n+1}^N c_{4m-1} + \frac{2}{2n+1} = 0, \quad n = 1..N. \quad (3.5.9)$$

Table 3 shows the values of conformal mapping coefficients c_m for different N . Those data are consistent with Table 1.

	$N = 100$	$N = 19$	$N = 15$	$N = 11$	$N = 7$	$N = 3$
c_3	0.14484	0.13940	0.13759	0.13448	0.12825	0.11111
c_7	0.01727	0.01511	0.01437	0.01306	0.01034	
c_{11}	0.00575	0.00435	0.00385	0.00288		
c_{15}	0.00271	0.00164	0.00119			
c_{19}	0.00152	0.00061				

Table 3. Coefficients of conformal mapping obtained as the solution of the inverse problem

Next section is devoted to investigation of the domain boundary near the corner. One shows that the corner angle is equal to the critical Carothers value (see Carothers [105], Markenscoff [60]).

3.6 Asymptotic expansion of the optimal solution near the corners

The results of the previous section show that any finite series of conformal map corresponds to an analytical boundary of the cavity. Thus, one needs a different technique to deal with the fields near the assumed corners on the boundary of the optimal cavity and we need to demonstrate that the necessary conditions are satisfied almost everywhere. Consider the infinite plane with the corner point and the opening angle close to $\pi/2$.

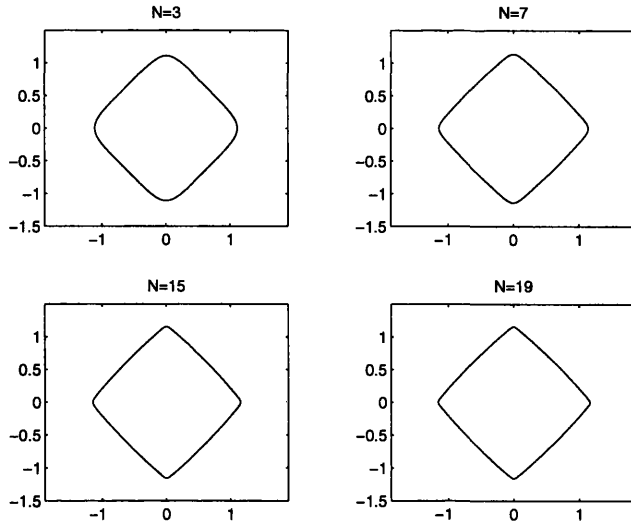


Figure 3-7: The shape of domain with piece-wise constant tangential stresses on the boundary.

The exterior of the corner is filled by an isotropic elastic material, and zero traction boundary conditions are specified on the boundary. Such problem can explain the behaviour of the boundary near the corner points.

One looks for a solution of specified boundary value problem using the Airy stress function $U(r, \theta)$ written in polar coordinates. This method is well presented in literature (see, for example, Muskhelishvili [83], Sokolnikoff [103]). The Airy stress function satisfies biharmonic equation

$$\nabla^2 \nabla^2 U(r, \theta) = 0, \quad (r, \theta) \in \Omega.$$

The components of the stress field in polar coordinates associated with the corner point are represented in the following form

$$\sigma_{rr} = \frac{1}{r^2} \frac{\partial^2 U}{\partial \theta^2} + \frac{1}{r} \frac{\partial U}{\partial r}, \quad \sigma_{\theta\theta} = \frac{\partial^2 U}{\partial r^2}, \quad \sigma_{r\theta} = -\frac{1}{r} \frac{\partial^2 U}{\partial r \partial \theta} + \frac{1}{r^2} \frac{\partial U}{\partial \theta}. \quad (3.6.1)$$

The polar displacements in the radial and circumferential directions are given by

$$\begin{aligned} 2\mu u_r &= -\frac{\partial U}{\partial r} + \frac{1}{4}(\nu + 1)r \frac{\partial \chi}{\partial \theta}, \\ 2\mu u_\theta &= -\frac{1}{r} \frac{\partial U}{\partial \theta} + \frac{1}{4}(\nu + 1)r^2 \frac{\partial \chi}{\partial r}, \end{aligned} \quad (3.6.2)$$

where χ is the harmonic function related to the Airy function by

$$\nabla^2 U = \frac{\partial}{\partial r} \left(r \frac{\partial \chi}{\partial \theta} \right).$$

The boundary value problem imposed in an infinite plane with corner point can be characterized by the Airy function of the following structure (Williams [121])

$$U(r, \theta) = r^{\Lambda_i+1} \{ b_1 \sin(\Lambda_i + 1)\theta + b_2 \sin(\Lambda_i - 1)\theta + b_3 \cos(\Lambda_i + 1)\theta + b_4 \cos(\Lambda_i - 1)\theta \}, \quad (3.6.3)$$

whereas the harmonic function χ is given by

$$\chi(r, \theta) = r^{\Lambda_i-1} \left\{ -\frac{4}{\Lambda_i-1} b_2 \cos(\Lambda_i - 1)\theta + \frac{4}{\Lambda_i-1} b_4 \sin(\Lambda_i - 1)\theta \right\}, \quad (3.6.4)$$

The eigenvalues Λ_i are uniquely defined by the corner opening and boundary conditions. For the case of homogeneous traction boundary conditions they are calculated as the roots of the equation

$$\sin 2\alpha\Lambda = \pm\Lambda \sin 2\alpha, \quad (3.6.5)$$

where $2\pi - 2\alpha$ is the corner opening. The main interest is in those solutions Λ of (3.6.5) that lie in $(0, 1]$. For the corner openings from the interval $(0, \pi)$ ($\alpha \in (\frac{\pi}{2}, \pi)$), there are at most three solutions $\Lambda_1 < \Lambda_2 \leq \Lambda_3 = 1$ in interval $(0, 1]$. For detailed analysis of the corresponding eigenvalue problem we refer to Karp and Karal [51]. For example, when $\alpha = \frac{3\pi}{4}$ corresponding to opening 90° , there are three real eigenvalues $\Lambda_1 = 0.54448$, $\Lambda_2 = 0.90853$ and $\Lambda_3 = 1$ in the interval $(0, 1]$.

The Airy function corresponding to the first eigenvalue has the form

$$U^{(1)} \sim r^{\Lambda_1+1} \left\{ \cos(\Lambda_1 + 1)\theta - \frac{\cos(\Lambda_1 + 1)\alpha}{\cos(\Lambda_1 - 1)\alpha} \cos(\Lambda_1 - 1)\theta \right\},$$

and satisfies the free-traction boundary conditions on the edges of the corner ($\theta = \pm\alpha$).

The corresponding displacement field in polar coordinate system is represented as

$$\mathbf{u}^{(1)} \sim r^{\Lambda_1} \begin{pmatrix} \cos(\Lambda_1 + 1)\theta + \frac{(\kappa - \Lambda_1) \cos(\Lambda_1 + 1)\alpha}{(\Lambda_1 + 1) \cos(\Lambda_1 - 1)\alpha} \cos(\Lambda_1 - 1)\theta \\ -\sin(\Lambda_1 + 1)\theta + \frac{(\kappa + \Lambda_1) \cos(\Lambda_1 + 1)\alpha}{(\Lambda_1 + 1) \cos(\Lambda_1 - 1)\alpha} \sin(\Lambda_1 - 1)\theta \end{pmatrix}, \quad (3.6.6)$$

$$\text{where } \varkappa = \frac{\lambda + 3\mu}{\lambda + \mu}.$$

These vectors describe the symmetric part of the displacement field. In other words, the displacement component u_r is an even function and the displacement component u_θ is an odd function of θ

$$U^{(2)} \sim r^{\Lambda_2+1} \left\{ \sin(\Lambda_2 + 1)\theta - \frac{\sin(\Lambda_2 + 1)\alpha}{\sin(\Lambda_2 - 1)\alpha} \sin(\Lambda_2 - 1)\theta \right\}.$$

and the corresponding displacement field in polar coordinate system has a form

$$\mathbf{u}^{(2)} \sim r^{\Lambda_2} \begin{pmatrix} \sin(\Lambda_2 + 1)\theta + \frac{(\varkappa - \Lambda_2)\sin(\Lambda_2 + 1)\alpha}{(\Lambda_2 + 1)\sin(\Lambda_2 - 1)\alpha} \sin(\Lambda_2 - 1)\theta \\ \cos(\Lambda_2 + 1)\theta - \frac{(\varkappa + \Lambda_2)\sin(\Lambda_2 + 1)\alpha}{(\Lambda_2 + 1)\sin(\Lambda_2 - 1)\alpha} \cos(\Lambda_2 - 1)\theta \end{pmatrix}, \quad (3.6.7)$$

and represents a skew-symmetric field (u_r is odd and u_θ is even).

The main interest is in the displacement field corresponding to the second eigenvalue Λ_2 (skew-symmetric field). Only this field occurs in the vicinity of the corner under the shear loading at infinity because of the symmetry of the problem. The displacement field (3.6.7) produces singularity at the vertex of the corner and the non-zero radial stress component on the boundary

$$\sigma_{rr} \sim \pm 4\Lambda_2 r^{\Lambda_2-1} \sin(\Lambda_2 + 1)\alpha. \quad (3.6.8)$$

The intention is to find such an angle α at which the singularity vanishes. Note that the third eigenvalue $\Lambda_3 = 1$ produces zero stress field. The free-traction conditions lead to b_1, b_2, b_3, b_4 being equal to zero in (3.6.3). The displacement field corresponding to this situation is the rigid body rotation field

$$\mathbf{u}^{(3)} \sim \begin{pmatrix} 0 \\ r \end{pmatrix}. \quad (3.6.9)$$

It is similar to the situation which occurs in the problem of the optimal cavity. There is no singularity in the vertex of the corner from inside. From outside, if we apply the external stress field (shear loading) that does not vanish at infinity

$$\boldsymbol{\sigma} = \begin{pmatrix} 0 & \sigma_{12} \\ \sigma_{12} & 0 \end{pmatrix},$$

then the radial stress component on the boundary can be found as

$$\sigma_{rr} = \pm\sigma_{12} \sin 2\alpha. \quad (3.6.10)$$

It characterises the piece-wise constant function and agrees with the optimality criterion formulated in the previous sections. Matching (3.6.8) and (3.6.10), one can see that $\Lambda_2 = 1$. In this case the singularity in (3.6.8) disappears. Observe that by decreasing the angle α from 0.75π (corner opening 90°) to $\alpha^* = 0.715\pi$ (corner opening 102.6°), we obtain that the second eigenvalue indeed approaches 1 (see Karp and Karal [51]). The precise value of this angle can be found as the solution of the following transcendental equation

$$\tan 2\alpha^* = 2\alpha^*. \quad (3.6.11)$$

For $\alpha \leq \alpha^$ and a skew-symmetric loading, there is no singularity near the vertex of the corner: the singularity in radial stress component in (3.6.8) vanishes.* For a skew-symmetric loading, the opening $2(\pi - \alpha^*) = 102.6^\circ$ is the critical one (Carothers [105]). Thus one has shown that the singularity in stress is absent near the optimal cavity contour for the case of external shear loading.

3.7 Numerical procedure and existence of the solution

Below one discusses two issues: existence of a solution and the numerical optimisation algorithm (see Sections 3.2 and 3.3). For more detailed analysis we refer to Sokolowski and Zolesio [104] and Press et al [91].

Existence of the solution. To prove the existence of the solution, the second constraint (finite size of the cavity) is essential. Consider a closure of a bounded domain in N -dimensional space (each point of this domain specifies a set of coefficients of the conformal mapping). All unbounded domains are excluded from our consideration as they lead to failure of the second constraint.

Also one excludes the sets of coefficients which lead to self-intersection boundary. Let an N -tuple of coefficients of the conformal mapping provide the boundary with self-intersections. Then so will N -tuples in the sufficiently small neighbourhood of the original point. Thus the region in N -dimensional space describing the boundaries with

self-intersection is open. Hence its complement is closed.

According to Weierstrass theorem such a function has both maximum and minimum (taking into account the condition $\delta W < 0$ which is true for all increments associated with cavities).

Downhill simplex method. has been used in this work is discussed below. The downhill simplex method, optimization method which has been used in earlier calculations requires the values of the function only, and it does not require the derivatives. This simplifies the procedure; it works effectively even for the case when the function we minimise is not specified in the explicit analytical form. It starts not just with a single point, but with $2N + 1$ points, defining an initial simplex in $2N$ -dimensional space. One assumes that the initial starting point P_0 corresponds to a unit circle $\{c_n = 0\}$ and take the other points to be $P_n = P_0 + \lambda_n e_n$, where e_n are $2N$ unit basis vectors and λ_n are constants representing the characteristic length scale along the direction e_n . They are chosen by using the value $1/\sqrt{n}$ (the upper bound for the modulus of the coefficient c_n) as the characteristic length scale.

The basic idea of the downhill simplex method is to compare the values of the function at the $2N + 1$ vertices of the initial simplex and move this simplex towards the minimum during the iterative process. On each step we evaluate the function at all vertices of the simplex and choose the maximal one, say P_m . Then we archive the "reflection" of the point P_m with maximal value of the function via the simplex boundary. It means that we define a new position P_r of the point P_m such that

$$P_r = (1 - \alpha)P_* - \alpha P_m,$$

where $P_* = \frac{1}{2N} \sum_{n=1, n \neq m}^{2N+1} P_n$ is the centroid of all points with the exception of P_m , and α is the reflection coefficient which is the ratio of distance between P_r and P_* and the distance between P_m and P_* .

The reflected point P_r will be on the line joining P_m and P_* on the opposite side of P_* . Repetitive application of the reflection process leads to a step-by-step approaching in the direction of the minimum.

In the particular situation when $f(P_r) > f(P_n)$ for all n except $n = m$ the simplex is contracted along the direction $P_r - P_m$ to P_* . Alternatively, if the reflection produces P_r such that $f(P_r) < f(P_n)$, the simplex is expanding, and we attempt to find a

local minimum on the line $P_r - P_m$ (the one-dimensional gradient method used in this particular situation).

After application of the "expansion" or "contraction" of the simplex we go back to the reflection procedure. The following convergence criterion is used with the simplex method

$$\left(\frac{\sum_{n=1}^{2N+1} [f(P_n) - f(P_*)]^2}{2N+1} \right)^{1/2} < \varepsilon,$$

where ε is a small positive parameter. In this work we used the Numerical Recipes routine "amoeba" Press et al [91] realising the downhill simplex method.

3.8 Conclusions

In this chapter the Pólya-Szegő tensors have been employed to solve the optimization problem. Namely, the shape optimization for a fixed area single cavity in an infinite elastic plane has been considered. This problem is of special interest since with homogenization technique it relates to the optimization of the dilute composites and defines new type of optimal microstructures subjected to shear. The last ones extend known types of structures (Vigdergauz structures, "confocal ellipse" structures by Grabovsky and Kohn, "second rank" laminates by Gibiansky and Cherkaev).

The problem has been studied in the following way. The elastic energy has been written in terms of coefficients of the Pólya-Szegő matrix. Optimization algorithm has used the downhill simplex method together with certain constraints on the coefficients of the conformal mapping. As a result, the shape of the optimal cavity has been specified in terms of conformal mapping coefficients.

Then we investigated the properties of the optimal cavity, such as the tensile stress on the boundary, the properties of the displacement and stress fields outside of the cavity, stress distribution near the corners on the boundary. The results of this analysis confirmed the necessary conditions of optimality and gave the value of the corner angle (the Carothers value).

The inverse problem for shape optimization has been solved. Assuming the energy density was constant on the boundary of the cavity we obtained the set of conformal mapping coefficients and showed an agreement with the direct optimization method.

Chapter 4

Crack-inclusion interaction problem

4.1 Background and motivation

The analysis of failure mechanisms of brittle-composite materials has design applications in a broad range of fields. These include defects-containing, porous, and fibre-reinforced materials. Examples of these materials are ceramic, which may contain flaws or pores, fibrous biological materials, porous rocks, porous high-strength metals at low temperature, and ceramic or metal composites. In other materials, like concrete or certain rocks, stiff inclusions co-exist in a soft matrix with pores and micro-cracks. In this context, fracture propagation is the dominant failure mechanism at the microscale.

It is obvious that fracture propagation is affected by the presence of inhomogeneities, which modify the crack trajectory and, consequently, the toughness of the material. For instance, the toughening effect of a diluted porosity remains controversial (see, e.g. Claussen [19]; Duan, Mai and Cotterell [23], where the porosity consists of small cracks). In fact, on one hand, pores may act as stress concentrators and initiate strain localisation and microcracking between cavities. On the other hand, pores may deviate the crack path from linearity and, when the crack tip intersects a cavity, this may produce a stress release. From the latter point of view, pores yield a shielding effect on crack propagation.

The above discussion elucidates the theoretical and practical relevance of developing analytical models capable of describing the fracture mechanisms in brittle materials containing voids or inclusions. This problem, analyzed numerically by Rose [93] and

Rubinstein [95], is the focus of the Chapter 4. In particular, an asymptotic solution is presented for the trajectory of a crack growing in an elastic-brittle isotropic material under plane strain conditions. With the term “brittle” we mean a material in which the fracture propagates according to the pure Mode I criterion or “criterion of local symmetry”, i.e. $K_{II} = 0$ (Banichuk [5], Goldstein and Salganik [32]). Two perturbed solutions are employed, one of which concerns the modification of the near-tip fields due to a perturbation from rectilinearity in the crack trajectory. In the other perturbed solution, defects are introduced and the modification on the near-tip field is evaluated. The former analysis is similar to some extent to that presented by Cotterell and Rice [20]. The latter analysis has been initiated by Movchan, Nazarov and Polyakova [77] and it is based on the concept of the Pólya-Szegő matrix [90], which characterizes the effect of the inclusion.

Below we apply the asymptotic technique to the crack propagation problem in thermo-elastic media. Fracture propagation in elastic media (no thermal effects) is analysed in the limit case. As a result of the asymptotic analysis, the formulae for the increment in stress intensity factor and for the crack trajectory have been derived.

4.2 Crack geometry and field equations

A quasi-static semi-infinite plane crack is considered, smoothly curved in the portion extending from the tip to a reference point where the crack profile becomes rectilinear, as indicated in Figure 4-1. With respect to a coordinate system with the origin in the reference point and the axis x_1 tangent to the rectilinear crack profile, the crack tip has abscissa l . If the curved portion of the crack is sufficiently regular and close to rectilinearity, it can be treated as perturbation of a straight crack. In this case, the crack geometry can be specified by introducing a smooth function h of x_1 which, multiplied by a perturbation parameter α , specifies the x_2 -coordinate of the curved portion of the crack. The semi-infinite crack is described by the set $M_\alpha(l) := \{(x_1, x_2) : x_1 < l, x_2 = \alpha h(x_1)\}$, with $0 < \alpha \ll 1$. A defect is considered in the form of a cavity or an elastic inclusion, and domain occupied by the defect is G_ε . The position of the defect is arbitrary, in the sense that it can be placed at an arbitrary point, but the ratio between the diameter of the defect and the distance from crack trajectory has to be small enough to allow to use a perturbation technique.

The boundary value problem is formulated as a plane strain problem of thermo-elastic,

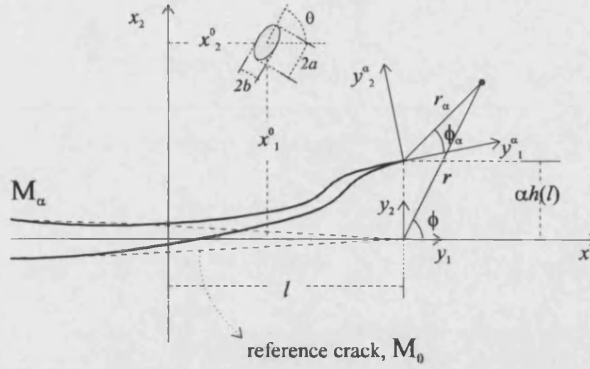


Figure 4-1: Crack geometry

isotropic materials, characterized by the Lamé constants λ , μ for the matrix material, λ_0 , μ_0 for the inclusion G_ε and the thermoelastic constants γ and γ_0 respectively. Alternatively, this region can be specified in terms of Young's modulus E , Poisson ratio ν and thermal expansion coefficient α_t . The following identities relate two possible sets of parameters

$$\mu = \frac{E}{2(1+\nu)}, \quad \lambda = \frac{E\nu}{(1+\nu)(1-2\nu)}, \quad \gamma = 2\alpha_t K = 2\alpha_t(\lambda + \mu),$$

where K is the bulk modulus in the plane strain.

Vectors \mathbf{u} and $\mathbf{u}^{(0)}$ representing the displacement fields in the matrix and inside the defect, respectively, satisfy the Navier equations

$$\begin{aligned} \mathfrak{L}_{xx}(\mathbf{u}; \mathbf{x}) &:= \mu \nabla^2 \mathbf{u} + (\lambda + \mu) \nabla \nabla \cdot \mathbf{u} = \gamma \nabla T(\mathbf{x}), & \mathbf{x} \in \mathbb{R}^2 \setminus \{\overline{G_\varepsilon} \cup M_0\}, \\ \mathfrak{L}_{0,xx}(\mathbf{u}_0; \mathbf{x}) &:= \mu_0 \nabla^2 \mathbf{u}_0 + (\lambda_0 + \mu_0) \nabla \nabla \cdot \mathbf{u}_0 = \gamma_0 \nabla T(\mathbf{x}), & \mathbf{x} \in G_\varepsilon. \end{aligned} \quad (4.2.1)$$

and the boundary conditions. The latter consist of ideal-contact conditions prescribed at the interface between the inclusion and the matrix

$$\boldsymbol{\sigma}^{(n)}(\mathbf{u}; \mathbf{x}) - \gamma \Delta T \mathbf{n} = \boldsymbol{\sigma}_0^{(n)}(\mathbf{u}_0; \mathbf{x}) - \gamma_0 \Delta T \mathbf{n}, \quad \mathbf{u} = \mathbf{u}_0, \quad \mathbf{x} \in \partial G_\varepsilon, \quad (4.2.2)$$

where $\Delta T = T - T_{rel}$, and T_{rel} is the temperature of the stress-free state.

On the crack faces we have the traction condition

$$\boldsymbol{\sigma}^{(n)}(\mathbf{u}; \mathbf{x}) = \mathbf{p}(\mathbf{x}) + \gamma \Delta T \mathbf{n}, \quad \mathbf{x} \in M_{\alpha}^{\pm}, \quad (4.2.3)$$

which reduces to the traction-free condition at the crack faces, if the temperature term is not taken into account

$$\boldsymbol{\sigma}^{(n)}(\mathbf{u}; \mathbf{x}) = \mathbf{0}, \quad \mathbf{x} \in M_{\alpha}^{\pm}. \quad (4.2.4)$$

In the case of a cavity and $\Delta T = 0$, the conditions (4.2.2) are replaced by the traction boundary condition

$$\boldsymbol{\sigma}^{(n)}(\mathbf{u}; \mathbf{x}) = \mathbf{0}, \quad \mathbf{x} \in \partial G_{\varepsilon}. \quad (4.2.5)$$

When the distance r from the crack tip tends to infinity, the displacement field has the following asymptotic form

$$\mathbf{u}(\mathbf{x}) \sim K_I^{\infty} r^{1/2} \boldsymbol{\Phi}^I(\phi) + K_{II}^{\infty} r^{1/2} \boldsymbol{\Phi}^{II}(\phi) \quad \text{as } r \rightarrow \infty, \quad (4.2.6)$$

where the stress intensity factors K_I^{∞} and K_{II}^{∞} are given, and the polar components of the vector functions $\boldsymbol{\Phi}^I = (\Phi_r^I, \Phi_{\phi}^I)^t$ and $\boldsymbol{\Phi}^{II} = (\Phi_r^{II}, \Phi_{\phi}^{II})^t$ are specified by (see, for example, Arutyunyan, Movchan and Nazarov [2])

$$\begin{aligned} \Phi_r^I(\phi) &= \frac{1}{4\mu\sqrt{2\pi}} [(2\kappa - 1) \cos \frac{\phi}{2} - \cos \frac{3\phi}{2}], \\ \Phi_{\phi}^I(\phi) &= \frac{1}{4\mu\sqrt{2\pi}} [\sin \frac{3\phi}{2} - (2\kappa + 1) \sin \frac{\phi}{2}], \\ \Phi_r^{II}(\phi) &= \frac{1}{4\mu\sqrt{2\pi}} [3 \sin \frac{3\phi}{2} - (2\kappa - 1) \sin \frac{\phi}{2}], \\ \Phi_{\phi}^{II}(\phi) &= \frac{1}{4\mu\sqrt{2\pi}} [3 \cos \frac{3\phi}{2} - (2\kappa + 1) \cos \frac{\phi}{2}], \end{aligned} \quad (4.2.7)$$

where $\kappa = (\lambda + 3\mu)(\lambda + \mu)^{-1}$ and $\phi \in [-\pi, \pi]$.

Further we suppose that our crack is a Mode-I crack, and K_{II}^{∞} is zero.

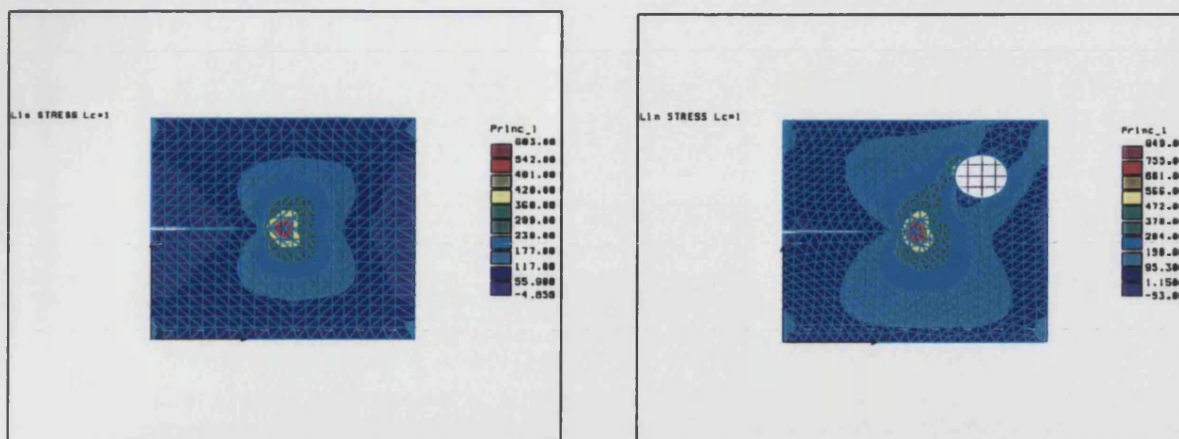


Figure 4-2: Crack in elastic region with and without a defect: distribution of the principal stresses

4.3 Asymptotic expansion for a solution of a thermo-elasticity problem

The thermo-elasticity boundary value problem (4.2.1), (4.2.2), (4.2.3) together with the condition at infinity (4.2.6) is specified in an infinite thermoelastic plane with a small inclusion G_ε and a crack M_0 . For illustration of the qualitative behaviour of the displacement field in both situations with and without an inclusion we perform two numerical experiments with the finite element package COSMOS/M. In Figure 4-2 the numerical approximation of a singular solution in unperturbed crack tip is shown. This solution can be easily obtained analytically in the form (4.2.6). The displacement field in the region with a crack and a defect is nonsymmetric, it can be seen in Figure 4-2(right plot). The distribution of the stresses shows that the crack more likely will move towards the cavity since the maximal tensile stresses occur in this direction.

In addition, the following heat conduction problem is considered for the temperature field

$$\begin{aligned}
 k\nabla^2 T(\mathbf{x}) &= w(\mathbf{x}), & \mathbf{x} \in \mathbb{R}^2 \setminus G_\varepsilon, & & k_0 \Delta T_0(\mathbf{x}) &= 0, & \mathbf{x} \in \overline{G_\varepsilon}, \\
 k \frac{\partial T}{\partial n} &= k_0 \frac{\partial T_0}{\partial n}, & T &= T_0, & \mathbf{x} \in \partial G_\varepsilon, \\
 T|_{M_0^+} &= T|_{M_0^-}, & \partial_n T|_{M_0^+} &+ \partial_n T|_{M_0^-} &= 0,
 \end{aligned}$$

4.3. ASYMPTOTIC EXPANSION FOR A SOLUTION OF A
THERMO-ELASTICITY PROBLEM

$$T \rightarrow T_\infty(x) \quad \text{as } x \rightarrow \infty,$$

where \mathbf{n} is a unit outward normal vector, k and k_0 are the thermal conductivities of both phases, $w(\mathbf{x})$ is the intensity of the heat sources. Assuming that $\text{diam } G_\varepsilon \ll \text{dist } \{G_\varepsilon, M_0\}$, one introduces a small parameter as follows

$$\varepsilon = \frac{1}{2} \frac{\text{diam } G_\varepsilon}{\text{dist } \{G_\varepsilon, M_0\}} \ll 1.$$

First, the temperature distribution in a plane with an inclusion is considered. In the case of equal thermal conductivities ($k = k_0$), the thermal boundary layers do not occur near the inclusion and the temperature field can be found as a solution of the following problem

$$\begin{aligned} k \nabla^2 T(\mathbf{x}) &= w(\mathbf{x}), \quad \mathbf{x} \in \mathbb{R}^2, \\ T &\rightarrow T_\infty \quad \text{as } \mathbf{x} \rightarrow \infty. \end{aligned} \tag{4.3.1}$$

In the case of different thermal conductivities of the inclusion and matrix and in the presence of heat sources, one shall construct the boundary layer and apply the asymptotic series expansion:

$$T(\mathbf{x}) = T^{(0)}(\mathbf{x}) + \varepsilon T^{(1)}(\mathbf{X}) + O(\varepsilon^2), \tag{4.3.2}$$

where $T^{(1)}(\mathbf{X})$ is a boundary layer solution which compensates the discrepancy in the interface boundary conditions produced by $T^{(0)}(\mathbf{x})$.

Second, given the temperature field (4.3.2), we seek the displacement vector \mathbf{u} which is a solution of the boundary value problem (4.2.1)-(4.2.3) in the following form

$$\mathbf{u}(\mathbf{x}) = \mathbf{u}^{(0)}(\mathbf{x}) + \varepsilon \mathbf{u}^{(1)}(\mathbf{X}) + \varepsilon^2 \mathbf{u}^{(2)}(\mathbf{x}) + O(\varepsilon^3). \tag{4.3.3}$$

Here the leading order term $\mathbf{u}^{(0)}(\mathbf{x})$ is a solution of the boundary value problem in $\mathbb{R}^2 \setminus M_0$ (without the defect)

$$\begin{aligned} \mu \nabla^2 \mathbf{u}^{(0)}(\mathbf{x}) + (\lambda + \mu) \nabla \nabla \cdot \mathbf{u}^{(0)}(\mathbf{x}) &= \gamma \nabla_x T^{(0)} + \gamma \nabla_X T^{(1)}, \quad \mathbf{x} \in \mathbb{R}^2 \setminus M_0, \\ \sigma^{(n)}(\mathbf{u}^{(0)}; \mathbf{x}) &= \mathbf{p}(\mathbf{x}) + \gamma T(\mathbf{x}) \mathbf{n}, \quad \mathbf{x} \in M_0^\pm. \end{aligned} \tag{4.3.4}$$

One introduces a set of linearly independent vector functions which satisfy the homo-

4.3. ASYMPTOTIC EXPANSION FOR A SOLUTION OF A
THERMO-ELASTICITY PROBLEM

geneous Navier system written in the stretched variables $\mathbf{X} = \mathbf{x} / \varepsilon$

$$\mathbf{U}^{(1)} = \begin{pmatrix} 1 \\ 0 \end{pmatrix}, \mathbf{U}^{(2)} = \begin{pmatrix} 0 \\ 1 \end{pmatrix},$$

$$\mathbf{V}^{(1)} = \begin{pmatrix} X_1 \\ 0 \end{pmatrix}, \mathbf{V}^{(2)} = \begin{pmatrix} 0 \\ X_2 \end{pmatrix}, \mathbf{V}^{(3)} = \begin{pmatrix} X_2 \\ X_1 \end{pmatrix}, \mathbf{V}^{(4)} = \begin{pmatrix} -X_2 \\ X_1 \end{pmatrix}.$$

The leading term $\mathbf{u}^{(0)}$ of the expansion (4.3.3) admits the following representation in the vicinity of the inclusion (coordinates \mathbf{x} are the Cartesian coordinates with the origin at the centre of the inclusion)

$$\begin{aligned} \mathbf{u}^{(0)}(\mathbf{x}) &\sim \mathbf{u}^{(0)}(\mathbf{0}) + \varepsilon X_1 \left. \frac{\partial \mathbf{u}^{(0)}(\mathbf{x})}{\partial x_1} \right|_0 + \varepsilon X_2 \left. \frac{\partial \mathbf{u}^{(0)}(\mathbf{x})}{\partial x_2} \right|_0 \\ &= A_1 \mathbf{U}^{(1)}(\mathbf{X}) + A_2 \mathbf{U}^{(2)}(\mathbf{X}) \\ &+ C_1 \varepsilon \mathbf{V}^{(1)}(\mathbf{X}) + C_2 \varepsilon \mathbf{V}^{(2)}(\mathbf{X}) + C_3 \varepsilon \mathbf{V}^{(3)}(\mathbf{X}) + C_4 \varepsilon \mathbf{V}^{(4)}(\mathbf{X}), \end{aligned} \quad (4.3.5)$$

where A_i, C_k are constants defined in terms of the components of the strain tensor $\varepsilon(\mathbf{u})$ evaluated for the leading term of the displacement field

$$C_1 = \frac{\partial u_1^{(0)}}{\partial x_1} = \varepsilon_{11}(\mathbf{u}^{(0)}), \quad C_2 = \frac{\partial u_2^{(0)}}{\partial x_2} = \varepsilon_{22}(\mathbf{u}^{(0)}),$$

$$C_3 = \frac{1}{2} \left\{ \frac{\partial u_2^{(0)}}{\partial x_1} + \frac{\partial u_1^{(0)}}{\partial x_2} \right\} = \varepsilon_{12}(\mathbf{u}^{(0)}).$$

The second term of the expansion (4.3.3) can be specified as a solution of the boundary value problem specified in an infinite plane

$$\begin{aligned} \mu \nabla^2 \mathbf{u}^{(1)}(\mathbf{X}) + (\lambda + \mu) \nabla \nabla \cdot \mathbf{u}^{(1)}(\mathbf{X}) &= 0, \quad \mathbf{X} \in \mathbb{R}^2 \setminus \overline{G}, \\ \mu_0 \nabla^2 \mathbf{u}_0^{(1)}(\mathbf{X}) + (\lambda_0 + \mu_0) \nabla \nabla \cdot \mathbf{u}_0^{(1)}(\mathbf{X}) &= 0, \quad \mathbf{X} \in G, \\ \sigma^{(n)}(\mathbf{u}^{(1)}; \mathbf{X}) - \sigma_0^{(n)}(\mathbf{u}_0^{(1)}; \mathbf{X}) & \\ = \sigma_0^{(n)}(\mathbf{u}_0^{(0)}; \mathbf{X}) - \sigma^{(n)}(\mathbf{u}^{(0)}; \mathbf{X}) + (\gamma - \gamma_0) T(\mathbf{X}) & \quad \mathbf{X} \in \partial G, \\ \mathbf{u}^{(1)}(\mathbf{X}) = \mathbf{u}_0^{(1)}(\mathbf{X}), & \quad \mathbf{X} \in \partial G, \\ \sigma^{(n)}(\mathbf{u}^{(1)}; \mathbf{X}) \rightarrow 0, & \quad |\mathbf{X}| \rightarrow \infty, \end{aligned} \quad (4.3.6)$$

where we replace the leading term $\mathbf{u}^{(0)}$ by its expression (4.3.5).

4.3. ASYMPTOTIC EXPANSION FOR A SOLUTION OF A
THERMO-ELASTICITY PROBLEM

The field $\mathbf{u}^{(1)}(\mathbf{X})$ is a boundary layer characterising the changes in the stress components near the defect. If we look at the interface traction conditions of the problem (4.3.6) one can note that the traction jump is defined by the leading term of the displacement field $\mathbf{u}^{(0)}$ and by the temperature field $T(\mathbf{X})$. Since both terms are uncoupled, one can split the jump in the traction boundary conditions (in (4.3.6)) associated with the term $\mathbf{u}^{(0)}$ and with the temperature. The solution $\mathbf{u}^{(1)}$ can be represented as a linear combination of a solution with an elastic jump and a jump due to the temperature. Note that stresses produced by the rigid body displacement $\mathbf{U}^{(1)}, \mathbf{U}^{(2)}$ and $\mathbf{V}^{(4)}$ are equal to zero. For other vector polynomials $\mathbf{V}^{(i)}, i = 1, 2, 3$, one constructs the fields $\mathbf{W}^{(i)}, i = 1, 2, 3$, which compensate the discrepancy left by $\mathbf{V}^{(i)}$ in the interface boundary conditions. At infinity the vector functions $\mathbf{W}^{(i)}$ admit the asymptotic representation (2.1.8) (see Chapter 2). The term $\mathbf{W}^{(4)}$ which compensates a thermal jump in interface conditions solves the problem

$$\begin{aligned} \mu \nabla^2 \mathbf{W}^{(4)}(\mathbf{X}) + (\lambda + \mu) \nabla \nabla \cdot \mathbf{W}^{(4)}(\mathbf{X}) &= 0, & \mathbf{X} \in \mathbb{R}^2 \setminus \bar{G}, \\ \mu_0 \nabla^2 \mathbf{W}_0^{(4)}(\mathbf{X}) + (\lambda_0 + \mu_0) \nabla \nabla \cdot \mathbf{W}_0^{(4)}(\mathbf{X}) &= 0, & \mathbf{X} \in G, \\ \sigma^{(n)}(\mathbf{W}^{(4)}; \mathbf{X}) - \sigma_0^{(n)}(\mathbf{W}_0^{(4)}; \mathbf{X}) &= (\gamma - \gamma_0) T^{(0)} \mathbf{n}, \quad \mathbf{u} = \mathbf{u}_0, & \mathbf{X} \in \partial G, \\ \sigma^{(n)}(\mathbf{W}^{(4)}; \mathbf{X}) &\rightarrow 0, & \mathbf{X} \rightarrow \infty, \end{aligned} \tag{4.3.7}$$

It admits the following asymptotic representation as $\|\mathbf{X}\| \rightarrow \infty$ (compare with the asymptotic expansions (2.1.8) of the fields $\mathbf{W}^{(i)}, i = 1, 2, 3$)

$$\boxed{\mathbf{W}^{(4)} = \sum_{k=1}^3 \mathcal{D}_k \mathfrak{D}^{(k)} \cdot \mathbf{T}(\mathbf{X}) + O(\|\mathbf{X}\|^{-2})}, \tag{4.3.8}$$

where \mathcal{D}_k are constants and the vector differential operators $\mathfrak{D}^{(k)}$ are defined by the following relations

$$\mathfrak{D}^{(1)} := \begin{pmatrix} \partial/\partial x_1 \\ 0 \end{pmatrix}, \quad \mathfrak{D}^{(2)} := \begin{pmatrix} 0 \\ \partial/\partial x_2 \end{pmatrix}, \quad \mathfrak{D}^{(3)} := \frac{1}{\sqrt{2}} \begin{pmatrix} \partial/\partial x_2 \\ \partial/\partial x_1 \end{pmatrix}. \tag{4.3.9}$$

Using the notations above, the second asymptotic term can be written in the form

$$\mathbf{u}^{(1)}(\mathbf{X}) = \sum_{i=1}^3 C_i \mathbf{W}^{(i)}(\mathbf{X}) + \mathbf{W}^{(4)}(\mathbf{X}). \tag{4.3.10}$$

The third term $\mathbf{u}^{(2)}(\mathbf{x})$ compensates the discrepancy in the boundary conditions on the crack surfaces M_0^\pm

$$\begin{aligned} \mu \nabla^2 \mathbf{u}^{(2)}(\mathbf{x}) + (\lambda + \mu) \nabla \nabla \cdot \mathbf{u}^{(2)}(\mathbf{x}) &= 0, \quad \mathbf{x} \in \mathbb{R}^2 \setminus M_0, \\ \sigma^{(n)}(\mathbf{u}^{(2)}; \mathbf{x}) &= -\sigma^{(n)} \left(\sum_{k=1}^3 \left\{ \sum_{n=1}^3 C_n \mathcal{P}_{nk} + \mathcal{D}_k \right\} \mathfrak{D}^{(k)} \cdot \mathbf{T}(\mathbf{x}); \mathbf{x} \right), \quad \mathbf{x} \in M_0^\pm, \end{aligned} \quad (4.3.11)$$

and it can be represented in the form

$$\begin{aligned} \mathbf{u}^{(2)}(\mathbf{x}) &= \sum_{n,k=1}^3 \mathcal{P}_{nk} \left(\mathbf{T}^{(k)}(\mathbf{x}) - \mathfrak{D}^{(k)} \cdot \mathbf{T}(\mathbf{x}) \right) C_n \\ &+ \sum_{k=1}^3 \mathcal{D}_k \left(\mathbf{T}^{(k)}(\mathbf{x}) - \mathfrak{D}^{(k)} \cdot \mathbf{T}(\mathbf{x}) \right). \end{aligned} \quad (4.3.12)$$

The field $\mathbf{T}^{(k)}$ can be found as a solution of the Navier system with dipole body forces acting at the centre of the small defect and zero tractions on the crack surfaces

$$\begin{aligned} \mu \nabla^2 \mathbf{T}^{(k)}(\mathbf{x}) + (\lambda + \mu) \nabla \nabla \cdot \mathbf{T}^{(k)}(\mathbf{x}) + \mathfrak{D}^{(k)} \delta(\mathbf{x}) &= 0, \quad \mathbf{x} \in \mathbb{R}^2 \setminus M_0, \\ \sigma^{(n)}(\mathbf{T}^{(k)}; \mathbf{x}) &= 0, \quad \mathbf{x} \in M_0^\pm. \end{aligned} \quad (4.3.13)$$

Note that the asymptotic expansion given here is a solution of the boundary value problem for the fixed crack. In real situation it is possible to consider either unperturbed crack (it propagates along a straight line) or perturbed one (due to the presence of the defect effect). The first situation is trivial since it reduces to analysis of a semi-infinite crack in an infinite space. The second one requires more accurate calculations.

4.4 Unperturbed crack

The perturbation introduced by a defect on the displacement fields is considered for a straight crack M_0 (note for $\alpha = 0$ there is no perturbation of crack trajectory). Following Movchan and Movchan [75] and Movchan and Serkov [79] the displacement field near the crack tip can be expanded as follows

$$\mathbf{u}(\mathbf{x}) \sim \mathbf{v}(\mathbf{x}) + \varepsilon^2 \mathbf{w}(\mathbf{x}), \quad (4.4.14)$$

where

$$\mathbf{v}(\mathbf{x}) = K_I r^{1/2} \Phi^I(\phi), \quad \text{as } |\mathbf{x}| \rightarrow 0$$

is the displacement field corresponding to a rectilinear crack in a plane without inclusion, and $\varepsilon^2 \mathbf{w}$ represents the correction term associated with the perturbation field produced by the small defect Ω_ε . Note that in the absence of tractions on the faces of a crack, the stress intensity factor $K_I = K_I^\infty$ (see (4.2.6)).

The reason why the correction term has the second-order in ε can be explained by considering the Neumann boundary value problem for a homogeneous elastic isotropic solid containing a defect (Movchan and Movchan [75], Section 1.3). The vector field \mathbf{w} satisfies the system of equation

$$\mathcal{L}_{xx}(\mathbf{w}; \mathbf{x}) = - \sum_{j,k=1}^3 \left[\mathfrak{D}^{(j)} \cdot \mathbf{v}(\mathbf{x}) \right]_{\mathbf{x}=\mathbf{x}_0} \mathcal{P}_{jk} \mathfrak{D}^{(k)} \delta(\mathbf{x} - \mathbf{x}^0), \quad \mathbf{x} \in \mathbb{R}^2 \setminus M_0, \quad (4.4.15)$$

where $\mathbf{x}_0 = (x_0, y_0)$ is the centre of the defect, δ is the Dirac function, \mathcal{P}_{jk} are the components of the Pólya-Szegő matrix, and the homogeneous traction boundary conditions on the crack faces

$$\boldsymbol{\sigma}^{(n)}(\mathbf{w}; \mathbf{x}) = \mathbf{0}, \quad \mathbf{x} \in M_0^\pm. \quad (4.4.16)$$

At infinity the correction field $\mathbf{w}(\mathbf{x})$ vanishes

$$\mathbf{w}(\mathbf{x}) \rightarrow \mathbf{0} \quad \text{as } \|\mathbf{x}\| \rightarrow \infty.$$

4.5 Perturbation of the crack

4.5.1 Asymptotic analysis

We are now in a position to investigate the problem of perturbation of the crack trajectory induced by the presence of a defect. In the absence of defects under Mode I loading the crack would propagate along x -axis, this condition satisfies the criterion $K_{II} = 0$. The presence of a defect, even a small one, produces a perturbation in terms of a smooth deflection from linear crack trajectory. Movchan, Gao and Willis [73] studied the out-of-plane perturbation for 2D and 3D cracks using the asymptotic analyses. Here the methodology of [73] is used for elastic and thermoelastic media. The main attention is paid to perturbation due to a defect, where the Pólya-Szegő tensors can be applied.

Let one consider the asymptotic expansion of the displacement field near the tip of the

perturbed crack M_α . A local system of coordinates \mathbf{y}^α can be introduced, which has the origin at the tip of the perturbed crack $(l, \alpha h(l))$ and the axis y_1^α tangent to the crack trajectory at the crack-tip (Figure 4-1)

$$\mathbf{y}^\alpha = \begin{pmatrix} 1 & \alpha h'(l) \\ -\alpha h'(l) & 1 \end{pmatrix} \mathbf{y} - \begin{pmatrix} 0 \\ \alpha h(l) \end{pmatrix}, \quad (4.5.17)$$

where \mathbf{y} is a system of coordinates translated with respect to \mathbf{x} , $\mathbf{y} = (y_1, y_2) = (x_1 - l, x_2)$ (α is supposed to be zero).

In the polar coordinate system \mathbf{y}^α (Figure 4-1), the asymptotic expansion of the displacement vector \mathbf{u} , relative to the perturbed crack, can be represented as follows

$$\mathbf{u}(\mathbf{y}^\alpha) \sim \sum_{j=I,II} r_\alpha^{1/2} K_j(\alpha) \Phi^{(j)}(\phi_\alpha), \quad K_j(\alpha) \sim K_j(l) + \alpha K_j'(l), \quad (4.5.18)$$

where $K_j(l)$ are referred to the unperturbed problem, so that $K_{II}(l) = 0$ by definition. Moreover, the displacement $\mathbf{u}(\mathbf{y}^\alpha)$ may be represented in the system \mathbf{y} through a rotation, i.e.

$$\mathbf{u}(\mathbf{y}, \alpha) = \begin{pmatrix} 1 & -\alpha h'(l) \\ \alpha h'(l) & 1 \end{pmatrix} \mathbf{u}(\mathbf{y}^\alpha), \quad (4.5.19)$$

and a Taylor series expansion of (4.5.19) can be performed near $\alpha = 0$

$$\mathbf{u}(\mathbf{y}, \alpha) = \mathbf{u}(\mathbf{y}, 0) + \alpha \left. \frac{\partial \mathbf{u}(\mathbf{y}, \alpha)}{\partial \alpha} \right|_{\alpha=0} + O(\alpha^2). \quad (4.5.20)$$

Therefore, using equations (4.5.18), (4.5.19), the formula (4.5.20) becomes

$$\begin{aligned} \mathbf{u}(\mathbf{y}, \alpha) = \mathbf{u}(\mathbf{y}, 0) + \alpha \left\{ \begin{pmatrix} 0 & -h'(l) \\ h'(l) & 0 \end{pmatrix} \mathbf{u}(\mathbf{y}, 0) + \frac{\partial \mathbf{u}(\mathbf{y}^\alpha)}{\partial y_1^\alpha} \frac{\partial y_1^\alpha}{\partial \alpha} \Big|_{\alpha=0} + \frac{\partial \mathbf{u}(\mathbf{y}^\alpha)}{\partial y_2^\alpha} \frac{\partial y_2^\alpha}{\partial \alpha} \Big|_{\alpha=0} \right. \\ \left. + \frac{\partial \mathbf{u}(\mathbf{y}^\alpha)}{\partial K_I(\alpha)} \frac{\partial K_I(\alpha)}{\partial \alpha} \Big|_{\alpha=0} + \frac{\partial \mathbf{u}(\mathbf{y}^\alpha)}{\partial K_{II}(\alpha)} \frac{\partial K_{II}(\alpha)}{\partial \alpha} \Big|_{\alpha=0} \right\} + O(\alpha^2), \end{aligned} \quad (4.5.21)$$

where the leading term $\mathbf{u}(\mathbf{y}, 0) = \mathbf{v}(\mathbf{y})$ is the same as in (4.4.14).

Now one can simplify this expression to the following form

$$\mathbf{u}(\mathbf{y}, \alpha) = \mathbf{v}(\mathbf{y}) + \alpha \left\{ h'(l) \begin{pmatrix} -v_2(\mathbf{y}) \\ v_1(\mathbf{y}) \end{pmatrix} + h'(l) y_2 \frac{\partial \mathbf{v}}{\partial y_1} - (h'(l) y_1 + h(l)) \frac{\partial \mathbf{v}}{\partial y_2} \right\}.$$

If one substitutes the expression for the asymptotic expansion (4.5.18) in the equation

above, the result can be rewritten in the form

$$\begin{aligned} \mathbf{u}(\mathbf{y}, \alpha) = & K_I(l)r^{1/2}\Phi^I(\phi) + \alpha \sum_{j=I,II} \left\{ K'_j(l)r^{1/2}\Phi^{(j)}(\phi) \right. \\ & + K_j(l) \left[-h(l)\frac{\partial}{\partial y_2} \left(r^{1/2}\Phi^{(j)}(\phi) \right) + h'(l) \left(y_2\frac{\partial}{\partial y_1} - y_1\frac{\partial}{\partial y_2} \right) \left(r^{1/2}\Phi^{(j)}(\phi) \right) \right] \\ & \left. + K_j(l) h'(l)r^{1/2}(-\Phi_2^{(j)}(\phi), \Phi_1^{(j)}(\phi))^t \right\}. \end{aligned}$$

It has been verified by direct calculations that

$$\begin{aligned} \frac{\partial}{\partial y_2} (r^{1/2}\Phi^I(\phi)) &= \frac{1+\varkappa}{4\mu} r^{-1/2}\Psi^{II}, \\ \left(y_2\frac{\partial}{\partial y_1} - y_1\frac{\partial}{\partial y_2} \right) \left(r^{1/2}\Phi^I(\phi) \right) &+ r^{1/2}(-\Phi_2^{(j)}(\phi), \Phi_1^{(j)}(\phi))^t = -\frac{1}{2}r^{1/2}\Phi^{II}(\phi), \end{aligned}$$

where

$$\begin{aligned} \Psi_r^{II}(\phi) &= \frac{1}{2\sqrt{2\pi}(1+\varkappa)} \left[(1+2\varkappa) \sin \frac{3\phi}{2} - \sin \frac{\phi}{2} \right], \\ \Psi_\phi^{II}(\phi) &= \frac{1}{2\sqrt{2\pi}(1+\varkappa)} \left[(2\varkappa-1) \cos \frac{3\phi}{2} - \cos \frac{\phi}{2} \right]. \end{aligned} \quad (4.5.22)$$

Using the calculation above the coefficient of the term multiplying α in (4.5.21) can be written as

$$\begin{aligned} \mathbf{w}(\mathbf{y}) := & -\frac{1+\varkappa}{4\mu} h(l)K_I(l)r^{-1/2}\Psi^{II}(\phi) + K'_I(l)r^{1/2}\Phi^I(\phi) \\ & + [K'_{II}(l) - \frac{1}{2}K_I(l)h'(l)]r^{1/2}\Phi^{II}(\phi), \end{aligned} \quad (4.5.23)$$

where the components of the vector function Φ^I , Φ^{II} are given by (4.2.7) and components of Ψ^{II} are presented by (4.5.22).

The stress components associated with (4.5.23) exhibit an unphysical strong singularity, and this fact indicates the presence of the boundary layer in the vicinity of the crack tip. This singularity may be eliminated as follows. First, let one introduce the weight function

$$\zeta^{II}(\mathbf{y}) := r^{-1/2}\Psi^{II}(\phi), \quad (4.5.24)$$

and define

$$\mathbf{w}^*(\mathbf{y}) := \mathbf{w}(\mathbf{y}) + \frac{1+\varkappa}{4\mu} h(l)K_I(l)\zeta^{II}(\mathbf{y}). \quad (4.5.25)$$

The function $\mathbf{w}^*(\mathbf{y})$ satisfies the Navier system (4.2.1) and the same boundary conditions on M_0^\pm as \mathbf{w} , but does not have a singularity at the crack tip $(l, 0)$. Second, let one consider the ring $\Xi_R = \{\mathbf{y} : \frac{1}{R} \leq \|\mathbf{y}\| \leq R\}$, surrounding the reference crack tip, and the integral

$$\int_{\Xi_R/M_0} \left\{ \zeta^{II}(\mathbf{y}) \cdot \mathcal{L}_{xx}(\mathbf{u}; \mathbf{y}) - \mathbf{u}(\mathbf{y}) \cdot \mathcal{L}_{xx}(\zeta^{II}; \mathbf{y}) \right\} d\mathbf{y}. \quad (4.5.26)$$

Here and further we suppose that the solution $\mathbf{u}(\mathbf{y})$ has no singularity at the crack tip

$$\mathbf{u}(\mathbf{y}) \sim \mathbf{v}(\mathbf{y}) + \varepsilon^2 \mathbf{w}^*(\mathbf{y}).$$

If the defect is far enough from the reference crack tip, the representation (4.4.14) holds, and therefore,

$$\begin{aligned} & \int_{\Xi_R \setminus M_0} \left\{ \zeta^{II}(\mathbf{y}) \cdot \mathcal{L}_{xx}(\mathbf{u}; \mathbf{y}) - \mathbf{u}(\mathbf{y}) \cdot \mathcal{L}_{xx}(\zeta^{II}; \mathbf{y}) \right\} d\mathbf{y} \\ &= -\varepsilon^2 \int_{\Xi_R \setminus M_0} \left\{ \zeta^{II}(\mathbf{y}) \cdot \sum_{j,k=1}^3 \left[\mathcal{D}^{(j)} \cdot \mathbf{v}(\mathbf{y}) \right]_{\mathbf{y}=\mathbf{y}_0} \mathcal{P}_{jk} \mathcal{D}^{(k)} \right\} \delta(\mathbf{y} - \mathbf{y}_0) d\mathbf{y} \\ &= \varepsilon^2 \sum_{j,k=1}^3 \mathcal{P}_{jk} \mathcal{F}_{jk}(\mathbf{v}(\mathbf{y}), \zeta^{II}(\mathbf{y}); \mathbf{y}_0), \end{aligned} \quad (4.5.27)$$

where $\mathbf{y}_0 = (x_0 - l, y_0)$ is the centre of the defect in the local coordinate system \mathbf{y} , and

$$\mathcal{F}_{jk}(\mathbf{v}(\mathbf{y}), \zeta^{II}(\mathbf{y}); \mathbf{y}_0) := \left[\mathcal{D}^{(j)} \cdot \mathbf{v}(\mathbf{y}) \right]_{\mathbf{y}=\mathbf{y}_0} \left[\mathcal{D}^{(k)} \cdot \zeta^{II}(\mathbf{y}) \right]_{\mathbf{y}=\mathbf{y}_0}, \quad (4.5.28)$$

If we reconsider integral (4.5.26), apply the Betti's formula and take the limit when R tends to infinity, one obtains

$$\begin{aligned} & \lim_{R \rightarrow \infty} \int_{\Xi_R \setminus M_0} \left\{ \zeta^{II}(\mathbf{y}) \cdot \mathcal{L}_{xx}(\mathbf{u}; \mathbf{y}) - \mathbf{u}(\mathbf{y}) \cdot \mathcal{L}_{xx}(\zeta^{II}; \mathbf{y}) \right\} d\mathbf{y} \\ &= \lim_{R \rightarrow \infty} \left\{ \int_{C_1} \left[\zeta_r^{II} \sigma_{rr}(\mathbf{u}) + \zeta_\phi^{II} \sigma_{r\phi}(\mathbf{u}) - u_r \sigma_{rr}(\zeta^{II}) - u_\phi \sigma_{r\phi}(\zeta^{II}) \right] ds \right. \\ & \quad - \int_{C_2} \left[\zeta_r^{II} \sigma_{rr}(\mathbf{u}(\mathbf{y}, 0) + \alpha \mathbf{w}^*(\mathbf{y})) + \zeta_\phi^{II} \sigma_{r\phi}(\mathbf{u}(\mathbf{y}, 0) + \alpha \mathbf{w}^*(\mathbf{y})) \right. \\ & \quad \left. \left. - \left(u_r(\mathbf{y}, 0) + \alpha w_r^*(\mathbf{y}) \right) \sigma_{rr}(\zeta^{II}) - \left(u_\phi(\mathbf{y}, 0) + \alpha w_\phi^*(\mathbf{y}) \right) \sigma_{r\phi}(\zeta^{II}) \right] ds \right\} \end{aligned}$$

$$\begin{aligned}
 & + \sum_{\pm} \int_{M_0} \left[\zeta_1^{II} \sigma_{12}(\mathbf{u}) + \zeta_2^{II} \sigma_{22}(\mathbf{u}) - u_1 \sigma_{12}(\zeta^{II}) - u_2 \sigma_{22}(\zeta^{II}) \right] ds \Big\} \\
 & = 0 + \alpha \left\{ \frac{1}{2} h'(l) K_I(l) - K'_{II}(l) \right\} + 0, \tag{4.5.29}
 \end{aligned}$$

where $C_1(R) = \{\mathbf{y} : \|\mathbf{y}\| = R\}$ and $C_2 = \{\mathbf{y} : \|\mathbf{y}\| = 1/R\}$.

Note that in the integral along C_1 , the field \mathbf{u} corresponds to (4.2.6), whereas in the integral along C_2 the approximation (4.5.23) regularized via the weight function is used. Finally, the integral along M_0 is zero because of the traction free boundary conditions. Matching (4.5.29) with (4.5.27), it can be concluded that $\alpha = \varepsilon^2$, and the derivative of K_{II} has the form

$$\boxed{K'_{II}(l) = K_I(l) \left[\frac{1}{2} h'(l) - \sum_{j,k=1}^3 \mathcal{P}_{jk} \mathcal{F}_{jk}(r^{-1/2} \Psi^{II}, r^{1/2} \Phi^I; \mathbf{y}_0) \right]}. \tag{4.5.30}$$

Note that if the crack remains straight, i.e. if $h = 0$, the relation (4.5.30) can be used to compare the present asymptotic solution to the numerical results of Rubinstein [95] referred to the influence of defects on the near tip fields of a straight crack.

4.5.2 Crack trajectory

If the pure Mode I criterion of fracture is adopted, the direction of the crack growth has to be chosen in such a way that $K_{II}(\alpha) = 0$, and therefore

$$K_{II}(\alpha) \sim \alpha K'_{II}(l) = 0, \tag{4.5.31}$$

which can be substituted into (4.5.30) to get

$$h'(l) = 2 \sum_{j,k=1}^3 \mathcal{P}_{jk} \mathcal{F}_{jk}(r^{-1/2} \Psi^{II}, r^{1/2} \Phi^I; \mathbf{y}_0). \tag{4.5.32}$$

Equation (4.5.32) can be easily integrated with the use of the following auxiliary identity

$$\zeta^{II} = \frac{4\mu}{1 + \nu} \frac{\partial(r^{1/2} \Phi^I)}{\partial y_2}.$$

One supposes that crack deflection at $-\infty$ is zero. Then the crack deflection function in the case when the centre of the inclusion is placed at the generic point (x_0, y_0) is given

by

$$h(l) = \frac{4\mu}{y_0(1+\varkappa)} \{ \cos \theta \mathcal{L}^t(\theta) \mathcal{P} \mathcal{L}(\theta) - \mathcal{L}^t(0) \mathcal{P} \mathcal{L}(0) \}, \quad (4.5.33)$$

where

$$\cos \theta = \frac{x_0 - l}{\sqrt{y_0^2 + (x_0 - l)^2}},$$

and

$$\mathcal{L}(\theta) = \begin{pmatrix} \frac{1}{4\mu\sqrt{2\pi}} \cos \frac{\theta}{2} [\varkappa - 1 - 2 \sin \frac{\theta}{2} \sin \frac{3\theta}{2}] \\ \frac{1}{4\mu\sqrt{2\pi}} \cos \frac{\theta}{2} [\varkappa - 1 + 2 \sin \frac{\theta}{2} \sin \frac{3\theta}{2}] \\ \frac{1}{4\mu\sqrt{\pi}} \sin \theta \cos \frac{3\theta}{2} \end{pmatrix}. \quad (4.5.34)$$

The Cartesian components of the vector \mathcal{L} are given by

$$\mathcal{L}_k = r^{1/2} \left[\mathcal{D}^{(k)} \cdot [r^{1/2} \Phi^I(\theta)] \right]_{\mathbf{y}=\mathbf{y}_0}.$$

It may be important to remark that the problem of the interaction of a crack with more than one defect can be solved in a straightforward way in the present framework under the assumption that defects do not interact. In particular, when a number of defects is considered, and they are supposed to have non-interactive behaviour (dilute composite limit) the total crack trajectory can be calculated using (4.4.14), where the sum of the perturbed terms relative to each defect replaces the single term $\varepsilon^2 \mathbf{w}$.

4.5.3 Effect of thermal stresses

Following the procedure thoroughly discussed above we obtain the following expressions for the right-hand side of (4.5.27)

$$I = \varepsilon^2 \sum_{i,k=1}^3 \mathcal{P}_{ik} \left[\mathcal{D}^{(i)} \cdot \mathbf{v}(\mathbf{y}) \right]_{\mathbf{y}=\mathbf{y}_0} \left[\mathcal{D}^{(k)} \cdot \zeta^{II}(\mathbf{y}) \right]_{\mathbf{y}=\mathbf{y}_0} + \varepsilon^2 \sum_{k=1}^3 \mathcal{D}_k \left[\mathcal{D}^{(k)} \cdot \zeta^{II} \right]_{\mathbf{y}=\mathbf{y}_0}. \quad (4.5.35)$$

For convenience, we rewrite the vector $\mathcal{L}(\theta)$ (4.5.34) in a slightly different form, which allows to simplify further calculations

$$\mathcal{L}(\theta) = \begin{pmatrix} \frac{1}{8\mu\sqrt{2\pi}} \left(\cos \frac{5\theta}{2} + (2\varkappa - 3) \cos \frac{\theta}{2} \right) \\ \frac{1}{8\mu\sqrt{2\pi}} \left(-\cos \frac{5\theta}{2} + (2\varkappa - 1) \cos \frac{\theta}{2} \right) \\ \frac{1}{8\mu\sqrt{\pi}} \left(\sin \frac{5\theta}{2} - \sin \frac{\theta}{2} \right) \end{pmatrix},$$

where θ denotes the angle between the x -axis and a line joining the crack tip and

the centre of the inclusion. Using the equality $[\mathfrak{D}^{(k)} \cdot (r^{1/2} \Phi^I)]_{\mathbf{y}=\mathbf{y}_0} = \mathcal{L}^{(k)} r^{-1/2}$, the formula (4.5.35) and the displacement field \mathbf{v} given by $K_I r^{1/2} \Phi^I(\phi)$, the representation for the changes in the stress intensity factor can be written in the form

$$K'_{II}(l) = \frac{1}{2} K_I h'(l) - \frac{2\mu K_I}{(1+\nu)r^2} \sum_{i,k=1}^3 \frac{\partial}{\partial \theta} \left(\cos \theta \mathcal{L}^{(i)}(\theta) \mathcal{P}_{ik} \mathcal{L}^{(k)}(\theta) \right) - \frac{4\mu}{(1+\nu)r^{3/2}} \sum_{k=1}^3 \mathcal{D}_k \left(\cos \theta \frac{\partial}{\partial \theta} \mathcal{L}^{(k)}(\theta) - \frac{1}{2} \sin \theta \mathcal{L}^{(k)}(\theta) \right). \quad (4.5.36)$$

Now the Sih criterion [102], [101] of the crack propagation is taken into account. The crack propagates if the stress intensity factor K_I is greater than the critical value K_I^c and it propagates as a pure Mode-I crack if the stress intensity factor K_{II} is equal to zero. The crack path deflection is obtained after the integration of the expression (4.5.36) using the equality $h(-\infty) = 0$. The result is formulated as the following theorem

Theorem 4.1 *If a semi-infinite crack propagates quasi-statically in an elastic plane subject to a constant temperature stress, and its perturbation is caused by a remote small defect then the resulting crack trajectory can be obtained by the following formula*

$$h(l) = \frac{4\mu}{(1+\nu)y_0} \sum_{i,k=1}^3 \left(\cos \phi \mathcal{L}^{(i)}(\phi) \mathcal{P}_{ik} \mathcal{L}^{(k)}(\phi) \right) \Big|_0^\theta + \frac{8\mu}{K_I(1+\nu)\sqrt{y_0}} \sum_{k=1}^3 \int_0^\theta \mathcal{D}_k \left(\cos \phi \frac{\partial}{\partial \phi} \mathcal{L}^{(k)}(\phi) - \frac{1}{2} \sin \phi \mathcal{L}^{(k)}(\phi) \right) \frac{d\phi}{\sqrt{\sin \phi}}. \quad (4.5.37)$$

In (4.5.37) the effect of inhomogeneity is specified in terms of the Pólya-Szegő matrix \mathcal{P} and the thermo-elastic vector \mathcal{D} , θ denotes the angle between the x -axis and the line drawn through the crack tip and the centre of the inclusion, $h(l)$ is the crack deflection about the x -axis. The following auxiliary identities have been used for integration

$$dl = \frac{y_0 d\phi}{\sin^2 \phi}, \quad y_0 = r \sin \phi = \text{const}$$

4.6 Conclusions

In conclusion of this chapter one can note that the formula (4.5.37) holds for thermoelastic inhomogeneities of arbitrary shape. The only quantities required in (4.5.37) are the Pólya-Szegő matrix of the inclusion and the thermal vector \mathcal{D} . These quantities

are specified by the geometry of the inclusion and the thermoelastic properties of the materials. In the next chapter we consider some examples where the expression (4.5.37) could be simplified further.

Asymptotic derivation of the formula (4.5.37) presented here is mainly based on two asymptotic solutions. The first problem is the thermoelasticity problem in an infinite plane with an unperturbed crack and a small defect which is located far away from the crack line. This problem has been solved by expanding the solution in the asymptotic series where the second and the third terms are evaluated in terms of the Pólya-Szegö matrix. The second problem is a perturbation of a crack due to non-zero tractions on the crack faces. By combining these problems together one obtained a desirable result.

Chapter 5

Fracture propagation due to different inhomogeneities

The model described in Chapter 4 makes possible to investigate the effects of different inclusions on the trajectory of a crack. It is assumed that the characteristic size of defects is small compared to the distance from the crack trajectory and no interaction takes place between the defects. In subsections 5.1.1-5.2 a number of examples is presented for the cases where defects are circular elastic inclusions, elliptical voids and elliptical elastic inclusion. Results obtained agree with those presented by Rubinstein [95] and are qualitatively consistent with crack patterns in brittle materials observed in experiments. Further we investigate the crack propagation due to interaction with thermo-elastic effects. The Pólya-Szegő tensors are employed on this stage of the algorithm to obtain analytical formulae for the crack deflection. Temperature effects can cause reduction in the amplitude of deflection. The elastic deflection (deflection corresponding to zero increment of the temperature) and thermal deflection (difference between total deflection and the elastic one) are considered separately. The conditions when thermal deflection and elastic deflection compensate each other are analysed. This problem can be regarded as the problem of residual stresses in a composite media. Thermal stresses in an inclusion produce a jump in the displacement field on the interface. Jump conditions of the same kind correspond to residual stresses occurring under cooling. One can reformulate the problem to be a problem of interaction of a crack and an inclusion with non-perfect interface. The interface is specified by the jump, which is the function of the temperature, either in displacement or in traction boundary conditions or both. In the last part of this chapter we analyse non-perfect interface conditions. Namely,

interface conditions of the debonding type (sometimes it is called linear interface). The crack-inclusion interaction problem is considered and it yields the conditions corresponding to the case when the interface layer compensates the effect of the inclusion.

5.1 Some examples of the crack path

5.1.1 Interaction between a semi-infinite crack and a cavity

As a first application of the theory presented, we consider the case of interaction of a semi-infinite crack and an elliptical cavity G_ε with the largest axis inclined at an angle β to the x -axis. The centre of the ellipse is located at (x_0, y_0) , a and b are the semi-axes of an ellipse, $m = \frac{a-b}{a+b}$ is the eccentricity of the ellipse. One uses the representation for the Pólya-Szegő matrix for an elliptical cavity which is obtained from the formula for an arbitrary cavity (see (2.2.14) in Chapter 2) with the conformal mapping coefficients

$$c_1 = \frac{1}{2}(a+b), \quad c_{-1} = \frac{1}{2}(a-b) \exp 2\beta = c_1 m \exp 2\beta,$$

and all other coefficients of the conformal mapping (2.2.1) are zero. Under such conditions the representation for the Pólya-Szegő matrix (2.2.14) can be simplified to the following form

$$\mathcal{P} = -\frac{1}{4\mu}(a+b)^2\pi(\lambda+2\mu) \begin{pmatrix} \Xi + \Omega + \Sigma & \Xi - \Omega & \Lambda \\ \Xi - \Omega & \Xi + \Omega - \Sigma & \Lambda \\ \Lambda & \Lambda & 2\Theta \end{pmatrix}, \quad (5.1.1)$$

where

$$\begin{aligned} \Omega &= \frac{2\mu^2}{\lambda + \mu}, & \Xi &= (\lambda + \mu)(1 + m^2), \\ \Sigma &= -4\mu m \cos 2\beta, & \Lambda &= -2\sqrt{2}\mu m \sin 2\beta. \end{aligned} \quad (5.1.2)$$

This representation for the Pólya-Szegő matrix can be compared with the one given by (2.2.17); the latter has been constructed for three non-zero coefficients of the conformal mapping.

Now we use the asymptotic formula (4.5.33) for the crack trajectory. Substituting (5.1.1) into (4.5.33) one obtains

$$H(l) = \varepsilon^2 h(l) = \frac{R^2}{2y_0} \left[2(1+m^2) - z \left(2 + z - z^2 + m^2(1+z) \right) \right]$$

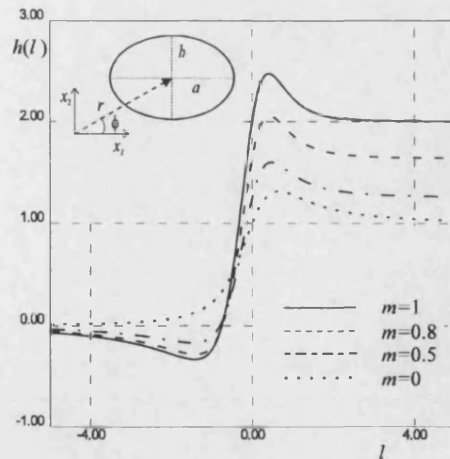


Figure 5-1: Crack trajectory $h(l)$ versus crack tip position l , resulting from interaction with an elliptic cavity whose major axis is parallel to the main crack. Results are reported for different aspect ratios a/b .

$$+2 m \cos 2\beta (1 + 2z)(1 - z^2) - 2 m \sin 2\beta (2z - 1)(1 + z)\sqrt{1 - z^2} \Big], \quad (5.1.3)$$

where

$$z = \frac{x_0 - l}{\sqrt{y_0^2 + (x_0 - l)^2}}, \quad R = \frac{a + b}{2}, \quad m = \frac{a - b}{a + b}.$$

It should be noted that the conditions $m = 0$ and $m = 1$ correspond to the cases of a circular void and of a Griffith crack, respectively.

The crack trajectories $h(l)$ obtained from (5.1.3) are reported in Figures 5-1 and 5-2. In particular, the crack trajectories plotted in Figure 5-1 show the interaction of a semi-infinite crack with ellipses having the major axis parallel to x -axis. Different aspect ratios are investigated. Figure 5-2 describes the case of a semi-infinite crack interacting with a Griffith crack inclined at different angles.

It should be noted that in the case of a circular cavity, $m = 0$, $H(l)$ takes positive values for every l . Therefore, a circular cavity always "attracts" a crack. In the case of an elliptical void, the situation is more complicated. In fact the trajectory of the crack is influenced by the orientation of the ellipse and by the aspect ratio a/b . In particular, the crack may suffer a slight repulsion, followed by a strong attraction (so that curves in Figure 5-1 have a minimum followed by a maximum). In any case, the deflection at infinity always corresponds to attraction. This can be verified by observing the limit as $l \rightarrow +\infty$ of (4.5.33). The following lemma holds

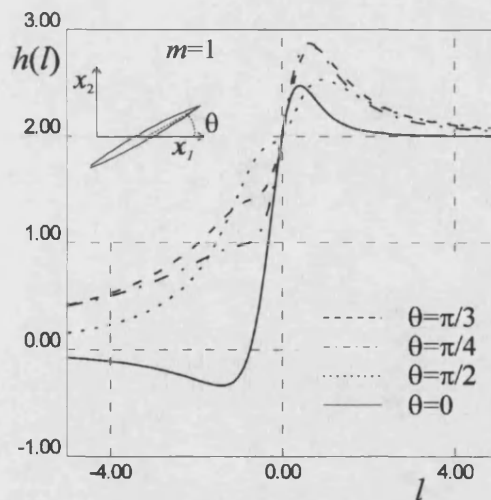


Figure 5-2: Crack trajectory $h(l)$ versus crack tip position l , resulting from interaction with a Griffith crack at different inclinations.

Lemma 5.1 *Crack deflection $H(l)$ due to the presence of an elliptical cavity in an infinitely remote point is specified by the formula*

$$H_{\infty} = -\frac{\varepsilon^2 4\mu}{1 + \varkappa} [\mathcal{L}(0) \mathcal{P} \mathcal{L}(0)] = \frac{R^2}{y_0} [1 + m^2], \quad (5.1.4)$$

The deflection is always positive and does not depend on the rotation of the main axis of elliptical defect. This is a direct consequence of the fact that the dipole matrix \mathcal{P} is negative definite for any cavity of finite dimension. Moreover, H_{∞} increases when parameter m increases (Figure 5-1). The latter means that the deflection due to interaction with a thin ellipse is greater than the deflection produced by a circular cavity with the diameter equal to the crack length (equal sum of semi-axes $a + b = 2R$ should be taken into account).

One can note from Figure 5-2 that, for any orientation of the Griffith crack, all crack trajectories intersect at the point corresponding to $l = 0$. Moreover, $H(0) = H_{\infty}$. The second observation, that the crack deflection is independent of the orientation of the small defect, is valid in the vicinity of infinite remote point. The change of the angle β affects the shape of the crack trajectory in the vicinity of the origin.

A SEM photograph (Figure 5-3) shows the crack path induced by Vickers indenter in a sample of porcelain stoneware. This particular ceramic contains a dilute concentration

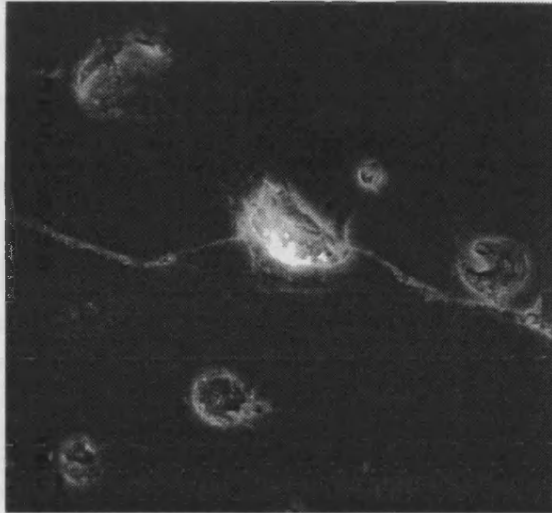


Figure 5-3: SEM photograph of a crack in a porcelain stoneware

of near-ellipsoidal voids. These voids have been modelled as ellipses in Figure 5-4 where the crack trajectory shown has been obtained using the technique above. Obviously, certain approximations of the model may be anticipated. In particular, interactions between voids has been neglected; moreover, the assumption of small ratio of the void dimension to the distance from the crack tip is often required. However, from Figure 5-4 we note that, in spite of all the approximations, the mathematical model gives a good description of the physical situation. The experimental photographs have been kindly provided by the Ceramic Centre (Bologna, Italy) and published in Bigoni, Movchan, Exposito, Serkov and Valentini [9], [114].

The comparison of the theory developed with the numerical solution of the singular integral equation for the complex crack opening given by Rubinstein [95] leads to interesting results. Taking $h'(l) = 0$ in (4.5.30) gives the formula for the normalised Mode-II stress intensity factor in the case when the unperturbed state corresponds to the Mode-I load (characterised by the stress-infinity factor K_I^∞)

$$K_{II}/K_I^\infty \sim \frac{R^2}{r^2} \sum_{j,k=1}^3 \mathcal{P}_{jk} \mathcal{F}_{jk}(r, \phi), \quad (5.1.5)$$

with (r, ϕ) being polar coordinates of a small defect.

Comparison with Rubinstein's results [95] is shown in Figures 5-5(a) and 5-5(b) for a Griffith crack and a circular cavity respectively. Note that the Mode-II normalised stress intensity factors are given as functions of ϕ , the angle of orientation of the position vector

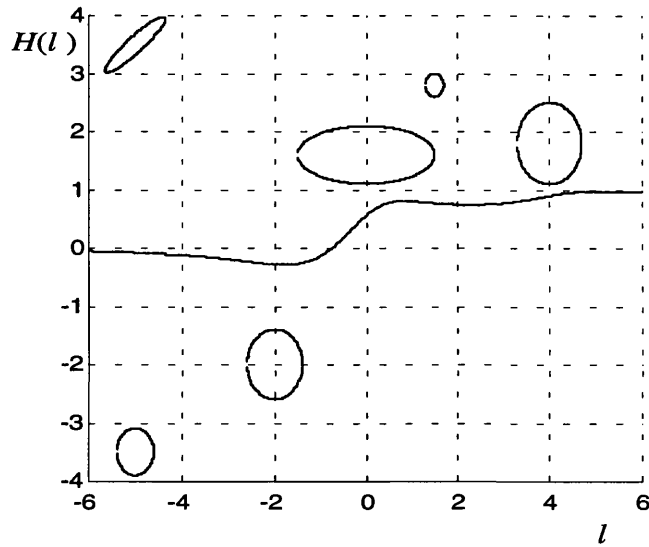


Figure 5-4: Matlab simulation corresponding to SEM photograph 5-3

relative to the small defect (Figure 4-1). Since the expression (5.1.5) is an approximate asymptotic formula, a discrepancy with the numerical results of Rubinstein can be expected. The error is however quite small and the results of an explicit asymptotic analysis show the right qualitative behaviour of the stress intensity factor as a function of the angular variable ϕ .

5.1.2 Interaction between a crack and a circular elastic inclusion

Another important example is an interaction of a crack with an elastic inclusion. It allows one to analyse the effect of the elastic moduli of the inclusion on the crack trajectory. In the frame of this section we restrict ourselves by analysing the problem for an elastic circular inclusion.

First, for reader's convenience, we rewrite the formula for the Pólya-Szegő matrix corresponding to an elastic circular inclusion (see (2.2.39) in Chapter 2)

$$\mathcal{P} = \frac{2 R^2 \pi \mu (\lambda + 2\mu)}{\lambda + \mu} \begin{pmatrix} \Xi + \Theta & \Xi - \Theta & 0 \\ \Xi - \Theta & \Xi + \Theta & 0 \\ 0 & 0 & 2\Theta \end{pmatrix}, \quad (5.1.1)$$

where

$$\Theta = \frac{\mu_0 - \mu}{\varkappa \mu_0 + \mu}, \quad \Xi = \frac{1}{(\varkappa - 1)^2} \frac{2\mu_0(\varkappa - 1) - 2\mu(\varkappa_0 - 1)}{\mu(\varkappa_0 - 1) + 2\mu_0}. \quad (5.1.2)$$

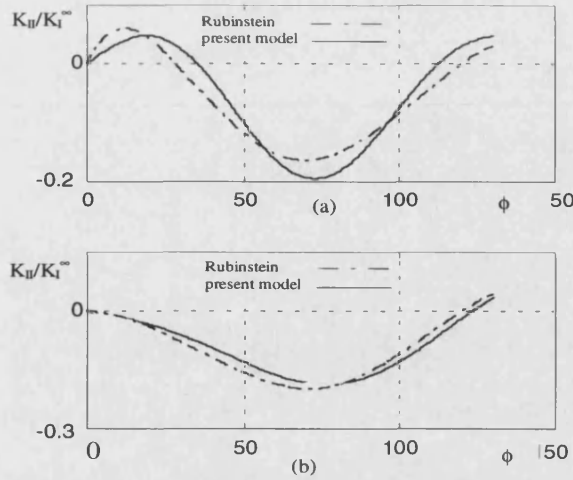


Figure 5-5: Comparison with Rubinstein's [95] results, Mode II normalized stress intensity factor versus defect position ϕ :
 (a) interaction with a Griffith crack;
 (b) interaction with a circular cavity.

Consequently, the formula (4.5.33) gives

$$\begin{aligned}
 H(l) = \varepsilon^2 h(l) = \frac{R^2}{2y_0} & \left[(z^2 + z - 2) \frac{\mu_0(\kappa - 1) - \mu(\kappa_0 - 1)}{\mu(\kappa_0 - 1) + 2\mu_0} \right. \\
 & \left. + (z - z^3) \frac{\mu_0 - \mu}{\kappa\mu_0 + \mu} \right], \quad (5.1.3)
 \end{aligned}$$

where R is the radius of the inclusion and

$$z = \frac{x_0 - l}{\sqrt{y_0^2 + (x_0 - l)^2}}.$$

In the particular case when $\mu_0 = 0$ the formula (5.1.3) reduces to (5.1.3) with $m = 0$ which corresponds to the case of a circular cavity. The Pólya-Szegő matrix \mathcal{P} of a circular inclusion is positive definite when

$$\frac{\mu_0}{\mu} > 1 \quad \text{and} \quad \frac{\lambda_0 + \mu_0}{\lambda + \mu} > 1, \quad (5.1.4)$$

and it is negative definite when the inequalities (5.1.4) are both reversed. Otherwise, the matrix \mathcal{P} is indefinite.

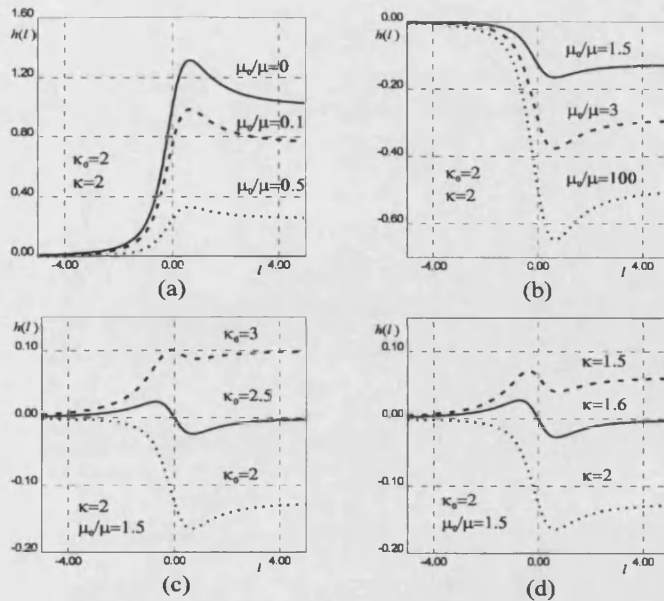


Figure 5-6: Crack trajectory $h(l)$ versus crack tip position l , resulting from interaction with an elastic circular inclusion: (a) inclusion more rigid than the matrix; (b) inclusion less rigid than the matrix; (c) and (d) \mathcal{P} is indefinite.

The crack deflection at infinity is given by

$$H_{\infty} = \varepsilon^2 h_{\infty} = \frac{R^2}{y_0} \left\{ 1 - \frac{\mu_0(\kappa + 1)}{2\mu_0 + (\kappa_0 - 1)\mu} \right\}. \quad (5.1.5)$$

The crack trajectories corresponding to the interaction of a semi-infinite crack with an elastic circular inclusion are reported in Figure 5-6 for different values of elastic parameters. In particular, when the inclusion is more rigid than the matrix, the conditions (5.1.4) hold, and therefore, the defect attracts the crack (Figure 5-6(a)). In the case of an inclusion which is softer than the matrix, the inverse conditions hold, and therefore, the crack is repelled by the defect (Figure 5-6(b)). Figure 5-6(c) and Figure 5-6(d) refer to the cases in which matrix \mathcal{P} is indefinite. Note that in this case a set of parameters can be chosen such that the deflection at infinity is equal to zero. These observations can be summarised in the following propositions:

Lemma 5.2 *Defects with the positive definite Pólya-Szegő matrices repel the macro-crack, and defects characterised by the negative definite Pólya-Szegő matrices attract the macro-crack.*

For circular elastic inclusions the condition of positive definiteness can be expressed in the form:

$$\mu_0 > \mu \quad \text{and} \quad \lambda_0 + \mu_0 > \lambda + \mu. \quad (5.1.6)$$

The Pólya-Szegő matrix is negative definite, if

$$\mu_0 < \mu \quad \text{and} \quad \lambda_0 + \mu_0 < \lambda + \mu. \quad (5.1.7)$$

Lemma 5.3 *The macro-crack has zero deflection at infinity if and only if the coefficients of the Pólya-Szegő matrix satisfy the conditions*

$$\mathcal{P}_{11} + \mathcal{P}_{22} + 2\mathcal{P}_{12} = 0.$$

For instance, such a condition written for the circular elastic inclusion reduces to equal bulk moduli of the inclusion and the matrix

$$\lambda_0 + \mu_0 = \lambda + \mu \quad (5.1.8)$$

As an example, in Figure 5-7 we present the experimental SEM photo of a sample of Zirconia-Alumina composite (ZrO_2/Al_2O_3). The aluminium inclusions can be modelled as circular elastic inclusions with the moduli $\lambda_0 = 140GPa$ and $\mu_0 = 180GPa$. The characteristics of the Zirconia matrix are $\lambda = 125GPa$ and $\mu = 75GPa$ (see, for example, Claussen [19]).

5.2 The influence of an elliptic elastic inclusion on the crack trajectory

5.2.1 Model problem

Before going further in consideration of crack-inclusion interaction we shall stop for a moment and return to the problem of Pólya-Szegő matrices. In Chapter 2 these matrices have been calculated for cavities and rigid inclusions, here our intention is to construct a matrix for an elliptical inclusion. The main methodology in this section is similar to the one used in Chapter 2, but at the same time calculation of the Pólya-Szegő tensor

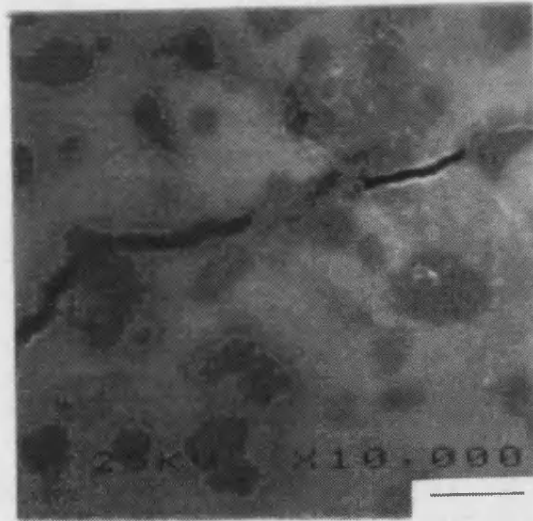


Figure 5-7: Crack propagation in Zirconia-Alumina composite

for an elastic elliptical inclusion look extremely laborious even under the right choice of notations.

To construct the Pólya-Szegő matrix, we consider a model problem for an inclusion in an infinite plane subject to a homogeneous loading at infinity. The inclusion is characterized by the Lamé constants λ_0, μ_0 and the infinite medium by the constants λ, μ . The surrounding medium is loaded at infinity by prescribing a generic homogeneous deformation. In particular, with reference to a Cartesian coordinate system, the three displacement fields at infinity are important for further analysis ((2.1.6) in Chapter 2). These displacements correspond to three linearly independent deformations, a linear combination of which gives a general homogeneous deformation. Subjected to these conditions at infinity and due to the presence of the inclusion, the elastic matrix deforms with non-linear distribution of stresses. However, the deformation in the inclusion remains homogeneous (constant stress field). The latter has been shown by Hardiman [36] and Eshelby [24] and is known as the Eshelby theorem.

Now we are looking for a displacement field satisfying the Navier equation in both the matrix and the inclusion. The following interface boundary conditions are imposed

$$\mathbf{u}_0(\mathbf{x}) = \mathbf{u}(\mathbf{x}) \quad \text{and} \quad \boldsymbol{\sigma}_0^{(n)}(\mathbf{u}_0; \mathbf{x}) = \boldsymbol{\sigma}^{(n)}(\mathbf{u}; \mathbf{x}), \quad \mathbf{x} \in \partial G_\varepsilon, \quad (5.2.1)$$

where \mathbf{u} is the displacement field, $\boldsymbol{\sigma}^{(n)}$ is the traction vector on the elliptical boundary

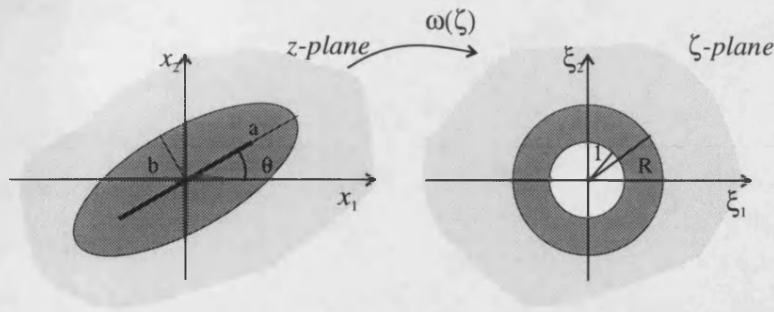


Figure 5-8: Elliptical inclusion and its conformal map

∂G_ϵ , \mathbf{n} is the unit normal vector and the index $(\)_0$ denotes fields inside the inclusion. The displacement field $\mathbf{u} = (u_1, u_2)$ satisfying the Navier equation inside and outside the inclusion can be represented, in terms of complex Kolosov-Muskhelishvili potentials $\varphi(z)$ and $\psi(z)$ as

$$u_1 + iu_2 = \frac{1}{2\mu} [\kappa\varphi(z) - z\overline{\varphi'(z)} - \overline{\psi(z)}], \quad (5.2.2)$$

where $z = x_1 + ix_2$, $\kappa = \frac{\lambda+3\mu}{\lambda+\mu} = 3 - 4\nu$, ν is the Poisson ratio. The resultant force acting on a generic arc AB of any curve drawn in the material (i.e. in the xy -plane) can be represented as

$$F_x + iF_y = -i \left[\varphi(z) + z\overline{\varphi'(z)} + \overline{\psi(z)} \right]_B^A. \quad (5.2.3)$$

5.2.2 Conformal mapping

Let us consider the complex plane z where the inclusion is an ellipse with the semi-axes a and b , with the major axis oriented at an angle β with respect the x -axis (Figure 5-8). Following Sokolnikoff [103], one investigates the properties of the Zukovskij function

$$z = \omega(\xi) = c_1\xi + c_{-1}\xi^{-1}, \quad (5.2.4)$$

where

$$c_1 = \frac{\sqrt{a^2 - b^2}}{2} \quad \text{and} \quad c_{-1} = c_1 \exp 2i\beta. \quad (5.2.5)$$

This function maps conformally a ring in the ξ -plane with internal radius

$$\mathcal{R} = \sqrt{\frac{a-b}{a+b}},$$

and external one

$$\mathcal{R}^{-1} = \sqrt{\frac{a+b}{a-b}},$$

to an elliptical inclusion in the z -plane with a slit along the major axis of the ellipse between two points $-\exp i\beta\sqrt{a^2-b^2}$ and $\exp i\beta\sqrt{a^2-b^2}$. Note that $0 < \mathcal{R} < 1$ and the limit value 1 corresponds to mapping of the exterior of a slit to the exterior of a unit disk. The same function (5.2.4) maps the region outside the circle of radius \mathcal{R}^{-1} to the exterior of the ellipse.

The map (5.2.4) can be inverted to give the following relation

$$\xi = \frac{z}{2c_1} + \frac{1}{2c_1} \sqrt{z^2 - 4c_1c_{-1}}, \quad (5.2.6)$$

that, for $|z| \rightarrow \infty$, can be expanded in the series representation

$$\xi = \frac{z}{c_1} - \frac{c_{-1}}{z} + O(|z|^{-3}). \quad (5.2.7)$$

Note that the map (5.2.4) does not have a limit when semi-axes of ellipse coincide (the ellipse reduces to a circle). In this situation $\mathcal{R} \rightarrow 0$ and $\mathcal{R}^{-1} \rightarrow \infty$. To resolve this problem, one shall introduce new complex variable ξ^* such that

$$\xi^* = \sqrt{\frac{a-b}{a+b}} \xi.$$

Its substitution in the conformal mapping (5.2.4) yields

$$z = \omega(\xi^*) = \frac{a+b}{2} \xi^* + \frac{a-b}{2} \exp 2i\beta \frac{1}{\xi^*}. \quad (5.2.8)$$

5.2.3 Series representation for potentials

Taking into account the conformal mapping (5.2.4), the complex representation for the displacement field (5.2.2) can be represented in the following form

$$u_1(\xi) + iu_2(\xi) = \frac{1}{2\mu} \left[\kappa\varphi(\xi) - \frac{\omega(\xi)}{\omega'(\xi)} \overline{\varphi'(\xi)} - \overline{\psi(\xi)} \right]. \quad (5.2.9)$$

A series expansion of potentials $\varphi(\xi)$ and $\psi(\xi)$ can be performed

$$\varphi(\xi) = \sum_{n=-\infty}^1 a_n \xi^n, \quad \psi(\xi) = \sum_{n=-\infty}^1 b_n \xi^n, \quad (5.2.10)$$

5.2. THE INFLUENCE OF AN ELLIPTIC ELASTIC INCLUSION ON THE CRACK TRAJECTORY

where, in particular, the coefficients a_0 and b_0 , representing the rigid body translation, can be set equal to zero, i.e. $a_0 = b_0 = 0$. Inside the inclusion the following series representation of the complex potentials is adopted (note that the result of the Eshelby theorem is not used here and it will follow from the solution for the displacement field)

$$\varphi_0(\xi) = \sum_{k=-\infty}^{+\infty} d_k \xi^k, \quad \psi_0(\xi) = \sum_{n=-\infty}^{+\infty} e_n \xi^n, \quad (5.2.11)$$

where, once again, $d_0 = e_0 = 0$ can be assumed. Let one consider the conformal mapping (5.2.4) shown in Figure 5-8 and two generic points lying on the circle $|\xi| = 1$ inclined at $\beta + \vartheta$ and $\beta - \vartheta$ with respect to the ξ_1 -axis. These points correspond to the same point on the slit in z -plane inclined of the angle β . Therefore, the conditions

$$\varphi_0(e^{i(\beta+\vartheta)}) = \varphi_0(e^{i(\beta-\vartheta)}), \quad \psi_0(e^{i(\beta+\vartheta)}) = \psi_0(e^{i(\beta-\vartheta)}), \quad (5.2.12)$$

hold for any ϑ . The substitution of (5.2.12) into (5.2.11) gives

$$\begin{aligned} \sum_{k=-\infty}^{k=+\infty} d_k e^{ki(\beta+\vartheta)} &= \sum_{k=-\infty}^{k=+\infty} d_k e^{ki(\beta-\vartheta)}, \\ \sum_{k=-\infty}^{k=+\infty} e_k e^{ki(\beta+\vartheta)} &= \sum_{k=-\infty}^{k=+\infty} e_k e^{ki(\beta-\vartheta)}, \end{aligned} \quad (5.2.13)$$

so that, comparing terms multiplied by $e^{ki\vartheta}$, we obtain the useful conditions

$$d_{-k} = d_k \exp 2ki\beta, \quad e_{-k} = e_k \exp 2ki\beta. \quad (5.2.14)$$

Coefficients a_1 and b_1 are determined from the conditions at infinity; we supposed that they are known, i.e.

$$a_1 = \alpha_j, \quad b_1 = \gamma_j, \quad \text{where } \alpha_j \in \mathbb{R}, \quad \gamma_j \in \mathbb{C} \quad (5.2.15)$$

For exact value α_j, γ_j corresponding to linear fields $V^{(j)}$ one refers to (2.2.7) in Chapter 2.

The other coefficients of (5.2.10) and (5.2.11) can be determined from the boundary conditions (5.2.1) which can be rewritten in terms of complex potentials in the following

form

$$\begin{aligned} \left[\varkappa\varphi(\xi) - \frac{\omega(\xi)}{\omega'(\xi)}\overline{\varphi'(\xi)} - \overline{\psi(\xi)} \right] &= \frac{\mu}{\mu_0} \left[\varkappa_0\varphi_0(\xi) - \frac{\omega(\xi)}{\omega'(\xi)}\overline{\varphi'_0(\xi)} - \overline{\psi_0(\xi)} \right], \\ \varphi(\xi) + \frac{\omega(\xi)}{\omega'(\xi)}\overline{\varphi'(\xi)} + \overline{\psi(\xi)} &= \varphi_0(\xi) + \frac{\omega(\xi)}{\omega'(\xi)}\overline{\varphi'_0(\xi)} + \overline{\psi_0(\xi)}, \end{aligned} \quad (5.2.16)$$

where $|\xi| = \mathcal{R}^{-1}$.

The series representation of $[\omega'(\xi)]^{-1}$ at infinity yields

$$\omega'(\xi)^{-1} = \frac{1}{c_1} \left(1 + \frac{c_{-1}}{c_1}\xi^{-2} + \left(\frac{c_{-1}}{c_1} \right)^2 \xi^{-4} + O(|\xi|^{-6}) \right), \quad (5.2.17)$$

so that on the boundary of external circle with radius \mathcal{R}^{-1} the following expansion holds

$$\frac{\omega(\xi)}{\omega'(\xi)} = \sum_{k=-1}^{+\infty} g_k \xi^k,$$

where $g_{-1} = \exp 2i\beta$,

$$\begin{aligned} g_k &= \left(1 + \mathcal{R}^4 \right) \mathcal{R}^{2(k-1)} \exp \{-i\beta(k-1)\}, \quad \text{for } k = 2m-1, \quad m \in \mathbb{N}, \\ g_k &= 0, \quad \text{for } k = 2m, \quad m \in \mathbb{N} \cup \{0\}. \end{aligned} \quad (5.2.18)$$

The system (5.2.16) can be rewritten in the form of sums if we take into account the series representations (5.2.11) for the complex potentials

$$\begin{aligned} \varrho &\left(\varpi \sum_{n=-\infty}^{+1} a_n \xi^n + \sum_{n=-1}^{+\infty} g_n \xi^n \sum_{n=-\infty}^{+1} n \bar{a}_n \bar{\xi}^{n-1} + \sum_{n=-\infty}^{+1} \bar{b}_n \bar{\xi}^n \right) \\ &= \varrho_0 \left(\varpi_0 \sum_{n=-\infty}^{+\infty} d_n \xi^n + \sum_{n=-1}^{+\infty} g_n \xi^n \sum_{n=-\infty}^{+\infty} n \bar{d}_n \bar{\xi}^{n-1} + \sum_{n=-\infty}^{+\infty} \bar{e}_n \bar{\xi}^n \right), \end{aligned} \quad (5.2.19)$$

where parameters ϖ and ϱ take the values,

$$\varrho = (2\mu)^{-1}, \quad \varrho_0 = (2\mu_0)^{-1}, \quad \varpi = -\varkappa, \quad \varpi_0 = -\varkappa_0,$$

and

$$\varrho = 1, \quad \varrho_0 = 1, \quad \varpi = 1, \quad \varpi_0 = 1.$$

Taking $|\xi| = \mathcal{R}^{-1}$ we rewrite the system (5.2.19)

$$\begin{aligned}
 & \varrho \left(\varpi \sum_{n=-\infty}^{+1} a_n \xi^n + \sum_{n=1}^{+\infty} \bar{a}_1 g_n \xi^n - \sum_{n=1}^{+\infty} \sum_{m=1}^{+\infty} m g_n \bar{a}_{-m} \mathcal{R}^{2(m+1)} \xi^{n+m+1} \right. \\
 & \quad \left. + g_{-1} \bar{a}_1 \xi^{-1} - \sum_{n=1}^{+\infty} n g_{-1} \bar{a}_{-n} \mathcal{R}^{2(n+1)} \xi^n + \sum_{n=1}^{+\infty} \bar{b}_{-n} \mathcal{R}^{2n} \xi^n + \bar{b}_1 \mathcal{R}^{-2} \xi^{-1} \right) \\
 & = \varrho_0 \left(\varpi_0 \sum_{n=-\infty}^{+\infty} d_n \xi^n + \sum_{n=1}^{+\infty} \sum_{m=1}^{+\infty} m g_n \bar{d}_m \mathcal{R}^{2(1-m)} \xi^{1-m+n} - \sum_{n=1}^{+\infty} \sum_{m=1}^{+\infty} m g_n \bar{d}_{-m} \mathcal{R}^{2(m+1)} \xi^{n+m+1} \right. \\
 & \quad \left. + \sum_{n=1}^{+\infty} n g_{-1} \bar{d}_n \mathcal{R}^{2(1-n)} \xi^{-n} - \sum_{n=1}^{+\infty} n g_{-1} \bar{d}_{-n} \mathcal{R}^{2(n+1)} \xi^n + \sum_{n=-\infty}^{+\infty} \bar{e}_n \mathcal{R}^{-2n} \xi^{-n} \right), \quad (5.2.20)
 \end{aligned}$$

or in a simpler form

$$\begin{aligned}
 & \varrho \left[\varpi a_1 \xi + \varpi \sum_{n=1}^{+\infty} a_{-n} \xi^{-n} + \sum_{n=1}^{+\infty} g_n \bar{a}_1 \xi^n - \sum_{n=3}^{+\infty} \sum_{m=1}^{n-2} g_m (n-m-1) \bar{a}_{1-n+m} \mathcal{R}^{2(n-m)} \xi^n \right. \\
 & \quad \left. + g_{-1} \bar{a}_1 \xi^{-1} - \sum_{n=1}^{+\infty} n g_{-1} \bar{a}_{-n} \mathcal{R}^{2(n+1)} \xi^n + \bar{b}_1 \mathcal{R}^{-2} \xi^{-1} + \sum_{n=1}^{+\infty} \bar{b}_{-n} \mathcal{R}^{2n} \xi^n \right] \\
 & = \varrho_0 \left[\varpi_0 \sum_{n=-\infty}^{+\infty} d_n \xi^n + \sum_{n=1}^{+\infty} \sum_{m=1}^{+\infty} g_m (n+m+1) \bar{d}_{n+m+1} \mathcal{R}^{-2(n+m)} \xi^{-n} \right. \\
 & \quad + \sum_{n=1}^{+\infty} \sum_{m=1}^{+\infty} g_{m+n-1} m \bar{d}_m \mathcal{R}^{2(1-m)} \xi^n - \sum_{n=3}^{+\infty} \sum_{m=1}^{n-2} g_m (n-m-1) \bar{d}_{1-n+m} \mathcal{R}^{2(n-m)} \xi^n \\
 & \quad \left. + \sum_{n=1}^{+\infty} g_{-1} n \bar{d}_n \mathcal{R}^{2(1-n)} \xi^{-n} - \sum_{n=1}^{+\infty} g_{-1} n \bar{d}_{-n} \mathcal{R}^{2(n+1)} \xi^n + \sum_{n=-\infty}^{+\infty} \bar{e}_n \mathcal{R}^{-2n} \xi^{-n} \right]. \quad (5.2.21)
 \end{aligned}$$

Comparing terms of equal order yields a system of linear equations for the unknowns a_n, b_n, c_n, d_n, e_n :

$$\begin{aligned}
 & \varrho \left[\varpi a_1 + \bar{b}_{-1} \mathcal{R}^2 + \bar{a}_1 g_1 - g_{-1} \bar{a}_{-1} \mathcal{R}^4 \right] = \varrho_0 \left[\varpi_0 d_1 + \bar{e}_{-1} \mathcal{R}^2 - g_{-1} \bar{d}_{-1} \mathcal{R}^4 + \sum_{h=1}^{+\infty} g_h h \mathcal{R}^{2(1-h)} \bar{d}_h \right]; \\
 & \varrho \left[\bar{b}_{-2} \mathcal{R}^4 - 2g_{-1} \bar{a}_{-2} \mathcal{R}^6 \right] = \varrho_0 \left[\varpi_0 d_2 + \bar{e}_{-2} \mathcal{R}^4 - 2g_{-1} \bar{d}_{-2} \mathcal{R}^6 + \sum_{h=1}^{+\infty} g_{h+1} h \mathcal{R}^{2(1-h)} \bar{d}_h \right]; \\
 & \varrho \left[\bar{a}_1 g_n + \bar{b}_{-n} \mathcal{R}^{2n} - g_{-1} n \bar{a}_{-n} \mathcal{R}^{2(n+1)} - \sum_{h=1}^{n-2} g_h (n-h-1) \bar{a}_{-n+h+1} \mathcal{R}^{2(n-h)} \right] \\
 & = \varrho_0 \left[\varpi_0 d_n + \bar{e}_{-n} \mathcal{R}^{2n} - g_{-1} n \bar{d}_{-n} \mathcal{R}^{2(n+1)} + \sum_{h=1}^{+\infty} g_{n+h-1} h \bar{d}_h \mathcal{R}^{2(1-h)} \right. \\
 & \quad \left. - \sum_{h=1}^{n-2} g_h (n-h-1) \bar{d}_{-n+h+1} \mathcal{R}^{2(h-n)} \right], \quad n \geq 3;
 \end{aligned}$$

5.2. THE INFLUENCE OF AN ELLIPTIC ELASTIC INCLUSION ON THE
CRACK TRAJECTORY

$$\begin{aligned} \varrho \left[\varpi a_{-1} + \bar{b}_1 \mathcal{R}^{-2} + g_{-1} \bar{a}_1 \right] &= \varrho_0 \left[\varpi_0 d_{-1} + \bar{e}_1 \mathcal{R}^{-2} + g_{-1} \bar{d}_1 + \sum_{h=1}^{+\infty} g_h (h+2) \mathcal{R}^{-2(h+1)} \bar{d}_{h+2} \right]; \\ \varrho \left[\varpi a_{-n} \right] &= \varrho_0 \left[\varpi_0 d_{-n} + \bar{e}_n \mathcal{R}^{-2n} + g_{-1} n \bar{d}_n \mathcal{R}^{2(1-n)} \right. \\ &\left. + \sum_{h=1}^{+\infty} g_h (h+n+1) \bar{d}_{h+n+1} \mathcal{R}^{-2(h+n)} \right], \quad n \geq 2. \end{aligned} \quad (5.2.22)$$

Taking into account the relations (5.2.14), the system (5.2.22) can be solved, yielding

$$\begin{aligned} a_{-1} &= \left[1 + \mathfrak{Y} \Theta (\mathcal{R}^4 - 1) \right] \alpha_j e^{2i\beta} + \frac{\Theta (1 - \mathcal{R}^4)}{\mathcal{R}^2 (1 + \mathcal{R}^4 \Theta)} \left[\bar{\gamma}_j + \mathcal{R}^4 \Re(\gamma_j e^{2i\beta}) e^{2i\beta} \right], \\ b_{-1} &= \mathfrak{Y} (1 - \mathcal{R}^4) \mathcal{R}^{-2} (1 - \mathcal{R}^4 \Theta) \alpha_j + \left[1 + \mathfrak{Y} \Theta (\mathcal{R}^4 - 1) \right] \Re(\gamma_j e^{2i\beta}) + i \Im(\gamma_j e^{2i\beta}), \\ d_1 &= \frac{(\varkappa + 1) \mu_0 [(1 - \mathcal{R}^4 \Theta) \alpha_j - \Theta \mathcal{R}^2 \Re(\gamma_j e^{2i\beta})]}{[(\varkappa_0 - 1) \mu + 2\mu_0] + \mathcal{R}^4 \Theta [(\varkappa_0 - 1) \mu - 2\varkappa \mu_0]} + i \frac{(\varkappa + 1) \mu_0 \mathcal{R}^2 \Theta \Im(\gamma_j e^{2i\beta})}{(\varkappa_0 + 1) \mu (1 + \mathcal{R}^4 \Theta)}, \\ e_{-1} &= \Gamma \left\{ \frac{[(\varkappa_0 - 1) \mu + 2\mu_0] \Re(\gamma_j e^{2i\beta})}{[(\varkappa_0 - 1) \mu + 2\mu_0] + \mathcal{R}^4 \Theta [(\varkappa_0 - 1) \mu - 2\varkappa \mu_0]} - \mathfrak{Y} \mathcal{R}^2 \alpha_j + i \frac{\Im(\gamma_j e^{2i\beta})}{1 + \mathcal{R}^4 \Theta} \right\}, \\ a_{-n} &= d_{-n} = d_n = e_{-n} = e_n = 0, \quad n \geq 1, \\ b_{-n} &= (1 + \mathcal{R}^4) \mathcal{R}^{-2} e^{(n-1)i\beta} (a_{-1} e^{-2i\beta} - a_1), \quad n = 2k + 1, \quad k \in \mathbb{N}, \\ b_{-n} &= 0, \quad n = 2k, \quad k \in \mathbb{N}, \end{aligned}$$

$$\begin{aligned} \text{where } \Theta &= \frac{\mu_0 - \mu}{\varkappa \mu_0 + \mu}, \quad \Gamma = \frac{(\varkappa + 1) \mu_0}{\varkappa \mu_0 + \mu}, \\ \mathfrak{X} &= \frac{2\Theta (\varkappa + 1) \mu_0}{[(\varkappa_0 - 1) \mu + 2\mu_0] + \mathcal{R}^4 \Theta [(\varkappa_0 - 1) \mu - 2\varkappa \mu_0]}, \\ \mathfrak{Y} &= \frac{2[(\varkappa - 1) \mu_0 - (\varkappa_0 - 1) \mu]}{[(\varkappa_0 - 1) \mu + 2\mu_0] + \mathcal{R}^4 \Theta [(\varkappa_0 - 1) \mu - 2\varkappa \mu_0]}. \end{aligned} \quad (5.2.23)$$

It is important to note that the system of linear equations for defining the coefficients $a_{-1}, b_{-1}, d_1, e_{-1}$ can be written in the following compact form:

$$\begin{aligned} \bar{b}_{-1} \mathcal{R}^2 - \bar{a}_{-1} \mathcal{R}^4 e^{2i\beta} + \alpha_j (2 + \mathcal{R}^4) &= d_1 + \bar{d}_1 + \bar{e}_{-1} \mathcal{R}^2, \\ \bar{b}_{-1} \mathcal{R}^2 - \bar{a}_{-1} \mathcal{R}^4 e^{2i\beta} + \alpha_j (1 - \varkappa + \mathcal{R}^4) &= \frac{\mu}{\mu_0} (\bar{d}_1 - \varkappa_0 d_1 + \bar{e}_{-1} \mathcal{R}^2), \\ a_{-1} e^{-2i\beta} + \alpha_j + \overline{\gamma_j e^{2i\beta}} \mathcal{R}^{-2} &= d_1 + \bar{d}_1 + \bar{e}_{-1} \mathcal{R}^{-2}, \end{aligned}$$

5.2. THE INFLUENCE OF AN ELLIPTIC ELASTIC INCLUSION ON THE
CRACK TRAJECTORY

$$-\kappa a_{-1} e^{-2i\beta} + \alpha_j + \overline{\gamma_j e^{2i\beta}} \mathcal{R}^{-2} = \frac{\mu}{\mu_0} (\bar{d}_1 - \kappa_0 d_1 + \bar{e}_{-1} \mathcal{R}^{-2}).$$

With the help of relations (5.2.14) between d_{-1} and d_1 and e_{-1} and e_1 , the exact expression of complex potentials can be obtained inside the inclusion

$$\begin{aligned} \varphi_0(\xi) &= d_1 \xi + d_{-1} \xi^{-1}, \\ \psi_0(\xi) &= e_1 \xi + e_{-1} \xi^{-1}, \end{aligned} \quad (5.2.24)$$

and outside the inclusion

$$\begin{aligned} \varphi(\xi) &= a_1 \xi + a_{-1} \xi^{-1}, \\ \psi(\xi) &= b_1 \xi + b_{-1} \xi^{-1} + (\mathcal{R}^2 + \frac{1}{\mathcal{R}^2}) \frac{(a_{-1} e^{-2i\beta} - a_1)}{\xi(\xi^2 e^{-2i\beta} - 1)}. \end{aligned} \quad (5.2.25)$$

Note that except well-known solutions due to Hardiman [36], Jaswon and Bhargava [46], the formulae (5.2.25) can be compared with the recent work by Gong and Meguid [33] where the case of $\theta = 0$ has been considered.

5.2.4 Pólya-Szegő matrix

Following the approach discussed in Chapter 2, the perturbation induced by a generic defect in an elastic matrix subject to the homogeneous conditions at infinity (2.1.6) is approximated using the Pólya-Szegő representation. Formula (2.1.8) holds at a sufficient distance from the defect. The linear vector polynomials (2.1.6) admit the following representation in terms of complex variables

$$V^{(1)}(z) = \frac{(z + \bar{z})}{2}, \quad V^{(2)}(z) = \frac{(z - \bar{z})}{2}, \quad V^{(3)}(z) = \frac{i\bar{z}}{\sqrt{2}}.$$

The vector differential operators (4.3.9) have the following form in complex variables:

$$\begin{aligned} \mathfrak{D}_{\frac{\partial}{\partial z}}^{(1)} &= \left(\frac{\partial}{\partial z} + \frac{\partial}{\partial \bar{z}}, 0 \right)^t, & \mathfrak{D}_{\frac{\partial}{\partial z}}^{(2)} &= \left(0, i \frac{\partial}{\partial z} - i \frac{\partial}{\partial \bar{z}} \right)^t, \\ \mathfrak{D}_{\frac{\partial}{\partial z}}^{(3)} &= 2^{-1/2} \left(i \frac{\partial}{\partial z} - i \frac{\partial}{\partial \bar{z}}, \frac{\partial}{\partial z} + \frac{\partial}{\partial \bar{z}} \right)^t, \end{aligned} \quad (5.2.26)$$

Using (5.2.26) and complex representation for the Green's tensor (2.2.12) the field (2.1.8) $W^{(j)}(z) = W_1^{(j)} + iW_2^{(j)}$ can be written in the complex variable form (2.2.11) which,

5.2. THE INFLUENCE OF AN ELLIPTIC ELASTIC INCLUSION ON THE
CRACK TRAJECTORY

through a substitution of coefficients of T_{ij} , becomes

$$W^{(j)}(z) := W_1^{(j)} + iW_2^{(j)} = \frac{q\kappa}{z} \left(-\mathcal{P}_{j1} + \mathcal{P}_{j2} - i\sqrt{2}\mathcal{P}_{j3} \right) + \frac{q(1-\kappa)}{\bar{z}} \left(\mathcal{P}_{j1} + \mathcal{P}_{j2} \right) + \frac{qz}{\bar{z}^2} \left(-\mathcal{P}_{j1} + \mathcal{P}_{j2} + i\sqrt{2}\mathcal{P}_{j3} \right). \quad (5.2.27)$$

Comparing (5.2.27) and (5.2.2), the coefficients of Pólya-Szegő matrix can be written in terms of the coefficients a_{-1} , b_{-1}

$$\begin{aligned} \mathcal{P}_{j1} &= \frac{1}{4q\mu} \left\{ -\operatorname{Re}[a_{-1}^j c_1 - \alpha_j c_{-1}] + \frac{b_{-1}^j c_1 - \gamma_j c_{-1}}{\kappa - 1} \right\}, \\ \mathcal{P}_{j2} &= \frac{1}{4q\mu} \left\{ \operatorname{Re}[a_{-1}^j c_1 - \alpha_j c_{-1}] + \frac{b_{-1}^j c_1 - \gamma_j c_{-1}}{\kappa - 1} \right\}, \\ \mathcal{P}_{j3} &= \frac{\sqrt{2}}{4q\mu} \operatorname{Im}[\alpha_j c_{-1} - a_{-1}^j c_1]. \end{aligned} \quad (5.2.28)$$

Provided the coefficients a_{-1}^j and b_{-1}^j have been calculated, the Pólya-Szegő matrix is known and its coefficients can be written in the following form for the elliptical elastic inclusion with the axes a and b , the major of which is inclined at an angle θ with respect to the x_1 -axis

$$\begin{aligned} P_{11} &= \frac{ab}{4q} \left\{ \frac{\Theta}{1 + \mathcal{R}^4 \Theta} \left[1 + \mathcal{R}^4 \mathfrak{X} \cos^2 2\beta \right] + \frac{\mathfrak{Y}}{\kappa - 1} \left[\frac{1 - \mathcal{R}^4 \Theta}{\kappa - 1} + 2\mathcal{R}^2 \Theta \cos 2\beta \right] \right\}, \\ P_{12} &= \frac{ab}{4q} \left\{ -\frac{\Theta}{1 + \mathcal{R}^4 \Theta} \left[1 + \mathcal{R}^4 \mathfrak{X} \cos^2 2\beta \right] + \frac{\mathfrak{Y}(1 - \mathcal{R}^4 \Theta)}{(\kappa - 1)^2} \right\}, \\ P_{13} &= \frac{\sqrt{2}ab}{4q} \Theta \sin 2\beta \left[\frac{\mathcal{R}^2 \mathfrak{Y}}{\kappa - 1} + \frac{\mathcal{R}^4 \mathfrak{X}}{1 + \mathcal{R}^4 \Theta} \cos 2\beta \right], \\ P_{22} &= \frac{ab}{4q} \left\{ \frac{\Theta}{1 + \mathcal{R}^4 \Theta} \left[1 + \mathcal{R}^4 \mathfrak{X} \cos^2 2\beta \right] + \frac{\mathfrak{Y}}{\kappa - 1} \left[\frac{1 - \mathcal{R}^4 \Theta}{\kappa - 1} - 2\mathcal{R}^2 \Theta \cos 2\beta \right] \right\}, \\ P_{32} &= \frac{\sqrt{2}ab}{4q} \Theta \sin 2\beta \left[\frac{\mathcal{R}^2 \mathfrak{Y}}{\kappa - 1} - \frac{\mathcal{R}^4 \mathfrak{X}}{1 + \mathcal{R}^4 \Theta} \cos 2\beta \right], \\ P_{33} &= \frac{ab}{2q} \frac{\Theta}{1 + \mathcal{R}^4 \Theta} \left[1 + \mathcal{R}^4 \mathfrak{X} \sin^2 2\beta \right], \end{aligned} \quad (5.2.29)$$

where q , Θ , Γ , \mathfrak{X} , \mathfrak{Y} are given by (5.2.23).

5.2. THE INFLUENCE OF AN ELLIPTIC ELASTIC INCLUSION ON THE
CRACK TRAJECTORY

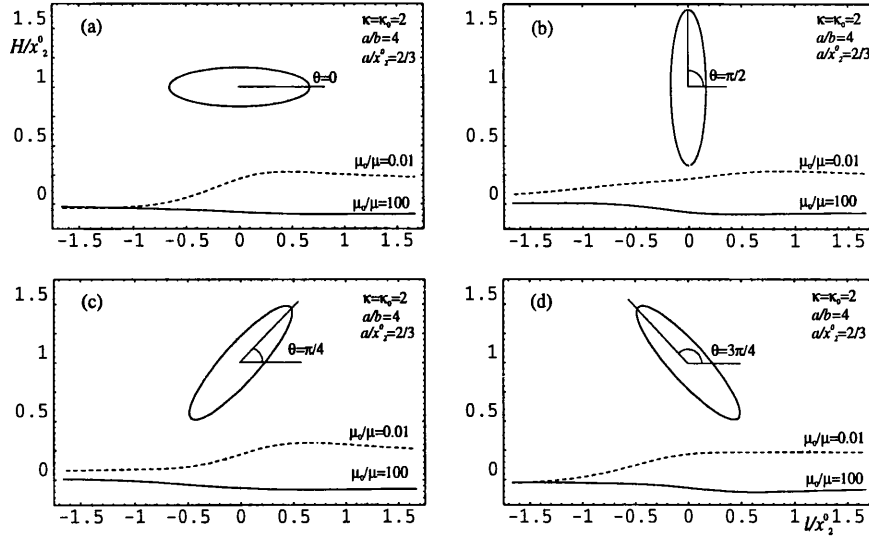


Figure 5-9: Crack trajectories $H(l)/y_0$ versus crack tip position l/y_0 , resulting from interaction with an elliptical inclusion, (a) more and (b) less stiff than the matrix. The major axis is inclined of different angles with respect to the unperturbed crack.

5.2.5 Trajectory of a perturbed crack

Since the Pólya-Szegő matrix has been calculated, one can investigate the trajectory of a semi-infinite crack that, in the absence of any disturbance, would propagate as a Mode I crack along the x -axis of an orthogonal coordinate system (x, y) . In the vicinity of the defect, a portion of length l of the crack is deflected. It has been shown in Chapter 4 that if the pure Mode-I propagation condition (i.e. the crack propagates such that $K_{II} = 0$) is accepted, the crack deflection can be described by a function $H(l)$ specifying the y coordinate of the crack (4.5.33), with \mathcal{L} given by (4.5.34). The crack path can therefore be expressed in a simplified form

$$\begin{aligned}
 H(l) = \frac{ab}{4y_0} & \left\{ \mathfrak{H}(1 - \mathcal{R}^4 \Theta)(t^2 + t - 2) + 2\mathcal{R}^2 \mathfrak{H} \Theta \left[\sin 2\beta(t + t^2)(2t - 1)\sqrt{1 - t^2} \right. \right. \\
 & \left. \left. - \cos 2\beta(t - t^3)(1 + 2t) \right] + \frac{\Theta}{1 + \mathcal{R}^4 \Theta}(t - t^3) \left[\left(1 + \mathcal{R}^4 \mathfrak{X} \cos^2 2\beta \right) \right. \right. \\
 & \left. \left. \times (1 - t)(1 + 2t)^2 + \left(1 + \mathcal{R}^4 \mathfrak{X} \sin^2 2\beta \right)(1 + t)(2t - 1)^2 \right. \right. \\
 & \left. \left. - \mathcal{R}^4 \mathfrak{X} \sin 4\beta \sqrt{1 - t^2}(4t^2 - 1) \right] \right\}, \tag{5.2.30}
 \end{aligned}$$

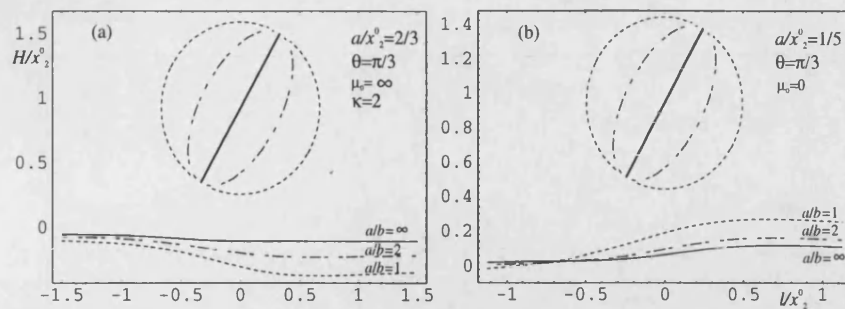


Figure 5-10: Crack trajectories $H(l)/y_0$ versus crack tip position l/y_0 , resulting from interaction with an elliptical rigid inclusion (a) and with an elliptical cavity (b) having major axis inclined of an angle $\theta = \pi/3$. Different aspect ratios are considered.

where

$$t = \cos \theta = \frac{x_0 - l}{\sqrt{(x_0 - l)^2 + y^2}}, \quad \text{and} \quad \mathcal{R}^2 = \frac{a - b}{a + b}.$$

Note that the expression (5.2.30) for the crack trajectory reduces to the known formulae for the cases of the elliptical void (5.1.3) when $\mu_0 = \lambda_0 = 0$ and circular elastic inclusion (5.1.3) when $a = b$. Analysing the deflection function, one can observe that the deflection of the crack at infinity is the same as at the origin, it can be evaluated by substitution $\theta = \pi$ and $\theta = \pi/2$ in (5.2.30) as specified in the following proposition:

Lemma 5.4 *Crack deflection at infinity caused by an elastic elliptical defect does not depend on the orientation of the ellipse and is given by*

$$H_\infty = H(0) = \frac{ab}{2y_0} \mathfrak{Y}(\mathcal{R}^4 \Theta - 1). \quad (5.2.31)$$

In Figures 5-9 to 5-11 the normalized crack deflection $H(l)$ (divided by the y_0 -coordinate of the centre of the defect) is plotted as a function of the crack tip horizontal position l (divided by y_0). Figures 5-9-5-11 represent crack trajectories in a non-dimensional scale. The centre of the ellipse is in all cases positioned at $(0, 1)$ and $a/y_0 = 0.04$ (in all figures, except for Figure 5-11, where the ellipses have the same area but different aspect ratio).

Four different ellipses are considered in Figure 5-11 with different inclinations and same aspect ratio $a/b = 4$. In particular, one ellipse is parallel, one is orthogonal and two are

5.2. THE INFLUENCE OF AN ELLIPTIC ELASTIC INCLUSION ON THE CRACK TRAJECTORY

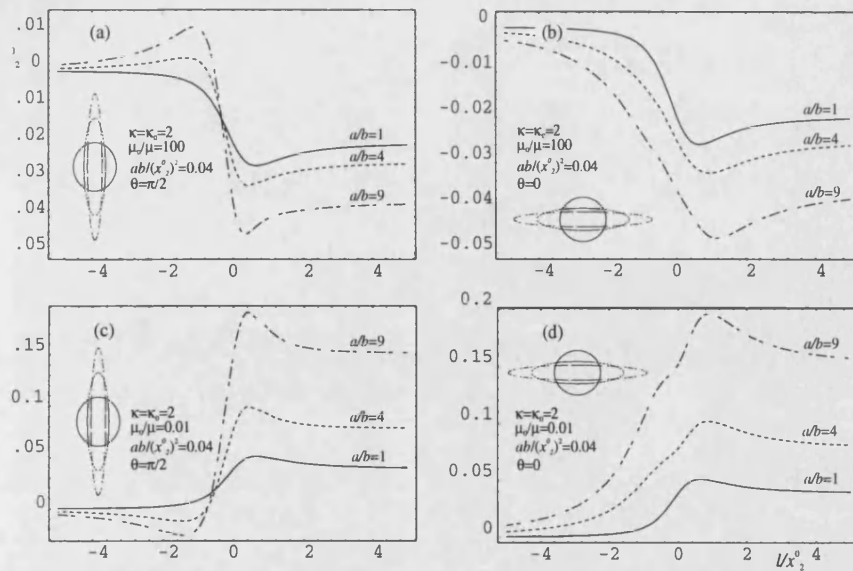


Figure 5-11: Crack trajectories $H(l)/y_0$ versus crack tip position l/y_0 , resulting from interaction with an elliptical inclusions of equal area: inclusion stiffer than the matrix, with major axis orthogonal (a) or parallel (b) to the unperturbed crack; inclusion weaker than the matrix, with major axis orthogonal (a) or parallel (b) to the unperturbed crack.

inclined (of $\pi/4$ and $3\pi/4$) with respect to the unperturbed crack trajectory, i.e. to the horizontal direction. The cases under consideration are referred to an ellipse stiffer and weaker than the matrix. It should be noted that, in order to give full evidence to the results, the ratio between the elastic moduli of the inclusion and matrix takes extreme values (μ_0/μ is equal to 0.01 and 100), whereas $\kappa_0 = \kappa = 2$. It can be observed from the figures that an inclusion more (less) rigid than the matrix tends to repel (attract) the crack. In particular, it can be shown that the crack repulsion and attraction correspond to a positive or negative definite Pólya-Szegő matrix respectively. Moreover, it can be observed that the asymptotes for $l/y_0 \rightarrow \infty$ of the various curves corresponding to different inclinations are the same, as predicted by (5.2.31).

The effect of the aspect ratio of the ellipse is investigated in Figure 5-10, in the particular cases of a rigid inclusion (Figure 5-10(a)) and an elliptical void (Figure 5-10(b)). The limit solution when $b/a = 0$ corresponds to the rigid line inclusion in the former case, and to a crack in the latter case. It may be concluded from these figures that the crack trajectory does not change significantly in shape when the aspect ratio changes, but the modulus of the deflection becomes less and less visible when the limit of the line inclusion is approached. It should be noted that the rigid inclusion repels the crack,

whereas the void attracts it. Moreover, voids affect the crack trajectory more than rigid inclusions.

In Figure 5-11, the comparison of the crack trajectories corresponding to elliptic inclusions having the same area $ab/(y_0)^2 = 4 \cdot 10^{-4}$ is presented. In particular, Figures 5-11(a,b) refer to the case of an inclusion which is more rigid than the matrix, whereas Figures 5-11(c,d) refer to the opposite case of a matrix stiffer than the inclusion. In both cases, it may be observed that the increase in the aspect ratio of the defect yields an increase in the crack deflection.

5.3 Fracture in thermo-elastic media

5.3.1 Interaction of a crack with a circular thermoelastic inclusion

The formula (4.5.37) characterizes the crack deflection for any possible types of the inclusions or their combinations. The morphology of the inclusion is specified in terms of the Pólya-Szegő matrix \mathcal{P} and the thermo-elastic vector \mathcal{D} . The only restriction on application of this formula is the non-interactive behaviour of inclusions. In other words, we suppose that the inclusion is located far away from the crack and it is small in comparison with the distance from the crack. If there are several inclusions in a plane, then the dilute limit is required. In this section we consider the interaction of a crack with a circular thermoelastic inhomogeneity. This is the simplest example, but it allows one to determine the main features of interaction mechanism in the presence of thermal effects.

In the problem where the inclusion is circular one needs to know the coefficients of the Pólya-Szegő matrix \mathcal{P} and the thermal vector \mathcal{D} . The Pólya-Szegő matrix for a circular inclusion is given by (5.1.1). Note that further it will be convenient to use the normalized form of the matrix, where R is supposed to be equal to one. To calculate the thermoelastic vector \mathcal{D} , one starts with the analysis of boundary conditions of the problem (4.3.7) written in terms of complex potentials

$$\varphi(z) + z\overline{\varphi'(z)} + \overline{\psi(z)} = \varphi_0(z) + z\overline{\varphi_0'(z)} + \overline{\psi_0(z)} + (\gamma - \gamma_0)\Delta Tz, \quad (5.3.1)$$

$$[\varkappa\varphi(z) - z\overline{\varphi'(z)} - \overline{\psi(z)}] \frac{\mu_0}{\mu} = \varkappa_0\varphi_0(z) - z\overline{\varphi_0'(z)} - \overline{\psi_0(z)}, \quad (5.3.2)$$

and looks for a solution which decays at infinity like $O(|z|^{-1})$. Due to Eshelby's theorem

[24] the solution is linear inside the inclusion. Note that here and further in the text we write the increment of temperature ΔT instead of $T - T_{rel}$. This value can be either positive or negative and depends on initial temperature at which the thermal stresses are zero.

The complex potentials $\varphi(z)$ and $\psi(z)$ obtained from the analysis of the boundary integral equations based on the boundary conditions (5.3.1) and (5.3.2) have the form

$$\varphi(z) = O\left(\frac{1}{|z|^2}\right), \quad \psi(z) = \frac{(\gamma - \gamma_0)\Delta T \mu(\kappa_0 - 1)}{2\mu_0 + \mu(\kappa_0 - 1)} \frac{1}{z} + O\left(\frac{1}{|z|^2}\right).$$

The components of the vector \mathcal{D} can be found as the coefficients multiplying the derivatives of the Green's tensor in the asymptotic expansion (4.3.8). After some routine calculations one obtains

$$\mathcal{D} = \frac{\mu\pi(\gamma - \gamma_0)\Delta T (\kappa_0 - 1)(\kappa + 1)}{(2\mu_0 + \mu(\kappa_0 - 1))(\kappa - 1)} \begin{pmatrix} 1 \\ 1 \\ 0 \end{pmatrix}. \quad (5.3.3)$$

Now, one has two characteristics of the thermoelastic inclusion: the Pólya-Szegő matrix and the thermoelastic vector \mathcal{D} . Finally, the formula for the crack deviation due to thermoelastic circular inclusion can be written in the form

$$\Delta h(l) = \varepsilon^2 \left(\Delta h_\varepsilon^\mu(l) + \frac{1}{K_I} \Delta h_\varepsilon^T(l) \right) + O(\varepsilon^3), \quad (5.3.4)$$

where

$$\Delta h_\varepsilon^T(l) = \frac{\mu\sqrt{2\pi}(\gamma_0 - \gamma)\Delta T (\kappa_0 - 1)}{2\mu_0 + \mu(\kappa_0 - 1)} \int_0^\theta \frac{\sin \frac{3\phi}{2}}{\sqrt{\sin \phi}} d\phi,$$

and $\Delta h_\varepsilon^\mu(l)$ is given by the formula (5.1.3), with $y_0 = 1, R = 1$.

If y_0 is not equal to 1 the formula (5.3.4) is given by

$$\Delta h(l) = \varepsilon^2 \left(\Delta h_\varepsilon^\mu(l)y_0 + \frac{1}{K_I} \Delta h_\varepsilon^T(l)y_0^{3/2} \right) + O(\varepsilon^3), \quad \varepsilon = \frac{R}{y_0}. \quad (5.3.5)$$

It corresponds to the case when the distance between the centre of the inclusion and the unperturbed crack y_0 is not normalized.

5.3.2 Interaction of a crack with an elliptical thermoelastic inclusion

In this section another example is considered: the perturbation of a crack due to an elliptical thermoelastic inhomogeneity. The elliptical inclusion has semi-axes a and b , with the major axis inclined at an angle β to the x -axis. As before, the problem of crack-inclusion interaction reduces to the formula (4.5.37) and requires the knowledge of Pólya-Szegő matrix \mathcal{P} and the vector \mathcal{D} . The components of Pólya-Szegő (symmetric) tensor have been calculated (see Chapter 4 formulae (5.2.29)).

To find the crack trajectory, we calculate the thermo-elastic vector \mathcal{D} for an elliptical inhomogeneity. The boundary value problem for determination of the auxiliary vector field $\mathbf{W}^{(4)}$ (4.3.7) is solved, and the components of the vector \mathcal{D} are extracted from the asymptotic expansion of the solution at infinity. The complex variables technique is applied. The following representation for the displacement fields (inside and outside of the defect) is used

$$\mathbf{u}^{(0)} = \mathbf{u}^{(0)*} + C^{(0)} z, \quad \mathbf{u} = \mathbf{u}^* + C z, \quad (5.3.1)$$

where $\mathbf{u}^{(\cdot)} = u_1^{(\cdot)} + iu_2^{(\cdot)}$ and $z = x_1 + ix_2$. The linear terms with the constant coefficients C and $C^{(0)}$ describe the thermal expansion. It follows from (5.3.1) and from the stress-strain relation that

$$\begin{aligned} \boldsymbol{\sigma}^{(n)}(\mathbf{u}^{(0)}) &= \boldsymbol{\sigma}^{(n)}(\mathbf{u}^{(0)*}) + 2(\lambda_0 + \mu_0)C^{(0)}\mathbf{n}, \\ \boldsymbol{\sigma}^{(n)}(\mathbf{u}) &= \boldsymbol{\sigma}^{(n)}(\mathbf{u}^*) + 2(\lambda + \mu)C\mathbf{n}, \end{aligned} \quad (5.3.2)$$

where \mathbf{n} is the normal vector. Taking into account the relations (5.3.1) and (5.3.2), the boundary conditions (4.3.7) can be rewritten as follows

$$\mathbf{u}^{(0)*} + C^{(0)} z = \mathbf{u}^* + C z,$$

$$\boldsymbol{\sigma}^{(n)}(\mathbf{u}^{(0)*}) + 2(\lambda_0 + \mu_0)C^{(0)}\mathbf{n} - \boldsymbol{\sigma}^{(n)}(\mathbf{u}^*) - 2(\lambda + \mu)C\mathbf{n} = (\gamma - \gamma_0)\Delta T\mathbf{n}.$$

The comparison of the terms of the same order shows that the constants C and $C^{(0)}$ are related to the thermal expansion coefficients α and α_0 by the relations

$$C = \alpha \Delta T, \quad C^{(0)} = \alpha_0 \Delta T. \quad (5.3.3)$$

The interface boundary conditions are reduced to

$$\begin{aligned}\sigma^{(n)}(u^{(0)*}) &= \sigma^{(n)}(u^*), \\ u^{(0)*} - u^* &= (\alpha - \alpha_0)\Delta T z,\end{aligned}\quad (5.3.4)$$

whereas the condition of decay at infinity

$$\mathbf{u} \rightarrow 0 \quad \text{as } |z| \rightarrow \infty$$

reduces to

$$u^* = -\alpha\Delta T z \quad \text{as } |z| \rightarrow \infty. \quad (5.3.5)$$

Using the complex potential method, we can rewrite the interface conditions (5.3.4) in the form

$$\begin{aligned}\frac{1}{2\mu} \left[\kappa\varphi(\xi) - \frac{\omega(\xi)}{\omega'(\xi)}\overline{\varphi'(\xi)} - \overline{\psi(\xi)} \right] - \frac{1}{2\mu_0} \left[\kappa_0\varphi_0(\xi) - \frac{\omega(\xi)}{\omega'(\xi)}\overline{\varphi'_0(\xi)} - \overline{\psi_0(\xi)} \right] \\ = (\alpha_0 - \alpha)\omega(\xi) \Delta T, \\ \varphi(\xi) + \frac{\omega(\xi)}{\omega'(\xi)}\overline{\varphi'(\xi)} + \overline{\psi(\xi)} = \varphi_0(\xi) + \frac{\omega(\xi)}{\omega'(\xi)}\overline{\varphi'_0(\xi)} + \overline{\psi_0(\xi)},\end{aligned}\quad (5.3.6)$$

where $|\xi| = 1$. Here, the complex potential $\varphi(\xi)$ and $\psi(\xi)$ are related to the field \mathbf{u}^* , whereas $\varphi_0(\xi)$ and $\psi_0(\xi)$ are related to the field $\mathbf{u}^{(0)*}$. The function $\omega(\xi)$ has the form

$$z = \omega(\xi) = c_1\xi + c_{-1}\xi^{-1}, \quad (5.3.7)$$

with c_1 and c_{-1} given by (5.2.5).

The boundary conditions (5.3.6) written in complex variables can be transformed into integral equations of Muskhelishvili type; and the last reduced to the system of linear equation for the coefficients in the series expansions of complex potentials. The corresponding technique has been discussed in Chapter 2 and Section 5.2. If the series expansions for the potentials $\varphi(\xi), \psi(\xi)$ is used in the form (5.2.10), (5.2.11) one obtains the linear system for the coefficients $a_{-1}, b_{-1}, d_1, e_{-1}$ which has the following form:

$$\bar{b}_{-1}\mathcal{R}^2 - \bar{a}_{-1}\mathcal{R}^4 e^{2i\beta} + a_1(2 + \mathcal{R}^4) = d_1 + \bar{d}_1 + \bar{e}_{-1}\mathcal{R}^2;$$

$$\bar{b}_{-1}\mathcal{R}^2 - \bar{a}_{-1}\mathcal{R}^4 e^{2i\beta} + a_1(1 - \varkappa + \mathcal{R}^2) = \frac{\mu}{\mu_0} (\bar{d}_1 - \varkappa_0 d_1 + \bar{e}_{-1}\mathcal{R}^2) - 2\mu(\alpha_0 - \alpha)\Delta T c_1;$$

$$a_{-1}e^{-2i\beta} + a_1 = d_1 + \bar{d}_1 + \bar{e}_{-1}\mathcal{R}^{-2};$$

$$-\varkappa a_{-1}e^{-2i\beta} + a_1 = \frac{\mu}{\mu_0} (\bar{d}_1 - \varkappa_0 d_1 + \bar{e}_{-1}\mathcal{R}^{-2} - 2\mu(\alpha_0 - \alpha)\Delta T c_1),$$

where $a_1 = -\frac{\gamma}{2}\Delta T c_1$ and $c_1 = \frac{\sqrt{a^2 - b^2}}{2}$ such that $(1 - \mathcal{R}^4)c_1^2 = ab\mathcal{R}^2$.

Solving the system of equation (5.3.6), we find the complex potentials which outside the defect have the following asymptotic representation

$$\begin{aligned} \varphi(z) &= -\frac{\gamma}{2}\Delta T z + \frac{1}{z} \frac{ab \mu(\varkappa_0 - 1)(\gamma_0 - \gamma)\Delta T \Theta \mathcal{R}^2}{(\varkappa_0 - 1)\mu + 2\mu_0 + \mathcal{R}^4\Theta[(\varkappa_0 - 1)\mu - 2\varkappa\mu_0]} e^{2i\beta} + o\left(\frac{1}{|z|}\right), \\ \psi(z) &= \frac{1}{z} \frac{ab \mu(\varkappa_0 - 1)(\gamma_0 - \gamma)\Delta T (\mathcal{R}^2\Theta - 1)}{(\varkappa_0 - 1)\mu + 2\mu_0 + \mathcal{R}^4\Theta[(\varkappa_0 - 1)\mu - 2\varkappa\mu_0]} + o\left(\frac{1}{|z|}\right), \end{aligned} \quad (5.3.8)$$

and therefore, the components of the vector \mathcal{D} have the form

$$\begin{aligned} \mathcal{D}_1 &= ab\pi(\varkappa + 1)\mathfrak{G} \left(\frac{\Theta\mathcal{R}^4 - 1}{\varkappa - 1} - \Theta\mathcal{R}^2 \cos 2\beta \right), \\ \mathcal{D}_2 &= ab\pi(\varkappa + 1)\mathfrak{G} \left(\frac{\Theta\mathcal{R}^4 - 1}{\varkappa - 1} + \Theta\mathcal{R}^2 \cos 2\beta \right), \\ \mathcal{D}_3 &= -\sqrt{2}ab\pi(\varkappa + 1)\mathfrak{G}\Theta\mathcal{R}^2 \sin 2\beta, \end{aligned} \quad (5.3.9)$$

where

$$\mathfrak{G} = \frac{\mu(\varkappa_0 - 1)(\gamma_0 - \gamma)\Delta T}{(\varkappa_0 - 1)\mu + 2\mu_0 + \mathcal{R}^4\Theta[(\varkappa_0 - 1)\mu - 2\varkappa\mu_0]}. \quad (5.3.10)$$

As before, one splits up the total deflection of a crack into an elastic deflection (deflection under zero increment of temperature) and thermal deflection (difference between total and elastic deflection). The elastic deflection is specified by the formula (5.2.30), whereas the thermal deflection is given by

$$\boxed{\Delta h^T(l) = \frac{ab\sqrt{2\pi}\mathfrak{G}}{\sqrt{y_0}K_I} \left\{ (1 - \mathcal{R}^4\Theta)I_1(\theta) + \mathcal{R}^2\Theta I_2(\theta) \cos 2\beta - \mathcal{R}^2\Theta I_3(\theta) \sin 2\beta \right\}}, \quad (5.3.11)$$

with the integrals I_1 , I_2 , I_3 defined below

$$\begin{aligned}
 I_1(\theta) &= \int_0^\theta \frac{\sin 3\phi/2}{\sqrt{\sin \phi}} d\phi, \\
 I_2(\theta) &= \int_0^\theta \frac{\cos \phi \sin 5\phi/2 + \sin 7\phi/2}{\sqrt{\sin \phi}} d\phi, \\
 I_3(\theta) &= \int_0^\theta \frac{\cos \phi \cos 5\phi/2 + \cos 7\phi/2}{\sqrt{\sin \phi}} d\phi.
 \end{aligned} \tag{5.3.12}$$

Analysing the behaviour of the function (5.3.11), we can conclude that the contribution of the thermal deflection at infinity is equal to zero

$$\begin{aligned}
 \Delta h^T(l)_\infty \rightarrow \frac{(a+b)\mathfrak{G}}{\sqrt{2\pi y_0}(\varkappa+1)K_I} \left\{ (\mathcal{R}^4\Theta - 1)I_1(\pi) + \right. \\
 \left. \mathcal{R}^2\Theta(I_3(\pi) \sin \beta - I_2(\pi) \cos \beta) \right\} = 0,
 \end{aligned} \tag{5.3.13}$$

The thermal deflection has only local effect: it affects the trajectory near the inclusion and does not affect it at infinity. This can also be seen from the numerical experiments presented in the next section.

5.3.3 Numerical experiments

A number of numerical experiments has been carried out to analyse the crack deviation. First, we recall that the cavities and soft inclusions attract the crack. On the other hand, the inclusions which are more rigid than the matrix material repel the crack. Since one treats uncoupled thermo-elasticity problems, it is possible to consider the “elastic” trajectory (trajectory of a crack in a elastic medium with zero increment of a temperature) and the thermal trajectory (difference between total and elastic trajectory). It is appropriate to refer to some numerical examples.

In Figure 5-12(top plot) one can see the crack trajectory due to soft inclusions. All trajectories correspond to attraction of the crack. At infinity the crack perturbation is still positive, but much less than near the inclusion.

In Figure 5-13(top plot) the crack trajectories due to rigid inclusions are shown. A negative deflection occurs in all points of trajectories including the infinite point. The more rigid the inclusion the more it repels the crack. It is important to note that all possible crack trajectories are in the region bounded by the curve corresponding to $\mu_0 \rightarrow \infty$ (lower boundary) and $\mu = 0$ (upper boundary).

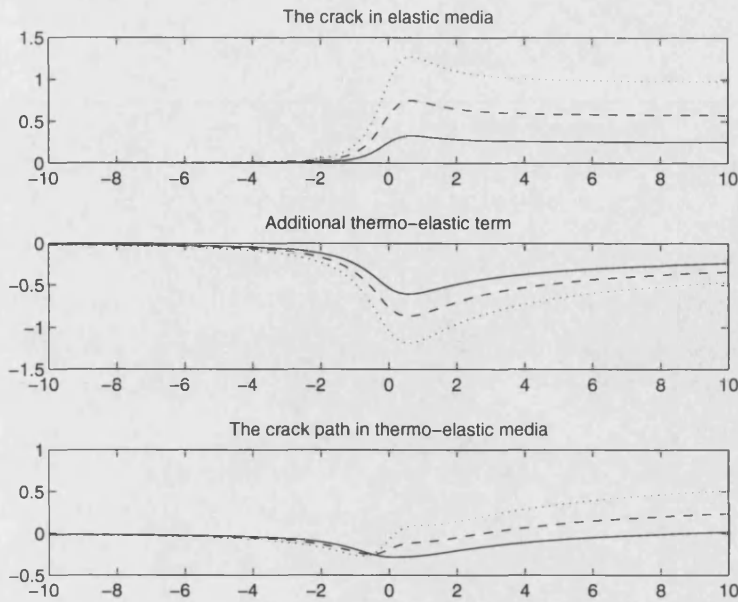


Figure 5-12: The crack deviation due to the soft thermoelastic inclusion: $\gamma = 4 \cdot 10^{-3}$, $\gamma_0 = 10^{-3}$, $\Delta T = 100K$, $\varkappa = 2$, $\varkappa_0 = 2$, $\mu_0/\mu = 0.5(-)$, $\mu_0/\mu = 0.2(--)$, $\mu_0/\mu = 0.01(\dots)$.

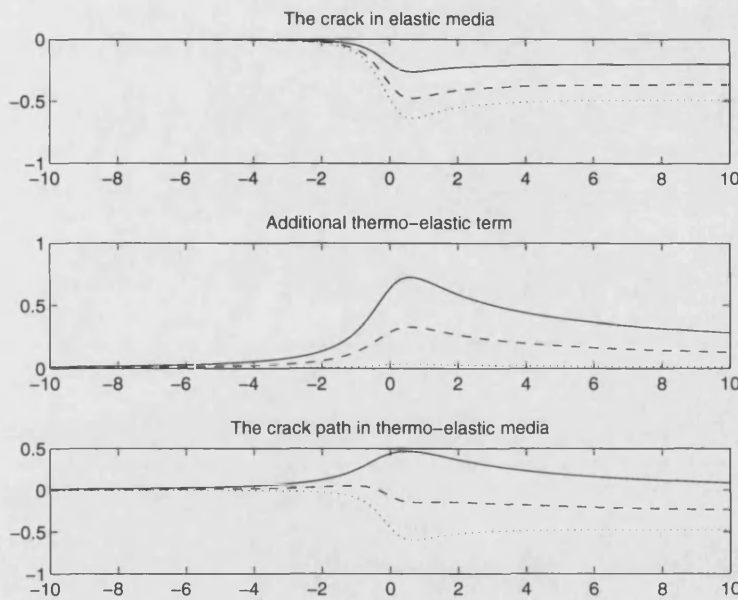


Figure 5-13: The crack deviation due to the rigid thermoelastic inclusion: $\gamma = 10^{-3}$, $\gamma_0 = 10^{-2}$, $\Delta T = 100K$, $\varkappa = 2$, $\varkappa_0 = 2$, $\mu_0/\mu = 2(-)$, $\mu_0/\mu = 5(--)$, $\mu_0/\mu = 50(\dots)$.

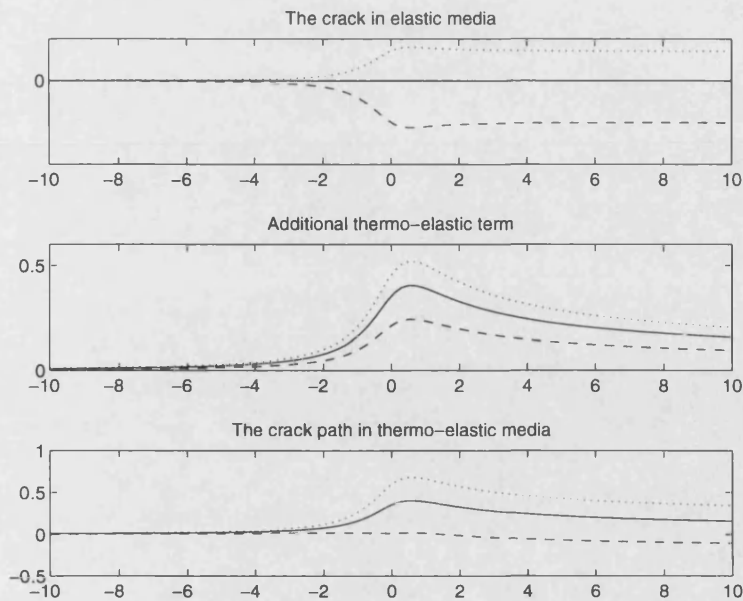


Figure 5-14: The crack deviation due to the thermoelastic inclusions with the same shear modulus: $\gamma = 10^{-3}$, $\gamma_0 = 4 \cdot 10^{-3}$, $\Delta T = 100K$, $\varkappa = 2$, $\mu_0/\mu = 1$, $\varkappa_0 = 2(-)$, $\varkappa_0 = 1.5(--)$, $\varkappa_0 = 2.5(\dots)$.

In Figure 5-14(top plot) the case of different Poisson ratio is considered. Shear moduli of matrix and inclusion are equal, but the parameters \varkappa and \varkappa_0 which characterize the Poisson ratios are different. If the Poisson ratio of the inclusion is less than of the matrix then the crack is attracted by the inclusion. In contrary, if Poisson ratio of the inclusion is greater, the crack is repelled by the inclusion.

By further analysis it is also possible to see that there are situations where the crack has zero deflection at infinity. It means that the macro-crack is not sensitive to such defects. Deflection has only local effect: some perturbations of a crack trajectory are possible only near the defect. When the crack propagates further all these effects vanish.

In Figure 5-15(top plot) we give an illustration of this statement: crack deflection at infinity is zero, at the same time there is a local perturbation of a crack trajectory near the origin. The latter is caused by differences in shear moduli of matrix and inclusion. The perturbation changes sign from positive to negative (or vice versa) depending on whether the shear modulus is greater in inclusion or in matrix.

The thermal deflection (difference between the total deflection and the elastic one) is analysed. This type of perturbation occurs only due to thermal expansion effect. If, for example, the coefficients of bulk thermal expansion γ and γ_0 are equal, then the

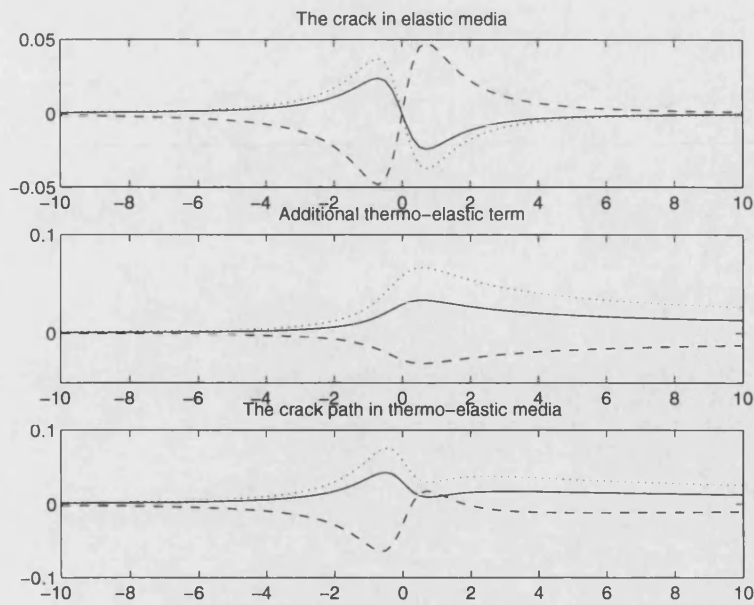


Figure 5-15: The crack deviation due to the thermoelastic inclusions with the same bulk modulus: $\gamma = 10^{-3}$, $\Delta T = 25K$, $\mu = 1$, $\lambda = 1$, $\mu_0 = 1.5$, $\lambda_0 = 0.5$, $\gamma_0 = 2 \cdot 10^{-3}(-)$, $\mu_0 = 0.5$, $\lambda_0 = 1.5$, $\gamma_0 = 10^{-4}(-)$, $\mu_0 = 1.95$, $\lambda_0 = 0.05$, $\gamma_0 = 3 \cdot 10^{-3}(\dots)$.

thermal deflection disappears even for non-zero temperature increment.

From the analysis of the thermoelastic term Δh_e^T , one can conclude that the difference of the thermal expansion coefficients plays an important role. To be more precise, whether the inclusion repels the crack or attracts it is defined by the sign of the expression $(\gamma - \gamma_0)\Delta T$. The inclusion with the greater thermal expansion coefficient repels the crack and, in contrary, the inclusion with the smaller thermal expansion coefficient attracts the crack.

Lemma 5.5 *The sign of the thermal deflection of the crack is the same as the sign of $(\gamma_0 - \gamma) \Delta T$.*

This simple proposition is illustrated in Figures 5-12 and 5-13. The middle plots show that $\gamma > \gamma_0$ and $\Delta T > 0$, the thermal crack trajectory is negative for an arbitrary combination of elastic parameters of inclusion and matrix. If $\gamma < \gamma_0$ and $\Delta T > 0$ the situation is the opposite.

Analysing further, we consider the total deflection. It is possible to find a situation when the temperature term compensates the influence of the elastic term, and the resulting crack deflection decreases. Such examples are presented in Figures 5-14, 5-15(bottom

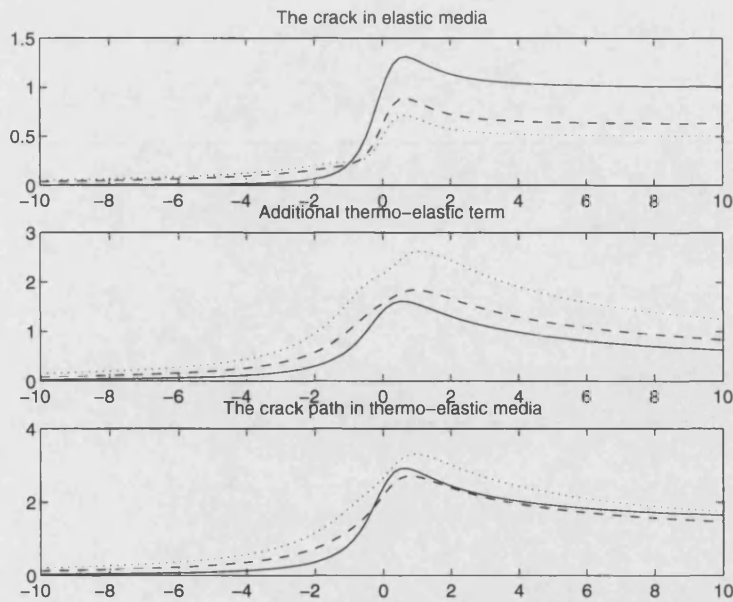


Figure 5-16: The crack deviation due to the elliptical thermoelastic inclusions with the same elastic and thermal moduli: $\gamma = 10^{-3}$, $\gamma_0 = 5 \cdot 10^{-3}$, $\Delta T = 100K$, $\varkappa = 2$, $\mu_0 = 0$, $\mu = 1$, $\varkappa_0 = 2$, $\beta = 45^\circ$, $a = 1$, $b = 1(-)$, $b = 0.5(--)$, $b = 0(\dots)$.

plots). The temperature reduces the crack deflection in comparison with the pure-elastic case on these plots.

One could emphasise that the elastic and the temperature deviation of the crack have different behaviour at infinity. The pure-elastic term tends to a non-zero constant at infinity (except for a special case considered in Chapter 4). At the same time, the thermal term vanishes at infinity, although with a very slowly rate. Thus, the temperature gives only a local effect in the crack propagation problem, the trajectory is perturbed near the inclusion only. Also, it means the total crack trajectory is never zero except for trivial cases.

Analysis of the crack trajectory due to an elliptical inclusion is more complicated. The number of parameters involved is greater (the ratio of the semi-axes specified by \mathcal{R} and the rotation β). In Figure 5-16 we give the example of crack deflection due to an elastic elliptical inclusion which shows that crack trajectories can have curious shapes. Detailed analysis is based on the crack trajectories which have been derived above in the form of explicit analytical functions (5.2.30) and (5.3.11).

5.4 Mathematical model of a debonding-type interface

In this section we analyse a different type of non-perfect interface conditions, namely, interface conditions of the debonding type (sometimes it is called linear interface conditions). We consider the crack-inclusion interaction problem and analyse the conditions on attraction and repulsion as functions of the stiffnesses characterizing the interface layer. In particular, the relation between the radial and tangential stiffnesses is found which leads to zero crack deflection at any point. The debonding layer of this type compensates the effect of inclusion.

First, we employ the asymptotic scheme for the analysis of dilute composites which contain inclusions with imperfect bonding at the interface. The interface is characterized by a discontinuous displacement field across which is linearly related to the tractions. Effects due to the interaction of a small circular defect and a crack are investigated. It is shown that the interfacial stiffness has a strong effect on the crack path and therefore may be an important design parameter for composites.

The description of the mechanical behaviour of fibrous and particulate-reinforced materials is crucial for design purposes. In these materials the inclusions may often be imperfectly bonded to the matrix. In some cases, a thin layer, called the *interphase*, is introduced to improve the performance of the composite. In other cases, the interphase may be the product of chemical interaction between phases or localised mechanical damage of one or both phases (see the detailed discussion by Aboudi [1]). It is obvious that such interface conditions have a strong effect on the mechanical behaviour of the composite. In the last few years, strong research effort has been devoted to analyse interfaces from the mechanical point of view. In particular, many different models of interfacial behaviour have been developed. The simplest model is the *linear interface*, in which a linear relation between the traction vector and the displacement jump holds at the interface. This interfacial constitutive law has been formulated by Jones and Whittier [48] and may be considered as a simplification of the behaviour of a thin, soft elastic layer (see Goland and Reissner [31]); a rigorous proof of this in terms of asymptotic analysis has been given by Klarbring [52], Geymonat and Krasucki [27]). The model of linear interface has been employed by Mal and Bose [59], Hashin [38], [39], Levy [56], Qu [92] and Lipton [57] in homogenization problems and by Suo, Needleman and Ortiz [109] and Bigoni, Ortiz and Needleman [10] in determining the bifurcation loads of layered elastic structures subject to large strain, and by Tullini, Savoia and Horgan [113]

in the Saint Venant analysis of layered elastic plates. Lipton and Vernescu [58] have considered composites filled by spheres with imperfect interfaces and have solved the corresponding problem using the variational approach when the tangential stiffness is equal to the radial one. Also, one could mention the paper by Bigoni, Serkov, Movchan and Valentini [11] where generic polynomial loading has been applied to the imperfectly bounded inclusion in an infinite elastic plane.

5.4.1 Asymptotic derivation of linear interface conditions

In this subsection an asymptotic expansion is presented for the solution of an isotropic elastic circular inclusion in an isotropic elastic plane, coated by a cylindrically-anisotropic, finite-thickness elastic coating. The asymptotic procedure yields the stiffness constants of the linear interface using the model of a thin and soft elastic layer in the limit when the layer thickness and stiffness tend to zero. The following notations for the geometry of the domain are used: Ξ_1 is the circular inclusion, Ξ_2 is the interphase, Ξ_3 is the remaining part of infinite domain. The inclusion and the infinite plane are isotropic elastic solids respectively characterised by the Lamé constants μ_1, λ_1 , and μ_3, λ_3 , respectively. The interphase is assumed, for generality, to be cylindrically anisotropic (in the plane), and therefore, it is characterized by the constitutive equation

$$\boldsymbol{\sigma} = \mathcal{H}\boldsymbol{\varepsilon},$$

where $\boldsymbol{\sigma}$ and $\boldsymbol{\varepsilon}$ are vectors collecting the components of stress and strain tensors, i.e.

$$\boldsymbol{\sigma} = (\sigma_{rr}, \sigma_{\theta\theta}, \sigma_{r\theta})^t, \quad \boldsymbol{\varepsilon} = (\varepsilon_{rr}, \varepsilon_{\theta\theta}, \varepsilon_{r\theta})^t,$$

and

$$\mathcal{H} = \begin{pmatrix} C_{rr} & C_{r\theta} & 0 \\ C_{\theta r} & C_{\theta\theta} & 0 \\ 0 & 0 & 2G_\theta \end{pmatrix}, \quad (5.4.1)$$

which depends on the four stiffness coefficients (in the particular case of isotropic elasticity $C_{rr} = \lambda + 2\mu$, $C_{r\theta} = C_{\theta r} = \lambda$ and $G_{\theta r} = \mu$). Therefore, the elasticity problem in compound domain can be formulated as follows

$$\mathfrak{L}_{r\theta}(\mathbf{u}^{(1)}, \mu_1, \lambda_1) = 0, \quad \mathbf{x} \in \Xi_1,$$

$$\begin{aligned}\mathfrak{L}_{r\theta}(\mathbf{u}^{(2)}, C_{ij}, G_{ij}) &= 0, & \mathbf{x} \in \Xi_2, \\ \mathfrak{L}_{r\theta}(\mathbf{u}^{(3)}, \mu_3, \lambda_3) &= 0, & \mathbf{x} \in \Xi_3,\end{aligned}\tag{5.4.2}$$

where $\mathfrak{L}_{r\theta}(\cdot)$ is the Navier operator written in the polar system of coordinates. In matrix form it can be represented by

$$\mathfrak{L}_{r\theta}(\cdot) := D_1 \mathcal{H} D_2^t(\cdot),$$

$$D_1 = \begin{pmatrix} \frac{\partial}{\partial r} + \frac{1}{r} & -\frac{1}{r} & \frac{1}{\sqrt{2}} \frac{1}{r} \frac{\partial}{\partial \theta} \\ 0 & \frac{1}{r} \frac{\partial}{\partial \theta} & \frac{1}{\sqrt{2}} \left(\frac{\partial}{\partial r} + \frac{2}{r} \right) \end{pmatrix}, \quad D_2 = \begin{pmatrix} \frac{\partial}{\partial r} & \frac{1}{r} & \frac{1}{\sqrt{2}} \frac{1}{r} \frac{\partial}{\partial \theta} \\ 0 & \frac{1}{r} \frac{\partial}{\partial \theta} & \frac{1}{\sqrt{2}} \left(\frac{\partial}{\partial r} - \frac{1}{r} \right) \end{pmatrix},$$

where \mathcal{H} is given by (5.4.1) for the interphase, whereas for the matrix and inclusion

$$\mathcal{H} = \begin{pmatrix} \lambda + 2\mu & \lambda & 0 \\ \lambda & \lambda + 2\mu & 0 \\ 0 & 0 & 2\mu \end{pmatrix}.$$

The boundary conditions on the outer and inner boundaries of the interphase are the conditions of the perfectly bonded interface

$$\begin{aligned}\boldsymbol{\sigma}^{(n)}(\mathbf{u}^{(1)}) &= \boldsymbol{\sigma}^{(n)}(\mathbf{u}^{(2)}), & \mathbf{u}^{(1)} &= \mathbf{u}^{(2)} & \text{when } r &= R, \\ \boldsymbol{\sigma}^{(n)}(\mathbf{u}^{(3)}) &= \boldsymbol{\sigma}^{(n)}(\mathbf{u}^{(2)}), & \mathbf{u}^{(3)} &= \mathbf{u}^{(2)} & \text{when } r &= R + \varepsilon,\end{aligned}\tag{5.4.3}$$

where ε is the thickness of the interphase, $\boldsymbol{\sigma}^{(n)}$ is the traction vector.

Solution of the above formulated problem is sought in the form of the asymptotic series

$$\mathbf{u}^{(1)} = \sum_{i=0}^{\infty} \varepsilon^i \mathbf{u}_i^{(1)}, \quad \mathbf{u}^{(2)} = \sum_{i=0}^{\infty} \varepsilon^i \mathbf{u}_i^{(2)}, \quad \mathbf{u}^{(3)} = \sum_{i=0}^{\infty} \varepsilon^i \mathbf{u}_i^{(3)}.$$

Let us introduce the scaled ("fast") variable ρ as

$$\rho = (r - R)\varepsilon^{-1},$$

where R is the radius of the inclusion, and apply this variable in the interphase (region Ξ_2) only. Then the equilibrium equations inside this region can be expanded in different

powers of ε with the leading term

$$\frac{1}{\varepsilon^2} \begin{pmatrix} C_{rr} \frac{\partial^2 u_{r,0}^{(2)}}{\partial \rho^2} \\ G_{\theta r} \frac{\partial^2 u_{\theta,0}^{(2)}}{\partial \rho^2} \end{pmatrix} = 0. \quad (5.4.4)$$

The solution of system (5.4.4) can be found in the form

$$\begin{pmatrix} u_{r,0}^{(2)} \\ u_{\theta,0}^{(2)} \end{pmatrix} = \begin{pmatrix} A(\theta)\rho + B(\theta) \\ C(\theta)\rho + D(\theta) \end{pmatrix}. \quad (5.4.5)$$

The radial traction vector at any point of the interphase can be rewritten in the form

$$\boldsymbol{\sigma}^{(n)}(\mathbf{u}_0^{(2)}) = \frac{1}{\varepsilon} \begin{pmatrix} C_{rr}A(\theta) \\ G_{\theta r}C(\theta) \end{pmatrix}. \quad (5.4.6)$$

From (5.4.3) we immediately deduce that the leading term of tractions on the outer and inner boundary of the interphase coincide, i.e.

$$\boldsymbol{\sigma}^{(n)}(\mathbf{u}_0^{(1)})|_{r=R} = \boldsymbol{\sigma}^{(n)}(\mathbf{u}_0^{(2)}) = \boldsymbol{\sigma}^{(n)}(\mathbf{u}_0^{(3)})|_{r=R+\varepsilon}. \quad (5.4.7)$$

Let us now analyze the continuity condition for the displacements. Following (5.4.5), the displacement jump between the outer boundary ($\rho = 1$) and inner boundary ($\rho = 0$) is specified by the functions $A(\theta)$ and $C(\theta)$. Employing (5.4.6), one obtains

$$u_{r,0}^{(3)}|_{r=R+\varepsilon} - u_{r,0}^{(1)}|_{r=R} = \frac{1}{C_{rr}^*} \sigma_{rr}(u_0^{(1)}) \Big|_{r=R}, \quad (5.4.8)$$

$$u_{\theta,0}^{(3)}|_{r=R+\varepsilon} - u_{\theta,0}^{(1)}|_{r=R} = \frac{1}{G_{\theta r}^*} \sigma_{r\theta}(u_0^{(1)}) \Big|_{r=R}, \quad (5.4.9)$$

where one has assumed that the elasticity coefficients of the interphase have the order ε

$$C_{rr} = \varepsilon C_{rr}^*, \quad G_{\theta r} = \varepsilon G_{\theta r}^*. \quad (5.4.10)$$

Now we expand first terms in (5.4.8) and (5.4.9) in the Taylor series (here we extend the functions $u_r^{(3)}$, $u_\theta^{(3)}$ smoothly in the thin interphase)

$$u_{(\cdot),0}^{(3)}|_{r=R+\varepsilon} = u_{(\cdot),0}^{(3)}|_{r=R} + \varepsilon \frac{\partial u_{(\cdot),0}^{(3)}}{\partial r} \Big|_{r=R} + O(\varepsilon^2). \quad (5.4.11)$$

Substituting the expansion (5.4.11) into (5.4.8) and (5.4.9) and considering only the

coefficients of zero order in ε , we obtain the interface conditions for a linear interface (viewed as a zero-thickness interphase)

$$u_{r,0}^{(3)} \Big|_{r=R} - u_{r,0}^{(1)} \Big|_{r=R} = \frac{1}{C_{rr}^*} \sigma_{rr}(u_0^{(1)}) \Big|_{r=R}, \quad (5.4.12)$$

$$u_{\theta,0}^{(3)} \Big|_{r=R} - u_{\theta,0}^{(1)} \Big|_{r=R} = \frac{1}{G_{\theta r}^*} \sigma_{r\theta}(u_0^{(1)}) \Big|_{r=R}. \quad (5.4.13)$$

It follows immediately from expressions (5.4.7), (5.4.12) and (5.4.13) that tractions are continuous across the linear interface, but displacement jumps occur. These jumps are related to the tractions at the interface with the stiffness coefficients

$$s_r = \frac{C_{rr}}{\varepsilon}, \quad s_\theta = \frac{G_{\theta r}}{\varepsilon}. \quad (5.4.14)$$

If one assumes that the elasticity coefficients of the interphase go to zero as

$$C_{rr} = \varepsilon^{1-\beta} C_{rr}^*, \quad G_{\theta r} = \varepsilon^{1-\beta} G_{\theta r}^*, \quad 0 < \beta < 1, \quad (5.4.15)$$

the perfectly bonded interface conditions are obtained

$$\sigma^{(n)}(\mathbf{u}^{(1)})|_{r=R} = \sigma^{(n)}(\mathbf{u}^{(3)})|_{r=R}, \quad \mathbf{u}^{(1)}|_{r=R} = \mathbf{u}^{(3)}|_{r=R} \text{ as } \varepsilon \rightarrow 0. \quad (5.4.16)$$

5.4.2 Circular inclusion with imperfect bonding

An isotropic, linearly-elastic infinite plane, which contains a circular, isotropic linearly-elastic inclusion of radius R is considered. The Lamé constants of the matrix and of the inclusion are denoted by λ , μ and λ_0 , μ_0 . The circular inclusion is connected to the matrix with a linear interface, which, according to results of previous section, is characterized (at $r = R$) by

$$\sigma_{rr} = \sigma_{rr,0}, \quad \sigma_{r\theta} = \sigma_{r\theta,0}, \quad (5.4.17)$$

$$\sigma_{rr} = s_r [u_r(\mathbf{x}^+) - u_{r,0}(\mathbf{x}^-)], \quad \sigma_{r\theta} = s_\theta [u_\theta(\mathbf{x}^+) - u_{\theta,0}(\mathbf{x}^-)], \quad (5.4.18)$$

where \mathbf{u} is the displacement vector, s_r and s_θ are the stiffness constants of the interface (assumed non-negative), \mathbf{x}^+ and \mathbf{x}^- are also the two limits of the same point on the boundary (from the matrix and from the inclusion). When both these coefficients tend to infinity, the perfect bonding is recovered. In opposite, when s_r and s_θ are equal to

zero, there is no connection between inclusion and matrix, and the problem reduces to that of a cavity in an infinite plane. The loading is prescribed at infinity by introducing a linear displacement field

$$\mathbf{u}(\mathbf{x}) \rightarrow \mathbf{u}_\infty(\mathbf{x}) \quad \text{as} \quad \mathbf{x} \rightarrow \infty, \quad (5.4.19)$$

where

$$\mathbf{u}_\infty(\mathbf{x}) = (p_1x_1 + q_1x_2, p_2x_1 + q_2x_2). \quad (5.4.20)$$

Thus, the problem considered in this subsection is to find a displacement field \mathbf{u} satisfying the Navier equations in the matrix and in the inclusion

$$\begin{aligned} \mu \nabla^2 \mathbf{u}(\mathbf{x}) + (\lambda + \mu) \nabla \nabla \cdot \mathbf{u}(\mathbf{x}) &= \mathbf{0}, \quad \mathbf{x} \in \mathbb{R}^2 \setminus \overline{G}, \\ \mu_0 \nabla^2 \mathbf{u}_0(\mathbf{x}) + (\lambda_0 + \mu_0) \nabla \nabla \cdot \mathbf{u}_0(\mathbf{x}) &= \mathbf{0}, \quad \mathbf{x} \in G, \end{aligned} \quad (5.4.21)$$

where G is the region occupied by the inclusion. The conditions (5.4.17) and (5.4.18) is prescribed at the interface and (5.4.20) - at infinity. The standard technique for solving two-dimensional problems reduces this boundary value problem to the calculation of the complex potentials $\varphi(z)$ and $\psi(z)$, which represent the displacement and stress field by

$$\begin{aligned} u_r + iu_\theta &= \frac{1}{2\mu} e^{-i\theta} (\kappa\varphi(z) - z\overline{\varphi'(z)} - \overline{\psi(z)}), \\ \sigma_{rr} + \sigma_{\theta\theta} &= 2(\varphi'(z) + \overline{\varphi'(z)}), \\ \sigma_{\theta\theta} - \sigma_{rr} + 2i\sigma_{r\theta} &= 2e^{2i\theta} (\overline{z}\varphi''(z) + \psi'(z)), \end{aligned} \quad (5.4.22)$$

where $z = x_1 + ix_2$ and $\kappa = (\lambda + 3\mu)(\lambda + \mu)^{-1}$ for plane strain. The complex potentials φ and ψ are analytical functions in the region where they specify the solution of the elastostatic problem. As a result, the solution is sought employing the following representation of the complex potentials

$$\varphi_0(z) = \sum_{k=0}^{+\infty} c_k z^k, \quad \psi_0(z) = \sum_{k=0}^{+\infty} d_k z^k, \quad (5.4.23)$$

which are analytic inside the disk of radius R , and

$$\varphi(z) = \sum_{k=-\infty}^{+\infty} a_k z^k, \quad \psi(z) = \sum_{k=-\infty}^{+\infty} b_k z^k, \quad (5.4.24)$$

which are analytic in the outer region $\{x : R + \varepsilon < \sqrt{x_1^2 + x_2^2} < +\infty\}$ and have a pole at infinity. The coefficients a_k, b_k are defined from the conditions (5.4.20) at infinity for $0 \leq k \leq N$, are zero for $k > N$ (i.e. $a_k = b_k = 0$, for $k > N$) and to be determined for N negative. The remaining coefficients can be found from the boundary conditions. In order to rewrite the interface boundary conditions in terms of the complex potentials, we note that the continuity of traction at the interface corresponds to the following condition

$$\varphi(z) + z\overline{\varphi'(z)} + \overline{\psi(z)} = \varphi_0(z) + z\overline{\varphi_0'(z)} + \overline{\psi_0(z)}, \quad (5.4.25)$$

where $z = Re^{i\theta}$. Using the standard Muskhelishvili [83] technique, the boundary integral equations holding in the whole plane are deduced

$$\begin{aligned} \oint_L \frac{[\varphi(t) + t\overline{\varphi'(t)} + \overline{\psi(t)}]dt}{t-z} &= \oint_L \frac{[\varphi_0(t) + t\overline{\varphi_0'(t)} + \overline{\psi_0(t)}]dt}{t-z}, \\ \oint_L \frac{[\overline{\varphi(t)} + \bar{t}\varphi'(t) + \psi(t)]dt}{t-z} &= \oint_L \frac{[\overline{\varphi_0(t)} + \bar{t}\varphi_0'(t) + \psi_0(t)]dt}{t-z}, \end{aligned} \quad (5.4.26)$$

where L denotes the circular boundary of the inclusion.

Solving this system of equations employing the theorems on Cauchy-type integrals and the expansion for the complex potentials (5.4.23-5.4.24), the condition (5.4.26) can be transformed into the form

$$\begin{aligned} \sum_{k=-\infty}^{+\infty} a_k R^k z^k + \sum_{k=-\infty}^{+\infty} k \bar{a}_k R^k z^{2-k} + \sum_{k=-\infty}^{+\infty} \bar{b}_k R^k z^{-k} \\ = \sum_{k=0}^{+\infty} c_k R^k z^k + \sum_{k=0}^{+\infty} k \bar{c}_k R^k z^{2-k} + \sum_{k=0}^{+\infty} \bar{d}_k R^k z^{-k}, \quad |z| = 1. \end{aligned} \quad (5.4.27)$$

Collecting coefficients near the same powers of z , we obtain the system of linear equations for the unknown coefficients a_k, b_k, c_k, d_k :

$$\begin{aligned} a_n R^n + (2-n)\bar{a}_{2-n} R^{2-n} + \bar{b}_{-n} R^{-n} \\ = c_n R^n + (2-n)\bar{c}_{2-n} R^{2-n} + \bar{d}_{-n} R^{-n}, \end{aligned} \quad (5.4.28)$$

where $n \in \mathbf{Z}$ and the coefficients a_n, b_n are known from the conditions at infinity for $n > 0$, whereas coefficients c_n, d_n are equal to zero for $n < 0$. More precisely, index n ranges between $-N$ and N .

Let us consider now the second boundary condition (5.4.18). Using the complex po-

tential representation, the radial and shearing components of the stress tensor can be rewritten in the form

$$\begin{aligned}\sigma_{rr} &= \varphi'(z) + \overline{\varphi'(z)} - \operatorname{Re}[e^{2i\theta}(\overline{z}\varphi''(z) + \psi'(z))], \\ \sigma_{r\theta} &= \operatorname{Im}[e^{2i\theta}(\overline{z}\varphi''(z) + \psi'(z))].\end{aligned}\quad (5.4.29)$$

Therefore, the boundary conditions (5.4.18) take the complex variable form

$$s_r(u_r - u_{r,0}) + is_\theta(u_\theta - u_{\theta,0}) = \sigma_{rr} + i\sigma_{r\theta}, \quad (5.4.30)$$

or, more explicitly,

$$\begin{aligned}& \frac{s_r + s_\theta}{2} \left[\frac{e^{-i\theta}}{2\mu} \left(\kappa\varphi(z) - z\overline{\varphi'(z)} - \overline{\psi(z)} \right) - \frac{e^{-i\theta}}{2\mu_0} \left(\kappa_0\varphi_0(z) - z\overline{\varphi'_0(z)} - \overline{\psi_0(z)} \right) \right] \\ & + \frac{s_r - s_\theta}{2} \left[\frac{e^{i\theta}}{2\mu} \left(\overline{\kappa\varphi(z)} - \overline{z}\varphi'(z) - \psi(z) \right) - \frac{e^{i\theta}}{2\mu_0} \left(\overline{\kappa_0\varphi_0(z)} - \overline{z}\varphi'_0(z) - \psi_0(z) \right) \right] \\ & = \varphi'(z) + \overline{\varphi'(z)} - e^{-2i\theta}(\overline{z}\varphi''(z) + \overline{\psi'(z)}).\end{aligned}\quad (5.4.31)$$

In terms of Cauchy integrals, the system (5.4.31) can be written as

$$\begin{aligned}& \frac{s_r + s_\theta}{4\mu} \oint_L \frac{e^{-i\theta}(\kappa\varphi(t) - t\overline{\varphi'(t)} - \overline{\psi(t)})dt}{t-z} - \frac{s_r + s_\theta}{4\mu_0} \oint_{L^-} \frac{e^{-i\theta}(\kappa_0\varphi_0(t) - t\overline{\varphi'_0(t)} - \overline{\psi_0(t)})}{t-z} \\ & + \frac{s_r - s_\theta}{4\mu} \oint_L \frac{e^{i\theta}(\overline{\kappa\varphi(t)} - \overline{t}\varphi'(t) - \psi(t))dt}{t-z} - \frac{s_r - s_\theta}{4\mu_0} \oint_L \frac{e^{i\theta}(\overline{\kappa_0\varphi_0(t)} - \overline{t}\varphi'_0(t) - \psi_0(t))dt}{t-z} \\ & = \oint_L \frac{[\varphi'(t) + \overline{\varphi'(t)} - e^{-2i\theta}(\overline{t}\varphi''(t) + \overline{\psi'(t)})]dt}{t-z}, \\ & \frac{s_r + s_\theta}{4\mu} \oint_L \frac{e^{i\theta}(\overline{\kappa\varphi(t)} - \overline{t}\varphi'(t) - \psi(t))dt}{t-z} - \frac{s_r + s_\theta}{4\mu_0} \oint_L \frac{e^{i\theta}(\overline{\kappa_0\varphi_0(t)} - \overline{t}\varphi'_0(t) - \psi_0(t))}{t-z} \\ & + \frac{s_r - s_\theta}{4\mu} \oint_L \frac{e^{-i\theta}(\kappa\varphi(t) - t\overline{\varphi'(t)} - \overline{\psi(t)})dt}{t-z} - \frac{s_r - s_\theta}{4\mu_0} \oint_{L^-} \frac{e^{-i\theta}(\kappa_0\varphi_0(t) - t\overline{\varphi'_0(t)} - \overline{\psi_0(t)})}{t-z} \\ & = \oint_L \frac{[\varphi'(t) + \overline{\varphi'(t)} - e^{2i\theta}(\overline{t}\varphi''(t) + \psi'(t))]dt}{t-z}.\end{aligned}\quad (5.4.32)$$

Taking the series expansion of (5.4.32), writing it on the circle of radius R and integrating

over L , one gets

$$\begin{aligned}
 & \frac{s_r + s_\theta}{2} \left[\frac{1}{2\mu} \left(\varkappa \sum_{j=-\infty}^{+\infty} a_j R^j z^{j-1} - \sum_{j=-\infty}^{+\infty} j \bar{a}_j R^j z^{1-j} - \sum_{j=-\infty}^{+\infty} \bar{b}_j R^j z^{-j-1} \right) \right. \\
 & \quad \left. - \frac{1}{2\mu_0} \left(\varkappa_0 \sum_{j=0}^{+\infty} c_j R^j z^{j-1} - \sum_{j=0}^{+\infty} j \bar{c}_j R^j z^{1-j} - \sum_{j=0}^{+\infty} \bar{d}_j R^j z^{-j-1} \right) \right] \\
 & + \frac{s_r - s_\theta}{2} \left[\frac{1}{2\mu} \left(\varkappa \sum_{j=-\infty}^{+\infty} \bar{a}_j R^j z^{1-j} - \sum_{j=-\infty}^{+\infty} j a_j R^j z^{j-1} - \sum_{j=-\infty}^{+\infty} b_j R^j z^{j+1} \right) \right. \\
 & \quad \left. - \frac{1}{2\mu_0} \left(\varkappa_0 \sum_{j=0}^{+\infty} \bar{c}_j R^j z^{1-j} - \sum_{j=0}^{+\infty} j c_j R^j z^{j-1} - \sum_{j=0}^{+\infty} c_j R^j z^{j+1} \right) \right] \\
 & = \sum_{j=-\infty}^{+\infty} j a_j R^{j-1} z^{j-1} + \sum_{j=-\infty}^{+\infty} j \bar{a}_j R^{j-1} z^{1-j} \\
 & \quad - \sum_{j=-\infty}^{+\infty} j(j-1) \bar{a}_j R^{j-1} z^{1-j} - \sum_{j=-\infty}^{+\infty} j \bar{b}_j R^{j-1} z^{-j-1}, \quad |z| = 1. \quad (5.4.33)
 \end{aligned}$$

After simplification and collection of the coefficients near the same power of z in (5.4.33), the following system of linear equations is obtained

$$\begin{aligned}
 & \frac{s_r + s_\theta}{4\mu} \left(\varkappa a_{n+1} R^{n+1} - (1-n) \bar{a}_{1-n} R^{1-n} - \bar{b}_{-n-1} R^{-n-1} \right) \\
 & \quad - \frac{s_r + s_\theta}{4\mu_0} \left(\varkappa_0 c_{n+1} R^{n+1} - (1-n) \bar{c}_{1-n} R^{1-n} - \bar{d}_{-n-1} R^{-n-1} \right) \\
 & + \frac{s_r - s_\theta}{4\mu} \left(\varkappa \bar{a}_{1-n} R^{1-n} - (n+1) a_{n+1} R^{n+1} - b_{n-1} R^{n-1} \right) \\
 & \quad - \frac{s_r - s_\theta}{4\mu_0} \left(\varkappa_0 \bar{c}_{1-n} R^{1-n} - (n+1) c_{n+1} R^{n+1} - d_{n-1} R^{n-1} \right) \\
 & = (n+1) a_{n+1} R^n + (1-n^2) \bar{a}_{1-n} R^{-n} + (n+1) \bar{b}_{-n-1} R^{-n-2}, \quad (5.4.34)
 \end{aligned}$$

where coefficients a_1 and b_1 are known from the condition at infinity for $n > 0$, whereas $c_n = d_n = 0$ for $n < 0$. More precisely, index n ranges between $-N - 1$ and $N - 1$.

The Eshelby condition of homogeneous stress at infinity, particularly relevant in view of applications (two of which, regarding crack propagation and homogenization of composite materials, are presented in Section 5.5), corresponds to a linearly varying displacement field. In this case, the general expression for the complex potentials becomes

$$\begin{aligned}
 \varphi(z) &= a_1 z + a_{-1} z^{-1}, & \psi(z) &= b_1 z + b_{-1} z^{-1} + b_{-3} z^{-3}, \\
 \varphi_0(z) &= c_1 z + c_3 z^3, & \psi_0(z) &= d_1 z,
 \end{aligned} \quad (5.4.35)$$

where coefficients a_1 and b_1 are related to the conditions at infinity given by (5.2.15) and α_j, γ_j correspond to the linear fields $\mathbf{V}^{(j)}$ with exact values (2.2.7). Coefficients $a_{-1}, b_{-1}, b_{-3}, c_1, c_3, d_1$ result

$$\begin{aligned}
 a_{-1} &= \frac{\bar{b}_1 R^2}{D_2} \left\{ s_r s_\theta R^2 \Gamma_0 (\mu_0 - \mu) + (s_r + s_\theta) R \mu \mu_0 (3(\mu_0 - \mu) - \Gamma_0) - 12\mu^2 \mu_0^2 \right\}, \\
 b_{-1} &= 2\text{Re}(a_1) R^2 \frac{s_r R (\mu_0 (\varkappa - 1) - \mu (\varkappa_0 - 1)) - 4\mu \mu_0}{s_r R (\mu (\varkappa_0 - 1) + 2\mu_0) + 4\mu \mu_0}, \\
 b_{-3} &= \frac{\bar{b}_1 R^4}{D_2} \left\{ s_r s_\theta R^2 \Gamma_0 (\mu_0 - \mu) - R \mu \mu_0 (s_r + s_\theta) (\Gamma_0 - 3\mu_0 + 3\mu) \right. \\
 &\quad \left. - R \mu \mu_0 (s_r - s_\theta) (\Gamma + \mu_0 - \mu) - 12\mu^2 \mu_0^2 \right\}, \\
 c_1 &= \frac{\text{Re}(a_1) R s_r (\varkappa + 1) \mu_0}{4\mu \mu_0 + s_r R (\mu (\varkappa_0 - 1) + 2\mu_0)} + i \frac{\text{Im}(a_1) (\varkappa + 1) \mu_0}{(\varkappa_0 + 1) \mu}, \\
 c_3 &= \frac{b_1 (s_\theta - s_r) (\varkappa + 1) \mu_0^2 \mu}{R D_2}, \\
 d_1 &= \frac{b_1 R (\varkappa + 1) \mu_0 (s_r s_\theta R \Gamma_0 + 6s_r \mu \mu_0)}{D_2}, \tag{5.4.36}
 \end{aligned}$$

where

$$D_2 = s_r s_\theta \Gamma \Gamma_0 R^2 + (s_r + s_\theta) R (3\Gamma + \Gamma_0) \mu \mu_0 + 12\mu^2 \mu_0^2.$$

$$\Gamma = \varkappa \mu_0 + \mu, \quad \Gamma_0 = \varkappa_0 \mu + \mu_0.$$

As noted by Gao [26], the Eshelby [24] theorem, stating that the deformation field is homogeneous inside the inclusion, holds if and only if $c_3 = 0$. Except for trivial cases, this occurs when the stiffness in radial and tangential directions are equal, i.e. $s_r = s_\theta = s$. In this case, the coefficients of the complex potentials reduce to

$$\begin{aligned}
 a_{-1} &= \bar{b}_1 R^2 \frac{sR(\mu_0 - \mu) - 2\mu\mu_0}{s\Gamma R + 2\mu\mu_0}, \\
 b_{-1} &= 2\text{Re}(a_1) R^2 \frac{sR(\mu_0(\varkappa - 1) - \mu(\varkappa_0 - 1)) - 4\mu\mu_0}{sR(\mu(\varkappa_0 - 1) + 2\mu_0) + 4\mu\mu_0}, \\
 b_{-3} &= \bar{b}_1 R^4 \frac{sR(\mu_0 - \mu) - 2\mu\mu_0}{s\Gamma R + 2\mu\mu_0}, \\
 c_1 &= \frac{\text{Re}(a_1) R s (\varkappa + 1) \mu_0}{sR(\mu(\varkappa_0 - 1) + 2\mu_0) + 4\mu\mu_0} + i \frac{\text{Im}(a_1) (\varkappa + 1) \mu_0}{(\varkappa_0 + 1) \mu},
 \end{aligned}$$

$$c_3 = 0,$$

$$d_1 = \frac{b_1 R s (\varkappa + 1) \mu_0}{s \Gamma R + 2 \mu \mu_0}. \quad (5.4.37)$$

5.5 Crack trajectory in a dilute composite

The solution obtained in Section 5.4.2 is applied to the problems of crack propagation in dilute composites. The examples show the strong effect of the interface conditions: the presence of a finite interfacial compliance yields a solution which is “intermediate” between the limit cases of zero and infinite interfacial stiffness, corresponding to a cavity and a perfectly bonded elastic inclusion, respectively.

5.5.1 Pólya-Szegő matrix

The Pólya-Szegő matrix for circular inclusion with linear interface may be written as

$$\mathcal{P} = \frac{R^2}{4q} \begin{pmatrix} \xi + \frac{2\eta}{(\varkappa-1)^2} & -\xi + \frac{2\eta}{(\varkappa-1)^2} & 0 \\ -\xi + \frac{2\eta}{(\varkappa-1)^2} & \xi + \frac{2\eta}{(\varkappa-1)^2} & 0 \\ 0 & 0 & 2\xi \end{pmatrix}, \quad (5.5.38)$$

where

$$\eta = \frac{s_r R (\mu_0 (\varkappa - 1) - \mu (\varkappa_0 - 1)) - 4 \mu \mu_0}{s_r R (\mu (\varkappa_0 - 1) + 2 \mu_0) + 4 \mu \mu_0},$$

$$\xi = \frac{s_r s_\theta R^2 \Gamma_0 (\mu_0 - \mu) + (s_r + s_\theta) R \mu \mu_0 (3(\mu_0 - \mu) - \Gamma_0) - 12 \mu^2 \mu_0^2}{s_r s_\theta \Gamma_0 R^2 + (s_r + s_\theta) R (3\Gamma + \Gamma_0) \mu \mu_0 + 12 \mu^2 \mu_0^2},$$

and

$$q = \frac{\lambda + \mu}{8\pi\mu(\lambda + 2\mu)}, \quad \Gamma = \varkappa\mu_0 + \mu, \quad \Gamma_0 = \varkappa_0\mu + \mu_0.$$

In the particular case of equal radial and tangential stiffness of the interface, $s_r = s_\theta = s$, the constant ξ reduces to

$$\xi = \frac{sR(\mu_0 - \mu) - 2\mu\mu_0}{s\Gamma R + 2\mu\mu_0}.$$

It should be noted that $\frac{R^2}{2q}\xi$ (with multiplicity 2) and $\frac{R^2}{2q}\eta$ are the two distinct eigenvalues of \mathcal{P} . It can be therefore easily verified that when one of the eigenvalues of \mathcal{P} is negative in the limit $s_r = s_\theta \rightarrow \infty$, i.e. for perfectly bonded interface, it remains negative for any finite (positive) value of interfacial parameters s_r and s_θ . On the other hand, when one of the eigenvalues of \mathcal{P} is positive in the limit $s_r = s_\theta \rightarrow \infty$, it may always become negative for a set of values of s_r and s_θ .

When the matrix \mathcal{P} is positive definite in the limit case of perfectly bonded interface, it may happen that the matrix \mathcal{P} becomes identically zero for an imperfectly bonded interface with a proper choice of parameters s_r and s_θ . The condition of vanishing of matrix \mathcal{P} can be obtained imposing $\eta = \xi = 0$ and thus obtaining

$$s_r = \frac{4\mu\mu_0}{R[\mu_0(\varkappa - 1) - \mu(\varkappa_0 - 1)]}, \quad (5.5.39)$$

and

$$s_\theta = \frac{4\mu\mu_0\{3(\Gamma - \mu_0 + \mu) - 2\Gamma_0\}}{R\{(\Gamma_0 + 3\Gamma)(\mu_0 - \mu) + \Gamma_0(\Gamma_0 - \Gamma)\}}. \quad (5.5.40)$$

When this condition is satisfied for non negative values of s_r and s_θ , the inclusion does not affect the matrix. In order to clarify this point, consider an example taking

$$\varkappa = \varkappa_0 = 1 + \varepsilon, \quad \rho = \frac{\mu}{\mu_0} < 1, \quad 0 < \varepsilon < 2.$$

Under these assumptions, both s_r and the denominator of s_θ are positive. Therefore,

$$s_\theta > 0, \quad \Leftrightarrow \quad \rho > \frac{\varepsilon}{\varepsilon - 2} + \frac{1}{2}.$$

5.5.2 Crack trajectory

The formulation is based on the asymptotic analysis from Chapter 4. In this subsection we are interested in effect of imperfect interface and stiffness parameters on the crack path. The crack is assumed to be at a sufficiently large distance from the defect (compared to the defect size) and the trajectory turns out to be representable by a function H of the generic crack tip position l . In the specific case under consideration, i.e. for a circular elastic inclusion with linear interface, this function is

$$H(l) = \frac{R^2}{2y_0} \left\{ \eta(t^2 + t - 2) + \xi(t - t^3) \right\}, \quad (5.5.41)$$

where R is the radius of the inclusion and

$$t = \frac{(x_0 - l)}{\sqrt{(y_0)^2 + (x_0 - l)^2}},$$

with x_0, y_0 being the coordinates of the centre of the inclusion in an orthogonal reference system having the x_1 axis coincident with the unperturbed crack trajectory.

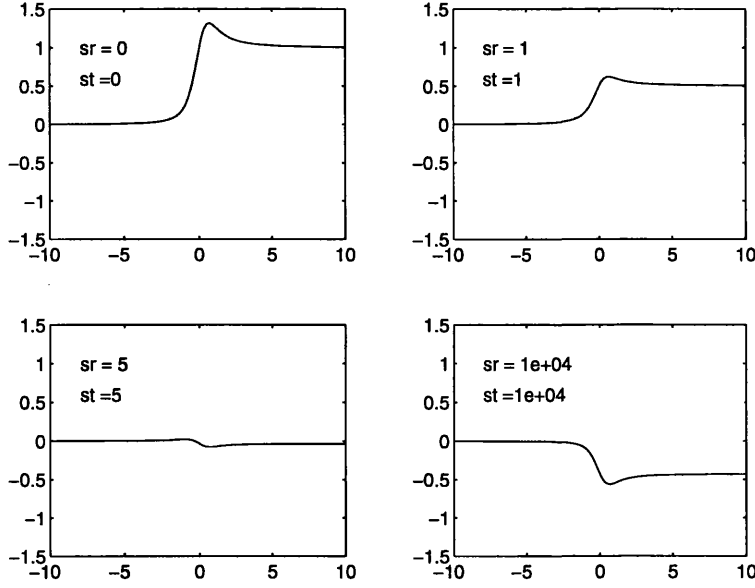


Figure 5-17: Crack trajectories $H(l)/y_0$ versus crack tip position l/y_0 , resulting from interaction with a circular elastic inclusion bonded with a linear interface with equal radial and tangential stiffness (the inclusion is stiffer than the matrix: $\mu_0/\mu = 10$).

It should be mentioned that the function $H(l)$ in (5.5.41) reduces to that corresponding to a circular void, for $s_r = s_\theta = 0$, and to that corresponding to a perfectly bonded inclusion, for $s_r = s_\theta \rightarrow \infty$.

The crack may be attracted or repelled by the inhomogeneity. For instance, an inclusion "stiffer" than the matrix repels the crack and a void attracts it. Formally, the attraction occurs when Pólya-Szegő matrix is negative definite and the repulsion when it is positive definite. The positive (or negative) definiteness depends on the values of material and interfacial parameters μ , μ_0 , \varkappa , \varkappa_0 , R , s_θ and s_r . For instance, if $s_r = s_\theta = s$ the Pólya-Szegő matrix is positive definite when

$$\frac{1}{\mu} - \frac{1}{\mu_0} > \frac{2}{sR}, \quad \frac{\varkappa - 1}{\mu} - \frac{\varkappa_0 - 1}{\mu_0} > \frac{4}{sR}, \quad (5.5.42)$$

and negative definite when the above inequalities have the opposite sign. Otherwise, the matrix \mathcal{P} is indefinite. From the analysis of the eigenvalues of matrix \mathcal{P} , it may be concluded that:

- if the crack is attracted in the limit case of perfectly bonded interface, it will be also attracted for imperfectly bonded interface;
- if the crack deflection is partly positive and partly negative (i.e. matrix \mathcal{P} is indefinite)

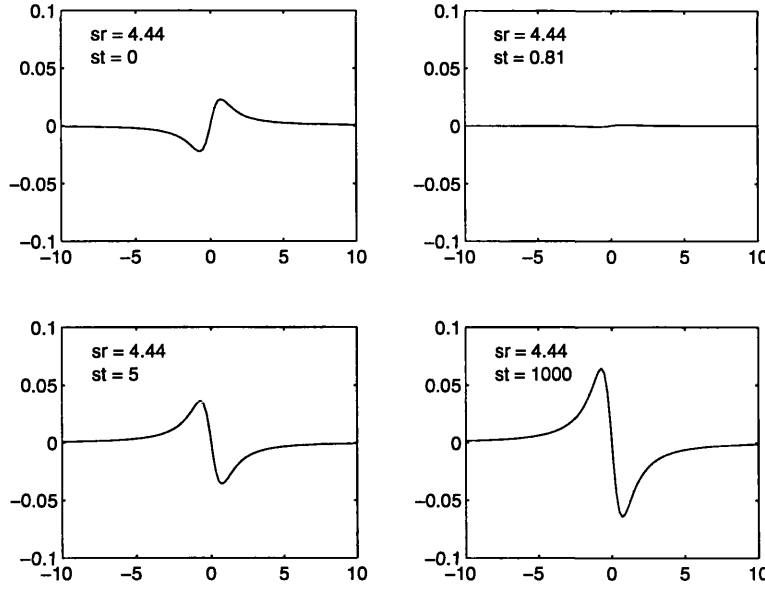


Figure 5-18: Crack trajectories $H(l)/y_0$ versus crack tip position l/y_0 , resulting from interaction with a circular elastic inclusion stiffer than the matrix and bonded with a linear interface. Different values of interfacial stiffness s_θ for the same parameter s_r , producing zero deflection of the crack path at infinity, are considered.

in the limit case of perfectly bonded interface, it will be not repelled for imperfectly bonded interface (i.e. matrix \mathcal{P} will be indefinite or negative definite);

- if the crack is repelled in the limit case of perfectly bonded interface, the crack deflection may be positive, negative, indefinite or zero for imperfectly bonded interface.

The condition for which the crack trajectory is zero at infinity, i.e. for $l \rightarrow \infty$, may be written as

$$H(\infty) = -\frac{R^2}{y_0}\eta = 0, \quad (5.5.43)$$

and therefore, it depends on the radial stiffness parameter s_r as specified by (5.5.39).

Crack trajectories $H(l)/y_0$ versus the crack tip position l/y_0 are shown in Figure 5-17 in a non-dimensional form (i.e. divided by the coordinate y_0 of the centre of the defect). These are the result of interaction with a circular elastic inclusion with a linear interface, positioned at $(0, 1)$. The stiffness of the interface enters in the non-dimensional form

$$\hat{s}_r = \frac{s_r y_0}{\mu}, \quad \hat{s}_\theta = \frac{s_\theta y_0}{\mu}. \quad (5.5.44)$$

In Figure 5-17 the equal radial and tangential stiffnesses of interface have been considered $\hat{s}_r = \hat{s}_\theta = s$. Various values of interfacial stiffness are considered, ranging between

the extreme cases of perfectly bonded interface $s \rightarrow \infty$ and circular void $s = 0$. Figure 5-17 shows the case when an inclusion stiffer than the matrix ($\mu_0/\mu = 10$), $k_- = k_+ = 2$. It can be observed that the crack trajectory changes even qualitatively, depending on the value of stiffness of the interface, for inclusion stiffer than the matrix (Figure 5-17). In the opposite case of inclusion weaker than the matrix, the effect of interfacial compliance is only quantitative.

The four values of tangential stiffness s_θ for the fixed value (5.5.39) of radial stiffness corresponding to zero crack deflection at infinity are considered in Figure 5-18. The stiffness of the interface enters in the non-dimensional form (5.5.44) and the values $\hat{s}_\theta = 100$, $\hat{s}_\theta = 5$, $\hat{s}_\theta \approx 0.81$, and $\hat{s}_\theta = 0$ are reported for $\hat{s}_r \approx 4.4444$. The Pólya-Szegő matrix is identically zero and crack remains straight when $\hat{s}_\theta \approx 0.81$. The case $\mu_0/\mu = 10$ and $k_- = k_+ = 2$ has been considered. It can be noted that the tangential stiffness parameter s_θ affects the crack path near the inclusion.

5.6 Conclusions

In this chapter the asymptotic models of crack propagation in the presence of different defects are given. One starts with the analysis of defects with perfect interface on the boundary and shows how these defects affect the crack trajectory. Then the crack-defect interaction in problems of uncoupled thermo-elasticity has been analysed. Finally, the effect of debonding on the interface boundary is considered. For all mentioned cases the crack trajectory has been analysed.

Chapter 6

Asymptotic analysis of thin-walled composites

6.1 Honeycomb structure under remote loading: formal asymptotic approach

In this chapter we consider the behaviour of a thin-walled structure under remote loading using the asymptotic methods. The approach is based on the asymptotic expansion of the model displacement fields and, as a result, the asymptotic expansions of the effective moduli are constructed. The leading term of this expansion (simplest geometries) agrees with the known "engineering approach" (see Gibson and Ashby [30], Davinge [22], Kalamkarov and Kolpakov [50], McClintock and Argon [66], Torquato, Gibiansky, Silva and Gibson [112]). In addition, the high order corrections are obtained here for the effective elastic moduli, and the accurate derivation of the junction boundary conditions is presented. That enables us to evaluate the shear modulus of the thin-walled composites, even for the cases unavailable in the general engineering literature.

One starts with the consideration of the periodic structure, in other words, the structure which can be obtained by a shift of the elementary periodic cell S in two non-parallel directions. In this structure (the union of K elementary periodic cells) the following

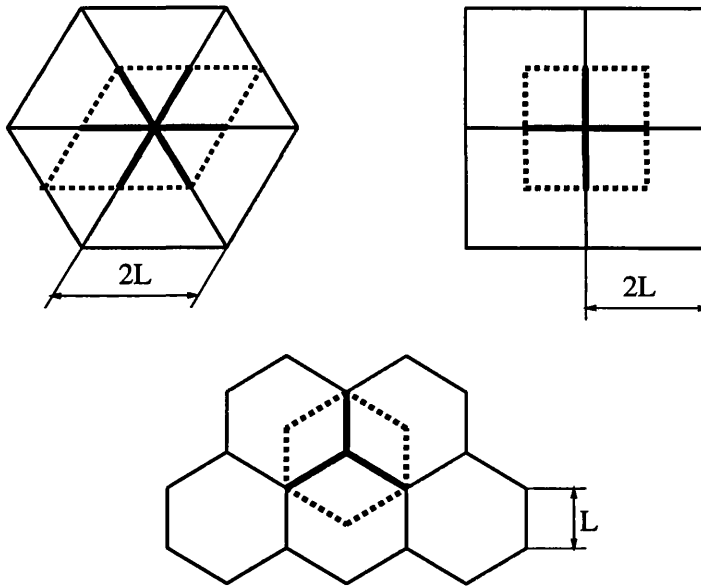


Figure 6-1: Types of thin-walled structures.

boundary value thermo-elasticity problem is specified

$$\begin{aligned}
 &\mu \nabla^2 \mathbf{U}(\mathbf{x}) + (\lambda + \mu) \nabla \nabla \cdot \mathbf{U}(\mathbf{x}) = \gamma \nabla T, \quad \mathbf{x} \in \mathcal{B}, \\
 &\boldsymbol{\sigma}^{(n)}(\mathbf{U}; \mathbf{x}) + \gamma T = \mathbf{p}(\mathbf{x}), \quad \mathbf{x} \in \partial \mathcal{B}, \\
 &k \nabla^2 T(\mathbf{x}) = w(\mathbf{x}), \quad \mathbf{x} \in \mathcal{B}, \\
 &T(\mathbf{x}) = T^*(\mathbf{x}), \quad \mathbf{x} \in \partial \mathcal{B},
 \end{aligned} \tag{6.1.1}$$

where \mathcal{B} is a composite medium defined as a union of periodic cells. In the simplest examples an elementary periodic cell \mathcal{S} could be parallelogram, square, rectangle or hexagon. The problem formulated for the whole composite (6.1.1) is reduced to the problem imposed for a single cell only. Let $\Xi^{(\varepsilon)}$ be a domain defined as a union of thin regions $\Pi_\varepsilon^{(n)} = \{(x^{(n)}, y^{(n)}) : 0 < x^{(n)} < L, |y^{(n)}| < \varepsilon/2\}, 0 < \varepsilon \ll 1, n = 1, \dots, N$, and the junction region is Ω_ε . $\Xi^{(\varepsilon)}$ covers the whole elementary cell of the periodic structure excluding voids. $\mathbf{x}^{(n)} = (x^{(n)}, y^{(n)})$ are the local coordinates specified in such a way that $x^{(n)}$ is always a longitudinal coordinate for the bridge $\Pi_\varepsilon^{(n)}$, and $y^{(n)}$ is its transversal coordinate, origin of these coordinates always coincides with the centre of the junction region, see Figure 6-2.

The junction region is specified such that $\Omega_\varepsilon \subset [-C\varepsilon, C\varepsilon] \times [-D\varepsilon, D\varepsilon]$, where C and D

are some constants. The junction region characterises the area where the bridges join each other $\Omega_\varepsilon \subset \cup_{n,k} (\Pi_\varepsilon^{(n)} \cap \Pi_\varepsilon^{(k)})$.

The boundary of the thin-wall structure inside the elementary cell \mathcal{S} is split up into two parts. First, $\partial\Xi_1^{(\varepsilon)}$ is defined as the lateral part of the boundary $\partial\Xi^{(\varepsilon)}$, $\partial\Xi^{(\varepsilon)} \cap \partial\mathcal{S} = \emptyset$. The remaining part is $\partial\Xi_2^{(\varepsilon)} = \partial\Xi^{(\varepsilon)} \setminus \partial\Xi_1^{(\varepsilon)}$ associated with the boundary of the periodic cell. The elasticity problem in $\Xi^{(\varepsilon)}$ can be reformulated in the following form

$$\begin{aligned} \mu \nabla^2 \mathbf{U}(\mathbf{x}) + (\lambda + \mu) \nabla \nabla \cdot \mathbf{U}(\mathbf{x}) &= 0, & \mathbf{x} \in \Xi^{(\varepsilon)}, \\ \boldsymbol{\sigma}^{(n)}(\mathbf{U}; \mathbf{x}) &= 0, & \mathbf{x} \in \partial\Xi_1^{(\varepsilon)}, \\ &+ \text{periodicity conditions.} \end{aligned} \quad (6.1.2)$$

The periodicity conditions on the boundary of the elementary cell correspond to periodical character of the structure. For example, in the case of square periodic cell $[0, 1] \times [0, 1]$ they can be specified in the form

$$\begin{aligned} U_1(0, y) &= U_1(1, y), & \frac{\partial}{\partial y} U_1(x, 0) &= \frac{\partial}{\partial y} U_1(x, 1), \\ U_2(x, 0) &= U_2(x, 1), & \frac{\partial}{\partial x} U_2(0, y) &= \frac{\partial}{\partial x} U_2(1, y), \quad \forall x, y \in [0, 1]. \end{aligned}$$

For the case of hexagonal periodic cell these conditions have more complicated form (Jikov, Koslov and Oleinik [47]).

In the limit case, when the thickness of the bridges tends to zero (or has the order $O(\varepsilon)$, where ε is a small parameter), the solution of the system (6.1.2) can be represented as a linear combination of solutions of model problems corresponding to each bridge and the solution of a model problem in the junction region. Using the asymptotic technique, the displacement field for each thin bridge $\Pi_\varepsilon^{(n)}$ can be represented as series (see Bakhvalov and Panasenko [4] and section 6.2.1 for the detailed analysis)

$$\mathbf{U}^{(n)}(\mathbf{x}) = \sum_{i=0}^{\infty} \varepsilon^i \left[\sum_{k=0}^2 \varepsilon^k \mathbf{u}_{i,k}^{(n)} + \sum_{k=0}^4 \varepsilon^k \mathbf{v}_{i,k}^{(n)} \right], \quad \mathbf{x} \in \Pi_\varepsilon^{(n)}. \quad (6.1.3)$$

If the lateral surface of the bridge is free of traction (which is true for a honeycomb with voids), the leading term of this expansion has the following vector polynomial form (it

is assumed that each thin bridge has a constant thickness)

$$\begin{aligned} \mathbf{U}^{(n)} &\sim \mathbf{u}_{0,0}^{(n)} + \mathbf{v}_{0,0}^{(n)}, & \mathbf{u}_{0,0}^{(n)} &= \begin{pmatrix} u_0^{(n)} \\ 0 \end{pmatrix} = \begin{pmatrix} A^{(n)}x^{(n)} + B^{(n)} \\ 0 \end{pmatrix}, \\ \mathbf{v}_{0,0}^{(n)} &= \begin{pmatrix} 0 \\ v_0^{(n)} \end{pmatrix} = \begin{pmatrix} 0 \\ C^{(n)}(x^{(n)})^3 + D^{(n)}(x^{(n)})^2 + E^{(n)}x^{(n)} + F^{(n)} \end{pmatrix}, \end{aligned} \quad (6.1.4)$$

where $x^{(n)}$ is the local coordinate along the bridge and the coefficients $A^{(n)}$, $B^{(n)}$, $C^{(n)}$, $D^{(n)}$, $E^{(n)}$, $F^{(n)}$ are defined from the boundary conditions on the edges of the bridges and the "junction boundary condition".

Our intention is to derive the "junction boundary condition" from the analysis of the boundary layer near the junction point. The smooth cut-off function is defined for each thin region and it is equal to 0 in the junction area and 1 in the thin bridge (i.e. far away from the junction point)

$$\chi(X^{(n)}) = 1, \text{ for } X^{(n)} > 1 \quad \text{and} \quad \chi(X^{(n)}) = 0, \text{ for } X^{(n)} < 1/2.$$

Here $\mathbf{X}^{(n)} = (X^{(n)}, Y^{(n)}) = \mathbf{x}^{(n)}/\varepsilon$ are the "fast" local variables. Under such notations the solution $\mathbf{u}(\mathbf{x})$ of the equilibrium equation (6.1.2) can be represented in the form

$$\mathbf{U}(\mathbf{x}) = \sum_{n=1}^N \chi(\mathbf{X}^{(n)}) \mathbf{U}^{(n)}(\mathbf{x}^{(n)}) + \mathbf{W}(\mathbf{X}), \quad (6.1.5)$$

where $\mathbf{U}^{(n)}(\mathbf{x})$ is the asymptotic expansion of the solution in the thin bridge (6.1.3), $\chi(\mathbf{X}^{(n)})$ is the cut-off function, $\mathbf{W}(\mathbf{X})$ is the boundary layer solution (it decays exponentially), which admits the asymptotic representation

$$\mathbf{W}(\mathbf{X}) = \sum_{i=0}^{\infty} \varepsilon^i \mathbf{W}^{(i)}(\mathbf{X}). \quad (6.1.6)$$

In the formulae above the "fast" global variables $\mathbf{X} = (X, Y)$ are such that $\mathbf{X} = \mathbf{x}/\varepsilon$ where $\mathbf{x} = (x, y)$.

Substituting (6.1.5) in the governing equations and collecting the coefficients near like powers of ε , one obtains the set of boundary value problems in the scaled region $\Xi(\varepsilon)$.

6.1.1 First-order boundary layer

The first-order boundary layer compensates the discrepancy left by the leading term of the asymptotic expansion in $\cup_{n=1}^N \Pi_\varepsilon^{(n)}$. As a result, the first boundary layer problem is the inhomogeneous problem, where the body forces and the surface traction are the functions of $u_0^{(n)}, v_0^{(n)}$ only. The condition of exponential decay of boundary layer at infinity is imposed

$$\begin{cases} \mu \nabla^2 \mathcal{W}^{(0)}(\mathbf{X}) + (\lambda + \mu) \nabla \nabla \cdot \mathcal{W}^{(0)}(\mathbf{X}) + \mathcal{F}_0(\mathbf{X}) = 0, & \mathbf{X} \in \Xi, \\ \sigma^{(n)}(\mathcal{W}^{(0)}; \mathbf{X}) + \mathcal{P}_0(\mathbf{X}) = 0, & \mathbf{X} \in \partial \Xi_1, \\ \mathcal{W}^{(0)} \rightarrow 0, & \|\mathbf{x}\| \rightarrow \infty. \end{cases} \quad (6.1.7)$$

In (6.1.7) the body forces $\mathcal{F}_0(\mathbf{X})$ and the surface tractions $\mathcal{P}_0(\mathbf{X})$ are specified by

$$\begin{aligned} \mathcal{F}_0(\mathbf{X}) &= \sum_{m=1}^N \chi''(X_1^{(m)}) \begin{pmatrix} (2\mu + \lambda) u_0^{(m)}(0) \\ \mu v_0^{(m)}(0) \end{pmatrix}, \\ \mathcal{P}_0(\mathbf{X}) &= \sum_{m=1}^N \chi'(X_1^{(m)}) \begin{pmatrix} \mu v_0^{(m)}(0) \\ \lambda u_0^{(m)}(0) \end{pmatrix}, \end{aligned} \quad (6.1.8)$$

and Ξ and $\partial \Xi_1$ are the domain Ξ and its boundary enlarged in ε^2 times.

The vector-valued functions (6.1.8) satisfy the orthogonality conditions

$$\int_{\Xi} \mathcal{F}^{(0)} d\mathbf{X} - \int_{\partial \Xi} \mathcal{P}^{(0)} ds = 0, \quad (6.1.9)$$

$$\int_{\Xi} \mathbf{X} \times \mathcal{F}^{(0)} d\mathbf{X} - \int_{\partial \Xi} \mathbf{X} \times \mathcal{P}^{(0)} ds = 0. \quad (6.1.10)$$

Now we can reduce this boundary layer problem to the problem for a finite domain. It corresponds to the fact that the body forces and the surface tractions located in the region of enlarged thin bridges where $\chi'(X^{(n)})$ and $\chi''(X^{(n)})$ are not equal to zero. Thus, the junction area is described by the homogeneous Navier system with zero traction on the lateral surface. In the region $\Xi \setminus \bar{\Omega}$ the solution of the problem (6.1.7) admits the following expansion

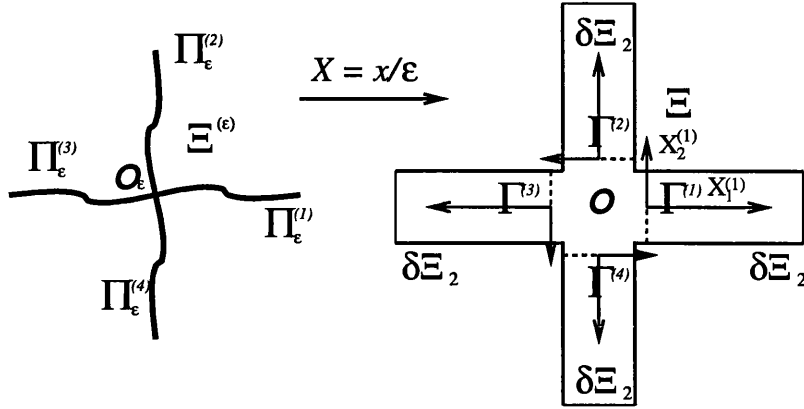


Figure 6-2: Honeycomb structure and junction area.

$$\mathbf{w}^{(0)} = \begin{cases} \begin{pmatrix} u_0^{(n)}(0) \\ v_0^{(n)}(0) \end{pmatrix} (1 - \chi(X_1^{(n)})), & \mathbf{X}^{(n)} \in \Xi \setminus \Omega, \\ \mathbf{w}^{(0,1)}, & \mathbf{X} \in \Omega, \end{cases} \quad (6.1.11)$$

where $\mathbf{X}^{(n)}$ are the local coordinates associated with the bridge. The field $\mathbf{w}^{(0,1)}$ satisfies the homogeneous Navier system with boundary conditions chosen in such a way that on $\Gamma^{(n)}$ continuity of traction and displacements holds. Thus, the problem initially specified in the infinite domain Ξ can be reduced to the problem in Ω (enlarged in ϵ^2 times junction region shown in Figure 6-2)

$$\begin{aligned} \mu \nabla^2 \mathbf{w}^{(0,1)}(\mathbf{X}) + (\lambda + \mu) \nabla \nabla \cdot \mathbf{w}^{(0,1)}(\mathbf{X}) &= 0, & \mathbf{X} \in \Omega, \\ \sigma^{(n)}(\mathbf{w}^{(0,1)}; \mathbf{X}) &= 0, & \mathbf{X} \in \partial\Omega \setminus \Gamma^{(n)}, \end{aligned} \quad (6.1.12)$$

$$\begin{aligned} \Gamma^{(1)} : \quad \mathbf{w}^{(0,1)} &= \begin{pmatrix} u_0^{(1)}(0) \\ v_0^{(1)}(0) \end{pmatrix}, & \Gamma^{(2)} : \quad \mathbf{w}^{(0,1)} &= \begin{pmatrix} -v_0^{(2)}(0) \\ u_0^{(2)}(0) \end{pmatrix}, \\ \Gamma^{(3)} : \quad \mathbf{w}^{(0,1)} &= \begin{pmatrix} -u_0^{(3)}(0) \\ -v_0^{(3)}(0) \end{pmatrix}, & \Gamma^{(4)} : \quad \mathbf{w}^{(0,1)} &= \begin{pmatrix} v_0^{(4)}(0) \\ -u_0^{(4)}(0) \end{pmatrix}, \end{aligned}$$

where $\Gamma^{(n)}$ (Figure 6-2) are the parts of the boundary corresponding to the attached thin bridges.

Now our intention is to find the solution of this system which provides the continuity of displacement and traction on $\Gamma^{(1)}$, $\Gamma^{(2)}$, $\Gamma^{(3)}$, $\Gamma^{(4)}$. Such conditions arise from the matching with the solution in thin bridges (6.1.11). Note that the solution (6.1.11) produces zero tractions on the boundary $\Gamma^{(n)}$. It follows from the fact that $\chi'(X^{(n)}) = 0$

when $\mathbf{X}^{(n)} \in \Gamma^{(n)}$. Therefore, on all parts of the boundary Ω we have zero traction, and the solution must be represented as a vector with constant components (it corresponds to the rigid translation of the region Ω).

Existence of a solution with constant components of the displacement fields yields the following relations between the boundary data of the problem (6.1.12)

$$\begin{aligned} u_0^{(1)}(0) &= -v_0^{(2)}(0) = -u_0^{(3)}(0) = v_0^{(4)}(0), \\ v_0^{(1)}(0) &= u_0^{(2)}(0) = -v_0^{(3)}(0) = -u_0^{(4)}(0). \end{aligned} \quad (6.1.13)$$

Under such conditions (6.1.13) the field $\mathcal{W}^{(0,1)}$ has zero energy and the condition of the continuity of tractions on $\Gamma^{(n)}$ is satisfied.

6.1.2 Second-order boundary layer

One can apply the procedure describing above to construct the boundary layer corresponding to the second asymptotic term of (6.1.6). As a result, the following boundary value problem for the field $\mathcal{W}^{(1)}$ is obtained

$$\begin{aligned} \mu \nabla^2 \mathcal{W}^{(1)}(\mathbf{X}) + (\lambda + \mu) \nabla \nabla \cdot \mathcal{W}^{(1)}(\mathbf{X}) + \mathcal{F}^{(1)}(\mathbf{X}) &= 0, \quad \mathbf{X} \in \Xi, \\ \sigma^{(n)}(\mathcal{W}^{(1)}; \mathbf{X}) + \mathcal{P}^{(1)}(\mathbf{X}) &= 0, \quad \mathbf{X} \in \partial \Xi, \\ \mathcal{W}^{(1)} &\rightarrow 0, \quad \|\mathbf{x}\| \rightarrow \infty, \end{aligned} \quad (6.1.14)$$

where

$$\begin{aligned} \mathcal{F}^{(1)}(\mathbf{X}) &= \sum_{m=1}^N \left\{ \chi''(X^{(m)}) \begin{pmatrix} (2\mu + \lambda)(X^{(m)} \frac{\partial}{\partial x} u_0^{(m)}(0) - Y^{(m)} \frac{\partial}{\partial x} v_0^{(m)}(0) + u_1^{(m)}(0)) \\ \mu(-\frac{\lambda Y^{(m)}}{\lambda+2\mu} \frac{\partial}{\partial x} u_0^{(m)}(0) + X^{(m)} \frac{\partial}{\partial x} v_0^{(m)}(0) + v_1^{(m)}(0)) \end{pmatrix} \right. \\ &\quad \left. + \chi'(X^{(m)}) \begin{pmatrix} \{2(2\mu + \lambda) - \frac{\lambda(\lambda+\mu)}{\lambda+2\mu}\} \frac{\partial}{\partial x} u_0^{(m)}(0) \\ (\mu + \lambda) \frac{\partial}{\partial x} v_0^{(m)}(0) \end{pmatrix} \right\}, \\ \mathcal{P}^{(1)}(\mathbf{X}) &= \sum_{m=1}^N \chi'(X^{(m)}) \begin{pmatrix} \mu(-\frac{\lambda Y^{(m)}}{\lambda+2\mu} \frac{\partial}{\partial x} u_0^{(m)}(0) + X^{(m)} \frac{\partial}{\partial x} v_0^{(m)}(0) + v_1^{(m)}(0)) \\ \lambda(X^{(m)} \frac{\partial}{\partial x} u_0^{(m)}(0) - Y^{(m)} \frac{\partial}{\partial x} v_0^{(m)}(0) + u_1^{(m)}(0)) \end{pmatrix}. \end{aligned}$$

This problem admits the solution which decays at infinity if and only if the following solvability conditions for (6.1.14) hold

$$\int_{\Xi} \mathcal{F}_1^{(1)} d\mathbf{X} - \int_{\partial \Xi} \mathcal{P}_1^{(1)} ds = 0, \quad (6.1.15)$$

$$\int_{\Xi} \mathcal{F}_2^{(1)} d\mathbf{X} - \int_{\partial\Xi} \mathcal{P}_2^{(1)} ds = 0, \quad (6.1.16)$$

$$\int_{\Xi} X_1 \mathcal{F}_2^{(1)} - X_2 \mathcal{F}_1^{(1)} d\mathbf{X} - \int_{\partial\Xi} X_1 \mathcal{P}_2^{(1)} - X_2 \mathcal{P}_1^{(1)} ds = 0. \quad (6.1.17)$$

The conditions (6.1.15), (6.1.16) can be represented in the following simplified form

$$\frac{\partial}{\partial x} u^{(1)}(0) - \frac{\partial}{\partial x} u^{(3)}(0) = 0, \quad \frac{\partial}{\partial x} u^{(2)}(0) - \frac{\partial}{\partial x} u^{(4)}(0) = 0. \quad (6.1.18)$$

The condition (6.1.17) is satisfied identically.

Following the procedure employed for the first boundary layer we reduce our problem in an infinite domain to the problem in a finite domain. We use the following properties of the system (6.1.14): it is homogeneous inside the region Ω , and the Dirichlet boundary conditions are imposed on $\Gamma^{(n)}$. As before, the field $\mathcal{W}^{(1)}$ is sought in the form

$$\mathcal{W}^{(1)}(\mathbf{X}) = \begin{cases} \left(\begin{array}{l} X^{(n)} \frac{\partial}{\partial x} u_0^{(n)}(0) + u_1^{(n)}(0) - Y^{(n)} \frac{\partial}{\partial x} v_0^{(n)}(0) \\ -\frac{\lambda Y^{(n)}}{\lambda+2\mu} \frac{\partial}{\partial x} u_0^{(n)}(0) + v_1^{(n)}(0) + X^{(n)} \frac{\partial}{\partial x} v_0^{(n)}(0) \end{array} \right) (1 - \chi(X^{(n)})), & \mathbf{X}^{(n)} \in \Xi \setminus \bar{\Omega}, \\ \mathcal{W}^{(1,1)}(\mathbf{X}), & \mathbf{X} \in \Omega. \end{cases} \quad (6.1.19)$$

The displacement vector $\mathcal{W}^{(1,1)}(\mathbf{X})$ satisfies the following system

$$\begin{aligned} \mu \nabla^2 \mathcal{W}^{(1,1)}(\mathbf{X}) + (\lambda + \mu) \nabla \nabla \cdot \mathcal{W}^{(1,1)}(\mathbf{X}) &= 0, & \mathbf{X} \in \Omega, \\ \sigma^{(n)}(\mathcal{W}^{(1,1)}; \mathbf{X}) &= 0, & \mathbf{X} \in \partial\Xi_1 \setminus \Gamma^{(n)}. \end{aligned} \quad (6.1.20)$$

The boundary conditions on $\Gamma^{(n)}$ are

$$\begin{aligned} \Gamma^{(1)} : \quad \mathcal{W}^{(1,1)} &= \begin{pmatrix} X \frac{\partial}{\partial x} u_0^{(1)}(0) + u_1^{(1)}(0) \\ -\frac{\lambda Y}{\lambda+2\mu} \frac{\partial}{\partial x} u_0^{(1)}(0) + v_1^{(1)}(0) \end{pmatrix} + \begin{pmatrix} -Y \frac{\partial}{\partial x} v_0^{(1)}(0) \\ X \frac{\partial}{\partial x} v_0^{(1)}(0) \end{pmatrix}, \\ \Gamma^{(2)} : \quad \mathcal{W}^{(1,1)} &= \begin{pmatrix} -\frac{\lambda X}{\lambda+2\mu} \frac{\partial}{\partial x} u_0^{(2)}(0) - v_1^{(2)}(0) \\ Y \frac{\partial}{\partial x} u_0^{(2)}(0) + u_1^{(2)}(0) \end{pmatrix} + \begin{pmatrix} -Y \frac{\partial}{\partial x} v_0^{(2)}(0) \\ X \frac{\partial}{\partial x} v_0^{(2)}(0) \end{pmatrix}, \\ \Gamma^{(3)} : \quad \mathcal{W}^{(1,1)} &= \begin{pmatrix} X \frac{\partial}{\partial x} u_0^{(3)}(0) - u_1^{(3)}(0) \\ -\frac{\lambda Y}{\lambda+2\mu} \frac{\partial}{\partial x} u_0^{(3)}(0) - v_1^{(3)}(0) \end{pmatrix} + \begin{pmatrix} -Y \frac{\partial}{\partial x} v_0^{(3)}(0) \\ X \frac{\partial}{\partial x} v_0^{(3)}(0) \end{pmatrix}, \\ \Gamma^{(4)} : \quad \mathcal{W}^{(1,1)} &= \begin{pmatrix} -\frac{\lambda X}{\lambda+2\mu} \frac{\partial}{\partial x} u_0^{(4)}(0) + v_1^{(4)}(0) \\ Y \frac{\partial}{\partial x} u_0^{(4)}(0) - u_1^{(4)}(0) \end{pmatrix} + \begin{pmatrix} -Y \frac{\partial}{\partial x} v_0^{(4)}(0) \\ X \frac{\partial}{\partial x} v_0^{(4)}(0) \end{pmatrix}, \end{aligned}$$

where $\mathbf{X} = (X, Y)$ are the global "fast" coordinates associated with the junction region. The traction on the boundary $\Gamma^{(n)}$ can be evaluated as follows

$$\sigma^{(n)}(\mathbf{W}^{(1)}; \mathbf{X}^{(n)}) = \begin{pmatrix} \frac{4\mu(\lambda+\mu)}{\lambda+2\mu} \frac{\partial}{\partial x} u_0^{(n)}(0) \\ 0 \end{pmatrix}.$$

The energy accumulated in the junction region is given by

$$\begin{aligned} \Delta \mathcal{E}_\Omega &= - \int_{\partial \Xi \cup \Gamma^{(n)}} \sigma^{(n)}(\mathbf{W}^{(1,1)}; \mathbf{X}^{(n)}) \mathbf{W}^{(1,1)}(\mathbf{X}^{(n)}) ds \\ &= \sum_{n=1}^N \frac{4\mu(\lambda+\mu)}{\lambda+2\mu} \frac{\partial}{\partial x} u_0^{(n)}(0) \left[X^{(n)} \frac{\partial}{\partial x} u_0^{(n)}(0) + u_1^{(n)}(0) \right], \end{aligned}$$

where $X^{(n)}$ is on the boundary $\Gamma^{(n)}$. One can see that the terms $\frac{\partial}{\partial x} v_0^{(n)}(0)$ are not present in the expression for the energy integral. The analysis of the Dirichlet boundary conditions of the problem (6.1.20) gives the following restrictions on the transversal displacements

$$\frac{\partial}{\partial x} v_0^{(1)}(0) = \frac{\partial}{\partial x} v_0^{(2)}(0) = \frac{\partial}{\partial x} v_0^{(3)}(0) = \frac{\partial}{\partial x} v_0^{(4)}(0). \quad (6.1.21)$$

As a result, the coefficients $\frac{\partial}{\partial x} v_0^{(n)}(0)$ correspond to the rigid rotation field of the whole body and produce zero traction and zero energy. Therefore, the continuity of the tractions for $\mathbf{W}^{(1)}$ is satisfied trivially. The condition (6.1.21) has a simple physical meaning. It corresponds to the fact that the *junction behaves like a rigid kernel* when we restrict ourselves by the leading term of the displacement field. This property holds for a junction of any shape (including three-beam and six-beam junctions).

If next-order junction layer problems are considered, the additional restrictions for the coefficients A, B, C, D, E, F can be obtained (as the solvability conditions of corresponding equations). Namely, from the analysis of the third-order junction layer

$$\sum_{m=1}^4 \frac{\partial^2}{\partial x^2} v_0^{(m)}(0) = 0, \quad (6.1.22)$$

and from the fourth-order junction layer

$$\frac{\partial^3}{\partial x^3} v_0^{(1)}(0) - \frac{\partial^3}{\partial x^3} v_0^{(3)}(0) = 0, \quad \frac{\partial^3}{\partial x^3} v_0^{(2)}(0) - \frac{\partial^3}{\partial x^3} v_0^{(4)}(0) = 0. \quad (6.1.23)$$

Due to the solvability conditions (6.1.18), (6.1.22), (6.1.23) and the continuity conditions (6.1.13), (6.1.21), the set of coefficients A, B, C, D, E, F is uniquely defined and the leading term of the asymptotic approximations of the displacement field is obtained in the closed form.

6.2 Asymptotic expansion of the solution in thin bridges

6.2.1 Thin bridge of a constant thickness

In this section one analyses the solution of linear isotropic elasticity in a thin region (see, for example, to Movchan and Movchan [75]). This problem is one of model problems which occur in analysis of the honeycomb structures (see Section 6.1). The corresponding boundary value problem can be written as follows

$$\begin{aligned}
 \mathfrak{L}_{xx}(U; \mathbf{x}) &:= \mathcal{D}_{\frac{\partial}{\partial \mathbf{x}}} \mathcal{H} \mathcal{D}_{\frac{\partial}{\partial \mathbf{x}}}^t U(\mathbf{x}) = 0, & \mathbf{x} \in \Pi_\varepsilon, \\
 \boldsymbol{\sigma}^{(n)}(U; \mathbf{x}) &= \begin{pmatrix} p_\pm^{(1)} \\ \varepsilon^2 p_\pm^{(2)} \end{pmatrix}, & \mathbf{x} \in \partial\Pi_\varepsilon^{(1)}, \\
 U &= \mathbf{a}_\pm, & \mathbf{x} \in \partial\Pi_\varepsilon^{(2)},
 \end{aligned} \tag{6.2.1}$$

where

$$\mathcal{D}_{\frac{\partial}{\partial \mathbf{x}}} = \begin{pmatrix} \frac{\partial}{\partial x_1} & 0 & \frac{1}{\sqrt{2}} \frac{\partial}{\partial x_2} \\ 0 & \frac{\partial}{\partial x_2} & \frac{1}{\sqrt{2}} \frac{\partial}{\partial x_1} \end{pmatrix}, \quad \mathcal{H} = \begin{pmatrix} 2\mu + \lambda & \lambda & 0 \\ \lambda & 2\mu + \lambda & 0 \\ 0 & 0 & 2\mu \end{pmatrix},$$

and $\Pi_\varepsilon = \{(x, \varepsilon t) : -1 < x < 1, -\frac{1}{2} < t < \frac{1}{2}\}$, $\partial\Pi_\varepsilon^{(1)} = \{t = \pm\frac{1}{2}\}$, $\partial\Pi_\varepsilon^{(2)} = \{x = \pm 1\}$.

Due to the presence of the small parameter ε , the thickness of the thin bridge, we can rewrite the Navier system in the stretched coordinates (x, t) and define the recurrent equations for the displacement vector

$$\begin{aligned}
 \frac{\partial^2}{\partial t^2} U_1^{(n)} &= -\frac{\lambda + \mu}{\mu} \frac{\partial^2}{\partial t \partial x} U_2^{(n-1)} - \frac{\lambda + 2\mu}{\mu} \frac{\partial^2}{\partial x^2} U_1^{(n-2)}, & |t| < 1/2, \\
 \frac{\partial}{\partial t} U_1^{(n)} &= -\frac{\partial}{\partial x} U_2^{(n-1)}, & |t| = \pm 1/2, \\
 \frac{\partial^2}{\partial t^2} U_2^{(n)} &= -\frac{\lambda + \mu}{\lambda + 2\mu} \frac{\partial^2}{\partial t \partial x} U_1^{(n-1)} - \frac{\mu}{\lambda + 2\mu} \frac{\partial^2}{\partial x^2} U_2^{(n-2)}, & |t| < 1/2, \\
 \frac{\partial}{\partial t} U_2^{(n)} &= -\frac{\lambda}{\lambda + 2\mu} \frac{\partial}{\partial x} U_1^{(n-1)}, & |t| = \pm 1/2.
 \end{aligned} \tag{6.2.2}$$

Now the recurrent formulae (6.2.2) is applied and the solvability conditions are checked

on each step. This procedure allows one to construct the asymptotic solution of the problem (6.2.2) in the form of the sets of two Jordan chains (6.1.3). For readers' convenience, we rewrite the definition of the Jordan chain given in the book [84]: the Jordan chain is a set of generalised eigenvectors corresponding to zero eigenvalue of the boundary value problem (6.2.1).

The first Jordan chain (6.1.3) corresponds to the longitudinal deformations and its leading term corresponds to the longitudinal displacement field, linear field in the absence of boundary tractions. It has multiplicity 2 and the elements

$$\mathbf{u}^{(0)} = \begin{pmatrix} u_0 \\ 0 \end{pmatrix}, \quad \mathbf{u}^{(1)} = \begin{pmatrix} 0 \\ -\frac{\lambda}{\lambda+2\mu} t \frac{\partial}{\partial x} u_0 \end{pmatrix}, \quad \mathbf{u}^{(2)} = \begin{pmatrix} \frac{\lambda}{\lambda+2\mu} \frac{t^2}{2} \frac{\partial^2}{\partial x^2} u_0 + \mathcal{U}(x, t) \\ 0 \end{pmatrix},$$

where \mathcal{U} is the solution of the following boundary value problem

$$\begin{aligned} \frac{\partial^2}{\partial t^2} \mathcal{U}(x, t) &= -\frac{4(\lambda+\mu)}{\lambda+2\mu} \frac{\partial^2}{\partial x^2} u_0, & |t| < 1/2, \\ \frac{\partial}{\partial t} \mathcal{U}(x, t) &= \pm \frac{1}{\mu} p_{\pm}^{(1)}, & t = \pm 1/2. \end{aligned} \tag{6.2.3}$$

The solvability condition of the system (6.2.3) gives the equation for the leading term of the longitudinal displacement

$$-\frac{4(\lambda+\mu)}{\lambda+2\mu} \frac{\partial^2}{\partial x^2} u_0 = p_+^{(1)} + p_-^{(1)}, \quad |x| < 1.$$

For the case of free-traction lateral surfaces, the leading term of the longitudinal displacement is a linear function.

Another Jordan chain describing the transversal deformation has the following form (it has multiplicity 4)

$$\begin{aligned} \mathbf{v}^{(0)} &= \begin{pmatrix} 0 \\ v_0 \end{pmatrix}, \quad \mathbf{v}^{(1)} = \begin{pmatrix} -t \frac{\partial}{\partial x} v_0 \\ 0 \end{pmatrix}, \quad \mathbf{v}^{(2)} = \begin{pmatrix} 0 \\ \frac{\lambda}{\lambda+2\mu} \frac{t^2}{2} \frac{\partial^2}{\partial x^2} v_0 \end{pmatrix}, \\ \mathbf{v}^{(3)} &= \begin{pmatrix} \left[\frac{4\mu+3\lambda}{6(\lambda+2\mu)} t^3 - \frac{\lambda+\mu}{2(\lambda+2\mu)} t \right] \frac{\partial^3}{\partial x^3} v_0 \\ 0 \end{pmatrix}, \\ \mathbf{v}^{(4)} &= \begin{pmatrix} 0 \\ \left[-\frac{3\lambda+2\mu}{24(\lambda+2\mu)} t^4 + \frac{(\lambda+\mu)(3\lambda+\mu)}{12(\lambda+2\mu)^2} t^2 \right] \frac{\partial^4}{\partial x^4} v_0 + \mathcal{V}(x, t) \end{pmatrix}, \end{aligned}$$

where \mathcal{V} satisfies the equations

$$\begin{aligned}\frac{\partial^2}{\partial t^2} \mathcal{V}(x, t) &= \frac{\mu(\lambda + \mu)}{3(\lambda + 2\mu)^2} \frac{\partial^4}{\partial x^4} v_0, \quad |t| < 1/2, \\ \frac{\partial}{\partial t} \mathcal{V}(x, t) &= \pm \frac{1}{\lambda + 2\mu} p_{\pm}^{(2)}, \quad |t| = \pm 1/2.\end{aligned}\tag{6.2.4}$$

From the solvability condition the equation for the leading term of the transversal displacement is derived in the form

$$\frac{\mu(\lambda + \mu)}{3(\lambda + 2\mu)} \frac{\partial^4}{\partial x^4} v_0 = p_+^{(2)} + p_-^{(2)}, \quad |x| < 1.$$

Note that in the case of free-traction lateral surfaces, the transversal displacement specified by the cubic polynomial.

6.2.2 Thin bridge of an orthotropic material

The objective of this section is to give an asymptotic solution for the thin bridge problem in an orthotropic medium. The axes of symmetry are parallel to the axes of the bridge. This is a generalisation of the analysis given in section 6.2.1. The solution below describes orthotropic thin bridges. The orthotropic symmetry, in contrary to general anisotropy, allows one to use the asymptotic expansions as the sets of ansatzes of finite length where the longitudinal and transversal modes are uncoupled. The boundary value problem we solve can be formulated in the form (6.2.1) where the elasticity matrix is

$$\mathcal{H} = \begin{pmatrix} c_1 & c_2 & 0 \\ c_2 & c_4 & 0 \\ 0 & 0 & c_6 \end{pmatrix}.$$

Using the method of compound asymptotic expansions we are looking for a solution of the boundary value problem (6.2.1) as the power series in ε . Also, similar to the asymptotic expansion for an isotropic thin bridge (see previous subsection) one can split up the series into two modes: the longitudinal and the transversal one and look for a solution in the form (6.1.3).

The longitudinal ansatz, also known as the first Jordan chain, has the following components

$$\mathbf{u}^{(0)} = \begin{pmatrix} u_0 \\ 0 \end{pmatrix}, \quad \mathbf{u}^{(1)} = \begin{pmatrix} 0 \\ -\frac{c_2 t}{c_4} \frac{\partial}{\partial x} u_0 \end{pmatrix}, \quad \mathbf{u}^{(2)} = \begin{pmatrix} \frac{c_2 t^2}{c_4} \frac{\partial^2}{\partial x^2} u_0 + \mathcal{U}(x, t) \\ 0 \end{pmatrix}.$$

The boundary value problem for the displacement vector \mathcal{U}

$$\begin{aligned}\frac{\partial^2}{\partial t^2}\mathcal{U}(x, t) &= \frac{2(c_2^2 - c_1 c_4)}{c_4 c_6} \frac{\partial^2}{\partial x^2} u_0, \quad |t| < 1/2, \\ \frac{\partial}{\partial t}\mathcal{U}(x, t) &= \pm \frac{2}{c_6} p_{\pm}^{(1)}, \quad t = \pm 1/2,\end{aligned}\tag{6.2.5}$$

is characterized by the following solvability condition

$$\frac{c_2^2 - c_1 c_4}{c_4} \frac{\partial^2}{\partial x^2} u_0 = p_+^{(1)} + p_-^{(1)}, \quad |x| < 1.$$

The components of the transversal ansatz, the second Jordan chain, are

$$\begin{aligned}\mathbf{v}^{(0)} &= \begin{pmatrix} 0 \\ v_0 \end{pmatrix}, \quad \mathbf{v}^{(1)} = \begin{pmatrix} -t \frac{\partial}{\partial x} v_0 \\ 0 \end{pmatrix}, \quad \mathbf{v}^{(2)} = \begin{pmatrix} 0 \\ \frac{c_2}{c_4} \frac{t^2}{2} \frac{\partial^2}{\partial x^2} v_0 \end{pmatrix}, \\ \mathbf{v}^{(3)} &= \begin{pmatrix} \left[\frac{2c_1 c_4 - 2c_2^2 - c_2 c_6}{6c_4 c_6} t^3 + \frac{c_2^2 - c_1 c_4}{4c_6} t \right] \frac{\partial^3}{\partial x^3} v_0 \\ 0 \end{pmatrix}, \\ \mathbf{v}^{(4)} &= \begin{pmatrix} 0 \\ \left[\frac{2c_2(c_2^2 + c_6 c_2 - c_1 c_4) - c_1 c_4 c_6}{24c_4^2 c_6} t^4 + \frac{(6c_2 + c_6)(c_1 c_4 - c_2^2)}{48c_4^2 c_6} t^2 \right] \frac{\partial^4}{\partial x^4} v_0 + \mathcal{V}(x, t) \end{pmatrix}.\end{aligned}$$

Equations for \mathcal{V} have the form

$$\begin{aligned}\frac{\partial^2}{\partial t^2}\mathcal{V}(x, t) &= \frac{c_1 c_4 - c_2^2}{12c_4^2} \frac{\partial^4}{\partial x^4} v_0, \quad |t| < 1/2, \\ \frac{\partial}{\partial t}\mathcal{V}(x, t) &= \frac{1}{c_4} p_{\pm}^{(2)}, \quad t = \pm 1/2,\end{aligned}\tag{6.2.6}$$

and this problem is solvable if and only if

$$\frac{c_1 c_4 - c_2^2}{12c_4} \frac{\partial^4}{\partial x^4} v_0 = \varepsilon(p_+^{(2)} - p_-^{(2)}), \quad |x| < 1.$$

One can note that the formulae above coincide with the ones for the isotropic case if we impose $c_1 = c_4 = 2\mu + \lambda$, $c_2 = \lambda$, $c_6 = 2\mu$.

6.2.3 Thin bridge of a varying thickness

In this subsection we analyse the structure of the solution in a thin bridge regions of variable thickness $\varepsilon h(x)$. This extends the analysis given in subsection 6.2.1 to the case of non-trivial geometry. We suppose that the bridge is symmetric with respect to the x -axis and the region which it occupies can be specified as follows $\{(x, y) : 0 < x < L; |y| < \varepsilon h(x)/2\}$. Using this assumption the solution can be expanded to the asymptotic series

of different powers of ε . The value of ε is defined as an average thickness of the bridge provided $\frac{1}{L} \int_0^L h(x) dx = 1$ and it coincides with the real thickness if $h'(x) = 0$ for all x . As for the case of a constant thickness (see subsection 6.2.1) we are looking for the asymptotic series which are split up into the longitudinal and the transversal modes in the form (6.1.3).

The system of the recurrent equations obtained from the homogeneous Navier system is similar to the constant-thickness bridge problem. New coordinates $(x, t) = (x, y/\varepsilon)$ are introduced, and the following recurrent system of equations arises

$$\begin{aligned} \frac{\partial^2}{\partial t^2} U_1^{(n)} &= -\frac{\lambda+\mu}{\mu} \frac{\partial^2}{\partial x \partial t} U_2^{(n-1)} - \frac{\lambda+2\mu}{\mu} \frac{\partial^2}{\partial x^2} U_1^{(n-2)}, \quad |t| < \frac{h(x)}{2}, \\ \frac{\partial^2}{\partial t^2} U_2^{(n)} &= -\frac{\lambda+\mu}{\lambda+2\mu} \frac{\partial^2}{\partial x \partial t} U_1^{(n-1)} - \frac{\mu}{\lambda+2\mu} \frac{\partial^2}{\partial x^2} U_2^{(n-2)}, \quad |t| < \frac{h(x)}{2}. \end{aligned} \quad (6.2.7)$$

The boundary conditions differ from the constant-thickness problem. Here (for the case of a variable thickness) the free-traction conditions imposed on the boundary ($t = \pm h(x)/2$), the outward normal vector on the top (and bottom) boundaries depends on the longitudinal coordinate x and, as a result, can be written in the form

$$n_+ = \begin{pmatrix} \frac{-\varepsilon h'(x)}{2\sqrt{1+\frac{1}{4}\varepsilon^2 h^2(x)}} \\ \frac{1}{\sqrt{1+\frac{1}{4}\varepsilon^2 h^2(x)}} \end{pmatrix}, \quad n_- = \begin{pmatrix} \frac{-\varepsilon h'(x)}{2\sqrt{1+\frac{1}{4}\varepsilon^2 h^2(x)}} \\ \frac{-1}{\sqrt{1+\frac{1}{4}\varepsilon^2 h^2(x)}} \end{pmatrix}.$$

With these relations in free-tractions boundary conditions on the lateral surfaces the recurrent system of equations (6.2.7) can be supplied with the system of recurrent boundary conditions specified by

$$\begin{aligned} \frac{\partial}{\partial t} U_1^{(n)} &= -\frac{\partial}{\partial x} U_2^{(n-1)} \pm \frac{\lambda}{2\mu} \frac{\partial}{\partial t} U_2^{(n-1)} h'(x) \\ &\quad \pm \frac{2\mu+\lambda}{2\mu} \frac{\partial}{\partial x} U_1^{(n-2)} h'(x) \pm \frac{1}{\mu} p_{\pm} \delta_{2n}, \quad |t| = \pm \frac{h(x)}{2}, \\ \frac{\partial}{\partial t} U_2^{(n)} &= -\frac{\lambda}{\lambda+2\mu} \frac{\partial}{\partial x} U_1^{(n-1)} \pm \frac{\mu}{2(2\mu+\lambda)} \frac{\partial}{\partial t} U_1^{(n-1)} h'(x) \\ &\quad \pm \frac{\mu}{2(2\mu+\lambda)} \frac{\partial}{\partial x} U_2^{(n-2)} h'(x) \pm \frac{1}{2\mu+\lambda} p_{\pm} \delta_{4n}, \quad |t| = \pm \frac{h(x)}{2}. \end{aligned} \quad (6.2.8)$$

Our next intention is to construct the set of generalised eigenvectors for the system (6.2.7)-(6.2.8). This procedure is similar to one mentioned for isotropic bridges of a constant thickness. However the eigenvectors are different due to new recurrent boundary conditions (6.2.8).

The first chain of the generalised eigenvectors can be specified as follows

$$\begin{aligned} \mathbf{u}^{(0)} &= \begin{pmatrix} u_0 \\ 0 \end{pmatrix}, \quad \mathbf{u}^{(1)} = \begin{pmatrix} 0 \\ -\frac{\lambda}{\lambda+2\mu} t \frac{\partial}{\partial x} u_0 \end{pmatrix}, \\ \mathbf{u}^{(2)} &= \begin{pmatrix} \frac{\lambda}{\lambda+2\mu} \frac{t^2}{2} \frac{\partial^2}{\partial x^2} u_0 + \frac{2(\mu+\lambda)}{2\mu+\lambda} t^2 \frac{h'(x)}{h(x)} \frac{\partial}{\partial x} u_0 + \mathcal{U}(x, t) \\ 0 \end{pmatrix}, \end{aligned}$$

where $\mathcal{U}(x, t)$ is the solution of the following boundary value problem

$$\begin{aligned} \frac{\partial^2}{\partial t^2} \mathcal{U}(x, t) &= -\frac{4(\lambda+\mu)}{\lambda+2\mu} \left(\frac{\partial^2}{\partial x^2} u_0 + \frac{h'(x)}{h(x)} \frac{\partial}{\partial x} u_0 \right), \quad |t| < \frac{h(x)}{2}, \\ \frac{\partial}{\partial t} \mathcal{U}(x, t) &= \pm \frac{1}{\mu} p_{\pm}^{(1)}, \quad t = \pm \frac{h(x)}{2}. \end{aligned} \quad (6.2.9)$$

The solvability condition of the system (6.2.9) gives one the equation for the leading term of the longitudinal displacement field

$$-\frac{4(\lambda+\mu)}{\lambda+2\mu} \frac{\partial}{\partial x} \left[h(x) \frac{\partial}{\partial x} u_0 \right] = p_+^{(1)} + p_-^{(1)}, \quad |x| < 1.$$

The second set of generalised eigenvectors specifies the transversal displacement and bending of the thin bridge

$$\begin{aligned} \mathbf{v}^{(0)} &= \begin{pmatrix} 0 \\ v_0 \end{pmatrix}, \quad \mathbf{v}^{(1)} = \begin{pmatrix} -t \frac{\partial}{\partial x} v_0 \\ 0 \end{pmatrix}, \quad \mathbf{v}^{(2)} = \begin{pmatrix} 0 \\ \frac{\lambda}{\lambda+2\mu} \frac{t^2}{2} \frac{\partial^2}{\partial x^2} v_0 \end{pmatrix}, \\ \mathbf{v}^{(3)} &= \begin{pmatrix} \left(\frac{4\mu+3\lambda}{6(\lambda+2\mu)} t^3 - \frac{\lambda+\mu}{2(\lambda+2\mu)} t h^2(x) \right) \frac{\partial^3}{\partial x^3} v_0 - \frac{\lambda+\mu}{2\mu+\lambda} h(x) h'(x) \frac{\partial^2}{\partial x^2} v_0 \\ 0 \end{pmatrix}, \\ \mathbf{v}^{(4)} &= \begin{pmatrix} 0 \\ -\frac{(3\lambda+2\mu)}{24(\lambda+2\mu)} \frac{\partial^4}{\partial x^4} v_0 t^4 + \frac{\mu(\lambda+\mu)[h^2(x) \frac{\partial^4}{\partial x^4} v_0 - 6(h'(x))^2 \frac{\partial^2}{\partial x^2} v_0]}{12(2\mu+\lambda)^2} t^2 \\ + \left(\frac{\lambda(\mu+\lambda) \frac{\partial^2}{\partial x^2} [h^2(x) \frac{\partial^2}{\partial x^2} v_0(x)]}{4(2\mu+\lambda)^2} t^2 + \mathcal{V}(x, t) \right) \end{pmatrix}, \end{aligned}$$

where $\mathcal{V}(x, t)$ is the solution of the ordinary differential equation with corresponding boundary conditions

$$\begin{aligned} \frac{\partial^2}{\partial t^2} \mathcal{V} &= \frac{\mu(\mu+\lambda)}{3(2\mu+\lambda)} \left[h^2(x) \frac{\partial^4}{\partial x^4} v_0 + 6h(x) h'(x) \frac{\partial^3}{\partial x^3} v_0 \right. \\ &\quad \left. + 3 \frac{\partial^2}{\partial x^2} v_0 \left(h(x) h''(x) + 2(h'(x))^2 \right) \right], \quad |t| < \frac{h(x)}{2}, \\ \frac{\partial}{\partial t} \mathcal{V}(x, t) &= \pm \frac{1}{\lambda+2\mu} p_{\pm}^{(2)}, \quad t = \pm \frac{h(x)}{2}. \end{aligned} \quad (6.2.10)$$

The solvability condition of the problem (6.2.10) is

$$\frac{\mu(\lambda + \mu)}{3(\lambda + 2\mu)} \frac{\partial^2}{\partial x^2} \left[h^3(x) \frac{\partial^2}{\partial x^2} v_0 \right] = p_+^{(2)} + p_-^{(2)}, \quad |x| < 1.$$

6.3 The leading order approximation for the effective moduli

The effective elastic moduli can be evaluated as the energy of some special fields in a unit periodic cell. This result can be found, for example, in Bakhvalov and Panasenko [4], Jikov, Koslov and Oleinik [47], Bensoussan, Lions and Papanicolaou [8], Milton [69] (see Appendix A)

$$\mathcal{H}_{nk} = \frac{1}{mes_2 \mathcal{S}} \int_{\Xi} \boldsymbol{\sigma}(\mathbf{U}^{(n)}; \mathbf{x}) : \boldsymbol{\varepsilon}(\mathbf{U}^{(k)}; \mathbf{x}) d\mathbf{x}, \quad (6.3.1)$$

where $\boldsymbol{\sigma}$ and $\boldsymbol{\varepsilon}$ are stress and strain tensors, \mathcal{S} is the elementary cell of the periodic structure (see Figure 6.2.1). The model fields $\mathbf{U}^{(n)}$, $\mathbf{U}^{(k)}$ describe the displacements in the elementary cell when the whole composite is loaded by the test fields. Namely, $\varepsilon_{11} = 1$ for $n = 1$; $\varepsilon_{22} = 1$ for $n = 2$; $\varepsilon_{12} = 1$ for $n = 3$ (all other components of the strain tensor are supposed to be zero). Thus, the homogenisation problem for elasticity equation reduces to the solutions of three boundary value problems corresponding to three types of loading. While one deals with the periodic elementary cell, the periodicity conditions on the outer boundary are imposed.

The problem of evaluation of the effective moduli for honeycomb structures has been treated by Torquato et al [112]. The authors used the approach based on the Hashin-Shtrikman estimates for the effective characteristics of the composite structures. Such kind of treatment gives approximations for bulk modulus. At the same time the shear modulus remains unknown.

The asymptotic approach is free of this restrictions. Estimates of the effective moduli matrix in terms of elastic energy allow one to take into account the high order terms. Moreover, this approach works for composites where the thickness of “thin bridges” is non-constant.

One can evaluate the energy of a single bridge assuming that the leading term of the asymptotic expansion (6.1.4) is known. Taking into account the fact that the lateral surface of the bridge is free of traction the first ansatz of the asymptotic expansion (see

section 6.2.1, for full expansion) can be written in the form

$$\mathbf{v}^{(n)}(x, y) = \begin{pmatrix} -y \frac{\partial}{\partial x} v_0(x) + \frac{4\mu+3\lambda}{6(\lambda+2\mu)} y^3 \frac{\partial^3}{\partial x^3} v_0(x) - \varepsilon^2 \frac{\mu+\lambda}{2(\lambda+2\mu)} y \frac{\partial^3}{\partial x^3} v_0(x) \\ v_0(x) + \frac{\lambda}{\lambda+2\mu} \frac{y^2}{2} \frac{\partial^2}{\partial x^2} v_0(x) \end{pmatrix},$$

$$\mathbf{u}^{(n)}(x, y) = \begin{pmatrix} u_0(x) \\ -\frac{\lambda}{\lambda+2\mu} y \frac{\partial}{\partial x} u_0(x) \end{pmatrix}, \quad (6.3.2)$$

where x, y are the coordinates associated with the thin bridge.

The equations for the leading term components reduce to

$$\frac{\partial^2}{\partial x^2} u_0(x) = 0, \quad \frac{\partial^4}{\partial x^4} v_0(x) = 0,$$

with the Dirichlet boundary conditions prescribed on the edges.

One can calculate the components of the strain tensor associated with the above mentioned fields

$$\begin{aligned} \varepsilon_{11} &= \frac{\partial}{\partial x} u_0(x) - y \frac{\partial^2}{\partial x^2} v_0(x), \\ \varepsilon_{22} &= -\frac{\lambda}{\lambda+2\mu} \frac{\partial}{\partial x} u_0(x) + \frac{\lambda}{\lambda+2\mu} y \frac{\partial^2}{\partial x^2} v_0(x), \\ \varepsilon_{12} &= \frac{2(\mu+\lambda)}{\lambda+2\mu} y^2 \frac{\partial^3}{\partial x^3} v_0(x) - \varepsilon^2 \frac{\lambda+\mu}{2(\lambda+2\mu)} \frac{\partial^3}{\partial x^3} v_0(x). \end{aligned} \quad (6.3.3)$$

Substitution (6.3.3) into the representation for the elastic energy allows one to obtain the leading term of the solution (6.3.2) in the formula for the energy

$$\Delta \mathcal{E}_0 = \int_0^L dx \int_{-\varepsilon/2}^{\varepsilon/2} \boldsymbol{\sigma}(\mathbf{U}^{(m)}; \mathbf{x}) : \boldsymbol{\varepsilon}(\mathbf{U}^{(k)}; \mathbf{x}) dy =$$

$$\frac{4\mu(\lambda+\mu)}{\lambda+2\mu} \int_0^L \left\{ A^{(m)} A^{(k)} \varepsilon + \frac{1}{3} (3C^{(m)} x + D^{(m)}) (3C^{(k)} x + D^{(k)}) \varepsilon^3 \right\} dx + O(\varepsilon^5), \quad (6.3.4)$$

where the quantities $A^{(k)}$, $C^{(k)}$ and $D^{(k)}$ are the same as in (6.1.4).

Due to specific geometry of the periodic cell one's energy (leading approximation of the energy) can be evaluated in terms of the energies of thin bridges. The following theorem can be formulated:

Theorem 6.1 *The asymptotic approximation of effective elastic moduli, which describe the "average" stress and strain fields in a thin-walled composite structure is given by*

$$\begin{aligned} \mathcal{H}_{mk} &= \frac{1}{mes_2\mathcal{S}} \sum_{n=1}^N \Delta \mathcal{E}_0^{(n)} = \frac{4\mu(\lambda + \mu)}{mes_2\mathcal{S}(\lambda + 2\mu)} \sum_{n=1}^N \int_0^L \left\{ A_n^{(m)} A_n^{(k)} \varepsilon \right. \\ &\quad \left. + \frac{1}{3} (3C_n^{(m)} x + D_n^{(m)}) (3C_n^{(k)} x + D_n^{(k)}) \varepsilon^3 \right\} dx + O(\varepsilon^5), \end{aligned} \quad (6.3.5)$$

where N is the number of bridges connected at the junction point ($N=3,4,6$), the index n corresponds to the number of the bridge, indices m, k correspond to the type of loading, L is the length of the bridge, $mes_2\mathcal{S}$ is the area of the elementary cell, ε is the normalized thickness of the bridge.

The junction area is considered as a point in the limiting problem when the thickness of bridges tends to zero. The junction gives the effect for next (high order) terms of the approximation of the effective moduli, which will be considered further. At the same time we note that the second term of the asymptotic expansion of the effective moduli has the order $O(\varepsilon^2)$ and can be evaluated by solving the problem (6.1.20).

6.3.1 Effective elastic moduli for square honeycombs

In this subsection we consider the square honeycomb structures and evaluate their effective elastic moduli. Following subsection 6.3 one evaluates the energy of the test fields $(x, 0)$, $(0, y)$ and $2^{-1/2}(y, x)$ imposed on the periodic cell. Inside each bridge the linear longitudinal displacement field and the cubic transversal bending field take place. These fields satisfy the homogeneous equations

$$\frac{\partial^2}{\partial x^2} u^{(n)} = 0, \quad \frac{\partial^4}{\partial x^4} v^{(n)} = 0, \quad n = 1, 2, 3, 4, \quad (6.3.6)$$

where x is the local longitudinal variable. The elementary cell is supposed to have a unit area, thus each bridge has the length $L = \frac{1}{2}$ (see Figure 6-1). If, in addition, the thickness of the bridge is ε , the area fraction of such composite is $f = 2\varepsilon$.

On the edges of the bridges the periodicity boundary conditions are imposed. They reduce to the Dirichlet boundary conditions given in terms of traces of the test fields. For the test field $(x, 0)$ one has the following conditions

$$\begin{aligned} u^{(1)}(L) &= 1/2, & u^{(2)}(L) &= 0, & u^{(3)}(L) &= 1/2, & u^{(4)}(L) &= 0, \\ v^{(1)}(L) &= 0, & v^{(2)}(L) &= 0, & v^{(3)}(L) &= 0, & v^{(4)}(L) &= 0. \end{aligned} \quad (6.3.7)$$

For the test field $(0, y)$ the displacements at the edges are given by

$$\begin{aligned} u^{(1)}(L) = 0, \quad u^{(2)}(L) = 1/2, \quad u^{(3)}(L) = 0, \quad u^{(4)}(L) = 1/2, \\ v^{(1)}(L) = 0, \quad v^{(2)}(L) = 0, \quad v^{(3)}(L) = 0, \quad v^{(4)}(L) = 0. \end{aligned} \quad (6.3.8)$$

For the test field $2^{-1/2}(y, x)$ the following values take place

$$\begin{aligned} u^{(1)}(L) = 0, \quad u^{(2)}(L) = 0, \\ u^{(3)}(L) = 0, \quad u^{(4)}(L) = 0, \\ v^{(1)}(L) = 1/(2\sqrt{2}), \quad v^{(2)}(L) = -1/(2\sqrt{2}), \\ v^{(3)}(L) = 1/(2\sqrt{2}), \quad v^{(4)}(L) = -1/(2\sqrt{2}). \end{aligned} \quad (6.3.9)$$

In the point of the bridge intersection one has the continuity of displacements

$$\begin{aligned} u_0^{(1)}(0) = -v_0^{(2)}(0) = -u_0^{(3)}(0) = v_0^{(4)}(0), \\ v_0^{(1)}(0) = u_0^{(2)}(0) = -v_0^{(3)}(0) = -u_0^{(4)}(0); \end{aligned} \quad (6.3.10)$$

the condition of the continuity of longitudinal forces

$$\frac{\partial}{\partial x} u^{(1)}(0) - \frac{\partial}{\partial x} u^{(3)}(0) = 0, \quad \frac{\partial}{\partial x} u^{(2)}(0) - \frac{\partial}{\partial x} u^{(4)}(0) = 0; \quad (6.3.11)$$

the condition of the continuity of transversal forces

$$\frac{\partial^3}{\partial x^3} v^{(1)}(0) - \frac{\partial^3}{\partial x^3} v^{(3)}(0) = 0, \quad \frac{\partial^3}{\partial x^3} v^{(2)}(0) - \frac{\partial^3}{\partial x^3} v^{(4)}(0) = 0; \quad (6.3.12)$$

and zero moment in the junction point

$$\frac{\partial^2}{\partial x^2} v^{(1)}(0) + \frac{\partial^2}{\partial x^2} v^{(2)}(0) + \frac{\partial^2}{\partial x^2} v^{(3)}(0) + \frac{\partial^2}{\partial x^2} v^{(4)}(0) = 0. \quad (6.3.13)$$

To close the system of differential equations one impose a "soft boundary conditions" on the edges of the bridges for the transversal displacement. They correspond to zero moment in these points

$$\frac{\partial^2}{\partial x^2} v^{(n)}(L) = 0, \quad n = 1, 2, 3, 4. \quad (6.3.14)$$

Equations (6.3.6) together with the boundary conditions (6.3.7)-(6.3.14) admit the so-

lution in the form

$$u^{(n)} = A^{(n)}x + B^{(n)}, \quad v^{(n)} = C^{(n)}x^3 + D^{(n)}x^2 + E^{(n)}x + F^{(n)}, \quad n = 1, 2, 3, 4.$$

with the coefficients given in the table

	$(x_1, 0)$				$(0, x_2)$				$2^{-1/2}(x_2, x_1)$			
	(1)	(2)	(3)	(4)	(1)	(2)	(3)	(4)	(1)	(2)	(3)	(4)
A	1	0	1	0	0	1	0	1	0	0	0	0
C	0	0	0	0	0	0	0	0	$-\sqrt{2}$	$\sqrt{2}$	$-\sqrt{2}$	$\sqrt{2}$
D	0	0	0	0	0	0	0	0	$3/\sqrt{2}$	$-3/\sqrt{2}$	$3/\sqrt{2}$	$-3/\sqrt{2}$

Further one can evaluate the energy of each thin bridge (see formula (6.3.4) from subsection 6.2.1) and, using (A.0.14) and (6.3.5), determine the effective elastic moduli. For unit cell with the bridges of the thickness ε the following representation holds for the matrix of effective elastic moduli

$$\mathcal{H} \sim \frac{4\mu(\lambda + \mu)}{2\mu + \lambda} \begin{pmatrix} \varepsilon & 0 & 0 \\ 0 & \varepsilon & 0 \\ 0 & 0 & \varepsilon^3 \end{pmatrix}. \quad (6.3.15)$$

Taking into account the relation between area fraction and the normalized thickness of the bridge $f = 2\varepsilon$, these formulae can be rewritten in the form

$$\mathcal{H} \sim \frac{4\mu(\lambda + \mu)}{2\mu + \lambda} \begin{pmatrix} \frac{1}{2}f & 0 & 0 \\ 0 & \frac{1}{2}f & 0 \\ 0 & 0 & \frac{1}{8}f^3 \end{pmatrix}. \quad (6.3.16)$$

The corresponding compliance matrix is

$$\mathcal{S} \sim \frac{1}{E} \begin{pmatrix} 2f^{-1} & 0 & 0 \\ 0 & 2f^{-1} & 0 \\ 0 & 0 & 8f^{-3} \end{pmatrix}. \quad (6.3.17)$$

6.3.2 Effective elastic moduli for triangular honeycombs

Triangular honeycomb structures and evaluation of the effective elastic moduli are considered below. Following the idea of the subsection 6.3.1 we evaluate the energy of the

test fields $(x, 0)$, $(0, y)$ and $2^{-1/2}(y, x)$ imposed on the periodic cell. In this particular situation one does not need to consider the bending of the thin bridges. For triangular honeycomb all components of the effective moduli tensor can be calculated in terms of the longitudinal deformation of the bridges only. The shear modulus for this structure has the same order as the bulk modulus. And the homogenized structure behaves similar to the isotropic structure if we restrict ourselves by the leading term of homogenized moduli only. The longitudinal displacement fields inside the thin bridges satisfy the following equations

$$\frac{\partial^2}{\partial x^2} u^{(n)} = 0, \quad n = 1, 2, 3, 4, 5, 6, \quad (6.3.18)$$

and x is the local longitudinal variable. The elementary cell has a unit area, and each bridge has the length $L = 1/(\sqrt{2}\sqrt[4]{27})$. If, in addition, the thickness of the bridge is ε , the area fraction of such a composite is $f = 3\sqrt{2}/\sqrt[4]{3}\varepsilon$.

Due to the small thickness of the bridges the periodicity conditions on the boundary of an elementary cell reduce to the Dirichlet boundary conditions on one edge of the bridges. In this case periodicity is satisfied without any additional restrictions. For the test field $(x, 0)$ the Dirichlet conditions on the bridges edges have the following form

$$\begin{aligned} u^{(1)}(L) &= u^{(4)}(L) = 1/(\sqrt{2}\sqrt[4]{3}), \\ u^{(2)}(L) &= u^{(3)}(L) = u^{(5)}(L) = u^{(6)}(L) = 1/(4\sqrt{2}\sqrt[4]{3}). \end{aligned} \quad (6.3.19)$$

For the test field $(0, y)$ the following conditions hold

$$\begin{aligned} u^{(1)}(L) &= u^{(4)}(L) = 0, \\ u^{(2)}(L) &= u^{(3)}(L) = u^{(5)}(L) = u^{(6)}(L) = 3/(4\sqrt{2}\sqrt[4]{3}). \end{aligned} \quad (6.3.20)$$

And for the test field $2^{-1/2}(y, x)$ they look as written below

$$\begin{aligned} u^{(1)}(L) &= u^{(4)}(L) = 0, \\ u^{(2)}(L) &= u^{(5)}(L) = \sqrt[4]{3}/4, \\ u^{(3)}(L) &= u^{(6)}(L) = -\sqrt[4]{3}/4. \end{aligned} \quad (6.3.21)$$

6.3. THE LEADING ORDER APPROXIMATION FOR THE EFFECTIVE
MODULI

At the point of the bridge intersection one impose continuity of the displacements

$$\begin{aligned}
 u^{(2)}(0) &= \frac{1}{2}u^{(1)}(0) + \frac{\sqrt{3}}{2}v^{(1)}(0), \\
 u^{(3)}(0) &= -\frac{1}{2}u^{(1)}(0) + \frac{\sqrt{3}}{2}v^{(1)}(0), \\
 v^{(2)}(0) &= -\frac{\sqrt{3}}{2}u^{(1)}(0) + \frac{1}{2}v^{(1)}(0), \\
 v^{(3)}(0) &= -\frac{\sqrt{3}}{2}u^{(1)}(0) - \frac{1}{2}v^{(1)}(0), \\
 u^{(4)}(0) &= -u^{(1)}(0), & v^{(4)}(0) &= -v^{(1)}(0), \\
 u^{(5)}(0) &= -u^{(2)}(0), & v^{(5)}(0) &= -v^{(2)}(0), \\
 u^{(6)}(0) &= -u^{(3)}(0), & v^{(6)}(0) &= -v^{(3)}(0),
 \end{aligned} \tag{6.3.22}$$

and condition of the continuity of the longitudinal forces which can be written as follows

$$\begin{aligned}
 \frac{\partial}{\partial x}u^{(1)}(0) - \frac{\partial}{\partial x}u^{(4)}(0) + \frac{1}{2}\frac{\partial}{\partial x}u^{(2)}(0) + \frac{1}{2}\frac{\partial}{\partial x}u^{(6)}(0) - \frac{1}{2}\frac{\partial}{\partial x}u^{(3)}(0) - \frac{1}{2}\frac{\partial}{\partial x}u^{(5)}(0) &= 0, \\
 \frac{\partial}{\partial x}u^{(2)}(0) + \frac{\partial}{\partial x}u^{(3)}(0) - \frac{\partial}{\partial x}u^{(2)}(0) - \frac{\partial}{\partial x}u^{(3)}(0) &= 0.
 \end{aligned} \tag{6.3.23}$$

The equations (6.3.18) together with the boundary conditions (6.3.19)-(6.3.23) have the linear solution

$$u^{(n)} = A^{(n)}x + B^{(n)}, \quad n = 1, 2, 3, 4, 5, 6,$$

with the results of calculation summarised in the following table

	$(x_1, 0)$						$(0, x_2)$					
	(1)	(2)	(3)	(4)	(5)	(6)	(1)	(2)	(3)	(4)	(5)	(6)
A	1	$\frac{1}{4}$	$\frac{1}{4}$	1	$\frac{1}{4}$	$\frac{1}{4}$	0	$\frac{3}{4}$	$\frac{3}{4}$	0	$\frac{3}{4}$	$\frac{3}{4}$
	$2^{-1/2}(x_2, x_1)$											
	(1)	(2)	(3)	(4)	(5)	(6)						
A	0	$\frac{\sqrt{3}}{2\sqrt{2}}$	$-\frac{\sqrt{3}}{2\sqrt{2}}$	0	$\frac{\sqrt{3}}{2\sqrt{2}}$	$-\frac{\sqrt{3}}{2\sqrt{2}}$						

Evaluating the energy of a thin bridge (see, (6.1.4)) one obtains the matrix of the effective elastic moduli. If an elementary cell (parallelogram for triangular thin-walled composites) has a unit area and bridges of the thickness ε the following representation

for the effective elastic moduli matrix holds

$$\mathcal{H} \sim \frac{4\mu(\lambda + \mu)}{2\mu + \lambda} \begin{pmatrix} \frac{9}{4\sqrt{2}\sqrt[4]{3}}\varepsilon & \frac{3}{4\sqrt{2}\sqrt[4]{3}}\varepsilon & 0 \\ \frac{3}{4\sqrt{2}\sqrt[4]{3}}\varepsilon & \frac{9}{4\sqrt{2}\sqrt[4]{3}}\varepsilon & 0 \\ 0 & 0 & \frac{3}{2\sqrt{2}\sqrt[4]{3}}\varepsilon^3 \end{pmatrix}. \quad (6.3.24)$$

Taking into account the area fraction which is related to the thickness of the bridge by $f = \frac{3\sqrt{2}}{\sqrt[4]{3}}\varepsilon$, we can rewrite these formulae in terms of f

$$\mathcal{H} \sim \frac{4\mu(\lambda + \mu)}{2\mu + \lambda} \begin{pmatrix} \frac{3}{8}f & \frac{1}{8}f & 0 \\ \frac{1}{8}f & \frac{3}{8}f & 0 \\ 0 & 0 & \frac{1}{4}f \end{pmatrix}. \quad (6.3.25)$$

The corresponding compliance matrix has the form

$$\mathcal{S} \sim \frac{1}{E} \begin{pmatrix} 3f^{-1} & -f^{-1} & 0 \\ -f^{-1} & 3f^{-1} & 0 \\ 0 & 0 & 4f^{-1} \end{pmatrix}. \quad (6.3.26)$$

6.3.3 Effective elastic moduli for hexagonal honeycombs

Hexagonal honeycomb structures are considered below and the effective elastic moduli are evaluated for them. If we impose test fields $(x, 0)$, $(0, y)$ and $2^{-1/2}(y, x)$ on the periodic cell, linear longitudinal displacement field and cubic transversal bending field occur in the bridges. These fields can be found as the solution of the homogeneous equations

$$\frac{\partial^2}{\partial x^2} u^{(n)} = 0, \quad \frac{\partial^4}{\partial x^4} v^{(n)} = 0, \quad n = 1, 2, 3, 4, \quad (6.3.27)$$

where x is the local longitudinal variable. Each bridge has the length $L = \sqrt{2}/\sqrt[4]{27}$ and the thickness of the bridge is ε . Thus the area fraction of such composite is $f = \sqrt{6}/\sqrt[4]{3}\varepsilon$. The Dirichlet conditions on the edges of the bridges correspond to the applied test fields. For field $(x, 0)$ these conditions have the following form

$$\begin{aligned} u^{(1)}(L) &= L, & u^{(2)}(L) &= L/4, & u^{(3)}(L) &= L/4, \\ v^{(1)}(L) &= 0, & v^{(2)}(L) &= \sqrt{3}L/4, & v^{(3)}(L) &= -\sqrt{3}L/4, \end{aligned} \quad (6.3.28)$$

or

$$\begin{aligned} u^{(1)}(L) &= \sqrt{2}/\sqrt[4]{27}, & u^{(2)}(L) &= 1/(2\sqrt{2}\sqrt[4]{27}), & u^{(3)}(L) &= 1/(2\sqrt{2}\sqrt[4]{27}), \\ v^{(1)}(L) &= 0, & v^{(2)}(L) &= 1/(2\sqrt{2}\sqrt[4]{3}), & v^{(3)}(L) &= -1/(2\sqrt{2}\sqrt[4]{3}). \end{aligned} \quad (6.3.29)$$

For the test field $(0, y)$ the fields are

$$\begin{aligned} u^{(1)}(L) &= 0, & u^{(2)}(L) &= 3L/4, & u^{(3)}(L) &= 3L/4, \\ v^{(1)}(L) &= 0, & v^{(2)}(L) &= -\sqrt{3}L/4, & v^{(3)}(L) &= \sqrt{3}L/4, \end{aligned} \quad (6.3.30)$$

or

$$\begin{aligned} u^{(1)}(L) &= 0, & u^{(2)}(L) &= \sqrt[4]{3}/(2\sqrt{2}), & u^{(3)}(L) &= \sqrt[4]{3}/(2\sqrt{2}), \\ v^{(1)}(L) &= 0, & v^{(2)}(L) &= -1/(2\sqrt[4]{3}\sqrt{2}), & v^{(3)}(L) &= 1/(2\sqrt[4]{3}\sqrt{2}), \end{aligned} \quad (6.3.31)$$

and for the test field $2^{-1/2}(y, x)$ they are given by

$$\begin{aligned} u^{(1)}(L) &= 0, & u^{(2)}(L) &= -\sqrt{3}L/(2\sqrt{2}), & u^{(3)}(L) &= \sqrt{3}L/(2\sqrt{2}), \\ v^{(1)}(L) &= L/\sqrt{2}, & v^{(2)}(L) &= -L\sqrt{2}/4, & v^{(3)}(L) &= -L\sqrt{2}/4. \end{aligned} \quad (6.3.32)$$

or

$$\begin{aligned} u^{(1)}(L) &= 0, & u^{(2)}(L) &= -1/(2\sqrt[4]{3}), & u^{(3)}(L) &= 1/(2\sqrt[4]{3}), \\ v^{(1)}(L) &= 1/(\sqrt{3}\sqrt[4]{3}), & v^{(2)}(L) &= -1/(2\sqrt{3}\sqrt[4]{3}), & v^{(3)}(L) &= -1/(2\sqrt{3}\sqrt[4]{3}). \end{aligned} \quad (6.3.33)$$

At the junction point we impose the continuity of the displacements. It corresponds to the fact that the edges of bridges join up together in one point and there is zero displacement jump between these three points. In other words, these conditions express the same displacements but in different coordinate systems. The longitudinal displacements $u^{(n)}$, $n = 1, 2, 3$, correspond to the longitudinal directions of bridges

$$\begin{aligned} u^{(2)}(0) &= -\frac{1}{2}u^{(1)}(0) + \frac{\sqrt{3}}{2}v^{(1)}(0), & u^{(3)}(0) &= -\frac{1}{2}u^{(1)}(0) - \frac{\sqrt{3}}{2}v^{(1)}(0), \\ v^{(2)}(0) &= -\frac{\sqrt{3}}{2}u^{(1)}(0) - \frac{1}{2}v^{(1)}(0), & v^{(3)}(0) &= \frac{\sqrt{3}}{2}u^{(1)}(0) - \frac{1}{2}v^{(1)}(0). \end{aligned} \quad (6.3.34)$$

In addition, the condition of the continuity of the longitudinal forces is imposed

$$\frac{\partial}{\partial x}u^{(1)}(0) - \frac{1}{2}\frac{\partial}{\partial x}u^{(2)}(0) - \frac{1}{2}\frac{\partial}{\partial x}u^{(3)}(0) = 0, \quad \frac{\partial}{\partial x}u^{(2)}(0) - \frac{\partial}{\partial x}u^{(3)}(0) = 0, \quad (6.3.35)$$

The condition of the continuity of the transversal forces is

$$\frac{\partial^3}{\partial x^3}v^{(1)}(0) + \frac{\partial^3}{\partial x^3}v^{(2)}(0) + \frac{\partial^3}{\partial x^3}v^{(3)}(0) = 0, \quad (6.3.36)$$

and zero moment in the junction point is given by

$$\frac{\partial^2}{\partial x^2}v^{(1)}(0) + \frac{\partial^2}{\partial x^2}v^{(2)}(0) + \frac{\partial^2}{\partial x^2}v^{(3)}(0) = 0. \quad (6.3.37)$$

The “soft boundary conditions” in the midpoints of the bridges are imposed for the transversal displacement. It corresponds to zero moment in these points. On the other hand, these conditions arise because of the symmetry. In the midpoints the moment is zero

$$\frac{\partial^2}{\partial x^2}v^{(n)}\left(\frac{L}{2}\right) = 0, \quad n = 1, 2, 3. \quad (6.3.38)$$

In terms of the coefficients A, C, D these conditions give one the following identity

$$D = -\frac{3}{2}CL.$$

Together with the conditions (6.3.36) and (6.3.37). The latter shows that

$$C_1 = C_2 = 2C_3.$$

The equations (6.3.27) together with the boundary conditions (6.3.29)-(6.3.38) admit the solution in the form

$$u^{(n)} = A^{(n)}x + B^{(n)}, \quad v^{(n)} = C^{(n)}x^3 + D^{(n)}x^2 + E^{(n)}x + F^{(n)}, \quad n = 1, 2, 3,$$

where the coefficients $A^{(n)}, B^{(n)}, C^{(n)}, D^{(n)}, E^{(n)}, F^{(n)}$ are the solution of the following linear system

$$\begin{aligned} A^{(1)} - \frac{1}{2}A^{(2)} - \frac{1}{2}A^{(3)} &= 0, & A^{(2)} - A^{(3)} &= 0, \\ D^{(1)} + D^{(2)} + D^{(3)} &= 0, & E^{(1)} = E^{(2)} = E^{(3)}, \\ C^{(1)} - \frac{1}{2}C^{(2)} - \frac{1}{2}C^{(3)} &= 0, & C^{(2)} + C^{(3)} &= 0, \\ B^{(2)} = -\frac{1}{2}B^{(1)} + \frac{\sqrt{3}}{2}F^{(1)}, & & B^{(3)} = -\frac{1}{2}B^{(1)} - \frac{\sqrt{3}}{2}F^{(1)}, \\ F^{(2)} = -\frac{\sqrt{3}}{2}B^{(1)} - \frac{1}{2}F^{(1)} & & F^{(3)} = \frac{\sqrt{3}}{2}B^{(1)} + \frac{1}{2}F^{(1)}, \end{aligned}$$

6.3. THE LEADING ORDER APPROXIMATION FOR THE EFFECTIVE
MODULI

$$\begin{aligned}
 D^{(1)} &= -\frac{3}{2}C^{(1)}L, & D^{(2)} &= -\frac{3}{2}C^{(2)}L, & D^{(3)} &= -\frac{3}{2}C^{(3)}L, \\
 A^{(1)}L + B^{(1)} &= u^{(1)}(L), & C^{(1)}L^3 + D^{(1)}L^2 + E^{(1)}L + F^{(1)} &= v^{(1)}(L), \\
 A^{(2)}L + B^{(2)} &= u^{(2)}(L), & C^{(2)}L^3 + D^{(2)}L^2 + E^{(2)}L + F^{(2)} &= v^{(2)}(L), \\
 A^{(3)}L + B^{(3)} &= u^{(3)}(L), & C^{(3)}L^3 + D^{(3)}L^2 + E^{(3)}L + F^{(3)} &= v^{(3)}(L).
 \end{aligned}$$

Note that under first type of loading $(x_1, 0)$ the junction point moves to a new position $(\frac{1}{\sqrt{2}\sqrt{3}\sqrt[4]{3}}; 0)$; under the second type of loading it moves to $(-\frac{1}{\sqrt{2}\sqrt{3}\sqrt[4]{3}}; 0)$. In both these cases bending of bridges does not occur. In the case of shear loading the junction point moves to $(0, -\frac{1}{\sqrt{3}\sqrt[4]{3}})$. The results of the calculation are summarised in the following table

	$(x_1, 0)$			$(0, x_2)$			$2^{-1/2}(x_2, x_1)$		
	(1)	(2)	(3)	(1)	(2)	(3)	(1)	(2)	(3)
A	1/2	1/2	1/2	1/2	1/2	1/2	0	0	0
B	$\frac{\sqrt[4]{3}\sqrt{2}}{6}$	$-\frac{\sqrt[4]{3}\sqrt{2}}{12}$	$-\frac{\sqrt[4]{3}\sqrt{2}}{12}$	$-\frac{\sqrt[4]{3}\sqrt{2}}{6}$	$\frac{\sqrt[4]{3}\sqrt{2}}{12}$	$\frac{\sqrt[4]{3}\sqrt{2}}{12}$	0	$-\frac{\sqrt[4]{27}}{6}$	$\frac{\sqrt[4]{27}}{6}$
C	0	-9/2	9/2	0	9/2	-9/2	$-3\sqrt{6}$	$\frac{3\sqrt{6}}{2}$	$\frac{3\sqrt{6}}{2}$
D	0	$\frac{9\sqrt[4]{3}\sqrt{2}}{4}$	$-\frac{9\sqrt[4]{3}\sqrt{2}}{4}$	0	$-\frac{9\sqrt[4]{3}\sqrt{2}}{4}$	$\frac{9\sqrt[4]{3}\sqrt{2}}{4}$	$3\sqrt[4]{27}$	$-\frac{3\sqrt[4]{27}}{2}$	$-\frac{3\sqrt[4]{27}}{2}$
E	0	0	0	0	0	0	0	0	0
F	0	$-\frac{\sqrt{2}\sqrt[4]{27}}{12}$	$\frac{\sqrt{2}\sqrt[4]{27}}{12}$	0	$\frac{\sqrt{2}\sqrt[4]{27}}{12}$	$-\frac{\sqrt{2}\sqrt[4]{27}}{12}$	$-\frac{\sqrt[4]{3}}{3}$	$\frac{\sqrt[4]{3}}{6}$	$\frac{\sqrt[4]{3}}{6}$

For the hexagonal elementary cell of unit area with the bridges of the thickness ε , the following representation holds for the matrix of elastic moduli

$$\mathcal{H} \sim \frac{4\mu(\lambda + \mu)}{2\mu + \lambda} \begin{pmatrix} \frac{1}{4}\sqrt[4]{3}\sqrt{2}\varepsilon + \frac{3}{4}\sqrt[4]{27}\varepsilon^3 & \frac{1}{4}\sqrt[4]{3}\sqrt{2}\varepsilon - \frac{3}{4}\sqrt[4]{27}\varepsilon^3 & 0 \\ \frac{1}{4}\sqrt[4]{3}\sqrt{2}\varepsilon - \frac{3}{4}\sqrt[4]{27}\varepsilon^3 & \frac{1}{4}\sqrt[4]{3}\sqrt{2}\varepsilon + \frac{3}{4}\sqrt[4]{27}\varepsilon^3 & 0 \\ 0 & 0 & \frac{3}{2}\sqrt[4]{27}\varepsilon^3 \end{pmatrix}. \quad (6.3.39)$$

Taking into account the correspondence between the area fraction and the thickness of the bridge, $f = \frac{\sqrt{6}}{\sqrt[4]{3}}\varepsilon$, we rewrite (6.3.39) in the following form

$$\mathcal{H} \sim \frac{4\mu(\lambda + \mu)}{2\mu + \lambda} \begin{pmatrix} \frac{1}{4}f + \frac{3}{8}f^3 & \frac{1}{4}f - \frac{3}{8}f^3 & 0 \\ \frac{1}{4}f - \frac{3}{8}f^3 & \frac{1}{4}f + \frac{3}{8}f^3 & 0 \\ 0 & 0 & \frac{3}{4}f^3 \end{pmatrix}. \quad (6.3.40)$$

The corresponding representation for the compliance matrix has the following form

$$\mathcal{S} \sim \frac{1}{E} \begin{pmatrix} f^{-1} + \frac{2}{3}f^{-3} & f^{-1} - \frac{2}{3}f^{-3} & 0 \\ f^{-1} - \frac{2}{3}f^{-3} & f^{-1} + \frac{2}{3}f^{-3} & 0 \\ 0 & 0 & \frac{4}{3}f^{-3} \end{pmatrix}, \quad (6.3.41)$$

where E is 2D Young's modulus. This Young's modulus is so-called 2D Young's modulus of the material. The following relations hold

$$E := E_{2D} = \frac{E_{3D}}{1 - \nu^2}, \quad E_{2D} = \frac{4\mu(\lambda + \mu)}{2\mu + \lambda},$$

where ν is the Poisson ratio.

Note that these formulae agree with the result due to Torquato, Gibiansky, Silva and Gibson [112], but here they are obtained by a different method and not using the optimality of the hexagon honeycombs. This condition of optimality formulated for the uniaxial tension follows from the fact that the constants $A^{(1)} = A^{(2)} = A^{(3)}$ are equal under the first and the second type of loading. In other words, in the case of tension (not necessary uniform tension) the longitudinal strain is the same in all bridges. It corresponds to behaviour of the optimal composite. Just for convenience of reading, one rewrite the formulae for the effective bulk modulus K_* and the effective shear modulus μ_* cited in [112]

$$K_* = \frac{1}{4}fE, \quad \mu_* = \frac{3}{8}f^3E. \quad (6.3.42)$$

6.3.4 Second term in effective moduli expansion

In subsection 6.3 the leading term of the effective elastic moduli has been considered. If the accuracy of the first order approximation is not suitable for calculations one should go further and consider the second (or maybe the other) terms of asymptotic expansion. There is an essential difference between the first and the next levels of approximations. As we noticed in section 6.3, on the first level of approximation, the effect of junction region is specified in terms of the junction boundary conditions and the energy of elastic junction region does not count.

At the second level of accuracy, the junction is considered as the elastic region and its energy contributes to the homogenized moduli. We can rewrite the boundary value problem (6.1.20) for the second junction layer $\mathcal{W}^{(1,1)}(\mathbf{X})$ taking into account the con-

ditions (6.1.21)

$$\begin{aligned} \mu \nabla^2 \mathcal{W}^{(1,1)}(\mathbf{X}) + (\lambda + \mu) \nabla \nabla \cdot \mathcal{W}^{(1,1)}(\mathbf{X}) &= 0, & \mathbf{X} \in \Omega, \\ \sigma^{(n)}(\mathcal{W}^{(1,1)}; \mathbf{X}) &= 0, & \mathbf{X} \in \partial \Xi \setminus \Gamma^{(n)}. \end{aligned} \quad (6.3.43)$$

Boundary conditions on $\Gamma^{(n)}$

$$\begin{aligned} \Gamma^{(1)} : \quad \mathcal{W}^{(1,1)} &= \begin{pmatrix} X \frac{\partial}{\partial x} u_0^{(1)}(0) + u_1^{(1)}(0) \\ -\frac{\lambda Y}{\lambda + 2\mu} \frac{\partial}{\partial x} u_0^{(1)}(0) + v_1^{(1)}(0) \end{pmatrix}, \\ \Gamma^{(2)} : \quad \mathcal{W}^{(1,1)} &= \begin{pmatrix} -\frac{\lambda X}{\lambda + 2\mu} \frac{\partial}{\partial x} u_0^{(2)}(0) - v_1^{(2)}(0) \\ Y \frac{\partial}{\partial x} u_0^{(2)}(0) + u_1^{(2)}(0) \end{pmatrix}, \\ \Gamma^{(3)} : \quad \mathcal{W}^{(1,1)} &= \begin{pmatrix} X \frac{\partial}{\partial x} u_0^{(3)}(0) - u_1^{(3)}(0) \\ -\frac{\lambda Y}{\lambda + 2\mu} \frac{\partial}{\partial x} u_0^{(3)}(0) - v_1^{(3)}(0) \end{pmatrix}, \\ \Gamma^{(4)} : \quad \mathcal{W}^{(1,1)} &= \begin{pmatrix} -\frac{\lambda X}{\lambda + 2\mu} \frac{\partial}{\partial x} \partial u_0^{(4)}(0) + v_1^{(4)}(0) \\ Y \frac{\partial}{\partial x} u_0^{(4)}(0) - u_1^{(4)}(0) \end{pmatrix}, \end{aligned}$$

It is important to note that the second junction layer $\mathcal{W}^{(1,1)}(\mathbf{X})$ has non-zero energy, whereas the energy of $\mathcal{W}^{(0)}(\mathbf{X})$ (constant solution of (6.1.12)) is zero. If one evaluates the elastic energy of the displacement field associated with $\mathcal{W}^{(1,1)}$ in the junction area, the correction term in the effective moduli matrix can be obtained. This additional terms have the order $O(\varepsilon^2)$

$$\begin{aligned} \Delta \mathcal{E}_j &= \int_{\Xi_\varepsilon} \sigma(\varepsilon \mathcal{W}^{(1,1)}; \mathbf{x}) : \varepsilon(\varepsilon \mathcal{W}^{(1,1)}; \mathbf{x}) d\mathbf{x} \\ &= \varepsilon^2 \int_{\Xi} \sigma(\mathcal{W}^{(1,1)}; \mathbf{X}) : \varepsilon(\mathcal{W}^{(1,1)}; \mathbf{X}) d\mathbf{X} \sim O(\varepsilon^2). \end{aligned}$$

Note that coupling between $\mathcal{W}^{(1,1)}$ and $\mathcal{W}^{(0)}$ does not occur since the field $\mathcal{W}^{(0)}$ has the constant components and its corresponding stress and strain fields are zero.

At the same time the solution of the problem (6.3.43) in explicit analytical form can not be obtained. In the boundary conditions on $\Gamma^{(n)}$ there are unknown constants $u_1^{(1)}(0)$, $u_1^{(2)}(0)$, $u_1^{(3)}(0)$, $u_1^{(4)}(0)$, $v_1^{(1)}(0)$, $v_1^{(2)}(0)$, $v_1^{(3)}(0)$ and $v_1^{(4)}(0)$. These constants specify the edge conditions for the second ansatz of (6.1.3) and should be chosen such that the continuity of traction is satisfied on $\Gamma^{(n)}$.

One numerical approach to the solution of the boundary value problem (6.3.43) has

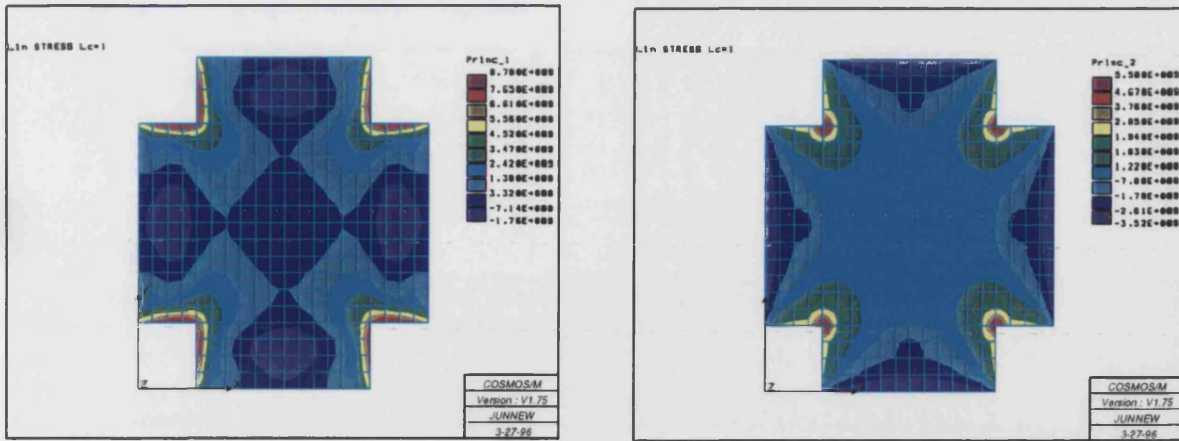


Figure 6-3: Distribution of principal stress field in junction area: "second junction layer"

been done using the finite element package COSMOS/M. The unknown constants have been evaluated by

$$u_1^{(n)}(0) = -X \frac{\partial}{\partial x} u_0^{(n)}(0), \quad v_1^{(n)}(0) = 0, \quad n = 1, 2, 3, 4,$$

and the continuity of traction has been checked numerically. Distributions of principal stresses are presented in Figure 6-3 for the case of $\frac{\partial}{\partial x} u_0^{(n)}(0) = 1$, $n = 1, 2, 3, 4$.

The third-order boundary layer gives the correction term of the order $O(\varepsilon^4)$, but the coupling can occur between the second-order and the third-order layers resulting in the correction $O(\varepsilon^3)$.

6.4 3D effective elastic moduli

In the text below we consider the 3D effective elastic moduli of thin-walled composites for a plane strain (the size of the elementary cell in the z -direction is bigger than in the x - and y -directions, and the displacement vector $\mathbf{u} = (u_1, u_2, 0)$ depends on the coordinates x and y only). The elementary cell of such a composite is a long thin cylinder with the cross section, as described above. To treat this problem, one shall introduce the set of the test fields

$$\mathbf{V}^{(1)} = \begin{pmatrix} x \\ -\frac{\lambda}{2(\mu+\lambda)}y \\ -\frac{\lambda}{2(\mu+\lambda)}z \end{pmatrix}, \quad \mathbf{V}^{(2)} = \begin{pmatrix} -\frac{\lambda}{2(\lambda+\mu)}x \\ y \\ -\frac{\lambda}{2(\lambda+\mu)}z \end{pmatrix}, \quad \mathbf{V}^{(3)} = \begin{pmatrix} -\frac{\lambda}{2(\lambda+\mu)}x \\ -\frac{\lambda}{2(\lambda+\mu)}y \\ z \end{pmatrix},$$

$$\mathbf{V}^{(4)} = \frac{1}{\sqrt{2}} \begin{pmatrix} y \\ x \\ 0 \end{pmatrix}, \quad \mathbf{V}^{(5)} = \frac{1}{\sqrt{2}} \begin{pmatrix} z \\ 0 \\ x \end{pmatrix}, \quad \mathbf{V}^{(6)} = \frac{1}{\sqrt{2}} \begin{pmatrix} 0 \\ z \\ y \end{pmatrix}.$$

These fields are chosen in such a way that the corresponding stress fields have only one non-zero component

$$\sigma_{11}^{(1)} = \frac{\mu(3\lambda + 2\mu)}{\lambda + \mu} = E, \quad \sigma_{22}^{(2)} = \frac{\mu(3\lambda + 2\mu)}{\lambda + \mu} = E, \quad \sigma_{33}^{(3)} = \frac{\mu(3\lambda + 2\mu)}{\lambda + \mu} = E,$$

$$\sigma_{12}^{(4)} = \mu\sqrt{2}, \quad \sigma_{12}^{(5)} = \mu\sqrt{2}, \quad \sigma_{12}^{(6)} = \mu\sqrt{2}.$$

Now one can evaluate the Young's modulus in z -direction as

$$E_3 = \int_{\Omega} [\varepsilon_{ij}^{(3)} : \sigma_{ij}^{(3)}] d\mathbf{x}, \quad i, j = 1, 2, 3.$$

Thus,

$$E_3 = Ef = \frac{\mu(3\lambda + 2\mu)f}{\mu + \lambda}.$$

The Poisson ratios in the $x - z$ and $y - z$ directions can be calculated in a similar way

$$\nu_{13} = - \int_{\Omega} [\varepsilon_{ij}^{(1)} : \sigma_{ij}^{(3)}] d\mathbf{x} E_3^{-1}, \quad i, j = 1, 2, 3,$$

$$\nu_{23} = - \int_{\Omega} [\varepsilon_{ij}^{(2)} : \sigma_{ij}^{(3)}] d\mathbf{x} E_3^{-1}, \quad i, j = 1, 2, 3.$$

$$\nu_{13} = \nu_{23} = \frac{\lambda}{2(\mu + \lambda)}.$$

For the coefficients S_{13}, S_{23}, S_{33} all calculations reduce to the evaluation of the integral of $\varepsilon_{i3}\sigma_{33}$, because all the other terms vanish

$$S_{33} = \frac{\mu + \lambda}{\mu(3\lambda + 2\mu)f} = \frac{1}{Ef}, \quad (6.4.1)$$

$$S_{13} = S_{31} = S_{23} = S_{32} = -\frac{\lambda}{2\mu(3\lambda + 2\mu)f}. \quad (6.4.2)$$

Now let us analyse the test fields $\mathbf{V}^{(5)}$ and $\mathbf{V}^{(6)}$. We consider the plane strain state. Thus, the components of the displacement field in the (x, y) -plane are independent of the z -coordinate. The modified test fields $\mathbf{V}^{(5)}$ and $\mathbf{V}^{(6)}$ is given by

$$\mathbf{V}^{(5)} = \frac{1}{\sqrt{2\mu}} \begin{pmatrix} 0 \\ 0 \\ x \end{pmatrix}, \quad \mathbf{V}^{(6)} = \frac{1}{\sqrt{2\mu}} \begin{pmatrix} 0 \\ 0 \\ y \end{pmatrix},$$

and the corresponding coefficients of the compliance matrix have the form

$$S_{55} = \frac{1}{\mu f}, \quad S_{66} = \frac{1}{\mu f}. \quad (6.4.3)$$

From the calculations of the 2D effective elastic moduli we know the 2D effective elastic moduli (3×3 -matrix) (see, (6.3.16), (6.3.25), (6.3.40)). They can be referred as plane strain moduli:

$$\mathcal{H} = \begin{pmatrix} \mathcal{H}_{11} & \mathcal{H}_{12} & 0 \\ \mathcal{H}_{12} & \mathcal{H}_{11} & 0 \\ 0 & 0 & \mathcal{H}_{33} \end{pmatrix}. \quad (6.4.4)$$

The 3D effective elastic moduli (6×6 -matrix) includes 3×3 -matrix (6.4.4) as one block without any changes. If the matrix \mathcal{H} (6.4.4) corresponds to an isotropic medium ($\mathcal{H}_{33} = \mathcal{H}_{11} - \mathcal{H}_{12}$), then 6×6 -matrix \mathcal{H} corresponds to a transversely isotropic medium. Now, taking into account the formulae (6.4.1), (6.4.2), (6.4.3), (6.4.4) and using the relation $\mathbf{S} = \mathcal{H}^{-1}$, one obtain the 3D effective compliance matrix in the form

$$\mathbf{S} = \begin{pmatrix} \frac{H_{11}}{H_{11}^2 - H_{12}^2} + \frac{\lambda^2}{4\mu f(\lambda + \mu)(3\lambda + 2\mu)} & -\frac{H_{11}}{H_{11}^2 - H_{12}^2} + \frac{\lambda^2}{4\mu f(\lambda + \mu)(3\lambda + 2\mu)} & -\frac{\lambda}{2\mu(3\lambda + 2\mu)f} & 0 & 0 & 0 \\ -\frac{H_{11}}{H_{11}^2 - H_{12}^2} + \frac{\lambda^2}{4\mu f(\lambda + \mu)(3\lambda + 2\mu)} & \frac{H_{11}}{H_{11}^2 - H_{12}^2} + \frac{\lambda^2}{4\mu f(\lambda + \mu)(3\lambda + 2\mu)} & -\frac{\lambda}{2\mu(3\lambda + 2\mu)f} & 0 & 0 & 0 \\ -\frac{\lambda}{2\mu(3\lambda + 2\mu)f} & -\frac{\lambda}{2\mu(3\lambda + 2\mu)f} & \frac{\mu + \lambda}{\mu(3\lambda + 2\mu)f} & 0 & 0 & 0 \\ 0 & 0 & 0 & \frac{1}{H_{33}} & 0 & 0 \\ 0 & 0 & 0 & 0 & \frac{1}{\mu f} & 0 \\ 0 & 0 & 0 & 0 & 0 & \frac{1}{\mu f} \end{pmatrix}.$$

The corresponding coefficients S_{11} , S_{22} and S_{12} are given by

$$S_{11} = S_{22} = \frac{H_{11}}{H_{11}^2 - H_{12}^2} + \frac{\lambda^2}{4\mu f(\lambda + \mu)(3\lambda + 2\mu)}, \quad (6.4.5)$$

$$S_{12} = -\frac{H_{11}}{H_{11}^2 - H_{12}^2} + \frac{\lambda^2}{4\mu f(\lambda + \mu)(3\lambda + 2\mu)}. \quad (6.4.6)$$

Note that the results above are consistent with Nemat-Nasser and Hori [85](p.97), but they have been obtained here by different method introducing test fields $\mathbf{V}^{(n)}$, $n = 1, 2, 3$.

6.5 Application of the homogenization procedure

6.5.1 Closely-located rigid inclusions: elasticity problem

In this subsection we discuss the alternative problem: the problem of closely located rigid inclusions with the Dirichlet conditions specified on their surfaces. In the section 6.3 the volume fraction of voids is supposed to be close to one and the volume fraction of elastic material approaches a small value. In the problem of closely-located rigid inclusions the volume fraction of rigid inclusions plays the same role as the volume fraction of the voids. However, as we will see later on, the volume fraction of the elastic material is not a small parameter in this problem. The important parameter is the distance between nearby rigid inclusions. If this distance is small, but the volume fraction of an elastic material is comparable with the volume fraction of rigid phase (it can happen for non-convex rigid inclusions like stars, for example) the first parameter dominates. Thus, a small parameter in this problem is the minimal distance between inclusions.

Mathematically, the problem is formulated as a homogenization problem in a periodic array of rigid inclusions. The elementary cell can be of arbitrary shape (square, parallelogram, hexagonal), and arbitrary number of rigid inclusions is admitted inside the cell. We emphasise that rigid inclusions are closely located: at least in a neighbourhood of one point, the distance between nearby inclusions is much smaller than the diameter of the inclusion. The shape of the inclusion can be arbitrary, and the boundary is specified in terms of a parametric function. Using the homogenization technique of Bakhvalov and Panasenko [4], the problem of defining the effective moduli is reduced to the problem for an elementary cell subject to external homogeneous loading and periodicity conditions. The boundary value problem on an elementary cell similar to (6.1.2) is imposed. The Dirichlet conditions are prescribed on $\partial\Xi_1^{(\epsilon)}$ instead of the Neumann ones.

Now, it is appropriate to consider a model boundary value problem for an elastic thin

bridge located between two rigid inclusions

$$\begin{aligned}
 \mathcal{L}_{xx}(\mathbf{U}; \mathbf{x}) &:= \mathcal{D}_{\frac{\partial}{\partial \mathbf{x}}} \mathcal{H} \mathcal{D}_{\frac{\partial}{\partial \mathbf{x}}}^t \mathbf{U}(\mathbf{x}) = 0, & \mathbf{x} \in \Pi_\varepsilon, \\
 \mathbf{U}(\mathbf{x}) &= \begin{pmatrix} C_\pm^{(1)} \\ C_\pm^{(2)} \end{pmatrix}, & \mathbf{x} \in \partial\Pi_\varepsilon^{(1)}, \\
 \mathbf{U} &= \mathbf{a}_\pm, & \mathbf{x} \in \partial\Pi_\varepsilon^{(2)},
 \end{aligned}$$

where $C_\pm^{(n)}$ are constants corresponding to the displacements of rigid inclusions. $\Pi_\varepsilon = \{(x, \varepsilon t) : -1 < x < 1, -h(x)/2 < t < h(x)/2\}$, $\partial\Pi_\varepsilon^{(1)} = \{t = \pm \frac{h(x)}{2}\}$, $\partial\Pi_\varepsilon^{(2)} = \{x = \pm 1\}$. The problem in a thin bridge subject to the Dirichlet boundary conditions on the lateral surfaces has been considered by Maz'ya and Nazarov [63], Maz'ya, Nazarov and Plamenevsky [65]. Here we follow the developed method to calculate the effective moduli of such structures in terms of energy of special fields.

Following Maz'ya and Nazarov [63], the leading term of the displacement field for this problem can be found as

$$\begin{aligned}
 U_1(x, y) &= C_-^{(1)} + \frac{t\varepsilon}{h(x)}(C_+^{(1)} - C_-^{(1)}), & t = y/\varepsilon, \\
 U_2(x, y) &= C_-^{(2)} + \frac{t\varepsilon}{h(x)}(C_+^{(2)} - C_-^{(2)}), & t = y/\varepsilon.
 \end{aligned} \tag{6.5.1}$$

The procedure for defining the effective moduli reduces to the evaluation of the energy of the deformation field concentrated in the gap between rigid inclusions. The formulae (6.3.1) and (6.3.4) are employed, and the stress and strain fields are calculated for the displacement fields (6.5.1). For simplicity, one supposes that all elastic bridges have the same geometry and specified by the thickness $h(x)$ and the length L^* . Rigid inclusions are supposed to be symmetric (this allows to reduce a number of required parameters), the thickness $h(x)$ specifies all bridges. As a result, we have the formulae for the effective elastic moduli matrices.

For a composite including symmetric triangular rigid inclusion an elementary cell is hexagonal (there are six inclusions in one periodic cell) or parallelogram (there are two inclusions in one periodic cell). In this case the effective moduli can be evaluated as follows

$$\mathcal{H} = \frac{\sqrt{3}}{12} \int_0^{L^*} \frac{dx}{h(x)} \begin{pmatrix} 7\mu + 3\lambda & \mu + \lambda & 0 \\ \mu + \lambda & 7\mu + 3\lambda & 0 \\ 0 & 0 & 6\mu + 2\lambda \end{pmatrix} + O(1), \quad (6.5.2)$$

$$L^* = 2\sqrt{3}\bar{h}f^{-1}, \quad \bar{h} = \int_0^{L^*} h(x)dx,$$

where f is the area fraction of the elastic material.

If the periodic cell has a shape of a square and there is one symmetric rigid inclusion inside, the following formula holds for the matrix of the elastic moduli

$$\mathcal{H} = \int_0^{L^*} \frac{dt}{h(t)} \begin{pmatrix} 2\mu + \lambda & 0 & 0 \\ 0 & 2\mu + \lambda & 0 \\ 0 & 0 & \mu \end{pmatrix} + O(1), \quad (6.5.3)$$

$$L^* = 2\bar{h}f^{-1}.$$

Finally, for the hexagonal periodic cell with a rigid symmetric inclusion inside, the matrix of the elastic moduli is given by

$$\mathcal{H} = \frac{\sqrt{3}}{4} \int_0^{L^*} \frac{dt}{h(t)} \begin{pmatrix} 7\mu + 3\lambda & \mu + \lambda & 0 \\ \mu + \lambda & 7\mu + 3\lambda & 0 \\ 0 & 0 & \frac{2}{3}(11\mu + 5\lambda) \end{pmatrix} + O(1), \quad (6.5.4)$$

$$L^* = \frac{2\sqrt{3}}{3}\bar{h}f^{-1}.$$

6.5.2 Thin-walled composites: conductive media

The homogenization of conductivity problems is simpler for consideration due to a scalar character of the corresponding boundary value problem. As a result, the effective conductivity tensor can be evaluated as a Dirichlet integral

$$\mathcal{K}_{mk} = \frac{1}{mes_2\mathcal{S}} \int_{\Xi} k(\mathbf{x}) \nabla T^{(n)} \cdot \nabla T^{(k)} d\mathbf{x}, \quad (6.5.5)$$

where $T^{(n)}$, $n = 1, 2$, are special solutions corresponding to applied linear test fields in the x - and y - directions.

The solution of the conductivity problems in thin bridges admits a simple asymptotic expansion. There is no bending mode, thus the leading terms of potentials (or temperature

fields) are linear functions. The asymptotic analysis is applied and after calculation the effective conductivity tensor for the thin-bridge composites is evaluated by the following expressions:

triangular honeycombs -

$$\mathcal{K} = k \left[\int_0^{L^*} \frac{dx}{h(x)} \right]^{-1} \begin{pmatrix} \sqrt{3} & 0 \\ 0 & \sqrt{3} \end{pmatrix} + O(f^2), \quad L^* = 2\sqrt{3}\bar{h}f^{-1}. \quad (6.5.6)$$

square honeycombs -

$$\mathcal{K} = k \left[\int_0^{L^*} \frac{dx}{h(x)} \right]^{-1} \begin{pmatrix} 1 & 0 \\ 0 & 1 \end{pmatrix} + O(f^2), \quad L^* = 2\bar{h}f^{-1}. \quad (6.5.7)$$

hexagonal honeycombs -

$$\mathcal{K} = k \left[\int_0^{L^*} \frac{dx}{h(x)} \right]^{-1} \begin{pmatrix} \frac{1}{\sqrt{3}} & 0 \\ 0 & \frac{1}{\sqrt{3}} \end{pmatrix} + O(f^2), \quad L^* = \frac{2\sqrt{3}}{3}\bar{h}f^{-1}, \quad (6.5.8)$$

$$\text{where } \bar{h} = \int_0^{L^*} h(x) dx.$$

6.5.3 Closely-located rigid inclusions: conductive media

In the case of the Dirichlet boundary conditions the problem reduces to defining the effective moduli in the media with closely located perfectly conductive inclusion. Here, it is important to note that if the Dirichlet conditions are imposed, then the effective moduli depend mainly on the distance between perfectly conductive inclusion. This effect is similar to one in elasticity problems. As a result of the calculation, one has the following effective conductivity tensors for the composites with perfectly conductive inclusions:

triangular honeycombs -

$$\mathcal{K} = k \int_0^{L^*} \frac{dt}{h(t)} \begin{pmatrix} \frac{1}{\sqrt{3}} & 0 \\ 0 & \frac{1}{\sqrt{3}} \end{pmatrix} + O(1), \quad L^* = 2\sqrt{3}\bar{h}f^{-1}. \quad (6.5.9)$$

square honeycombs -

$$\mathcal{K} = k \int_0^{L^*} \frac{dt}{h(t)} \begin{pmatrix} 1 & 0 \\ 0 & 1 \end{pmatrix} + O(1), \quad L^* = 2\bar{h}f^{-1}. \quad (6.5.10)$$

hexagonal honeycombs -

$$\mathcal{K} = k \int_0^{L^*} \frac{dt}{h(t)} \begin{pmatrix} \sqrt{3} & 0 \\ 0 & \sqrt{3} \end{pmatrix} + O(1), \quad L^* = \frac{2\sqrt{3}}{3}\bar{h}f^{-1}. \quad (6.5.11)$$

6.5.4 Thin-walled composites: thermo-elastic media

After the homogenization procedure applied to the uncoupled thermo-elastic equilibrium equations, we obtain the formulae for the thermal expansion matrix

$$\Upsilon_{mk} = \frac{1}{mes_2\mathcal{S}} \int_{\Xi} \gamma(\mathbf{x}) \nabla T^{(n)} \cdot \nabla T^{(k)} d\mathbf{x}, \quad (6.5.12)$$

where $\gamma(\mathbf{x})$ is the thermal expansion coefficient, and $T^{(n)}$, $n = 1, 2$, are the temperature fields corresponding to the test fields x and y imposed on the composite structure.

The asymptotic procedure for the Laplace equation is much simpler than one presented earlier for the Navier system, and the leading term of the temperature field inside each bridge can be obtained as the solution of the equation

$$\partial_{xx}^2 T^{(n)} = 0, \quad 0 < x < L,$$

Hence,

$$T^{(n)} = A^{(n)}x + B^{(n)}. \quad (6.5.13)$$

Combining (6.5.12) and (6.5.13), we obtain the formula for the components of the thermal expansion matrix in the form

$$\Upsilon_{mk} = \frac{\gamma}{mes_2G} \sum_{n=1}^N \int_0^L A_n^{(m)} A_n^{(k)} \varepsilon dx + O(\varepsilon^2). \quad (6.5.14)$$

For composite structures considered above (having triangular, square or hexagonal elementary cells) the volume fraction of the material f is supposed to be small, and all bridges are of a constant thickness ε . Under these conditions the following formula for effective thermal expansion coefficients for triangular, square and hexagonal honeycomb

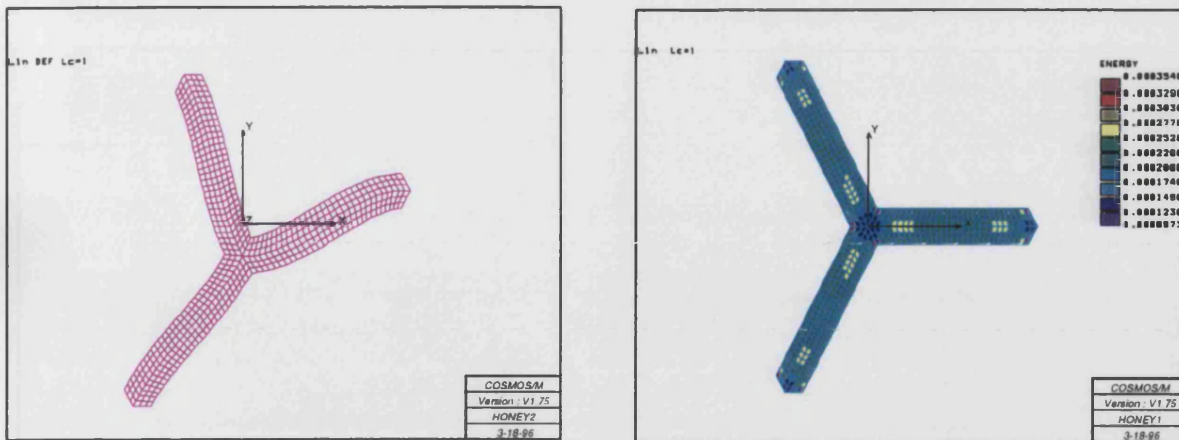


Figure 6-4: Honeycomb composite under shear loading: deformed state and distribution of energy density

holds

$$\Upsilon = \gamma \begin{pmatrix} \frac{1}{2}f & 0 \\ 0 & \frac{1}{2}f \end{pmatrix} + O(f^2). \quad (6.5.15)$$

6.6 Comparison with numerical experiments

In the sections above the formulae for the effective elastic, conductive and thermo-elastic moduli are given. They have been derived on the basis of the asymptotic expansion of the displacement field and the temperature in an elementary cell and take into account the whole first ansatz in the asymptotic representation, not only the leading terms. This technique differs from “engineering approach” by Kalamkarov and Kolpakov [50], where the displacement field in bridges is supposed to be linear. The advantage of the asymptotic technique appears, when we consider the bridges of varying thickness and the linear approach does not work any more. In this section we go further in consideration of the homogenized moduli. Some numerical experiments have been performed using the finite element technique. The following homogenization procedure has been applied: the problem has been reduced to a model problem imposed on the elementary cell; this problem has been solved numerically using the finite element package COSMOS/M and on the last step the effective moduli have been evaluated in terms of the formula (A.0.14).

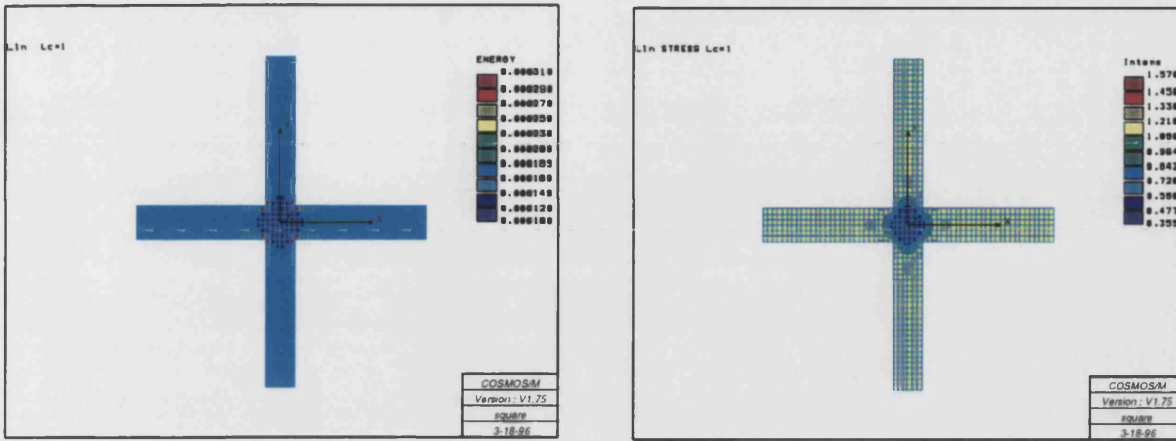


Figure 6-5: Square-type thin-walled composite under hydrostatic loading: energy and intensity distributions

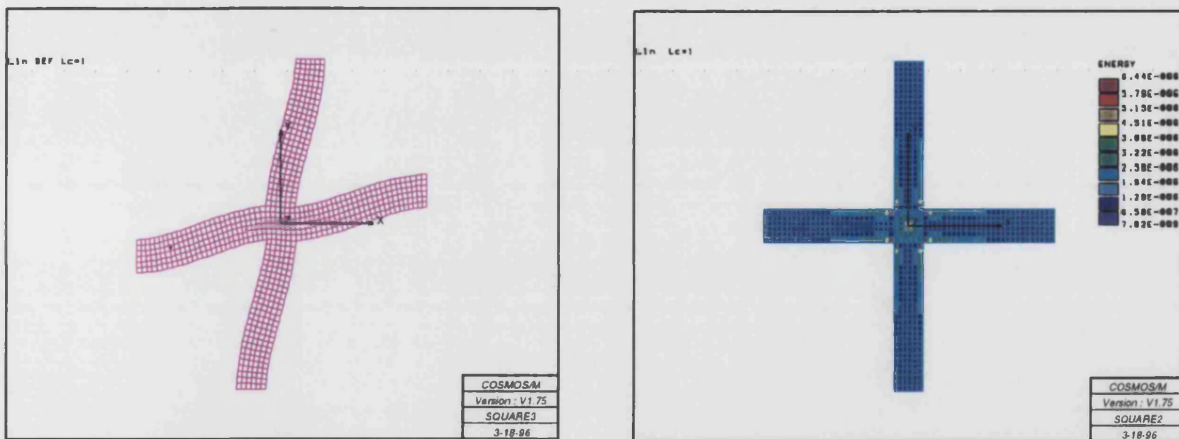


Figure 6-6: Square-type thin-walled composite under shear loading: deformed state and energy distribution

Here some of them are described and compared with the asymptotic solutions:

1. Hexagonal honeycomb composite subject to shear loading (see Figure 6-4). The energy of normalized periodic cell allows one to evaluate the shear modulus μ . It is equal to 0.04232 for the volume fraction $f = 0.1$ as the result of numerical simulations and to 0.05144 as the result of asymptotic formulae (6.3.40) (volume fraction $f = 0.19$, Poisson ratio $\nu = 0.3$ and Young's modulus $E = 1$).
2. Square thin-walled composite subject to hydrostatic loading (see Figure 6-5). We apply the loading (x, y) to a unit periodic cell with periodicity conditions on the edges of bridges. The energy of the field allows one to evaluate the bulk modulus. It is equal to 0.117709 after numerical integration and to 0.1 as a result of the formulae (6.3.16) (volume fraction $f = 0.19$, Poisson ratio $\nu = 0.3$ and Young's modulus $E = 1$).
3. Similar calculation for the shear modulus of square thin-walled composite has been performed. Shear modulus obtained by the numerical procedure is equal to 0.0006021 and calculated by the asymptotic formula (6.3.16) is 0.0008574. (volume fraction $f = 0.19$, Poisson ratio $\nu = 0.3$ and Young's modulus $E = 1$) (see Figure 6-6).

6.7 Conclusions

In this chapter the accurate asymptotic model of thin-walled composite structures have been constructed. The boundary value problem for the Navier system in region with thin bridges has been analysed. The junction conditions have been derived as the conditions of exponential decay of the boundary layer fields. This technique does not involve any additional assumptions adopted in engineering literature. The asymptotic formulae have been derived for effective elastic and thermo-conductive moduli, and the comparison with numerical data is presented.

Appendix A

Homogenisation of the linear elasticity equations

For readers' convenience we give a brief description of the homogenisation procedure for the Lamé system (the general theory is given in Jikov, Koslov and Oleinik [47]).

$$\mathcal{L}_{xx}(\mathbf{u}) := \mu \nabla^2 \mathbf{u} + (\lambda + \mu) \nabla \nabla \cdot \mathbf{u} = 0, \quad \mathbf{x} \in \Omega. \quad (\text{A.0.1})$$

The displacement vector \mathbf{u} depends on the "slow" variables \mathbf{x} and the "fast" variables $\boldsymbol{\xi} = \mathbf{x}/\varepsilon$. Fast coordinates are associated with the periodic structure (containing inclusions or cavities) characterized by the small parameter ε . The differential operator of the 2D Lamé system can be rewritten in the matrix form

$$\mathcal{L}_{tx} := \mathcal{D}_{\frac{\partial}{\partial \mathbf{x}}} \mathcal{H}(\boldsymbol{\xi}) \mathcal{D}_{\frac{\partial}{\partial \mathbf{x}}}^t, \quad (\text{A.0.2})$$

where

$$\mathcal{D}_{\frac{\partial}{\partial \mathbf{x}}} = \begin{pmatrix} \frac{\partial}{\partial x_1} & 0 & \frac{1}{\sqrt{2}} \frac{\partial}{\partial x_2} \\ 0 & \frac{\partial}{\partial x_2} & \frac{1}{\sqrt{2}} \frac{\partial}{\partial x_1} \end{pmatrix}, \quad \mathcal{H} = \begin{pmatrix} 2\mu + \lambda & \lambda & 0 \\ \lambda & 2\mu + \lambda & 0 \\ 0 & 0 & 2\mu \end{pmatrix}.$$

We are looking for a solution of the Lamé system $\mathcal{L}_{xx} \mathbf{u}(\mathbf{x}, \boldsymbol{\xi}) = 0$ in the following asymptotic form

$$\mathbf{u}(\mathbf{x}, \boldsymbol{\xi}) = \mathbf{u}^{(0)}(\mathbf{x}) + \varepsilon \mathbf{u}^{(1)}(\mathbf{x}, \boldsymbol{\xi}) + \varepsilon^2 \mathbf{u}^{(2)}(\mathbf{x}, \boldsymbol{\xi}) + O(\varepsilon^3). \quad (\text{A.0.3})$$

The coefficients in (A.0.3) solve the recurrent system of equations

$$\mathcal{L}_{\xi\xi}\mathbf{u}^{(0)}(\mathbf{x}) = 0, \quad (\text{A.0.4})$$

$$\mathcal{L}_{\xi\xi}\mathbf{u}^{(1)}(\mathbf{x}, \boldsymbol{\xi}) = -\mathcal{L}_{\xi x}\mathbf{u}^{(0)}(\mathbf{x}) - \mathcal{L}_{x\xi}\mathbf{u}^{(0)}(\mathbf{x}), \quad (\text{A.0.5})$$

$$\mathcal{L}_{\xi\xi}\mathbf{u}^{(2)}(\mathbf{x}, \boldsymbol{\xi}) = -\mathcal{L}_{\xi x}\mathbf{u}^{(1)}(\mathbf{x}, \boldsymbol{\xi}) - \mathcal{L}_{x\xi}\mathbf{u}^{(1)}(\mathbf{x}, \boldsymbol{\xi}) - \mathcal{L}_{xx}\mathbf{u}^{(0)}(\mathbf{x}). \quad (\text{A.0.6})$$

The first equation (A.0.4) is an identity. Note, that $\mathcal{L}_{x\xi}\mathbf{u}^{(0)}(\mathbf{x}) = 0$ as well. The right hand side of the equation (A.0.5) can be simplified as

$$\begin{aligned} \mathcal{L}_{\xi x}\mathbf{u}^{(0)}(\mathbf{x}) &= \mathcal{D}_{\frac{\partial}{\partial \xi}} \mathcal{H}(\boldsymbol{\xi}) \mathcal{D}_{\frac{\partial}{\partial x}}^t \mathbf{u}^{(0)} = \mathcal{D}_{\frac{\partial}{\partial \xi}} \mathcal{H}(\boldsymbol{\xi}) \left(\frac{\partial u_0}{\partial x_1}, \frac{\partial v_0}{\partial x_2}, \frac{1}{\sqrt{2}} \left(\frac{\partial u_0}{\partial x_2} + \frac{\partial v_0}{\partial x_1} \right) \right) \\ &= \sum_{n=1}^3 C_n(\mathbf{x}) \mathcal{D}_{\frac{\partial}{\partial \xi}} \mathcal{H}(\boldsymbol{\xi}) \mathcal{D}_{\frac{\partial}{\partial x}}^t \mathbf{V}^{(n)} = \sum_{n=1}^3 C_n(\mathbf{x}) \mathcal{L}_{\xi\xi} \mathbf{V}^{(n)}. \end{aligned} \quad (\text{A.0.7})$$

Here the following notations are used

$$\begin{aligned} \mathbf{u}^{(0)} &= \begin{pmatrix} u_0 \\ v_0 \end{pmatrix}, \quad C_1(\mathbf{x}) = \frac{\partial u_0}{\partial x_1}, \quad C_2(\mathbf{x}) = \frac{\partial v_0}{\partial x_2}, \quad C_3(\mathbf{x}) = \frac{1}{\sqrt{2}} \left(\frac{\partial u_0}{\partial x_2} + \frac{\partial v_0}{\partial x_1} \right), \\ \mathbf{V}^{(1)} &= \begin{pmatrix} \xi_1 \\ 0 \end{pmatrix}, \quad \mathbf{V}^{(2)} = \begin{pmatrix} 0 \\ \xi_2 \end{pmatrix}, \quad \mathbf{V}^{(3)} = \frac{1}{\sqrt{2}} \begin{pmatrix} \xi_2 \\ \xi_1 \end{pmatrix}, \quad \mathcal{D}_{\frac{\partial}{\partial \xi}}^t \mathbf{V}^{(n)} = \begin{pmatrix} \delta_{1n} \\ \delta_{2n} \\ \delta_{3n} \end{pmatrix}. \end{aligned}$$

It is possible to see that

$$\mathbf{u}^{(1)}(\mathbf{x}, \boldsymbol{\xi}) = \sum_{n=1}^3 \mathbf{W}^{(n)}(\boldsymbol{\xi}) C_n(\mathbf{x}), \quad (\text{A.0.8})$$

where the fields $\mathbf{W}^{(n)}$ satisfy the system

$$\mathcal{L}_{\xi\xi}(\mathbf{W}^{(n)}(\boldsymbol{\xi}) + \mathbf{V}^{(n)}(\boldsymbol{\xi})) = 0, \quad \mathbf{x} \in \mathbb{R}^2. \quad (\text{A.0.9})$$

This system has a solution if and only if the solvability conditions hold

$$\langle \boldsymbol{\xi} \times \mathbf{L}_{\xi\xi} \mathbf{u}^{(i)} \rangle = 0, \quad \text{and} \quad \langle \mathbf{L}_{\xi\xi} \mathbf{u}^{(i)} \rangle = 0, \quad (\text{A.0.10})$$

where $\langle \cdot \rangle$ denotes the average over an elementary cell of the periodic structure. The condition (A.0.10) is applied to each elementary cell separately and the periodicity

boundary conditions for the functions $\mathbf{W}^{(n)}$ are specified. In the case of the square periodical cell $[1 \times 1]$ the periodicity boundary conditions are formulated in the form

$$\begin{aligned}\mathbf{W}^{(n)}(0, \xi_2) &= \mathbf{W}^{(n)}(1, \xi_2), \quad \sigma(\mathbf{W}^{(n)}; 0, \xi_2) = \sigma(\mathbf{W}^{(n)}; 1, \xi_2), \\ \mathbf{W}^{(n)}(\xi_1, 0) &= \mathbf{W}^{(n)}(\xi_1, 1), \quad \sigma(\mathbf{W}^{(n)}; \xi_1, 0) = \sigma(\mathbf{W}^{(n)}; \xi_1, 1).\end{aligned}$$

Now consider the third equation (A.0.6). Employing the some useful notations

$$\begin{aligned}\mathbf{W} &= \begin{pmatrix} \mathbf{W}_1^{(1)} & \mathbf{W}_1^{(2)} & \mathbf{W}_1^{(3)} \\ \mathbf{W}_2^{(1)} & \mathbf{W}_2^{(2)} & \mathbf{W}_2^{(3)} \end{pmatrix}, \\ \mathbf{V} &= \begin{pmatrix} \mathbf{V}_1^{(1)} & \mathbf{V}_1^{(2)} & \mathbf{V}_1^{(3)} \\ \mathbf{V}_2^{(1)} & \mathbf{V}_2^{(2)} & \mathbf{V}_2^{(3)} \end{pmatrix}, \quad \mathbf{C} = (C_1 \quad C_2 \quad C_3)^t,\end{aligned}$$

one can write the right hand side of the equation (A.0.6) as

$$\begin{aligned}\mathcal{D}_{\frac{\partial}{\partial \xi}} \mathcal{H}(\xi) \mathcal{D}_{\frac{\partial}{\partial x}}^t \mathbf{W}(\xi) \mathbf{C}(\mathbf{x}) + \mathcal{D}_{\frac{\partial}{\partial x}} \mathcal{H}(\xi) \mathcal{D}_{\frac{\partial}{\partial \xi}}^t \mathbf{W}(\xi) \mathbf{C}(\mathbf{x}) + \mathcal{D}_{\frac{\partial}{\partial \xi}} \mathcal{H}(\xi) \mathbf{C}(\mathbf{x}) \\ = \mathcal{D}_{\frac{\partial}{\partial \xi}} \mathcal{H}(\xi) \mathbf{W}^t(\xi) \mathcal{D}_{\frac{\partial}{\partial x}} \mathcal{D}_{\frac{\partial}{\partial \xi}}^t \mathbf{u}^{(0)}(\mathbf{x}) \\ + \mathcal{D}_{\frac{\partial}{\partial x}} \left\{ \mathcal{H}(\xi) \mathcal{D}_{\frac{\partial}{\partial \xi}}^t \left(\mathbf{W}(\xi) + \mathbf{V}(\xi) \right) \right\} \mathcal{D}_{\frac{\partial}{\partial x}}^t \mathbf{u}^{(0)}(\mathbf{x}).\end{aligned}\quad (\text{A.0.11})$$

Now apply the solvability conditions (A.0.10). First term in (A.0.11) vanishes due to the periodicity boundary conditions imposed on the function $\mathbf{W}^{(n)}$. The second one gives the homogenized elasticity equation

$$\mathcal{D}_{\frac{\partial}{\partial x}} \widehat{\mathcal{H}} \mathcal{D}_{\frac{\partial}{\partial x}}^t \mathbf{u}^{(0)}(\mathbf{x}) = 0, \quad \mathbf{x} \in \Omega, \quad (\text{A.0.12})$$

and the expression for the matrix of effective elastic moduli

$$\widehat{\mathcal{H}} = \int_{[1 \times 1]} \mathcal{H}(\xi) \mathcal{D}_{\frac{\partial}{\partial \xi}}^t \left\{ \mathbf{W}(\xi) + \mathbf{V}(\xi) \right\} d\mathbf{x}. \quad (\text{A.0.13})$$

It is verified by direct calculations that

$$\mathcal{H}(\mathbf{x}) \mathcal{D}_{\frac{\partial}{\partial \xi}}^t \left\{ \mathbf{W}(\xi) + \mathbf{V}(\xi) \right\} = \begin{pmatrix} \sigma_{11} \\ \sigma_{22} \\ \sqrt{2}\sigma_{12} \end{pmatrix} = \boldsymbol{\sigma},$$

$$\mathcal{D}_{\frac{\partial}{\partial \xi}}^t \left\{ \mathbf{W}(\xi) + \mathbf{V}(\xi) \right\} = \begin{pmatrix} \varepsilon_{11} \\ \varepsilon_{22} \\ \sqrt{2}\varepsilon_{12} \end{pmatrix} = \boldsymbol{\varepsilon}.$$

Thus the final relation (A.0.13) for effective elastic moduli of periodical composite with square elementary cells can be rewritten in the form

$$\begin{aligned} \widehat{\mathbf{H}} &= \int_{[1 \times 1]} \left[\mathbf{H}(\xi) \mathcal{D}_{\frac{\partial}{\partial \xi}}^t \left\{ \mathbf{W}(\xi) + \mathbf{V}(\xi) \right\} \right]^t \mathcal{D}_{\frac{\partial}{\partial \xi}}^t \left\{ \mathbf{W}(\xi) + \mathbf{V}(\xi) \right\} dx \\ &= \int_{[1 \times 1]} \boldsymbol{\sigma}^t(\mathbf{W}(\xi) + \mathbf{V}(\xi)) \boldsymbol{\varepsilon}(\mathbf{W}(\xi) + \mathbf{V}(\xi)) dx. \end{aligned} \quad (\text{A.0.14})$$

List of Figures

2-1	The equivalent regions for Laplace operator:	33
2-2	Equivalent cavities for the case of plane strain:	38
2-3	The equivalent elliptical and nonelliptical cavities:	44
3-1	The shape of the optimal cavity.	55
3-2	Geometry of the optimal cavity as the function of applied stresses.	56
3-3	The normalized energy change versus applied stress.	57
3-4	The distribution of the energy density for the optimal domain.	57
3-5	The tangential stress on the boundary.	59
3-6	The regions obtained by the "modified" conformal mapping	60
3-7	The shape of domain with piece-wise constant tangential stresses on the boundary.	65
4-1	Crack geometry	73
4-2	Crack in elastic region with and without a defect: distribution of the principal stresses	75
5-1	Crack trajectory $h(l)$ versus crack tip position l , resulting from interaction with an elliptic cavity whose major axis is parallel to the main crack. Results are reported for different aspect ratios a/b	90
5-2	Crack trajectory $h(l)$ versus crack tip position l , resulting from interaction with a Griffith crack at different inclinations.	91
5-3	SEM photograph of a crack in a porcelain stoneware	92
5-4	Matlab simulation corresponding to SEM photograph 5-3	93

5-5	Comparison with Rubinstein's [95] results , Mode II normalized stress intensity factor versus defect position ϕ :	
	(a) interaction with a Griffith crack;	
	(b) interaction with a circular cavity.	94
5-6	Crack trajectory $h(l)$ versus crack tip position l , resulting from interaction with an elastic circular inclusion: (a) inclusion more rigid than the matrix; (b) inclusion less rigid than the matrix; (c) and (d) \mathcal{P} is indefinite.	95
5-7	Crack propagation in Zirconia-Alumina composite	97
5-8	Elliptical inclusion and its conformal map	98
5-9	Crack trajectories $H(l)/y_0$ versus crack tip position l/y_0 , resulting from interaction with an elliptical inclusion, (a) more and (b) less stiff than the matrix. The major axis is inclined of different angles with respect to the unperturbed crack.	106
5-10	Crack trajectories $H(l)/y_0$ versus crack tip position l/y_0 , resulting from interaction with an elliptical rigid inclusion (a) and with an elliptical cavity (b) having major axis inclined of an angle $\theta = \pi/3$. Different aspect ratios are considered.	107
5-11	Crack trajectories $H(l)/y_0$ versus crack tip position l/y_0 , resulting from interaction with an elliptical inclusions of equal area: inclusion stiffer than the matrix, with major axis orthogonal (a) or parallel (b) to the unperturbed crack; inclusion weaker than the matrix, with major axis orthogonal (a) or parallel (b) to the unperturbed crack.	108
5-12	The crack deviation due to the soft thermoelastic inclusion: $\gamma = 4 \cdot 10^{-3}$, $\gamma_0 = 10^{-3}$, $\Delta T = 100K$, $\varkappa = 2$, $\varkappa_0 = 2$, $\mu_0/\mu = 0.5(-)$, $\mu_0/\mu = 0.2(--)$, $\mu_0/\mu = 0.01(...)$	115
5-13	The crack deviation due to the rigid thermoelastic inclusion: $\gamma = 10^{-3}$, $\gamma_0 = 10^{-2}$, $\Delta T = 100K$, $\varkappa = 2$, $\varkappa_0 = 2$, $\mu_0/\mu = 2(-)$, $\mu_0/\mu = 5(--)$, $\mu_0/\mu = 50(...)$	115
5-14	The crack deviation due to the thermoelastic inclusions with the same shear modulus: $\gamma = 10^{-3}$, $\gamma_0 = 4 \cdot 10^{-3}$, $\Delta T = 100K$, $\varkappa = 2$, $\mu_0/\mu = 1$, $\varkappa_0 = 2(-)$, $\varkappa_0 = 1.5(--)$, $\varkappa_0 = 2.5(...)$	116

5-15	The crack deviation due to the thermoelastic inclusions with the same bulk modulus: $\gamma = 10^{-3}$, $\Delta T = 25K$, $\mu = 1$, $\lambda = 1$, $\mu_0 = 1.5$, $\lambda_0 = 0.5$, $\gamma_0 = 2 \cdot 10^{-3}(-)$, $\mu_0 = 0.5$, $\lambda_0 = 1.5$, $\gamma_0 = 10^{-4}(-)$, $\mu_0 = 1.95$, $\lambda_0 = 0.05$, $\gamma_0 = 3 \cdot 10^{-3}(\dots)$	117
5-16	The crack deviation due to the elliptical thermoelastic inclusions with the same elastic and thermal moduli: $\gamma = 10^{-3}$, $\gamma_0 = 5 \cdot 10^{-3}$, $\Delta T = 100K$, $\varkappa = 2$, $\mu_0 = 0$, $\mu = 1$, $\varkappa_0 = 2$, $\beta = 45^\circ$, $a = 1$, $b = 1(-)$, $b = 0.5(-)$, $b = 0(\dots)$	118
5-17	Crack trajectories $H(l)/y_0$ versus crack tip position l/y_0 , resulting from interaction with a circular elastic inclusion bonded with a linear interface with equal radial and tangential stiffness (the inclusion is stiffer than the matrix: $\mu_0/\mu = 10$).	131
5-18	Crack trajectories $H(l)/y_0$ versus crack tip position l/y_0 , resulting from interaction with a circular elastic inclusion stiffer than the matrix and bonded with a linear, interface. Different values of interfacial stiffness s_θ for the same parameter s_r , producing zero deflection of the crack path at infinity, are considered.	132
6-1	Types of thin-walled structures.	135
6-2	Honeycomb structure and junction area.	139
6-3	Distribution of principal stress field in junction area: "second junction layer"	162
6-4	Honeycomb composite under shear loading: deformed state and distribution of energy density	170
6-5	Square-type thin-walled composite under hydrostatic loading: energy and intensity distributions	171
6-6	Square-type thin-walled composite under shear loading: deformed state and energy distribution	171

Bibliography

- [1] J. Aboudi. *Mechanics of composite materials*. Elsevier, Amsterdam, 1991.
- [2] N. Kh. Arutyunyan, A. B. Movchan, and S. A. Nazarov. The problems of elasticity in infinite regions with parabolic and cylindrical inclusions or cavities. *Advances in Mechanics*, 10(4):3–91, 1987.
- [3] V. M. Babich, I. S. Zorin, M. I. Ivanov, A. B. Movchan, and S. A. Nazarov. Integral characteristics in problems of elasticity. preprint p-6-89, Steklov Mathematical Institute (LOMI), Leningrad, 1989. (in Russian).
- [4] N. S. Bakhvalov and G. P. Panasenko. *Homogenization: Averaging processes in periodic media*. Kluwer, Dordrecht, 1989.
- [5] N. V. Banichuk. Determination of the form of a curvilinear crack by small parameter technique. *Izv. An SSSR, Mekhanika Tverdogo Tela*, 7(2):130–137, 1970.
- [6] G. I. Barenblatt and G. P. Cherepanov. On brittle crack under longitudinal shear. *Applied Mathematics and Mechanics(PMM)*, 25:1654–1666, 1961.
- [7] M. P. Bendsoe. *Optimization of structural topology, shape, and material*. Springer-Verlag, Berlin, New York, 1995.
- [8] A. Bensoussan, J. L. Lions, and G. Papanicolaou. *Asymptotic analysis for periodic structures*. North-Holland publishing company, Amsterdam, New York, Oxford, 1978.
- [9] D. Bigoni, A. Movchan, L. Esposito, S. Serkov, and M. Valentini. Crack propagation in brittle, elastic solid with defects. In *Atti del XII Convegno Nazionale del Gruppo Italiano Frattura*, pages 59–67, Parma, 1996.

- [10] D. Bigoni, M. Ortiz, and A. Needleman. Effect of interfacial compliance on bifurcation of a layer bonded to a substrate. *International Journal of Solids and Structures*, 34(33-34):4305–4326, 1997.
- [11] D. Bigoni, S. K. Serkov, A. B. Movchan, and M. Valentini. Asymptotic models of dilute composites with imperfectly bounded inclusions. *International Journal of Solids and Structures*, 1998. (in press).
- [12] B. Budiansky. On the elastic moduli of some heterogeneous materials. *Journal of the Mechanics and Physics of Solids*, 13:223–227, 1965.
- [13] H. F. Bueckner. A novel principle for the computational of stress intensity factors. *ZAMM*, 50(9):529–546, 1970.
- [14] S. D. Carothers. Plane strain in a wedge. *Proceedings of the Royal Society, Edinburgh*, 23:292, 1912.
- [15] D. Chenaus. On the existence of a solution in a domain identification problem. *Journal of Mathematical Analysis and Applications*, 52:189–219, 1975.
- [16] G. P. Cherepanov. Inverse problems of the plane theory of elasticity. *Applied Mathematics and Mechanics(PMM)*, 38(6):963–979, 1974.
- [17] A. V. Cherkaev, Y. Grabovsky, A. B. Movchan, and S. K. Serkov. The cavity of the optimal shape under the shear loading. *International Journal of Solids and Structures*, 1998. (in press).
- [18] R. M. Christensen. *Mechanics of composite materials*. Wiley, New York, 1979.
- [19] N. Claussen. Fracture toughness of Al_2O_3 with an unstabilized ZrO_2 dispersed phase. *Journal of American Ceramical Society*, 59:49–51, 1976.
- [20] B. Cotterell and J. R. Rice. Slightly curved or kinked cracks. *International Journal of Fracture*, 16(2):155–169, 1980.
- [21] R. Courant and D. Hilbert. *Methods of Mathematical Physics*. Interscience Publishers, New York, London, 1962.
- [22] R. W. Davinge. *Mechanical behaviour of ceramics*. Cambridge University Press, Cambridge, 1979.
-

- [23] K. Duan, Y. W. Mai, and B. Cotterell. On the paradox between crack bridging and crack interaction in quasi-brittle materials. *Journal of European Ceramical Society*, 15:1061–1064, 1976.
- [24] J. D. Eshelby. The determination of the elastic field of an ellipsoidal inclusion, and related problems. *Proceedings of the Royal Society, London A*, 241:376–396, 1957.
- [25] H. Gao. Three dimensional slightly non-planar crack. *Journal of Applied Mechanics*, 59:335–343, 1992.
- [26] Z. Gao. A circular inclusion with imperfect interface: Eshelby’s tensor and related problems. *Journal of Applied Mechanics*, 62:860–866, December 1995.
- [27] G. Geymonat and F. Krasucki. A limit model of a soft thin joint. In T. Marcellini, G. Talenti, and E. Vesentini, editors, *Partial differential equations and applications, Lecture notes in Pure and Applied Mathematics*, volume 177, pages 165–173. Marcel Dekker, New York, 1996.
- [28] L. V. Gibiansky and A. V. Cherkaev. Design of composite plates of extremal rigidity. In A. Cherkaev and R. Kohn, editors, *Topics in the mathematical modelling of composite materials*, pages 95–138. Birkhauser, New York, 1997. (Russian original, 1984).
- [29] L. V. Gibiansky and A. V. Cherkaev. Microstructures of composites of extremal rigidity and exact estimates of provided energy density. In A. Cherkaev and R. Kohn, editors, *Topics in the mathematical modelling of composite materials*, pages 273–317. Birkhauser, New York, 1997. (Russian original, 1986).
- [30] L. J. Gibson and M. Ashby. *Cellular Solids*. Pergamon Press, New York, 1988.
- [31] M. Goland and E. Reissner. The stresses in cemented joints. *Journal of Applied Mechanics*, pages A17–A27, 1944.
- [32] R. V. Goldstein and R. L. Salganik. Brittle fracture of solids with arbitrary cracks. *International Journal of Fracture*, 10:507–523, 1974.
- [33] S. X. Gong and S. A. Meguid. On the elastic fields of an elliptical inhomogeneity under plane deformation. *Proceedings of the Royal Society, London A*, 443:457–471, 1993.

- [34] Y. Grabovsky and R. V. Kohn. Microstructures minimising the energy of a two phase elastic composite in two space dimensions. i: The confocal ellipse construction. *Journal of the Mechanics and Physics of Solids*, 43(6):933–947, 1995.
- [35] Y. Grabovsky and R. V. Kohn. Microstructures minimising the energy of a two phase elastic composite in two space dimensions. ii: The Vigdergauz microstructure. *Journal of the Mechanics and Physics of Solids*, 43(6):949–972, 1995.
- [36] N. J. Hardiman. Elliptic elastic inclusion in an infinite elastic plate. *Quarterly Journal of Mechanics and Applied Mathematics*, 7, Pt.2:226–230, 1954.
- [37] Z. Hashin. Thermal-expansion coefficients of cracked laminates. *Composites Science and Technology*, 31(4):247–260, 1988.
- [38] Z. Hashin. Thermoelastic properties of fibre composites with imperfect interface. *Mechanics of Materials*, 8:333–348, 1990.
- [39] Z. Hashin. Composite materials with viscoelastic interphase: creep and relaxation. *Mechanics of Materials*, 11:135–148, 1991.
- [40] Z. Hashin. Thermoelastic properties of particulate composites with imperfect interface. *Journal of the Mechanics and Physics of Solids*, 39(6):745–762, 1991.
- [41] E. J. Haug, K. K. Choi, and V. Komkov. *Design Sensitivity Analysis of Structural System. Mathematics in Science and Engineering*, volume 177. Academic Press, Inc., 1986.
- [42] J. H. Hetherington and M. F. Thorpe. The conductivity of a sheet containing inclusions with sharp corners. *Proceedings of the Royal Society, London A*, 438:591–604, 1992.
- [43] R. Hill. The elastic behaviour of a crystalline aggregate. *Proceedings of Physical Society, A*, 65:349–354, 1952.
- [44] I. Jasiuk. Cavities vis-a-vis rigid inclusions: elastic moduli of materials with polygonal inclusions. *International Journal of Solids and Structures*, 32(3/4):407–422, 1995.
- [45] I. Jasiuk, J. Chen, and M.F. Thorpe. Elastic moduli of two dimensional materials with polygonal and elliptical holes. *Applied Mechanics Reviews*, 47(1, Pt.2):S18–S28, January 1994.
-

- [46] M. A. Jaswon and R. D. Bhargava. Two-dimensional elastic inclusion problems. *Proceedings of the Cambridge Philosophical Society: mathematical and physical sciences*, 57:669–680, 1961.
- [47] V. V. Jikov, S. M. Koslov, and O. A. Oleinik. *Homogenization of differential operators and integral functionals*. Springer-Verlag, New York, 1994.
- [48] J. P. Jones and J. S. Whittier. Waves at a flexibly bonded interface. *Journal of Applied Mechanics*, 34:905–909, 1967.
- [49] R. M. Jones. *Mechanics of composite materials*. McGraw-Hill, New York, 1975.
- [50] A. L. Kalamkarov and A. G. Kolpakov. *Analysis, design and optimization of composite structures*. Wiley, Chichester, New York, Toronto, 1997.
- [51] S. N. Karp and F. C. Karal. The elastic-field behaviour in the neighbourhood of a crack of arbitrary angle. *Communications on Pure and Applied Mathematics*, 15:413–421, 1962.
- [52] A. Klarbring. Derivation of a model of adhesively bonded joints by the asymptotic expansion method. *International Journal of Engineering Science*, 29:493–512, 1991.
- [53] R. V. Kohn and G. Strang. Optimal design and relaxation of variational problems. *Communications on Pure and Applied Mathematics*, 39:113 – 137, 139 – 182, 353 – 377, 1986.
- [54] V. A. Kondrat'ev. Boundary problems for elliptic equations on domains with conical or angular points. *Transactions of the Moscow Mathematical Society*, 16:227–313, 1967.
- [55] V. A. Kondrat'ev and O. A. Oleinik. Boundary value problems for partial differential equations in non-smooth domains. *Russian Mathematical Surveys*, 38(2):1–86, 1983.
- [56] A. J. Levy. The debonding of elastic inclusions and inhomogeneities. *Journal the Mechanics and Physics of Solids*, 39(4):477–505, 1991.
- [57] R. Lipton. Variational methods, bounds, and size effects for composites with highly conducting interface. *Journal of the Mechanics and Physics of Solids*, 45:361–384, 1997.
-

-
- [58] R. Lipton and B. Vernescu. Variational methods, size effects and extremal microstructures for elastic composites with imperfect interface. *Mathematical Models and Methods in Applied Sciences*, 5:1139–1173, 1995.
- [59] A. K. Mal and S. K. Bose. Dynamic elastic moduli of a suspension of imperfectly bonded spheres. *Proceedings of the Cambridge Philosophical Society: mathematical and physical sciences*, 76:587–599, 1974.
- [60] X. Markenscoff. Some remarks on the wedge paradox and Saint-Venant’s principle. *Journal of Applied Mechanics*, 61:519–523, September 1994.
- [61] P. A. Martin. Mapping flat cracks onto penny-shaped cracks: shear loading. *Journal of the Mechanics and Physics of Solids*, 43(2):275–294, 1995.
- [62] P. A. Martin. Mapping flat cracks onto penny-shaped cracks, with applications to somewhat circular tensile cracks. *Quarterly of Applied Mathematics*, LIV(4):663–675, 1996.
- [63] V. G. Maz’ya and S. A. Nazarov. Dirichlet problems in domains with thin bridges. *Sibirskii Matematicheskii Zhurnal*, 25(2):297–313, 1984.
- [64] V. G. Maz’ya and S. A. Nazarov. Asymptotics of energy ranges for small perturbation of the boundary in the vicinity of nodal and conical points. *Transactions of the Moscow Mathematical Society*, 50:79, 1987.
- [65] V. G. Maz’ya, S. A. Nazarov, and B. A. Plamenevsky. *Asymptotische Theorie Elliptischer Randwertanfgaben in Singulär Gestörten*. Akademie-Verlag, Berlin, B.1, 1991; B.2, 1992.
- [66] F. A. McClintock and A. S. Argon. *Mechanical Behaviour of Materials*. Addison Wesley, Reading, Mass., 1966.
- [67] L. M. Milne-Thomson. *Antiplane elastic system*. Springer-Verlag, Berlin, 1962.
- [68] G. W. Milton. Modelling the properties of composites by laminates. In J. L. Ericksen, D. Kinderlehrer, R. V. Kohn, and J. L. Lions, editors, *Homogenization and effective moduli of materials and media*, pages 150–174. Springer-Verlag, New York, 1986.
-

- [69] G. W. Milton. On characterizing the set of possible effective tensors of composites - the variational method and the translation method. *Communications on Pure and Applied Mathematics*, 43(1):63–125, 1990.
- [70] G. W. Milton and A. B. Movchan. A correspondence between plane elasticity and the two-dimensional real and complex dielectric equations in anisotropic media. *Proceedings of the Royal Society, London A*, 450:293–317, 1995.
- [71] A. B. Movchan. Brittle failure of an elastic plane with a thin rectangular hole. *Vestnik Leningrad University*, 63(1), 1988.
- [72] A. B. Movchan. Integral characteristics of elastic inclusions and cavities in the two-dimensional theory of elasticity. *European Journal of Applied Mathematics*, 3:21–30, 1992.
- [73] A. B. Movchan, H. Gao, and J. R. Willis. On perturbation of plane cracks. *International Journal of Solids and Structures*, 1998. (in press).
- [74] A. B. Movchan, N. F. Morozov, and S. A. Nazarov. Cracks with smoothly closing edges under plane deformation. *Applied Mathematics and Mechanics(PMM)*, 51(1):99–107, 1987.
- [75] A. B. Movchan and N. V. Movchan. *Mathematical Modelling of Solids with Non-regular Boundaries*. CRC Press, New York, London, Tokyo, 1995.
- [76] A. B. Movchan and S. A. Nazarov. Asymptotic behaviour of stress-strain state in the vicinity of sharp defects in an elastic body. *IMA Journal of Applied Mathematics*, 49:245–272, 1992.
- [77] A. B. Movchan, S. A. Nazarov, and O. R. Polyakova. The quasi-static growth of a semi-infinite crack in a plane containing small defects. *Comptes Rendus de L'Academie des Sciences Paris, Série II*, 313:1223–1228, 1991.
- [78] A. B. Movchan and S. K. Serkov. Longitudinal loading of rectangular notches. *Soviet Applied Mechanics*, 27(10):966–973, 1991.
- [79] A. B. Movchan and S. K. Serkov. Elastic polarization matrices of polygonal domains. *Izv. AN SSSR. Mekhanika Tverdogo Tela*, 26(3):63–68, 1992.

-
- [80] A. B. Movchan and S. K. Serkov. The Pólya-Szegő tensors in mathematical modelling of composite media. In *19th ICTAM-96, Abstracts*, Kyoto, Japan, 1996.
- [81] A. B. Movchan and S. K. Serkov. The Pólya - Szegő matrices in asymptotic models of dilute composites. *European Journal of Applied Mathematics*, 8:595–621, 1997.
- [82] A. B. Movchan and J. R. Willis. Dynamical weight-functions for a moving crack. ii: Shear loading. *Journal of the Mechanics and Physics of Solids*, 43(9):1369–1383, 1997.
- [83] N. I. Muskhelishvili. *Some basic problems of the mathematical theory of elasticity*. Nordhoff, Groningen, 1953.
- [84] S. A. Nazarov and B. A. Plamenevsky. *Elliptic Problems in Domains with Piecewise Smooth Boundaries*. Walter de Gruyter, Berlin, New York, 1994.
- [85] S. Nemat-Nasser and M. Hori. *Micromechanics: Overall Properties of Heterogeneous Solids*. 1992. 687 pages.
- [86] O. A. Oleinik, G. P. Panasenko, and G. A. Yosifian. Homogenization and asymptotic expansion for solution of the elasticity system with rapidly oscillating periodic coefficients. *Applicable Analysis*, 15:15–32, 1983.
- [87] N. Olhoff and G. I. N. Rozvany, editors. *First World Congress of Structural and Multidisciplinary Optimization*. Pergamon Press, 1995.
- [88] P. J. Olver. Canonical elastic moduli. *Journal of Elasticity*, 19:189–212, 1988.
- [89] O. Pironneau. *Optimal Shape Design for Elliptic Systems*. Springer-Verlag, New York, 1984.
- [90] G. Pólya and G. Szegő. *Isoperimetric inequalities in mathematical physics*. Princeton University Press, Princeton, 1951.
- [91] W. H. Press, B. P. Flannery, S. A. Teukolsky, and W. J. Vetterling. *Numerical Recipes in FORTRAN. The art of scientific computing*. Cambridge University Press, second edition, 1992.
- [92] J. Qu. The effect of slightly weakened interfaces on the overall elastic properties of composite materials. *Mechanics of Materials*, 14:269–281, 1993.
-

- [93] L. R. F. Rose. Microcrack interaction with a main crack. *International Journal of Fracture*, 31:233–242, 1986.
- [94] G. I. N. Rozvany, M. P. Bendsoe, and U. Kirsch. Layout optimization of structures. *Applied Mechanical Review*, 48(2):41–119, 1994.
- [95] A. A. Rubinstein. Macro-crack-micro-defect interaction. *Journal of Applied Mechanics*, 53:505–510, September 1986.
- [96] F. J. Sabina, V. P. Smyshlyaev, and J. R. Willis. Self-consistent analysis of waves in matrix-inclusion composite - i. aligned spheroidal inclusions. *Journal of the Mechanics and Physics of Solids*, 41(10):1573–1588, 1993.
- [97] G. N. Savin. *Stress concentration around holes*. Pergamon Press, New York, 1961.
- [98] E. Schnack and U. Spörl. A mechanical dynamic programming algorithm for structure optimization. *International Journal for Numerical Methods in Engineering*, 23(11):1985–2004, 1986.
- [99] G. P. Sendeckyj. *Mechanics of Composite Materials*. Academic Press, New York, London, 1974.
- [100] S. K. Serkov, A. B. Movchan, A. V. Cherkaev, and Y. Grabovsky. Optimality of dilute composites under shear load. In *IUTAM Symposium on Transformation Problems in Composite and Active Materials*. 1997. (in press).
- [101] G. C. Sih, editor. *Mechanics of fracture*. Nordhoff International Publishing, Leyden, 1978.
- [102] G. C. Sih and A. M. Skudra, editors. *Failure mechanics of composites*. North-Holland, Amsterdam, Oxford, 1984.
- [103] I. S. Sokolnikoff. *Mathematical theory of elasticity*. McGraw-Hill, New York, 1956.
- [104] J. Sokolowski and J.-P. Zolesio. *Introduction to Shape Optimization. Shape Sensitivity Analysis*. Springer-Verlag, New York, 1992.
- [105] E. Sternberg and W. T. Koiter. The wedge under a concentrated couple: a paradox in the two-dimensional theory of elasticity. *Journal of Applied Mechanics*, pages 575–581, December 1958.
-

- [106] Y. Sumi. Computational crack path prediction for brittle fracture in welding residual stress fields. *International Journal of Fracture*, 44:189–207, 1990.
- [107] Y. Sumi, S. Nemat-Nasser, and L. M. Keer. On crack branching and curving in a finite body. *International Journal of Fracture*, 21:67–79, 1983.
- [108] Y. Sumi and Z. N. Wang. A finite-element simulation method for a system of growing cracks in a heterogeneous material. (to be published).
- [109] Z. Suo, A. Needleman, and M. Ortiz. Stability of solids with interfaces. *Journal of the Mechanics and Physics of Solids*, 40:613–640, 1992.
- [110] G. I. Taylor. The energy of a body moving in an infinite fluid, with an application to airships. *Proceedings of the Royal Society. London A*, 120:13–21, 1928.
- [111] M. F. Thorpe and I. Jasiuk. New results in the theory of elasticity for two-dimensional composites. *Proceedings of the Royal Society, London A*, 438:531–544, 1992.
- [112] S. Torquato, L. V. Gibiansky, M. A. Silva, and L. J. Gibson. Effective mechanical and transport properties of cellular solids. *International Journal of Mechanical Sciences*, 40(1):71–82, 1998.
- [113] N. Tullini, M. Savoia, and C. O. Horgan. End effects in multi-layered orthotropic strips with imperfect bonding. *Mechanics of Materials*, 26(1):23–34, 1997.
- [114] M. Valentini, S. Serkov, D. Bigoni, and A. Movchan. Crack propagation in a brittle elastic material with defects. *Journal of Applied Mechanics*. (submitted).
- [115] S. B. Vigdergauz. Integral equation of the inverse problem of the plane theory of elasticity. *Applied Mathematics and Mechanics(PMM)*, 40(3):566–569, 1976.
- [116] S. B. Vigdergauz. Stressed state of an elastic plane with constant-stress holes. *Izv. AN SSSR. Mekhanika Tverdogo Tela*, 23(3):101–104, 1988.
- [117] S. B. Vigdergauz. Piecewise-homogeneous plates of extremal stiffness. *Applied Mathematics and Mechanics(PMM)*, 53(1):76–80, 1989.
- [118] S. B. Vigdergauz. Two-dimensional grained composites of extreme rigidity. *Journal of Applied Mechanics*, 61:390–394, June 1994.
-

- [119] S. B. Vigdergauz and A. V. Cherkaev. A hole in a plate, optimal for its biaxial extension - compression. *Applied Mathematics and Mechanics(PMM)*, 50(3):524–528, 1986.
- [120] V. I. Weingarten. *Cosmos/M User Guide*. Structural Research and Analysis Corporation, Santa Monica, California, 1993. Vol.I, Vol.II, Vol.III, Vol.IV.
- [121] M. L. Williams. Stress singularities resulting from various boundary condition in angular corners of plate in extension. *Journal of Applied Mechanics*, 19(4), 1952.
- [122] J. R. Willis. Elasticity theory of composites. In H. G. Hopkins and M. J. Sewell, editors, *Mechanics of Solids. The Rodney Hill Sixtieth Anniversary Volume*, pages 653–686. Pergamon Press, Oxford, 1982.
- [123] J. R. Willis. The overall elastic response of composite material. *Journal of Applied Mechanics*, 50:1202–1209, December 1983.
- [124] J. R. Willis and A. B. Movchan. Dynamical weight-functions for a moving crack. i: Mode-i loading. *Journal of the Mechanics and Physics of Solids*, 43(3):319–341, 1997.
- [125] J. R. Willis and A. B. Movchan. Three-dimensional dynamic perturbation of a propagating crack. *Journal of the Mechanics and Physics of Solids*, 45(4):591–610, 1997.
- [126] G. Xu, A. F. Bower, and M. Ortiz. An analysis of non-planar crack growth under mixed mode loading. *International Journal of Solids and Structures*, 31(16):2167–2193, 1994.
- [127] I. S. Zorin, A. B. Movchan, and S. A. Nazarov. Use of the elastic polarization tensor in problems of crack mechanics. *Izv. AN SSSR. Mekhanika Tverdogo Tela*, 23(6):128–134, 1988.